UNIVERSITY OF IOANNINA
COLLEGE OF SCIENCES AND TECHNOLOGIES
DEPARTMENT OF MATERIALS SCIENCE ENGINEERING

MISICHRONIS KONSTANTINOS
MATERIALS SCIENCE ENGINEER

SYNTHESIS, MOLECULAR AND MORPHOLOGICAL CHARACTERIZATION OF LINEAR AND COMPLEX ARCHITECTURE BLOCK COPOLYMERS CONSISTING OF POLY(CYCLOHEXADIENE)

PhD THESIS

IOANNINA 2012

ΠΑΝΕΠΙΣΤΗΜΙΟ ΙΩΑΝΝΙΝΩΝ
ΣΧΟΛΗ ΕΠΙΣΤΗΜΩΝ & ΤΕΧΝΟΛΟΓΙΩΝ
ΤΜΗΜΑ ΜΗΧΑΝΙΚΩΝ ΕΠΙΣΤΗΜΗΣ ΥΛΙΚΩΝ

ΜΙΣΙΧΡΟΝΗΣ ΚΩΝΣΤΑΝΤΙΝΟΣ
ΜΗΧΑΝΙΚΟΣ ΕΠΙΣΤΗΜΗΣ ΥΛΙΚΩΝ

ΣΥΝΘΕΣΗ, ΜΟΡΙΑΚΟΣ ΚΑΙ ΜΟΡΦΟΛΟΓΙΚΟΣ ΧΑΡΑΚΤΗΡΙΣΜΟΣ ΓΡΑΜΜΙΚΩΝ ΚΑΙ ΠΟΛΥΠΛΟΚΗΣ ΑΡΧΙΤΕΚΤΟΝΙΚΗΣ ΣΥΜΠΟΛΥΜΕΡΩΝ ΚΑΤΑ ΣΥΣΤΑΔΕΣ ΟΠΟΥ Η ΜΙΑ ΣΥΣΤΑΔΑ ΕΙΝΑΙ ΠΟΛΥ(ΚΥΚΛΟΕΞΑΔΙΕΝΙΟ)

ΔΙΔΑΚΤΟΡΙΚΗ ΔΙΑΤΡΙΒΗ

ΙΩΑΝΝΙΝΑ 2012

ΤΡΙΜΕΛΗΣ ΣΥΜΒΟΥΛΕΥΤΙΚΗ ΕΠΙΤΡΟΠΗ

Αυγερόπουλος Απόστολος, Αναπληρωτής Καθηγητής (επιβλέπων Καθηγητής)

Μπέλτσιος Κωνσταντίνος, Αναπληρωτής Καθηγητής

Βλάχος Κωνσταντίνος, Επίκουρος Καθηγητής

ΕΠΤΑΜΕΛΗΣ ΕΞΕΤΑΣΤΙΚΗ ΕΠΙΤΡΟΠΗ

Mays Jimmy W., Καθηγητής……...

Κοσμάς Μάριος, Καθηγητής ……...

Καρακασίδης Μιχαήλ, Αναπληρωτής Καθηγητής……...

Μπέλτσιος Κωνσταντίνος, Αναπληρωτής Καθηγητής……...

Αυγερόπουλος Απόστολος, Αναπληρωτής Καθηγητής…….

Βλάχος Κωνσταντίνος, Επίκουρος Καθηγητής……

Ζαφειρόπουλος Νικόλαος, Επίκουρος Καθηγητής……..

3-MEMBER ADVISING COMMITTEE

Avgeropoulos Apostolos, Associate Professor (Advisor)

Beltsios Konstantinos, Associate Professor

Vlahos Konstantinos, Assistant Professor

7-MEMBER EXAMINING COMMITTEE

Mays Jimmy W., Professor…….....

Kosmas Marios, Professor…….....

Karakassides Michael, Associate Professor…….....

Beltsios Konstantinos, Associate Professor…….....

Avgeropoulos Apostolos, Associate Professor……...

Vlahos Konstantinos, Assistant Professor……

Zafeiropoulos Nikolaos E., Assistant Professor……...

Acknowledgements

A big part of my life has come to an end. I have been member of this laboratory since February of 2005 and going back to that day, only positive thoughts and emotions overwhelm me. Numerous people accompanied me to this 7 year route towards this moment and I would like to thank all of them.

Above all I would like, from the deepest parts of my heart, to express my gratitude to my Advisor, Associate Professor Avgeropoulos Apostolos. He was the person who, through his lecturing, inspired me to follow this field. All these years, he never stopped guiding me with all his efforts in order to help and support me overcome any difficulties and our discussions were always very interesting and effective. I am grateful for providing me with the knowledge and principals in order to become a better scientist and I am truly thankful for giving me the opportunity to travel two times to the US, to the University of Tennessee at Knoxville and to Oak Ridge National Laboratory, and opening my mind to new perspectives and doors to new collaborations. After all these years he became something more than an Advisor to me, he is my mentor and my friend, I owe him a lot for being what I am and it was really honorable to meet him and work together.

I would like to express also my gratitude to Professor Jimmy W. Mays, who honored me with his presence by accepting the invitation of being a member of my 7-member examining committee and for giving me the opportunity to visit his laboratories, at Chemistry Department of the University of Tennessee at Knoxville and at Oak Ridge National Laboratory, and finalize a very significant part of my studies there. He is a distinguished Professor and a great man, and his reputation comes before him. Also, I would like to thank several people from Oak Ridge National Lab who helped me complete my dissertation. First of all, I want to thank Dr. Hong Kunlun who made sure that my experiments and my stay at Oak Ridge and at the Center for Nanophase Materials Science (CNMS) will be productive and without any obstacles. Furthermore, I would like to express my gratitude to Dr. Youjun He, who was a great help inside and outside the laboratory. I am grateful to Dr. Jihua Chen who helped me at most with the ultramicrotoming and TEM images consuming many hours of his day in order to make sure that everything will be on schedule. I want to thank also Dr. Keum Jong Kahk who did his best in order to help me with the SAXS measurements and Dr. Jamie Messman who helped me with the

DSC measurements. I would like also to thank every single person at the CNMS building who helped me less or more at any aspect that had to do with the everyday life inside the laboratory. Finally, I am very thankful to Dr. Xiaojun Wang from the University of Tennessee at Knoxville for his help with the staining procedure.

I would like also to thank the rest members of the committee, Beltsios Konstantinos, Associate Professor at Materials Science and Engineering Department of the University of Ioannina, Karakassides Michael, Associate Professor at Materials Science and Engineering Department of the University of Ioannina, Zafeiropoulos Nikolaos, Assistant Professor at Materials Science and Engineering Department of the University of Ioannina, Kosmas Marios, Professor at Chemistry Department of the University of Ioannina and Vlachos Konstantinos, Assistant Professor at Chemistry Department of the University of Ioannina, for their presence and their useful observations.

I would like also to express my gratefulness to every member of the Polymers Laboratory, either to those who already left or to those who are still here. Their help, to every aspect of my everyday life in the lab, was something more than great and I am thankful for that. I want to thank especially Liontos Giorgos for his help with the GPC results, Ntetsikas Konstantinos and Polymeropoulos Giorgos for the ^{1}H-NMR results, Katsigiannopoulos Dimitris and Zapsas Giorgos for their help with the DSC measurements and everybody else who made sure to create a nice working environment all these years. At the end of this route, I am very thankful that I made good friends and as I look back, I have only good moments to remember.

Finally, I am more than grateful to my parents, Fotis and Eirini, who have been to my side all these years supporting me with all their strengths. They have taught me selflessness and patience and that only good can come, when working hard for every aspect of your life. They helped me make the right choices when needed and they put always my well-being above themselves. They stood always by me in difficult situations and they made me look things only from the positive point of view. I feel that words are not enough to express my feelings for them and one thing I know for sure is that their love is overwhelming and unique.

Θα ήθελα να εκφράσω την απεριόριστη ευγνωμοσύνη μου και αγάπη στους γονείς μου, Φώτη και Ειρήνη, που βρισκόντουσαν πάντα στον πλευρό μου με όλες

τους τις δυνάμεις. Τα εφόδια που μου έδωσαν από μικρό παιδί με βοήθησαν να αντιμετωπίζω τις δύσκολες καταστάσεις και με έκαναν καλύτερο άνθρωπο. Η ανιδιοτέλεια τους είναι μοναδική και πάντα με έβαζαν πάνω από τους εαυτούς τους. Με έμαθαν να έχω υπομονή, να δουλεύω σκληρά και να βλέπω πάντα τα πράγματα από την θετική τους πλευρά. Η αγάπη τους είναι μοναδική και τα λόγια δεν φτάνουν για να περιγράψουν τα συναισθήματά που νιώθω για την αμέριστη συμπαράσταση όλα αυτά τα χρόνια. Πραγματικά, τους ευχαριστώ για όλα.

Ioannina, June 5th 2012
Konstantinos Misichronis

Ιωάννινα, 5 Ιουνίου 2012
Κωνσταντίνος Μισιχρόνης

Αφιερωμένο στην οικογένειά μου…

Table of Contents

CHAPTER 1

Introduction

1.1 General Information

Polymers are a remarkably significant class of materials with various properties suitable for numerous applications. The suitability of a polymer for a particular application is controlled by its molecular and structural characteristics such as molecular weight, molecular weight distribution, microphase separation, architecture and functionality. Well-defined polymers synthesized by living addition polymerization processes are a very useful tool to understand the relationship between structure and properties. Therefore, great progress has been achieved in living polymerization techniques over the past three decades by the development of new polymerization technologies. Especially, living anionic polymerization is the most important technique for synthesizing novel polymers with low heterogeneity and well-defined structures. By using anionic polymerization, many new polymeric materials have been synthesized with narrow molecular weight distributions and controlled architectures, molecular weights and functionalities. Initially, most of the studies had been limited to several hydrocarbon monomers (such as styrene, butadiene, isoprene etc.) due to their controlled polymerization behavior. However, during the last two decades more monomers, especially with functional groups, have been polymerized anionically [such as ethylene oxide, methyl methacrylate, 2- and 4-vinylpyridine, hexamethylcyclotrisiloxane (D_3)] introducing an enormous variety of new properties and applications for polymeric materials.

One of these monomers is also 1,3-cyclohexadiene (1,3-CHD). Its polymers (PCHD) are of a great interest from both scientific and practical views. PCHD and its derivatives lead to better thermal and chemical stability and higher mechanical strength due to their six-membered ring structure in the main chain. It can be dehydrogenated to poly(paraphenylene - PPP), a highly conducting polymer and also it can be hydrogenated to poly(cyclohexylene - PCHE) which exhibits significantly increased glass temperatures ($T_g \sim 200^0$C for 95% 1,4-PCHE and $T_g \sim 232^0$C for 52% 1,2-PCHE), low specific gravity, high heat resistance and high flexural modulus etc[1-3].

Anionic polymerization of 1,3-cyclohexadiene has proven to be the most effective technique among all others, despite the fact that it is less controlled than the polymerization of other dienes due to side reactions, such as chain transfer and chain termination. These side reactions have been almost restricted and controlled by using polar additives resulting in narrower molecular weight distributions. Nevertheless, the maximum attainable molecular weight of PCHD is limited approximately to 50.000 g/mol.

For this thesis, two types of samples were synthesized and studied. Initially, a series of linear diblocks copolymers consisting of polystyrene and 1,4-poly(cyclohexadiene) were synthesized. Particularly, seventeen (17) polystyrene-*b*-poly(cyclohexadiene) (PS-b-PCHD) or poly(cyclohexadiene)-b-polystyrene (PCHD-b-PS) linear diblock copolymers were synthesized via anionic synthesis polymerization by using the sequential monomer addition method and high vacuum techniques. By using these methods and techniques, narrow molecular weight distributions (> 1.1) were ensured as well as chemical and compositional homogeneity. These diblock copolymers were synthesized in order to study their molecular and especially their morphological behavior in terms of microphase separation in a wide variety of volume fractions ranging from 95% to 25% for the PS block. For this reason, their molecular weights range from 15.000 to 57.000 g/mol approximately resulting in a wide range of values for the degree of polymerization *N* and consequently in microphase separation near the order-disorder transition (ODT), the weak and the intermediate segregation limit. In this way, a comparison with other well-known similar systems with theoretically and experimentally confirmed phase diagrams was performed, such as the polystyrene-*b*-poly(isoprene) system. Observing and analyzing the morphological characterization results, it was possible to understand the mechanisms of self-assembly for this type of copolymers and gather information concerning their interaction parameter, which has not been estimated yet, and the ways that the molecular weight, the volume fraction and the conformational asymmetry influence their microphase separation. Most of the samples synthesized are of PS majority because it is difficult to increase significantly the molecular weight of the PCHD block as the second monomer due to undesirable side and termination reactions that occur, leading to homopolymerization of cyclohexadiene and increased molecular weight distributions.

For the other type of samples, five (5) copolymers with complex architectures were synthesized. The synthesis of one (1) linear triblock copolymer, one (1) linear pentablock copolymer, one (1) H-type and two (2) super H-type copolymers is presented in this research, by using the difunctional initiator sodium/naphthalenide and well established chlorosilane chemistry. The use of this difunctional initiatior involved highly purified reagents and challenging procedures, while the final materials were received after several weeks or months (1,5-2) depending on the linking agent used and the targeted molecular weights. The main purpose was to successfully synthesize the difunctional middle block, exhibiting low molecular weight distribution and predictable molecular weight. Furthermore, the linking reaction with the corresponding linking agent was of a great importance, in order to synthesize precursors with suitable number of Cl atoms, as well as the final linking reaction with the corresponding living arms for the synthesis of the final copolymer. The synthesis of copolymers bearing PS as the backbone and PCHD or PS-b-PCHD as living arms, has never

been reported in the literature, therefore, their successful synthesis provided information concerning their molecular properties rising from the complex architectures. A schematic representation of the complex architectures synthesized in this thesis is observed in Figure 1.1.

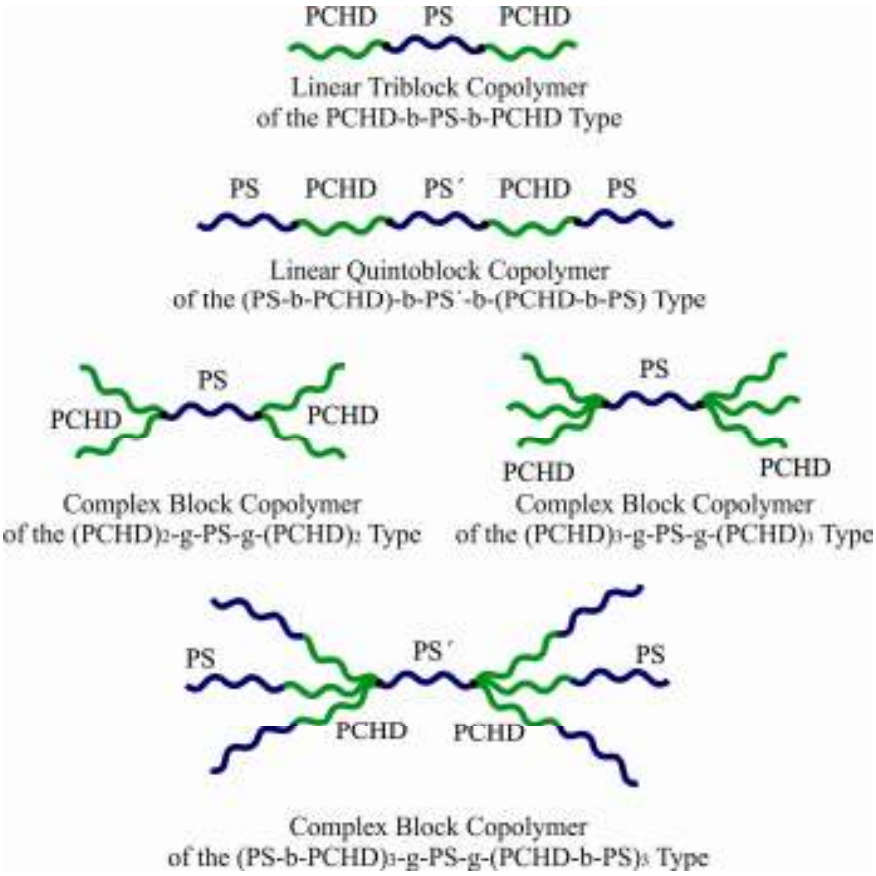

Figure 1.1: *Schematic of the complex architectures synthesized in this thesis.*

The complete synthesis of all samples was accomplished by using anionic polymerization and high vacuum techniques. The molecular characterization of the samples was performed via size exclusion chromatography (SEC), in order to confirm the molecular weight distribution, and membrane osmometry (MO) in order to confirm the $\overline{M}_n$ values. Also ^{1}H-nuclear magnetic resonance spectroscopy (^{1}H-NMR) was adopted to verify the type of microstructure for the polydiene as well as to identify the composition of each segment in the copolymers. Thermal analysis via differential scanning calorimetry (DSC) was also performed in order to examine the variations of the glass transition temperature and its dependence from the molecular weight and the weight fraction of each segment. Morphological characterization via transmission electron microscopy (TEM) and small angle X-ray scattering (SAXS) was performed only for the linear diblock copolymers in order to verify their microphase separation and to provide significant information concerning the different morphologies which are observed.

1.2 Overview

Chapter 2 provides information concerning the fundamentals of anionic polymerization synthesis and the basic principles of scientific glassblowing. Furthermore, information for the already reported cases of the polymerization of 1,3-cyclohexadiene and its copolymerization with other well studied monomers such as styrene, isoprene and butadiene are provided, as well as, information concerning the synthetic routes for linear diblocks and complex architecture copolymers already established.

In Chapter 3, information concerning the physical properties of block copolymers and their microphase separation is given.

Chapter 4 describes the basic theory and instrumentation used for the molecular characterization and the thermal analysis of the synthesized samples [Size exclusion chromatography (SEC), membrane osmometry (MO), proton nuclear magnetic resonance (^{1}H-NMR) spectroscopy, differential scanning calorimetry (DSC)].

Chapter 5 details the theory and instrumentation for the morphological characterization of the synthesized samples [transmission electron microscopy (TEM), small angle X-ray scattering (SAXS)]. Tailored procedures, especially for the preparation of the segments for TEM measurements, are exhibited.

In Chapter 6, the experimental procedures adopted for the synthesis of the linear diblock as well as for the complex architecture copolymers are provided as well as detailed description of the purification procedures in order to minimize the traces from the unwanted reagents.

In Chapter 7, the thermal analysis and the molecular and morphological characterization results of the synthesized samples are presented. Thorough investigation and discussion of the results is performed in order to conclude on the observed morphologies for the synthesized linear diblock copolymers.

CHAPTER 2

Anionic Polymerization

2.1 Basic Concepts

Anionic polymerization[4-5] is the most well-known and most studied technique for synthesizing well-defined polymers with controlled characteristics. Its main advantage, as compared to radical and cationic polymerization, is the absolute control of the termination step. For that reason, anionic polymerization is also described as living polymerization. This concept indicates that the macromolecular living ends can be used further for polymerizing additional monomer or for reacting with a suitable linking reagent in order to modify them. It is clearly understood, therefore, that through anionic polymerization, architecture, composition, molecular weight and molecular weight distribution can be easily controlled.

In each polymerization of vinyl monomers (anionic, cationic or radical) there are three steps: initiation, propagation and termination. According to the above mentioned criteria, in anionic polymerization only two steps exist as exhibited in Scheme 2.1:

Initiation

$$Bu^-Li^+ + CH_2{=}CH\Psi \longrightarrow BuCH_2CH\Psi^-Li^+$$

Propagation

$$BuCH_2CH\Psi^-Li^+ + nCH_2{=}CH\Psi \longrightarrow Bu(CH_2CH\Psi)_nCH_2CH\Psi^-Li^+$$

Scheme 2.1: *Initiation and propagation of living anionic polymerization.*

Free radical polymerization, though, is considered to be the most common technique from the industrial point of view since most industrial polymers are synthesized by this procedure. Nevertheless, these polymers do not exhibit predictable molecular characteristics and narrow distributions (over 1.5). Furthermore, in radical polymerization various chemical reagents which lead to free radicals are used as initiators, as well as heat and/or light. Another important difference between anionic and radical polymerization is that in the latter uncontrolled termination reactions occur through redistribution or conjunction between macromolecular radicals.

A very significant issue which limits the use of anionic polymerization in industry and large scale applications is that the macroinitiator and the macroanions, due to their reactivity, are very sensitive in oxygen, humidity and carbon dioxide traces. The reactions that occur and describe this drawback are shown in Scheme 2.2. Consequently, it is of great importance that all reactions must occur in the absence of atmospheric air and reagents (initiators, monomers, solvents etc.) must exhibit high purity (> 99.9%). For that reason all

reactions occur under high vacuum conditions (10^{-6} - 10^{-7} mmHg) in purified and suitably modified glass vessels.

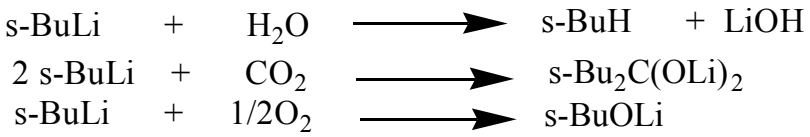

Scheme 2.2: *Termination reactions occurring for an anionic polymerization initiator with water, oxygen and carbon dioxide.*

The greatest advantage of anionic polymerization is that it can proceed up to 100% yield. Practically, this means that the polymerization reaction will be completed when all the monomer quantity has reacted during the propagation reactions. As a result, the molecular weight of the final polymer can be easily estimated by the quantities of the monomer and initiator, using the following equation:

$$\overline{M}_n = \frac{gr_{monomer}}{moles_{initiator}} \qquad (2.1)$$

One very important feature of the polymers synthesized with anionic polymerization technique is the narrow molecular weight distribution (< 1.1) which ensures the compositional and molecular homogeneity. Low polydispersities are secured by the proper choice of the solvent, monomer and initiator system in which it is crucial that the rate of the initiation reaction must be higher than the rate of the propagation step. When these conditions apply, polymerization of the monomer units starts simultaneously and almost identical numbers, of monomer units are added to each chain, until they are consumed.

In non-polar solvents the initiation rate depends on the organometallic initiator used and on the solvent composition (aliphatic or aromatic). Usually organolithium reagents are used which form aggregates in hydrocarbon solvents, polar and non-polar. The lower the aggregation rate of the initiator, the higher will be the reactivity. The organolithium initiator structure affects its aggregation rate in each solvent. Consequently, organolithium initiators normally form hexameric aggregates in hydrocarbon solvents, while those which are branched on α- or β- carbon form quatermeric aggregates. Below, the reactivity sequence of organolithium initiators for diene polymerization in hydrocarbon solvents is demonstrated whereas in parenthesis the aggregation number is shown:

Methyllithium (2) > secondary butyllithium (sec-BuLi) (4) > isopropyllithium (i-PrLi) (4-6) > tertiary butyllithium (tert-BuLi) (4) > normal butyllithium (n-BuLi) (6)

For the styrene polymerization in hydrocarbon solvents the same sequence is applied except from a change that occurs between the two last organolithium initiators (n-BuLi > tert-BuLi). The main parameters which decrease the aggregation rate are the following:

a) The concentration reduction.
b) The temperature increase.
c) The use of relatively strong solvating media (aromatic hydrocarbon solvents are stronger than aliphatic ones).

During the propagation step the negatively charged polymer chains with the lithium cation can also aggregate. The aggregation degree for (polystyryl)lithium (PS^-Li^+) in aromatic and aliphatic hydrocarbon solvents has been calculated to be equal with 2. Furthermore, the aggregation degree for (polybutadienyl)lithium (PB^-Li^+) in hydrocarbon solvents is 4-6 and for (polyisoprenyl)lithium 3-4 respectively.

Nevertheless, it has been observed that the aggregation degree of initiators and polymer chains is decreased in polar environments. It has been estimated through kinetic studies that the aggregation rate of (polystyryl)lithium in tetrahydrofuran (THF) is decreased from 2 to 1 while for (polybutadienyl)lithium and (polyisoprenyl)lithium the relative value is decreased to 2. Such behaviour occurs since a minor quantity of the polar reagent can shift the equilibrium between the aggregated and non-aggregated polymer chains towards the non-aggregated ionic pairs (PS^-Li^+). All forms of ionic pairs for polystyrene (PS) segments can be seen in Figure 2.1.

$$(PS^-Li^+)_2 \leftrightarrow 2(PS^-Li^+) \leftrightarrow PS^-, Li^+ \leftrightarrow PS^- // Li^+ \leftrightarrow PS^- + Li^+$$

Aggregated ionic pairs | **Non-aggregated ionic pairs** | **In contact ionic pairs** | **In distance ionic pairs** | **Free ions**

Figure 2.1: *Forms of aggregated and non-aggregated ionic pairs of (polystyryl)lithium in the presence of polar reagents.*

Each one of these ionic pairs can be considered as a living centre and can lead to polymerization. Such free ions are extremely functional and can significantly increase the propagation rate even in lower concentrations. In the presence of polar reagents, an increase in the free ions' concentration is observed leading to a relative increase in the propagation rate.

Monomers subject to anionic polymerization are those which can create stable anionic centres under certain polymerization conditions. A variety of monomers has been polymerized through this method such as styrenic (e.g. a-methylstyrene, para-methylstyrene)[6-10], dienes (e.g. isoprene[11], butadiene[12], 2-methyl-1,3-pentadiene[13,14], 1,3-cyclohexadiene)[15,16], methacrylic esters (e.g. methyl methacrylate)[17] and cyclic monomers(e.g. ethylene oxide[18], hexamethylcyclotrisiloxane)[19].

2.2 Scientific Glassblowing

2.2.1 General Information

Scientific glassblowing[20] is the process of creating pyrex glass apparatuses and glassware systems used in research and production. Many chemical, medical, pharmaceutical and engineering laboratories use scientific glassware extensively. Especially, in polymer science and in anionic polymerization synthesis, scientific glassblowing is one of the most basic skills that a scientist has to develop in order to respond to the requirements of this method. Scientific glassblowing is performed by using a torch or burner so as to heat, form and seal glass tubes, rods and preformed components into glass apparatuses. The type of glass most commonly used in a laboratory is the borosilicate glass. It is a heat-resistant glass which contains approximately 5% boric oxide. In addition to outstanding resistance in heat and thermal shocks, borosilicate glasses are known for their chemical durability and low coefficients of thermal expansion. Trade names one may be familiar with are PYREX (Dow Corning), KIMAX (Kimple) and DURAN (Schott). In scientific glassblowing the glass comes usually in tubing or rod forms with varying diameters, depending on the required needs.

2.2.2 Glass Strain and Annealing

Scientific glassblowers fabricate simple to complex apparatuses which are used under laboratory conditions. Standard usage of these apparatuses can involve harsh chemical exposure, high and/or low pressures and a variety of other hostile environments. An awareness of product design is essential as well as the integrity of the glass structure by itself. A critical product safety element is the fabrication of strain or stress-free glass apparatuses and systems.

In order to fabricate the glassware, a torch or burner is used. The flame is adjusted to varying degrees of sharpness ranging from a pinpoint for precision work, to large “bushy” flame used for heating and forming broad areas. This process of heating, forming and cooling will introduce strain, often referred to as stress, into the glassware. Invisible most of the times to the naked eye, the strain is nevertheless present and is a potential point of failure in the glass apparatus unless relieved. The degree of stress will be determined by a number of factors including the intensity and size of the torch flame, glass wall thickness and the complexity of the seal itself. The severity of stress may be enough to cause glass failure, sometimes while the glass piece is under construction. It is therefore recommended to hand-anneal the work during the fabrication process, with full furnace annealing at the end prior to the usage of the apparatus or system.

Some glassblowers use a device called polariscope to help detect the presence of glass strain. By looking through two polarized filters held in varying orientation, one can

visualize the stress patterns in a piece of glass (Figure 2.2). Relieving stresses in the glass can be performed by hand annealing, which is a process of using a torch flame of diminishing intensity and size over time, slowly and evenly allowing the glass to return to room temperature. An alternative solution is to use a glass annealing furnace which can be programmed to allow pre-determined ramps up to the annealing temperature and then back down to room temperature.

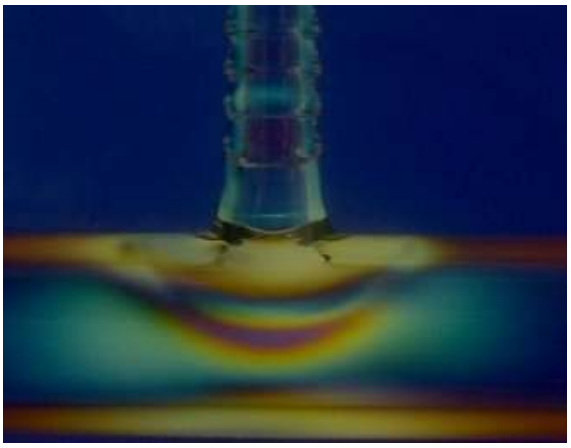

Figure 2.2: *Stress patterns in a piece of glass.*

2.2.3 Glass Blowing Tools

Torches: Torches are most commonly used in glassware fabrication for anionic polymerization procedures than burners. The gases normally used for working with borosilicate glasses are propane or natural gas mixed with oxygen. A typical glassblowing torch can be seen in the following Figure (Figure 2.3).

Figure 2.3: *A glassblowing hand torch. The red valve adjusts gas and the green oxygen.*

They are usually small and light in order to handle them easily. This kind of torch uses a chamber within its body to mix propane/oxygen and it is the most popular type. The

experience gained by time in handling properly the torch and using the appropriate flame is very important for making easier all glassblower's tasks.

Callipers: Callipers are used by glassblowers to measure outer diameters, inner diameters, wall thickness and other dimensions of the glassware. Vernier callipers and electronic callipers are two of the most widely used types of callipers used (Figure 2.4). Electronic callipers are relatively expensive compared to the standard vernier style but they are not as tolerant to heat and chemical exposure. However, they are quite accurate and easier to read.

Figure 2.4: *Vernier (up) and electronic (down) callipers.*

Basic Hand Tools: Glassblowers use a wide assortment of standard and custom-made hand tools and equipment in the fabrication of glass apparatuses. The following examples are representative and very commonly used.

- The glassblowing process produces visible and UV light transmissions that are harmful to the eyes. Didymium lenses have been used for years by scientific glassblowers, offering protection from glass shards and providing sodium light filtration (Figure 2.5).

Figure 2.5: *Various types of didymium lenses for glassblowing.*

- The blowhose and the attachments shown in Figure 2.6 are what glassblowers use to blow air into the glassware. On the left of the image is a latex tube (blowhose) with a mouthpiece at one end and a swivel at the other. The swivel is a device that serves as a transition piece between the blowhose and the glass. The swivel allows glass

rotation without any twisting and kinking of the flexible blowhose tubing. Latex or rubber tubes and rubber stoppers of assorted sizes are used to connect to the glass.

- Graphite tools are used extensively in glassworking because they can withstand high temperature exposures and are easy to machine and form into custom shapes. Depending on their shape, they can be used in forming glass bottoms on glassware, in reducing outer diameters of tubes or to enlarge a hole blown in a tube.

Figure 2.6: *Blowhose, swivels and rubber tubes for glassblowing.*

- In the following picture (Figure 2.7), some useful additional tools can be seen. From left to right, two strikers or flint lighters can be seen which are used to light the torch or burner.

Figure 2.7: *Additional tools for glassblowing.*

Nowadays the use of a simple lighter is more common. Tweezers can be used also to pull or hold hot glass or tools. The next two tools are tungsten carbide glass knives or scorers that are used to scratch glass surfaces when cutting tubes or rods. The tungsten pick on the right is used to move small amounts of heated glass in order to help close small openings

found during glass repair or fabrication. The scalloped piece of wood is normally used as a rest for placing glass (hot or cold) components used during the fabrication.

2.3 Vinyl Monomers with Double C-C Bonds (Dienes)

Dienes are a significant class of chemical compounds as they exhibit very interesting physical and chemical properties when polymerized. Poly(isoprene) (PI) and poly(butadiene) (PB) were the first polydienes synthesized and studied extensively for their properties. They belong to the category of elastomers, which are viscoelastic polymers generally having noticeably low Young's modulus and high yield strain compared to other polymers. Elastomers are usually thermosets (requiring vulcanization) or thermoplastic. Thermosets are vulcanized polymers (chemically forming networks between polymer chains in the presence of other atoms i.e. sulfur) having the ability to reconfigure themselves in order to distribute an applied external stress. The covalent cross-links ensure that the elastomer will return to its original configuration when the stress is removed. As a result of this extreme flexibility elastomers can reversibly extend from 5-700%, depending on the specific material. Without the cross-links or with short, not easily reconfigured chains, the applied stress would result in a permanent deformation. Thermoset elastomers have also low melt temperatures (T_m) and glass transition temperatures (T_g). Specifically, 1,4-poly(butadiene) exhibits $T_m = 6^0C$ and very low T_g = -85 to -90^0C, while cis-1,4 poly(isoprene) has $T_m = 35^0C$ and $T_g = -67^0C$[21]. These two dienic polymers are widely employed in laboratory and industrial scale in a variety of applications such as automobile tires, water proof membranes etc. Over the last two decades scientists focused their interest to other polydienes also, such as poly(2-methyl-1,3-pentadiene) which through hydrogenation is converted (up to >99%) to polypropylene, exhibiting an almost perfect atactic structure with various architectures as well as unique thermal and mechanical properties[13]. This interesting polydiene exhibits high 1,4-microstructure (~99%) when polymerized via alkyllithium initiators (e.g. sec-BuLi) and in hydrocarbon solvents (e.g cyclohexane) and also exhibits higher glass transition temperature than the polydienes previously mentioned ($T_g = 4^0C$).[14]

2.4 Homopolymers and Copolymers of 1,3-Cyclohexadiene

Another diene that has been successfully polymerized is 1,3-cyclohexadiene (1,3-CHD), leading to poly(cyclohexadiene) with various percentages of 1,2 and 1,4 microstructure (Scheme 2.3) depending on the method of polymerization used, the solvent, the initiator and the presence or not of polar additives.

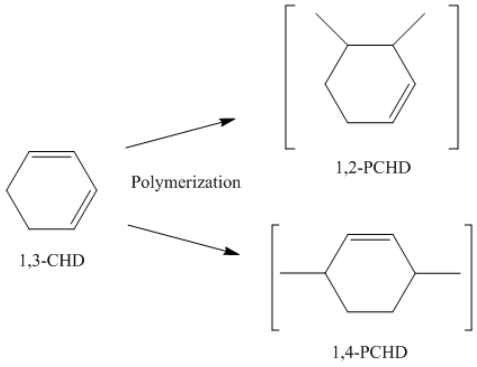

Scheme 2.3: *Polymerization of 1,3-CHD leading to PCHD with 1,2- or 1,4-microstructure.*

Poly(cyclohexadiene) can exhibit very interesting and different, from other polydienes, properties such as increased thermal and chemical stability as well as improved mechanical properties[2,3] due to its alicyclic rings in the main chain. The use of poly(cyclohexadiene) has been reported in ion-exchange resins, photo resistance films and in low density plastics for underwater applications[22-24].

The first attempts of polymerizing 1,3-cyclohexadiene were performed via radical polymerization using various initiators[25-27] but in all cases the results were not encouraging since either oligomers were synthesised with very low yield or no polymer at all. Via radical polymerization, though, 1,3-cyclohexadiene substituted in carbons 5 and/or 6 was polymerized leading to polymers with high molecular weights, high yields (~90%) and with 1,4-microstructure (~85-90%)[28,29]. These polymers were chemically modified to poly(paraphenylene) or PPP.

Better results for the polymerization of 1,3-cyclohexadiene have been reported by using transition metals catalysts or Ziegler-Natta catalysts[30-34]. The most effective report lies upon the polymerization of 1,3-cyclohexadiene, substituted in carbon 5 and/or 6, with nickel catalyst leading to 100% 1,4-poly(cyclohexadiene), which was then chemically modified to PPP[35]. Also, via Ziegler-Natta catalysts, cyclohexadiene polymers were synthesized (80-90% yield) with 1,4-microstructure but relatively low molecular weights[36]. Additionally, cationic polymerization was adopted leading to similar results[37].

Anionic polymerization of 1,3-cyclohexadiene also displays several problems due to transfer and termination reactions that occur during the polymerization (Scheme 2.4)[38].

a)

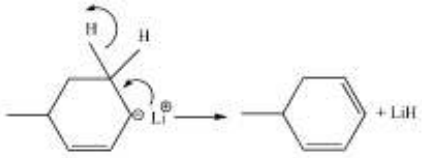

b)

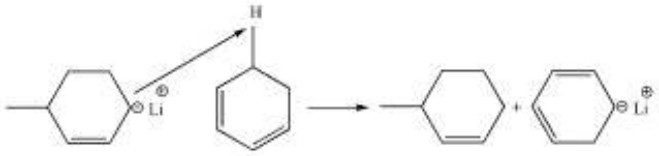

c)

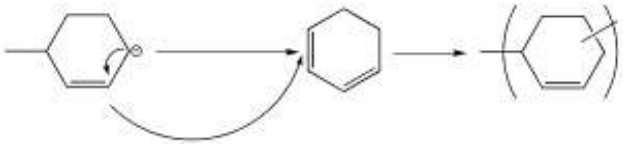

Scheme 2.4: *Termination and transfer reactions during the polymerization of 1,3-cyclohexadiene.*

One main side reaction during the chain propagation is chain termination via hydride abstraction. During the propagation of the polymerization and the creation of more polymer chains, lithium is converted into LiH by reacting with one of the hydrogen atoms of the six-member ring resulting in the termination of the polymerization (Scheme 2.4a). Another main side reaction that leads to high distributions is chain transfer through proton elimination (Scheme 2.4b). This occurs during the reaction of the monomer hydrogen as indicated in the Scheme, with the chain lithium resulting in the termination of the living anion and the creation of a new much smaller reactive anion. Finally, during chain propagation, is not possible to control the 1,2- or 1,4-addition resulting in undesirable ratios of microstructure (Scheme 2.4c).

Several studies have been reported in which anionic polymerization was adopted for 1,3-cyclohexadiene, leading to much better results than the previous mentioned methods of polymerization, such as higher molecular weights and yields.

The polymerization of 1,3-cyclohexadiene is reported using alkyllithium initiator (n-BuLi) in hydrocarbon solvents leading to high yields of 100% amorphous soluble poly(cyclohexadiene) with increased percentage of 1,4-microstructure[39]. Also, polymerizations in THF using various initiators such as n-BuLi, sodium naphthalene, lithium naphthalene and potassium naphthalene were performed leading to polymers with both 1,4 and 1,2 microstructures. However, the formation of undesirable products such as benzene, cyclohexene and 1,4-cyclohexadiene was observed due to termination and transfer reactions. Furthermore, 1,4-cyclohexadiene is not polymerized but it decreases the molecular weight and the yield of the polymerization of 1,3-cyclohexadiene[40]. By lowering the temperature in

both hydrocarbon solvents and THF, the decrease of these termination and transfer reactions was accomplished leading to higher molecular weights and yields.

Francois and co-workers were the first that studied extensively the polymerization of 1,3-cyclohexadiene. They estimated that the aggregation degree of (polycyclohexadienyl)lithium in cyclohexane is 2[41], in agreement with Young's[42] results who estimated this value to be approximately 1,7 in hydrocarbon solvents. Francois and co-workers reported that (polystyryl)lithium can inititate the polymerization of 1,3-cyclohexadiene, but the synthesis of PS-b-PCHD diblock copolymers is performed simultaneously with the formation of side products such as benzene, 1,4-cyclohexadiene and homopolymer of poly(cyclohexadiene). The formation of the homopolymer was inevitable especially in high concentrations of 1,3-cyclohexadiene. These termination and transfer reactions were minimized by lowering the polymerization temperature from 20^0C to 5^0C or even as low as -10^0C resulting in the relative decrease of the formation of PCHD homopolymer. These diblock copolymers of the PS-b-PCHD type were dehydrogenated leading to diblock copolymers of the PS-b-PPP type[43]. In all these previous mentioned cases of anionic polymerization of 1,3-cyclohexadiene, termination and transfer reactions were not eliminated resulting in not well-defined polymers with molecular weights only up to 20,000 g/mol and broad molecular weight distributions.

Natori and co-workers reported the successful living anionic polymerization of 1,3-cyclohexadiene in 1997[15]. Termination and transfer reactions were eliminated, by using the polar additive N, N, N′,N′-tetramethylethylenediamine (TMEDA) with n-BuLi as initiator in a molar ratio $n_{TMEDA}/n_{n\text{-}BuLi}$= 5/4, leading to a significant increase of the initiation rate. PCHD homopolymers were synthesized following this procedure with well-defined molecular weights, narrow molecular weight distribution and linear increase of the molecular weight in terms of the yield. By adding styrene in (polycyclohexadienyl)lithium living ends, the synthesis of a diblock copolymer of the PCHD-b-PS type is reported with well-defined composition and narrow molecular weight distributions. The absence of polystyrene or poly(cyclohexadiene) homopolymer proved that the termination and transfer reactions were eliminated at a significant degree. The addition of the polar additive TMEDA led to the raise of the 1,2-microstructure which was estimated by Natori et al. to be approximately to 54%[44]. Using this method, Natori et al. synthesized random copolymers of styrene, butadiene or isoprene with 1,3-cyclohexadiene as well as triblock copolymers of the ABA type of styrene or butadiene with 1,3-cyclohexadiene (PCHD-b-PS-b-PCHD and PCHD-b-PB-b-PCHD). Natori et al. found that the glass transition temperature of PCHD is increased when higher percentages of 1,2-microstructure are observed when compared to 1,4-microstructure, while identical behavior was observed also during higher values of the number average molecular weight. Furthermore, it was verified that the 1,2-microstructure in the polymer chain leads to

better stretch strain and thermal stability[3] than the 1,4-microstructure. Also, the PCHD-b-PB-b-PCHD series of samples were hydrogenated into their derivative copolymers of poly(cyclohexene-ethylene/butylene-cyclohexene) (PCHE-b-PEB-b-PCHE)[2]. Natori et al. showed that both mechanical strength and heat-resistant temperature tended to increase with an increase of 1,3-cyclohexadiene/butadiene ratio. Also, the heat resistance of hydrogenated block copolymers was found to be higher than that of the unhydrogenated samples. However, the mechanical strength was lower than those of the unhydrogenated block copolymers with the same ratio of CHD to butadiene. The n-BuLi/TMEDA system was also used successfully in synthesizing poly(cyclohexadiene) stars by reacting with the difunctional reagent divinylbenzene (DVB)[45]. The difunctional initiator bis-(1-phenylethylene) benzene (PEB) was also used with TMEDA for the synthesis of miktoarm star terpolymers of styrene, isoprene and 1,3-cyclohexadiene by applying a "seeding" technique with small amount of (polyisoprenyl)lithium as a capping reagent[46]

Another polar additive, 1,4-diazabicyclo[2,2,2]octane (DABCO), was used with sec-BuLi, in a molar ratio $n_{DABCO}/n_{sec\text{-}BuLi}$ = 2/1, for the polymerization of 1,3-cyclohexadiene by Hong and Mays[16]. The poly(cyclohexadienes) synthesized displayed controlled molecular weights and smaller molecular weight distributions than the n-BuLi/TMEDA system, while the microstructure was approximately 93% 1,4. Using this initiation system, at 20^0C, the same authors synthesized diblock copolymers of polystyrene and 1,4-poly(cyclohexadiene) polymerizing either styrene or cyclohexadiene first (PS-b-PCHD or PCHD-b-PS). These materials exhibited polydispersities less than 1.1 when the targeted molecular weights were lower than 20 kg/mol and the compositions of PCHD lower than 30 wt %[47]. By using trichloromethylsilane, PCHD stars with three arms [$(PCHD)_3$] as well as star block copolymers containing PS and PCHD [$(PCHD\text{-}b\text{-}PS)_3$ and $(PS\text{-}b\text{-}PCHD)_3$] were synthesized as well[48]. Under careful experimental conditions, fractionation with solvent/non-solvent mixtures was possible leading to near-monodisperse materials. Miktoarm stars copolymers with one poly(cyclohexadiene) arm and two or three poly(butadiene) arms were also prepared using the same system and were transformed to the corresponding miktoarm stars of PCHE and PE by complete hydrogenation[49]. A series of linear block co-, ter- and quaterpolymers of 1,3-cyclohexadiene with styrene, isoprene and butadiene were synthesized successfully using either the TMEDA/n-BuLi or the DABCO/sec-BuLi initiation system by Hadjichristidis and Mays groups. In order to minimize side reactions, they polymerized CHD in ~5^0C when using the DABCO/secBuLi system. The combined results from the molecular characterization indicated a high degree of molecular and compositional homogeneity[50]. The synthesis of a miktoarm star terpolymer of 1,3-cyclohexadiene, styrene and 2-vinylpyridine is reported also using the difunctional initiator 1,4-bis-(1-phenylethylene)benzene (1,4-PEB) and the sec-BuLi/DABCO initiation system[51]. Further studies report the fluorination of

poly(cyclohexadiene) homopolymers synthesized with both TMEDA/n-BuLi and DABCO/sec-BuLi systems via thermolysis of hexafluoropropylene oxide (HFPO) which generates difluorocarbenes ($:CF_2$). The results indicated that the optimum fluorination is achieved, when the concentration of HFPO was 40g/L and the average fluorination time was 4-6 hours while the T_g as well as the T_{decomp} of the homopolymers increased with an increase of the fluorination degree[52].

2.5 Chemical Modifications of Poly(cyclohexadiene)

Poly(cyclohexadiene) is considered a very interesting polymer since it can lead to the synthesis of two other significant polymers. By hydrogenation it is possible to transform it into poly(cyclohexylene) or poly(cyclohexane) (PCHE), which consists of six-member rings of cyclohexane directly connected in the main chain. Dehydrogenation of PCHD can lead to the formation of poly(phenylene) (PPh), which consists of aromatic rings directly connected in the main chain (Figure 2.5). PCHE exhibits a high glass transition temperature (T_g = 231^0C), which is among the highest from all hydrocarbon polymers[3]. Furthermore, it displays other excellent properties such as low specific gravity (1,03 for PCHD and 0,99 for PCHE), low dielectric constant (ε_{PCHD} = 2.5, ε_{PCHE} = 2.3), low water absorption (< 0.01%), high heat resistance, high transparency (92% for PCHD and 91% for PCHE), high flexural modulus (4.0 GPa for PCHD and 6.1 GPa for PCHE), high UV resistance and similar refractive index with glass (SiO_2)[1]. Dehydrogenation of PCHD with high 1,4-microstructure leads to the formation of poly(paraphenylene) (PPP), which is a polymer with high thermal stability (T_{dec} ~ 660^0C) and very low friction coefficient. Also PPP can be doped with AsF_5 becoming a highly conductive polymer (conductivity as high as 500 S/m) leading to the use as an active material and as an electrode of polymer batteries[54-64].

Williamson and co-workers synthesized a series of poly(cyclohexadiene-*alt*-styrene)-*block*-polystyrene copolymers using only sec-BuLi in cyclohexane as a solvent and chemically modified them with either hydrogenation or dehydrogenation in a controlled fashion[65]. The hydrogenated copolymers exhibited improved thermal stability as expected whereas the copolymers resulting from dehydrogenation, exhibited reduced thermal stability in both oxygen and nitrogen environments.

Mays and Hong synthesized several star-shaped, star-block-linear and hyperbranched poly(cyclohexadiene) polymers and copolymers with styrene through a convergent living anionic polymerization (CLAP) process by using (chlorodimethylsilyl)styrene, divinylbenzene and DABCO[66]. The star-shaped PCHDs were chemically modified by hydrogenation, dehydrogenation, fluorination and sulfonation in order to study the chemical and physical properties of these materials. Fluorination and hydrogenation were found to increase significantly the T_g as well as the decomposition temperature (T_{decomp}).

2.6 Block Copolymers

Block copolymers are polymers consisting of multiple sequences, or blocks, of the same monomer alternating in series with different monomer blocks[67]. The blocks are covalently bound to each other leading to diblock, triblock etc. copolymers, terpolymers etc. There are classifications based on the number of blocks they contain or how the blocks are arranged such as di-, tri- or multi-block copolymers depending on the block number or linear, star, hyperbranched etc. depending on the architecture. A block copolymer contains two or more blocks (group of polymer chains) attached at their ends. Linear block copolymers are comprised from two or more blocks in sequence, whereas, starblock copolymers are comprised from at least three linear block copolymers attached at a common branch point. In most cases, the different polymeric chains of block copolymers are thermodynamically incompatible giving rise to a variety of microstructures in bulk and in solution. Therefore, the microstructures are highly coupled to the chemical and physical characteristics of the molecules of each block and materials with applications ranging from thermoplastic elastomers and high-impact plastics to pressure-sensitive adhesives, additives, foams etc. can be created. For example, thermoplastic elastomers are block copolymers of a rubbery state (polyisoprene or polybutadiene) containing glassy hard domains (often polystyrene). This block copolymer behaves as a rubber at ambient conditions but can be thermally treated at relatively high temperatures due to the presence of the glassy domains that act like physical crosslinks. In addition, block copolymers are very good candidates for potential applications in advanced technologies such as information storage, drug delivery and photonic crystals.

Anionic polymerization is one well established technique for the synthesis of tailored block copolymers[68]. To prepare well-defined copolymers, the technique is demanding, requiring high purity reagents and the use of high vacuum procedures to prevent accidental termination due to the presence of impurities. Under appropriate experimental conditions[69,70], due to the absence of termination and chain transfer reactions, carbanions remain active after complete consumption of the monomer. Such behavior leads to the formation of block copolymers by introducing a second monomer into the polymerization mixture, which is the simplest case. The need of combining even more properties in block copolymer systems have directed recent advances in the synthesis of block copolymers with complex architectures, such as miktoarm stars[71-74], star block, H-shaped, super H-shaped[72], ring-shaped copolymers[75] etc.

2.6.1 Linear Diblock Copolymers (AB)

Linear diblock copolymers[76] are the simplest case of copolymerization where two blocks with different chemical structures are linked together via a common junction point. The most common method to synthesize diblock copolymers is sequential monomer addition,

where one of the two monomers polymerizes first and the second is added after complete polymerization of the first, allowing to polymerize through the living macroanions of the first block until its complete consumption. At this point a termination reagent is added and the diblock copolymer is precipitated in a non-solvent, dried and collected.

The most important parameters that must be fulfilled in order to achieve the synthesis of well-defined diblock copolymers are:

a) The macroanion of the first monomer must be a stronger nucleophile than the corresponding one obtained from the second monomer in order to be able to initiate its polymerization.
b) The initiation rate for the polymerization of the second monomer by the macroanions of the first monomer must be higher than the propagation rate during the polymerization of the second monomer. In this way, narrow molecular weight distribution is ensured as well as molecular homogeneity.
c) The purity of the second monomer must be equally high with that of the first monomer. Otherwise, macroanions of the first monomer can be partially terminated leading to the presence of homopolymer in the final material. Furthermore, there will be no control of the molecular weight as well as of the composition of the second monomer (and consequently of the final product) due to the decrease in the concentration of the active centers.

Taking into account all the above major parameters, a variety of AB diblock copolymers has been synthesized by sequential addition of monomers. The most widely studied diblock copolymers are those that consist of styrene and isoprene or butadiene[77,78]. The styrene anionic centers can initiate efficiently the polymerization of dienes in hydrocarbon solvents. Additionally, by using organolithium initiators, high percentage of 1,4-microstructure is achieved for the polydienes leading to copolymers with thermoelastomeric properties. Alternatively, copolymerization of dienes as the first block in hydrocarbon solvents with styrene as the second block is possible by adding a small amount of polar media (e.g THF) prior to the initiation of the polymerization of styrene. The presence of polar reagents alters the stereochemistry and the activity of the polydiene macroanions, enabling a fast initiation rate for the second monomer (styrene) and leading to diblock copolymers with predictable molecular weights and narrow molecular weight distributions[79]

The copolymerization of styrene with other dienes, such as 2-methyl-1,3-pentadiene, has also been investigated[13] leading to diblock copolymers with well defined molecular weights, narrow molecular weight distributions and compositional homogeneity. As it has been already mentioned, latest interest for dienes has been focused on the polymerization of 1,3-cyclohexadiene leading to several AB linear diblock copolymers of the PS-b-PCHD type or PCHD-b-PS type, with controlled molecular weights and molecular weight distributions

and almost complete elimination of side reactions by using polar additives (DABCO or TMEDA). The use of polar additives for the polymerization of cyclohexadiene changes the stereochemistry and enables a fast initiation rate for styrene leading to controlled polymerization conditions, when styrene is used as the second monomer.

The synthesis of diblock copolymers containing styrene/styrenic monomers or dienes (isoprene,butadiene) and (meth)acrylic monomers has been reported in the literature[79]. These diblocks are synthesized by polymerizing first the styrenic monomer or the diene and then the (meth)acrylic monomer. Polymerization of (meth)acrylic monomers requires low polymerization temperatures (-78^{0}C), polar solvents (usually THF)[80] and relatively less active and more sterically hindered initiators in order to avoid side reactions of carboanions with the active carbonyl group. For this reason, a non homopolymerizable reagent such as 1,1-DPE (1,1-diphenylethylene) is usually used together with additives like LiCl, enhancing the control of the polymerization of (meth)acrylic monomers even in higher temperatures (e.g. -30^{0}C)[81].

A large number of linear diblock copolymers containing only (meth)acrylic monomers have been also synthesized due to the fact that there is a variety of different side groups in this type of monomers [e.g poly(methylmethacrylate-b-poly(tert-butyl acrylate)][82]. Depending on the desired properties, one can choose the suitable side groups on the monomers that will be used for the copolymerization[83-85].

Linear diblock copolymers containing 2- or 4- vinylpyridine and styrenic or dienic blocks have also been synthesized in low temperatures and polar solvents in order to avoid the attack of the anionic centers on the nitrogen atom at the pyridine ring of each monomeric unit, therefore avoiding quaternization[86,87]. Also, the nitrogen atom provides lower reactivity to the monomer; therefore, the vinylpyridine monomers are added always second and the propagation rate is rather fast. Furthermore, the ability to synthesize polyelectrolyte blocks gives this kind of copolymer interesting properties and potential applications.

The synthesis of diblock copolymers of styrene and ethylene oxide has also been reported in the literature using initiators with Na or K counteriors[88,89]. These materials present unique properties due to the solubility of poly(ethylene oxide) in water and its ability to crystallize. The C-O-Na or C-O-K centers have lower reactivity resulting always in the use of ethylene oxide as the second monomer. Under appropriate conditions such as polar solvents and polymerization temperatures above room temperature (~40^{0}C to 45^{0}C), propagation of ethylene oxide proceeds rather slowly compared to initiation. Nevertheless, diblock copolymers with no traces of homopolymer from the first block and narrow molecular weight distributions can be prepared. Furthermore, a synthetic procedure involving Li reagents initiated in the presence of strong phosphazene bases such as $tBuP_4$ has been reported[90] for the synthesis of well-defined diblock copolymers containing styrene or dienes and ethylene oxide.

Another class of significant diblock copolymers is those containing siloxane monomers and especially hexamethylcyclotrisiloxane. For the last few decades, siloxane containing polymers are widely used in numerous applications leading to advanced research on these materials as well as to their increased production. Anionic polymerization of cyclosiloxanes has been investigated in synthesizing diblock copolymers with styrene or dienes as the first block[91]. Initiators containing Li as the counterion have been used as long as the purity of the siloxane monomer is high enough and the back biting reactions have been minimized by using low polymerization temperatures (-20^0C)[19].

2.6.2 Linear Symmetric Triblock Copolymers Containing Two Different Monomers (ABA)

Triblock copolymers, meaning polymers consisting of three block sequences of monomers, provide a variety of different architectures since they can be comprised of either two monomers (ABA type copolymers) or three (ABC type terpolymers). The case of ABA triblock copolymers will be investigated. Linear symmetric triblock copolymers, containing two different monomers arranged in such a manner where the first and the third block (outer blocks) exhibit the same chemical nature and molecular weight while the second (middle) block is of different chemical nature, can be synthesized by employing three procedures: a) sequential addition of monomers, b) coupling of the living AB chains and c) use of a difunctional initiator.

Sequential Monomer Addition: In this procedure, the first monomer is polymerized followed by the polymerization of the second by simply adding the appropriate amount. After complete consumption, an equal amount of the first monomer is added to the mixture resulting in the synthesis of an ABA triblock copolymer[78]. This technique provides a relatively easy way of synthesizing symmetric triblock copolymers but the sequential addition of the monomers can result in partial termination of the growing chains leading to the presence of undesirable homopolymer A and/or diblock AB in the final product. Furthermore, it is possible that the amount of the monomer used in steps one and three will be different, resulting in outer blocks with different molecular characteristics (not perfectly symmetric). Additionally, the reactivity of each monomer must be investigated and its ability to initiate the polymerization of the other one and vice versa. This procedure cannot be applied in the case when the outer block is a polydiene, since the second addition results in different ratios for the microstructures.

Coupling of Living AB Chains: In this technique, a living diblock copolymer of the AB type is synthesized via sequential addition of monomers, having the same composition but half the molecular weight of the final triblock copolymer. After this step, an appropriate coupling agent is used, usually dichlorodimethylsilane, having two functional groups (Cl in this case)

which can react with the living Li counteranions forming covalent bonds, resulting in the formation of a symmetric triblock ABA copolymer. The advantage of this method is the formation of an exact symmetric triblock copolymer with identical molecular characteristics for the outer A blocks as well as the two step (instead of three) polymerization procedure. On the contrary, this technique is more time consuming since the coupling of the living chains lasts more. Furthermore, caution should be given on the stoichiometry of the coupling reaction. For that reason, an excess of living anions is used to ensure that both groups (Cl) of the coupling agent have reacted completely. Additionally fractionation of the final product is needed in order to separate the undesirable products of the coupling reaction (unwanted diblock of the AB type from the wanted ABA triblock copolymer).

Use of Difunctional Initiator: In this methodology, the symmetric triblock copolymer is formed by using a difunctional initiator, i.e. an organometallic compound exhibiting two anionic sites able to initiate polymerization in a two-step addition of monomers. The middle block (B) is synthesized first followed by the polymerization of the second monomer (A). This technique will be investigated more since it is the one that has been used for the synthesis of the copolymers with the complex architectures of this thesis described in a following chapter. The polymerization in polar as well as in non-polar solvents has been reported[92-97] in the literature for this technique. The most important issue in this method is the quality of the initiator and its ability to lead in pure difunctional polymer. The chemical structure of the initiator, the solvent and the chemical nature of the monomer used play significant role in this approach. If the difunctional initiator cannot form pure difunctional polymers, the final product will be a mixture of homopolymer, diblock and triblock copolymer.

Well-defined symmetric linear triblock copolymers, with poly(butadiene) or poly(isoprene) as the middle block and polystyrene as the outer (SBS and SIS respectively), have been synthesized in hydrocarbon solvents using a difunctional initiator derived from 1,3-bis(1-phenylethenyl)benzene (1,3-PEB) and Li compounds, which is a well-studied and widely used type of difunctional initiators (DLi's)[94,95,98].

Furthermore, a series of triblock copolymers with poly(butadiene) as the middle block and methacrylic outer blocks, have been successfully synthesized by using difunctional initiators based on the biadduct of tert-butyllithium (t-BuLi) to either 1,3-bis(1-phenylethenyl)benzene or m-diisopropenylbenzene (m-DIB)[99-102].

Triblock copolymers with poly(isoprene) as the middle block and poly(cyclohexadiene) as the outer blocks were synthesized in the presence of TMEDA and a difunctional initiator derived also from m-diisopropenylbenzene (m-DIB) and Li. A multistep seeding technique with isoprene was developed to promote the efficiency of the dillithium

initiator. The PCHD-b-PI-b-PCHD triblock copolymers exhibited relatively wide molecular weight distributions (I~1,5) despite the anionic polymerization techniques involved[103].

Symmetric triblock copolymers containing only methacrylic blocks, with the middle block exhibiting low T_g [poly(n-butyl acrylate) (PnBA) or poly(isooctylacrylate) (PIOA)] and the outer blocks exhibiting relatively high T_g [poly(methylmethacrylate)] have been successfully synthesized showing interesting anti-oxidative properties[104,105].

The difunctional initiator derived from m-diisopropenylbenzene and t-BuLi has also been used for the synthesis of ABA triblock copolymers where A was poly(4-vinylpyridine) and B poly(butadiene)[106].

The synthesis of ABA triblock copolymers, where the middle block was poly(2-vinylpyridine) and the outer blocks were poly(tert-butyl acrylate), has been reported by using the difunctional initiator sodium tetraphenyldiisobutane in the presence of LiCl[107]. The final products, exhibiting narrow molecular weight polydispersities, were investigated in aqueous solutions as a function of pH versus rheology and viscometry measurements.

Various symmetric linear triblock copolymers have been synthesized by using difunctional initiators based on sodium, potassium or lithium naphthalene. In the early 90's, ABA triblock copolymers of the poly(tert-butyl acrylate)-polystyrene-poly(tert-butyl acrylate) (PtBuA-b-PS-b-PtBuA) were synthesized by using naphthalene-Li added with Li-Cl as an initiator for the styrene polymerization leading to final products with predictable molecular weights and monomodal molecular weight distributions (I~1,2)[79]. Furthermore, by using the same initiation system, symmetric triblock copolymers of the PMMA-b-PtBuA-b-PMMA or PtBuA-b-PMMA-b-PtBuA type have been synthesized leading to well-defined polymers[81]. A series of PEO-b-PI-b-PEO [poly(ethylene oxide)-poly(isoprene)-poly(ethylene oxide)] symmetric triblock copolymers exhibiting a variety of block compositions and molecular weights, have been synthesized by using sodium or potassium naphthalene as the difunctional initiator[108]. The final products had narrow molecular weight distributions while the PI block obtained was mostly of the 3,4-microstructure (~ 60%). Triblock copolymers comprising of 2-vinylpyridine (2VP) (middle block) and n-hexyl isocyanate (HIC) (outer blocks) were synthesized by using the difunctional initiator Na-naphthalene[109,110]. The polymerization temperatures were held at -78^0C for 2-vinylpyridine and -98^0C for n-hexyl isocyanate. The initiation system was effective leading to well-defined final materials with narrow molecular weight distributions.

2.6.3 Non-Linear Copolymers of H- And Super H-Architecture

Non-linear block copolymers have attracted also the interest of polymer scientists in an attempt to study the possible effect of macromolecular architecture on block copolymer properties. A variety of block copolymers has been synthesized with complex macromolecular architectures and many have proven to exhibit many interesting properties, in many cases completely different from their linear precursors. Non-linear block copolymers include star block, graft, miktoarm star and a variety of other complex architectures such as graft block, H- and super H-shaped copolymers etc.

The synthetic approaches of synthesizing non-linear block copolymers via anionic polymerization involve in many cases the combination of chlorosilane chemistry and difunctional reactive sites. This technique has been applied for the synthesis of H- and super H-shaped copolymers. The first attempt was reported by Roovers[111] who synthesized H-shaped polystyrenes by using the difunctional initiator sodium-naphthalene and methyltrichlorosilane ($MeSICl_3$) as the linking agent. Later on, H-shaped copolymers were synthesized by reacting initially PS^-Li^+ with the same linking agent in a ratio SiCl:Li = 3:2.1[112]. In this approach, only two (2) Cl atoms are substituted reacting with the living centers in a quantitative, fast and controlled way without the indication of undesirable byproducts and resulting in a PS dimer with an active Si-Cl bond. The macromolecular linking agent was then reacted in a 2.1:1 ratio with a difunctional PI chain synthesized by the difunctional initiator derived from PEB and sec-BuLi in the presence of tert-butoxide, forming the final H-shaped copolymer $[(PS)_2PI(PS)_2]$ as shown in Scheme 2.5.

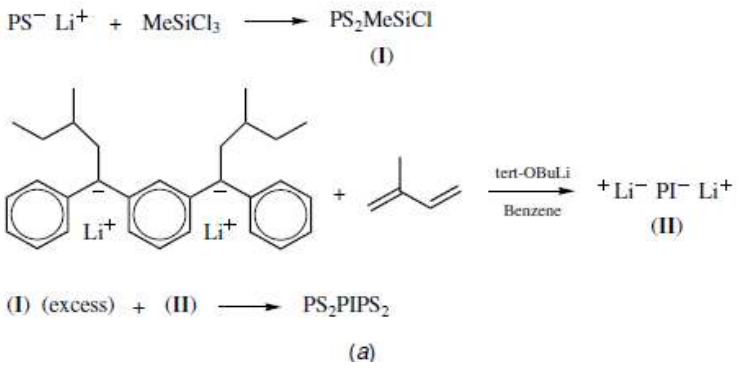

Scheme 2.5: *Synthesis reactions of a $(PS)_2PI(PS)_2$ H-type copolymer by combining the chlorosilane linking agent method and the difunctional polymerizable monomers method.*

Super H-shaped copolymers were synthesized by first forming a difunctional backbone of PS chain derived from the polymerization of styrene with the difunctional initiator sodium naphthalene in a mixture of benzene/THF (1.2:1)[113]. The PS backbone was then reacted with a large excess of tetrachlorosilane ($SiCl_4$) leading to a PS chain with three (3) active sites at each end due to the existence of three (3) chlorosilane atoms. After

removing the excess of tetrachlorosilane under high vacuum conditions, an excess of PI living arms is added in a Li:SiCl = 6.1:1 ratio resulting in the final super H-shaped copolymer [$(PI)_3PS(PI)_3$]. The excess of arms was eliminated by fractionation in a solvent/non-solvent system (toluene/methanol) and the pure final product was received.

CHAPTER 3

Physical Properties of Block Copolymers

3.1 Microphase Separation of Linear Diblock Copolymers

Block copolymers consist of incompatible polymer segments which are chemically connected to each other with covalent bonds. Copolymers depend on the value of the Gibbs free energy (ΔG_M), for the simplest case which is the mixing of two chemically different homopolymers, which is given by the following equation:

$$\Delta G_M = \Delta H_M - T\Delta S_M \quad (3.1)$$

where ΔH_M and ΔS_M are the enthalpy and entropy of mixing, respectively. For the phase separation of a linear diblock copolymer, the final free energy F is given by the following equation:

$$\frac{F}{kT} = \chi_{AB}\phi_A\phi_B + \left(\frac{\phi_A}{N_A}\right) \ln(\phi_A) + \left(\frac{\phi_B}{N_B}\right) \ln(\phi_B) \qquad (3.2)$$

where ϕ_A and ϕ_B correspond to the volume fraction of block A and B respectively, N_A and N_B is the degree of polymerization of block A and B respectively which is proportional to the molecular weight and χ is the interaction parameter Flory-Huggins between A and B polymer segments. The first two factors, ϕ and N, are related to the composition of the copolymer and affect the entropy of mixing while χ is a parameter related to the enthalpic interaction of the blocks and is inversely proportional to the temperature according to the equation:

$$\chi = aT^{-1} + \beta \quad (3.3)$$

where α and β are non-unit constants depending on the ϕ and N values. It is easily understood, from equation 3.2, that entropic interactions are related to N^{-1} and enthalpic interactions are related to χ, while $\chi << N$, resulting in a phase separation dependence on the χN value.

Thermodynamics of block copolymers depend also on the fact that chains tend to maintain their unperturbed dimensions. The entropic interactions enhance the mixture of the polymeric phases while the enthalpic interactions promote their separation. Consequently, the mechanism of phase separation in linear block copolymers depends on the following parameters:

a) The interaction parameter χ.
b) The total degree of polymerization N.
c) The volume fraction ϕ.

At the equilibrium state, polymer chains tend to form such shapes that the total free energy of the system is minimized. When the interaction parameter χ is decreased (e.g. by increasing the temperature) the junction points between A and B blocks are less favored. If the value of the degree of polymerization N is relatively high, then the junction points of A and B blocks are even less favored leading to the decrease of the chain conformation entropy. The result is that the chains do not maintain anymore their unperturbed dimensions and the enthalpy requirement for minimizing the junction points between dissimilar chain segments leads to a local phase separation which is called microphase separation (Figure 3.1).

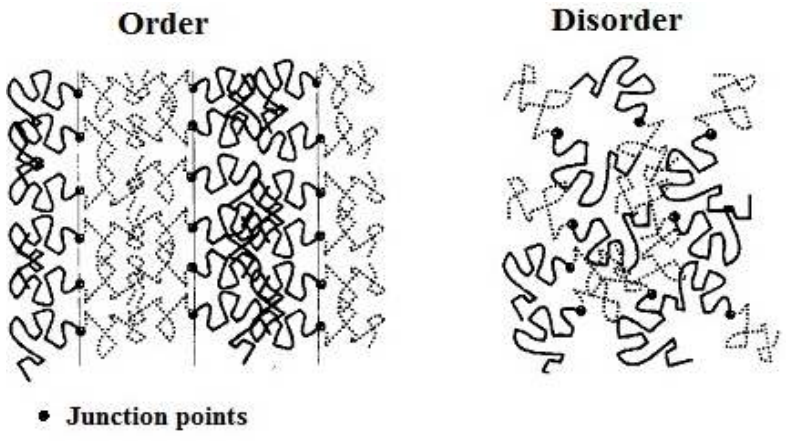

Figure 3.1: *Ordered state (left) and disordered state (right) of a symmetric linear diblock copolymer. The ordered state consists of separated microphases of the two components with the junction points located on the interface.*

In the case where χ or N decreases significantly, the entropic factors become greater than the enthalpic factors leading the system to the disordered state. The change related to a transition from a disordered state to a microphase ordered state is called order-disorder transition (ODT) and the temperature where this change happens is called microphase separation temperature or order-disorder temperature (T_{ODT}). For a symmetric copolymer ($\phi_A = \phi_B = 0.5$) with two symmetric blocks, the order-disorder transition is observed for $\chi N \sim 10.5$, which has been verified experimentally and from theoretical calculations.

The separated microphases assemble forming various structures. The morphology that will be adopted by the polymeric melt, when it is microphase separated, is determined by the entropic and enthalpic factors adjusting the free energy value. The enthalpic term is related to the interaction energy and favors the minimization of the interface size which separates the two different blocks. The entropic term is related to the extension energy of the chains and favors chain conformations at both sides of the interface. The adopted morphology of the copolymer at the equilibrium state is a result of the combination of these entropic and enthalpic terms. For a symmetric diblock copolymer ($\phi_A = \phi_B = 0.5$), the chains from both

sides of the interface will have almost the same size (which means that they will have similar conformation) leading to alternating lamellar formation. While the asymmetry between the blocks from both sides of the interface is increased ($\phi_A > 0.5$, $\phi_B < 0.5$), the asymmetry between the chain size is also increased resulting in the formation of more curved interfaces towards the block with the lowest content (ϕ_B) (Figure 3.2)

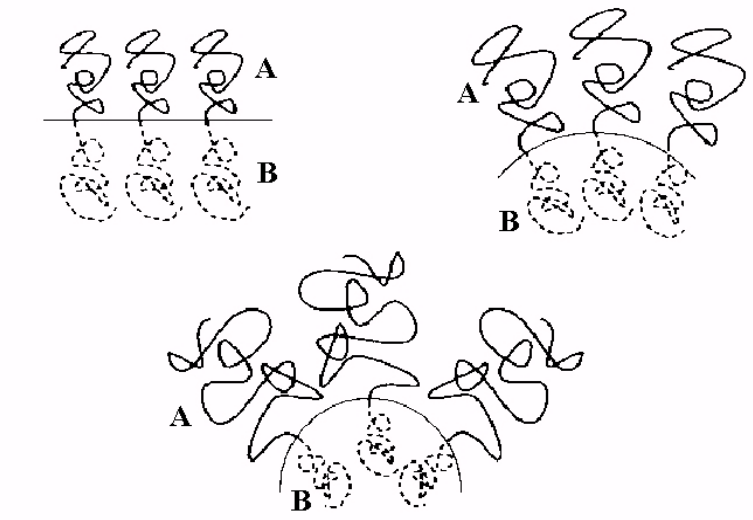

Figure 3.2: *The effect of the asymmetry of the blocks on the interface curving in a diblock copolymer. The more asymmetric the macromonomer is, the larger the curving of the interface becomes. The overall morphology of the system depends on the local curving of the interface.*

At the beginning of the microphase separation, the system goes through the ODT to the weak segregation limit (WSL) when $\chi N \sim 10.5$. At the weak segregation limit, the thickness of the interface is not small but significant enough, due to the high mixing of the two blocks and the macromolecular conformations are similar to the unperturbed dimensions. The other regime is the strong segregation limit (SSL) for cases in which $\chi N > 100$, where the interactions between the asymmetric blocks are so strong that the chains are almost immediately separated in homogenous microdomains with very thin interfaces. Each microphase contains only one of the two components and by moving from one microphase to another there is a sharp change of the composition. It is important to emphasize that the dimensions of the intermediate surface at the strong segregation limit are negligible in contrast with the case of the weak segregation limit. Consequently, the enthalpic term of the free energy is related only to the area of the interface since this is the domain where the junction points between the two different blocks are located. The enthalpic term is significantly reduced by the stretching of the chains away from the interface (the macromolecular conformations are far from the unperturbed dimensions resulting in absolute absence of mixing between the blocks. The third regime is the intermediate segregation limit

(ISL) ranging between the two already mentioned above. Each regime is discussed separately in the following paragraphs.

3.2 Strong Segregation Limit (SSL)

Many theories were developed in order to describe the strong segregation limit. The first one was introduced by Meier[114] who estimated that the width of microphase A (D_A) scale with the molecular weight according to the equation:

$$D_A \sim (N_A + N_B)^{2/3} \sim N^{2/3} \qquad (3.4)$$

Other theoretical studies followed and two of the most important are described below. The first was developed by Helfand and Wasserman[115-117] who introduced a self-consistent field theory with three principal contributions to the free energy: a) contact enthalpy between the A and B microdomains at the interface, b) minimization of entropy due to the stretching of chains and c) confinement entropy due to the localization of the junction points at the interface. Their result for the microdomain thickness was:

$$d \sim a N^{\delta} \chi^{\nu} \qquad (3.5)$$

with $\delta \sim 9/14$ and $\nu = 1/7$. The second theoretical study was developed by Semenov[118] who estimated the free energy in the asymptotic limit arguing that polymer chains are strongly stretched. This situation resembles grafted polymer brushes and surfactant interfaces and estimates that the microdomain size in the asymptotic limit is given by the following equation:

$$d \sim a N^{2/3} \chi^{1/6} \qquad (3.6)$$

Equation 3.6 predicts a strong dependence of the microdomain size on N and a weak dependence on χ. Since there is weak dependence of the interaction parameter χ, the experimental verification of this equation was a difficult task, however experiments in symmetric diblock copolymers[119] have shown a weaker dependence as $d \sim N^{0.6}$, for $\chi N > 29$, with a bizarre N-dependence ($d \sim N^{0.8}$) at weaker segregation, implying that this SSL predictions that $d \sim N^{2/3}$ are only correct for $\chi N > 100$.

3.3 Weak Segregation Limit (WSL)

This is the regime where most of the experiments are made, when χN is slightly larger than 10.5. Leibler[120] was the first who considered a monodisperse linear diblock copolymer (AB) with equal monomer volumes and statistical segment lengths ($\alpha_A = \alpha_B$). The conclusion was that the morphological behavior is related to the interaction parameter χ, the degree of polymerization N and the volume fraction ϕ, which is a fraction of the copolymer molecular composition f, according to the equation:

$$\phi_A = \frac{f_A d_A}{f_A d_B + f_B d_A} \qquad (3.7)$$

where ϕ_A is the volume fraction of block A, d_A and d_B are the densities of A and B blocks respectively and f_A and f_B are the molecular fraction values of A and B blocks respectively. The molecular fraction of block A is given by the following equation:

$$f_A = \frac{\overline{M}_{n,A}}{\overline{M}_{n,A} + \overline{M}_{n,B}} \qquad (3.8)$$

The phase diagram obtained is shown on Figure 3.3. As it can be observed from the phase diagram, the phase limits are more curved with the volume fraction as the segregation becomes weaker. For a symmetric copolymer with volume fraction ϕ = 0,5 the order-disorder transition is predicted that is happening when χN = 10.495, where a second order transition from the disordered phase straight to lamellar domains occurs. For a specific range of compositions and χN values larger than 10.5, for systems exhibiting large asymmetry between the two blocks, Leibler predicted that at the ODT the system undergoes a first order transition from the disorder phase to a body centered cubic (bcc) sphere phase.

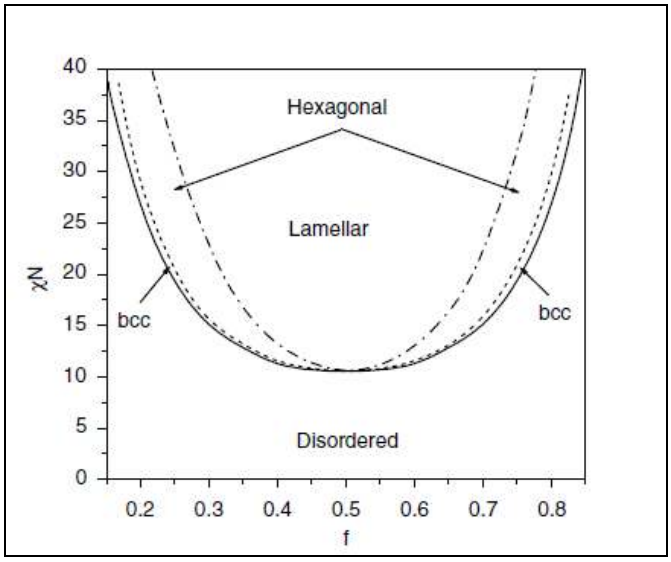

Figure 3.3: *Theoretical phase diagram for linear diblock copolymers within the mean-field theory assuming equal monomer volumes and statistical segment lengths for the two blocks. On this phase diagram, f corresponds to the volume fraction*[121].

By further increase of χN at specific volume fractions, and by using the mean-field theory (MFT), the system undergoes a transition to hexagonally packed cylinder (hpc) phase and then to lamellar phase. Mayes and Olvera de la Cruz[121] using the Hartree approximation resulted in the following equation:

$$(\chi N)_{ODT} = 10{,}495 + 39{,}053\, N^{-1/2} \qquad (3.9)$$

As it can be concluded and in contrast with strong segregation limit theory where d ~ $N^{2/3}$, at weak segregation limit theory the microdomain size (d) is analogous to $N^{1/2}$.

3.4 Intermediate Segregation Limit (ISL)

The previously reported approaches from Helfand, Leibler and Semenov were very successful in predicting the three classical phases but failed to account for the more complex ones. Matsen[122] showed that a self-consistent field theory (SCFT) results, at intermediate segregation, in more complex structures as it can be observed by the phase diagram given in Figure 3.4. The most important aspect of this phase diagram is the existence of a new phase, the double gyroid phase, in addition to the usual lamellar, hexagonal and spherical phases predicted from Leibler's work.

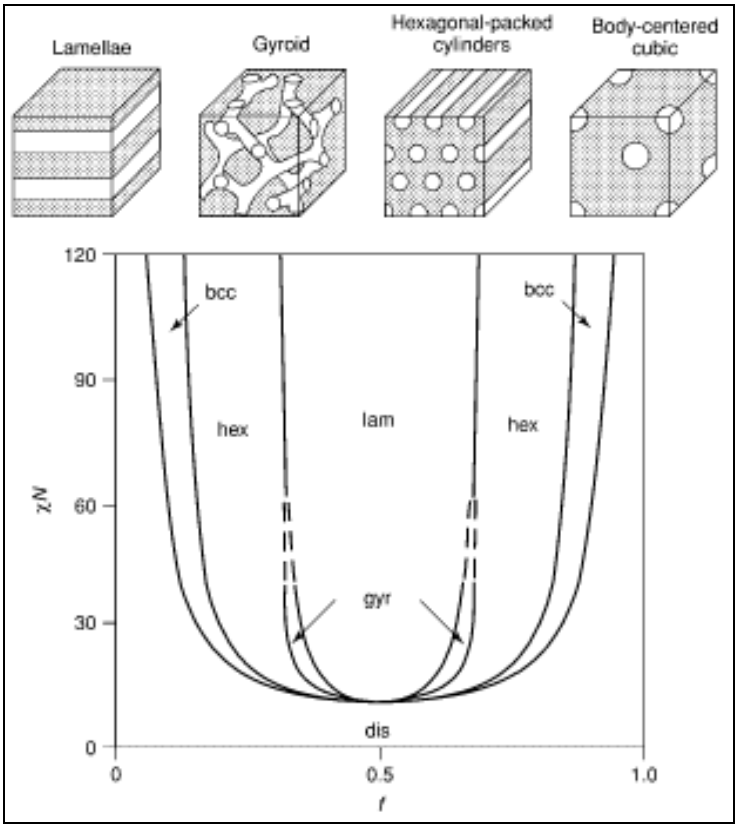

Figure 3.4: *Mean field phase diagram within the SCFT approximation for conformationally symmetric diblock copolymers where f = volume fraction. The differences with Leibler's MFT phase diagram (Fig. 3.3) are notable. The phases are: L: lamellar, C: hexagonally packed cylinders, S: spheres packed in a bcc lattice, G: bicontinuous Ia3d cubic (double gyroid), Scp: closed packed spheres*[123].

The SCFT predicts for intermediate segregation the sequence of lamellar-gyroid-hexagonal-spheres-disordered phases as ϕ progresses from 0.5 to 0 or 1. Both perforated lamellar (PL) phase and ordered bicontinuous double diamond (OBDD) phase are absent from the diagram because they were found to be relatively unstable.

3.5 Conformational Asymmetry

At 1997 Matsen and Bates[123] suggested, through SCFT calculations, that conformational asymmetry (ζ) plays a significant role to the order-order and order-disorder phase boundaries. By compiling the free energy values found for classical and more complex diblock copolymers, very interesting phase diagrams were produced corresponding to the cases where α_A/α_B = 1.5 and α_A/α_B = 2 (Figure 3.5). The main effect of conformational asymmetry is to shift the phase boundaries towards compositions richer in the blocks exhibiting the higher stiffness. This asymmetry has been attributed to differences in monomer volume and in chain flexibilities of the blocks, leading to an overall conformational asymmetry described by equation 3.10.

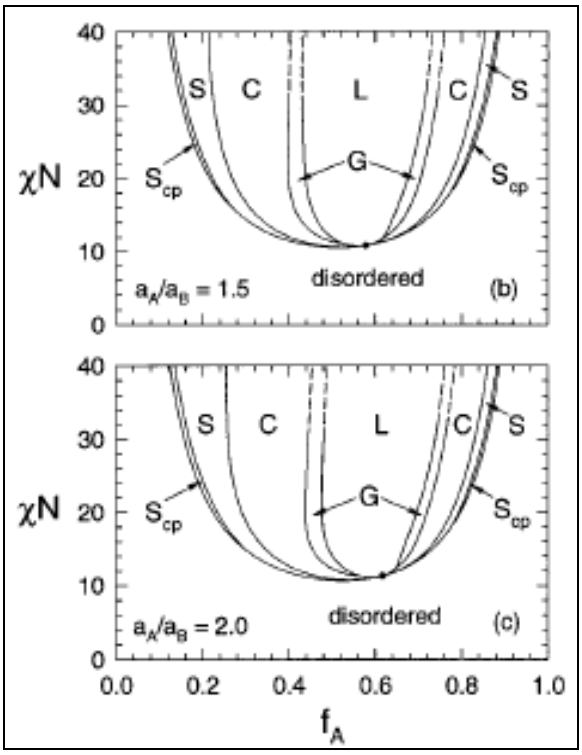

Figure 3.5: *Phase diagrams for linear diblock copolymers with different conformational asymmetries within the SCFT with f = volume fraction. Top: a_A/a_B = 1,5; Bottom: a_A/a_B = 2: The ordered phases are L (lamellar), G (gyroid), C (hexagonally packed cylinders), S (spheres in bcc lattice), and Scp (spheres in fcc lattice)*[124].

$$\zeta = \frac{\alpha_A^2 / 6u_A}{\alpha_B^2 / 6u_B} \qquad (3.10)$$

where u is the statistical segment volume and a the statistical segment length. As it can be easily observed from Figure 3.5, the conformational asymmetry has a greater impact on the order-order transitions (OOT) than on the order-disorder transitions (ODT) producing larger shifts. The larger shifts in the OOT can be explained from the fact that as α_A/α_B increases, the A blocks become easier to stretch, while the opposite happens for the B blocks. The interface

acquires the tendency to curve towards the A blocks, while allowing the B blocks to relax at the expense of A blocks. At a certain composition ϕ_A, the lamellar phase will tend to transform to the hexagonal one where cylinders of A blocks will be embedded in a matrix of B blocks. This tendency causes the OOT to shift towards the larger A-block volume fractions. On the other hand, the effect of conformational asymmetry on the ODT is much smaller. For example, disordering from spherical structure formed by A block requires a thermal energy applied on the blocks forming the spheres which is approximately $\chi N\phi_A$, thus independent of the statistical segment lengths α_A and α_B. Therefore, the ODT is relatively unaffected by the conformational asymmetry. Apart from the differences on the phase state, conformational asymmetry strongly affects the relative domain spacing between structures along their boundaries. This is expected to affect the kinetics of the respective order-to-order transitions.

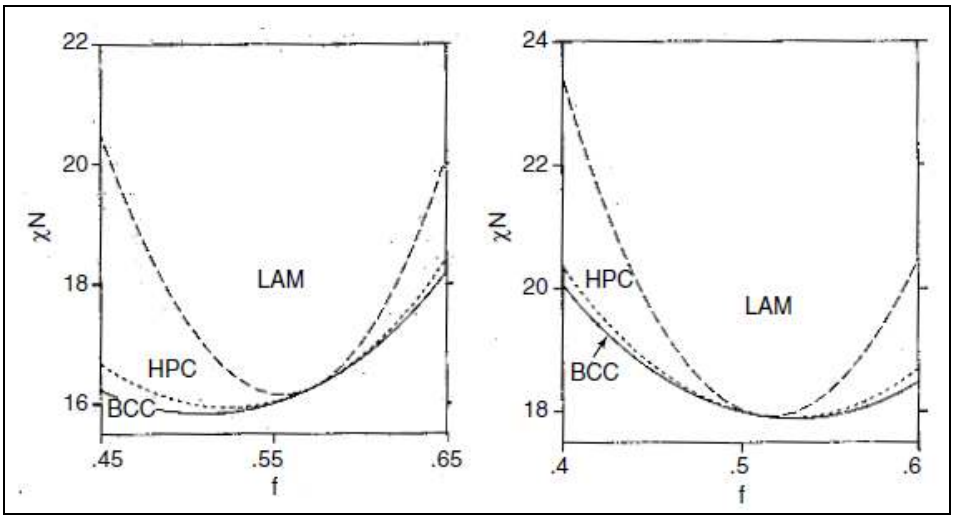

Figure 3.6: *Phase diagrams for linear ABA triblock copolymers with τ = 0.25 (left) and τ = 0.5 (right) and f = volume fraction.*

Milner showed also that chain architecture plays a significant role in the morphological behavior of block copolymers[124]. More specifically, he showed that for a specific volume fraction (e.g φ = 0.4), and assuming elastically symmetric blocks, diblocks ($n_A = n_B = 1$) would form lamellae, Y polymers ($n_A = 2$) would form cylinders and Ψ polymers ($n_A = 3$) would form spheres. The mean-field theory (MFT) approach proposed by Leibler was also used by Mayes[125] to predict phase diagrams for ABA triblock copolymers. The calculated phase diagrams are shown in Figure 3.6 for two ABA triblocks with τ = 0.25 and τ = 0.5, where τ is a symmetry parameter ($\tau = \phi_1/\phi$, with the cases of τ = 0 and τ = 1 corresponding to a diblock phase). These triblock phase diagrams are highly asymmetric due to the high deformation of the central B blocks in order to accommodate the outer A blocks into their domains. Increasing τ creates important differences for each morphology at a given composition. For example, at ϕ= 0.5, a diblock copolymer goes for the disordered state

directly to the lamellar, while for an ABA triblock copolymer for $\tau = 0.25$ at the same composition, there are large areas with BCC and hexagonal cylinder phases. For more symmetric triblock copolymers, these domains become narrower.

3.6 The Known Phase Diagrams of Diblock Copolymers

The most investigated systems in bulk of diblock copolymers are the poly(isoprene)-b-polystyrene and poly(ethyleneoxide)-b-poly(isoprene). For the first case 16 samples were synthesized while for the second case 25 samples were synthesized.

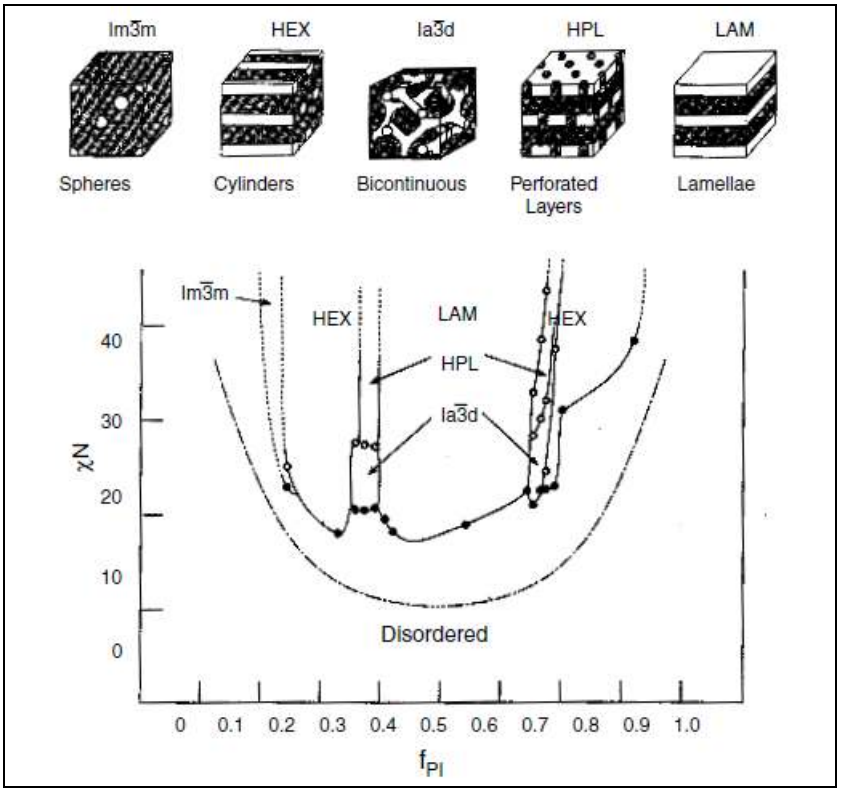

Figure 3.7: *Equilibrium morphologies experimentally observed for linear diblock copolymers of the PI-b-PS type and corresponding phase diagram. The dashed line gives the spinodal line from Leibler's MFT, where f=volume fraction*[126].

For the PI-b-PS phase diagram (Figure 3.7) the morphologies that were observed are the following:

- Spheres of the minority component arranged in a body centered cubic (BCC) lattice in a matrix of the majority component (lm3m).
- Hexagonally packed cylinders of the minority component in a matrix of the majority component (HEX).
- Double gyroid, where two independently interpenetrating and not interconnected bicontinuous networks of the minority component are formed in a matrix of the majority component (la3d).

- Hexagonally perforated layers (HPL – not equilibrium).
- Alternating lamellae of the two components (LAM).

As it can be observed, the phase diagram is asymmetric around ϕ= 1/2. Furthermore, the gyroid face is stabilized for a significant range of compositions and χN values, ranging from 0.35 to 0.40 and from 0.64 to 0.69. For the second volume fraction this order-order transition occurs also for a limited range of χN values.

For the PEO-b-PI phase diagram (Figure 3.8), which is constructed by 25 samples, five ordered phases have been identified based on their scattering, TEM and viscoelasticity results: crystalline lamellar (L_C), amorphous lamellar (lam), spheres in a bcc lattice, cylinders packed in an hexagonal structure (hex) and finally the gyroid phase (shaded areas). In addition a perforated lamellar structure was observed but found to be unstable.

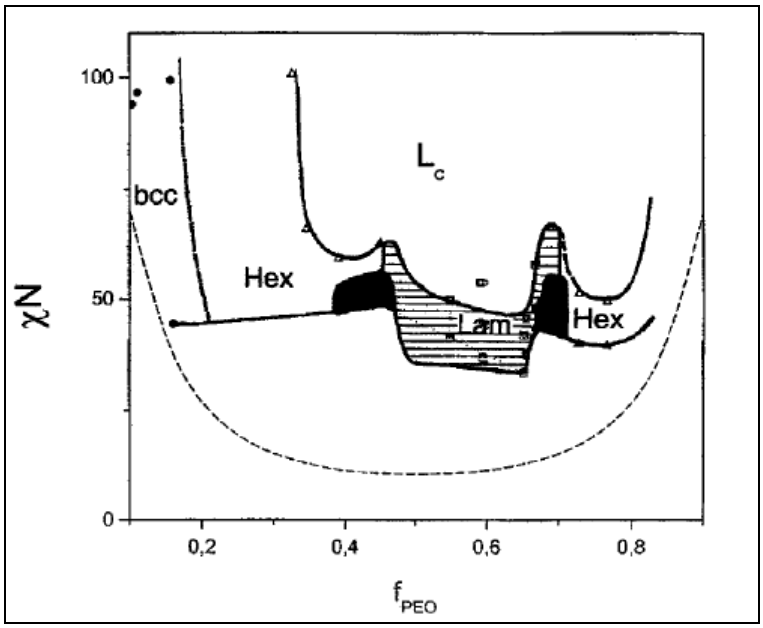

Figure 3.8: *Equilibrium morphologies observed for linear diblock copolymers of the PEO-PI type, where f = volume fraction.*

This phase diagram allows order-order transitions between hexagonally packed cylinders and gyroid phases for 0.38 < ϕ_{PEO} < 0.46 and between lamellar and gyroid phases for 0.66 < ϕ_{PEO} < 0.7. It is easily understood that there is a correlation of the phase asymmetry with the conformational asymmetry parameter ζ. The higher the value of ζ, the more asymmetric the phase diagram (it has been calculated that ζ = 2.7 for the PEO-b-PI system). Nevertheless, the high asymmetry does not seem to affect the gyroid phase which is present for both ϕ < 1/2 and ϕ > 1/2 and also stabilized for a wide range of *f* and χN values.

CHAPTER 4

Instrumentation and Theory of Molecular Characterization and Thermal Analysis

4.1 Size Exclusion Chromatography (SEC)

Size exclusion chromatography (SEC) or gel permeation chromatography (GPC) is one of the most dynamic and most used methods for molecular characterization of polymers in a laboratory and industrial scale[127]. The main reasons which make this method so widely used are the simplicity, the fast rate of its analytical potential and the ability to estimate the molecular weight distribution ($I = \frac{\overline{M}_w}{\overline{M}_n}$) as well as the number and weight average molecular weights ($\overline{M}_n$ and $\overline{M}_w$ respectively). Furthermore, it is also used for monitoring the progress of synthesis reactions such as linking reactions.

The main parts of size exclusion chromatography are: a) a reservoir of pure solvent, b) a high pressure isocratic pump, c) a sample injection port, d) columns with porous material (at least 3), e) UV and RI detectors, f) a recording system and g) a waste disposal reservoir. In Figure 4.1 is a typical schematic scene of a size exclusion chromatography set-up is presented.

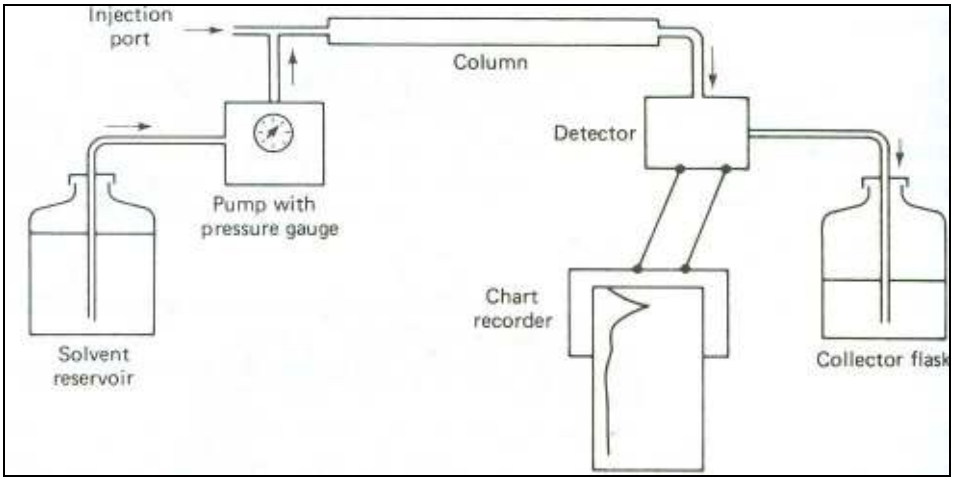

Figure 4.1: *Schematic of a size exclusion chromatography set up.*

The solvent that is mainly used is tetrahydrofuran (THF). Chloroform is used as well as dimethylformamide for high temperature GPCs and distilled water for water soluble polymers. Volumes (5-50 %) of triethylamine or pyridine are also used in mixtures with THF. The pump secures stable flow of the solvent as well as high and stable pressure in order to drive the solution throughout the columns. Separation columns are the most important part of the instrument. One column with different pore size areas or many columns connected in

series with a wide variety of pores (500-10^6Å) may be used. Columns of crosslinked polystyrene with well-known pore size or specially treated silica gel are applied for organic solvents. The separation procedure of an ideal polymer mixture consisting of two sizes of macromolecules is presented in Figure 4.2. In the first frame, the sample is shown immediately after injection at the top of the column. The liquid mobile phase (e.g. THF) is passed through the column at a fixed flow rate, setting up a pressure across its length. In the next frame, the sample polymer molecules pass into the column as a result of this pressure. The smaller macromolecules are able to penetrate the pores as they pass through the column but the larger ones are too large to be accommodated and remain mainly in the space between the pores, as shown in the third frame. The smaller molecules are only temporarily retained and flow down the column until they encounter other pores to enter. The larger molecules flow more rapidly down the length of the column since they cannot reside inside most of the pores. Finally the two molecular sizes are separated completely as shown in the fourth frame.

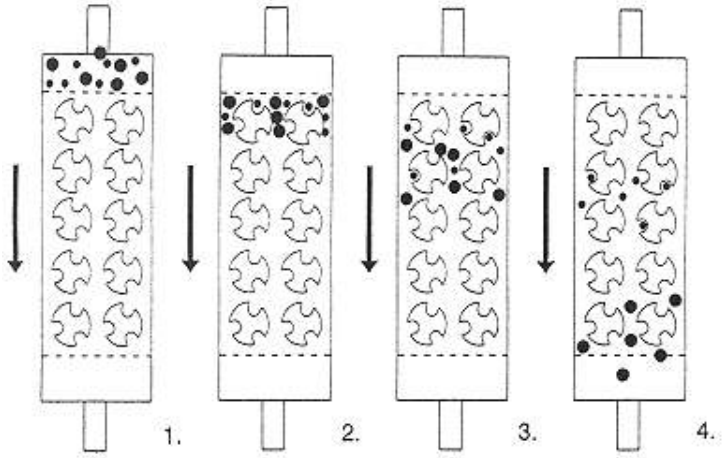

Figure 4.2: *SEC separation of two macromolecular sizes: 1) sample solution before entering the column, 2) sample solution upon the head of the column, 3) size separation begins, 4) complete resolution*[127].

The detectors used in this equipment can vary and they all must be very accurate and sensitive in order to respond to the dissolved polymer. The most common type is the differential refractive index detector (DRI). It senses differences in refractive index between the sample solution and a static reference of the mobile phase (solvent) using a split cell. It responds well, at a moderate concentration level, to most polymer samples, provided that they are different in refractive index from the solvent in which they are dissolved. It is generally assumed that the response of the DRI is equally proportional to polymer concentration in all molecular weight regimes. Unfortunately, this assumption does not stand at low molecular weights (less than several hundred monomer units) at which the polymer end groups represent a non-negligible portion of the molecular mass and change the refractive index of the

material. Other common types of detectors are the ultraviolet (UV) and infrared (IR) detectors. The IR detector is slightly more sensitive than the DRI detector while the UV detector is several orders of magnitude more sensitive. The last is most commonly employed for polymers containing aromatic rings or for calculating the molecular fraction of the segment in a copolymer as long as one of the chains absorbs in UV wavelength (e.g. PS with $\lambda = 269nm$). Detectors of laser light scattering (dual angle - DALLS, low angle - LALLS etc.) are also employed providing accurate results for the weight average molecular weight, the radius of gyration and the second Virial coefficient (A_2). It is easily understood that depending on the detector employed, one can estimate with great accuracy the molecular characteristics of a polymer.

Size exclusion chromatography is an indirect method of molecular weight characterization, which means that calibration is required in order to monitor the elution volume time of novel monodisperse polymers with well-known molecular weights (e.g. polystyrenes). The elution volume of each macromolecule of the polymer is given by the following equation:

$$V_e = V_0 + K_{sec} V_E \qquad (4.1)$$

where V_0 is the void volume or total exclusion volume which is the volume of the column that is not occupied by any porous material, K_{sec} is the ratio of the concentration *i* of the macromolecule in the pores to the concentration of the macromolecule in V_o and V_E is the total volume of all pores. For macromolecules that cannot flow down the column it is known that $V_e = V_0$ ($K_{sec} = 0$) while for macromolecules that can reside inside all of the pores the value of V_e equals to $V_o + V_E$ ($K_{sec} = 1$). In these two situations, the macromolecular separation is not successful and the columns must be replaced. Macromolecular separation is applied when $0 < K_{sec} < 1$ for all the macromolecular chains. Consequently, the pore size of the column material is a very significant parameter for the effective and needed separation of the various types of macromolecules. The pores size should be similar to the size of the macromolecules in the solution and the column material should exhibit quite high overall pore volume, usually $0.5 < V_E / V_0 < 1.65$. Therefore, in order to separate the polymer samples in a wide range of hydrodynamic volume, either a series of columns each one covering a different molecular size or columns connected in series with variable pore size should be used.

Calibration of the instrument can be performed by using novel polymers, meaning polymers with well-known molecular weight and narrow molecular weight distribution ($\frac{\overline{M}_w}{\overline{M}_n} \leq 1{,}05$). Depending on their hydrodynamic volume, these novel polymers will elute at different elution volumes resulting in the calibration curve described as $\log M = f(V_e)$ where M is the molecular weight per sample (M_{peak}) and V_e the elution volume. It can be easily

understood that macromolecular separation is directly associated with hydrodynamic volume of the polymer, which is given by the following equation:

$$CV_h = [n]M = \Phi\left\langle \overline{S}^2 \right\rangle^{3/2} \qquad (4.2)$$

where V_h is the hydrodynamic volume, [n] is the intrinsic viscosity, $\left\langle \overline{S}^2 \right\rangle^{1/2}$ is the mean square root of radius of gyration of the polymer chain and C and Φ are constants. Therefore, it can be easily understood that [n]M is proportional to the hydrodynamic volume. This product versus elution volume [log([η]M) = f(V_e)] for a number of chemically and architecturally different polymers was investigated under identical SEC conditions and it was concluded that all points lie on the same calibration curve. This calibration curve was established as universal for all polymer types studied[127].

4.2 Proton Nuclear Magnetic Resonance (^{1}H-NMR) Spectroscopy

Proton nuclear magnetic resonance spectroscopy, commonly referred to as ^{1}H-NMR, is one of the most versatile tools for characterizing molecular structure, and its application to polymer solutions has provided qualitative and quantitative information concerning these materials[128]. Although larger amounts of sample are needed than mass spectroscopy, NMR is non-destructive, and with modern instruments much information can be obtained from samples weighing less than a milligram.

The nuclei of many elemental isotopes have a characteristic spin (I). Some nuclei have integral spins (e.g. I = 1, 2, 3…), some have fractional spins (e.g. I = 1/2, 3/2, 5/2…), and a few have no spin, I = 0 (e.g. ^{12}C, ^{16}O, ^{32}S…). Isotopes of particular interest are ^{1}H, ^{13}C, ^{19}F and ^{31}P, all of which have I = 1/2. The nucleus that has been widely used and studied in NMR is that of the hydrogen atom (proton).

The following features lead to the NMR phenomenon:

1. A spinning charge generates a magnetic field. The resulting spin-magnet has a magnetic moment (μ) proportional to the spin.
2. In the presence of an external magnetic field (B_0), two spin states exist, +1/2 and -1/2. The magnetic moment of the lower energy +1/2 spin state is aligned with the external field while that of the higher energy -1/2 spin state is opposed to the external field.
3. The difference in energy between the two spin states is dependent on the external magnetic field strength and is always very small. At a field equal to B_x, a formula for the energy difference ΔE is given (I = 1/2):

$$\Delta E = \mu B_\chi / I \qquad (4.3)$$

Strong magnetic fields are necessary for NMR spectroscopy. The earth's magnetic field is not constant, but is approximately 10^{-4} Tesla at ground level. Modern NMR

spectrometers use powerful magnets having fields of 1 to 20 T (Figure 4.3). Even with these high fields, the energy between the two spin states is less than 0.1 cal/mol. For NMR purposes this small energy difference (ΔE) is usually given as a frequency in units of MHz (10^6Hz), ranging from 100 to 900 Mz for proton nuclei and depending on the magnetic field strength (Figure 4.4). Irradiation of a sample with radio frequency (rf) energy corresponding exactly to the spin state separation of a nuclei will cause excitation of this nuclei in the +1/2 state to the higher -1/2 spin state.

Figure 4.3: *900 MHz, 21.2 Tesla NMR magnet.*

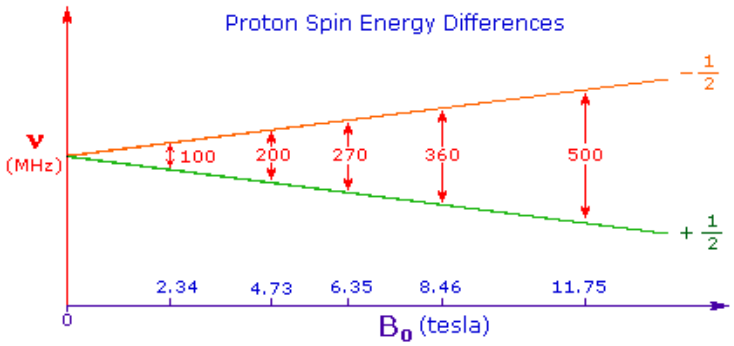

Figure 4.4: Proton *spin energy differences (ΔE) for a range of magnetic field strength (B_0).*

In order to obtain a good NMR spectrum, except from the external magnetic field, homogeneity of the opposing local magnetic field near the sample is also required, which means that the same power of magnetic field must be applied on the sample. This secondary local field generates from the movement of the charged electrons responding to the external magnetic field (B_0). Furthermore, this field shields the nucleus from the applied field, thus B_0 must be increased in order to achieve resonance (absorption of radio frequency energy). The

increase is very small though and it is usually referred to as in units of parts per million (ppm). Instead of designating a range of NMR signals in terms of magnetic field differences, it is more common to use a frequency scale, even though the spectrometer may operate by changing the magnetic field. Most organic compounds exhibit resonances that fall within a 12 ppm range and it is therefore necessary to use very sensitive and precise spectrometers.

Unlike IR and UV spectroscopy, where absorption peaks are uniquely located by a frequency or wavelength, the location of different NMR resonance signals is dependent on both the external magnetic field and the radio frequency. Since no two magnets will have exactly the same field, resonance frequencies will vary accordingly and an alternative method for characterizing and specifying the locations of the NMR signals is needed. The method of solving this problem is to report the location of an NMR signal in a spectrum relative to a reference signal from a standard compound added/or not to the sample. In the case of the external standard compound the advantage of not reacting with the sample is very important, since it lies in a different capillary tube, but the main disadvantage is that its magnetic susceptibility is different from that of the sample. In the case of a reference standard added in the sample, the magnetic susceptibility for both the reference standard and the sample is the same but care should be taken for the reference standard to be chemically inactive. Also it should be easily removed from the sample after the measurement and it should contain only one type of magnetic nuclei as well as large number of nucleus in order to give a single sharp NMR signal that does not interfere with the resonances normally observed for organic compounds. Tetramethylsilane, $(CH_3)_4Si$, usually referred to as TMS, meets all these requirements and has become the reference compound of choice for proton NMR. Since the separation of NMR signals is magnetic field dependent, one additional step must be taken in order to provide a clear location unit. To correct the frequency differences from the field dependence, they are divided by the spectrometer frequency (e.g. 100 MHz) resulting in numbers that are very small (e.g. 2.15 for 215 Hz frequency difference). This operation gives a locator number called chemical shift, having units of parts per million (ppm) and is designated by the symbol δ. In order to take the NMR spectra of a solid, it is usually necessary to dissolve it in a suitable solvent. This solvent must be deuterated in order to avoid extremely sharp resonances of the solvent. Commonly used solvents are chloroform-d ($CDCL_3$), acetone-d_6 (CD_3COCD_3) and DMSO-d_6 (CD_3SOCD_3).

4.3 Membrane Osmometry (MO)

Determining the average molar mass of polymers is of considerable importance since the chain length is a controlling factor in the evolution of solubility, elasticity, fiber formation and mechanical strength properties. Membrane osmometry (MO) (Figure 4.5) is an absolute method for determining the number average molecular weight of polymers ($\overline{M}_n$) as well as

the second Virial coefficient (A_2), which means that no calibration with samples of known molecular weight is needed such as in size exclusion chromatography. This technique is useful in several molecular weight ranges (10.000-500.000 g/mol) and depends on the change in osmotic pressure from polymers in solution.

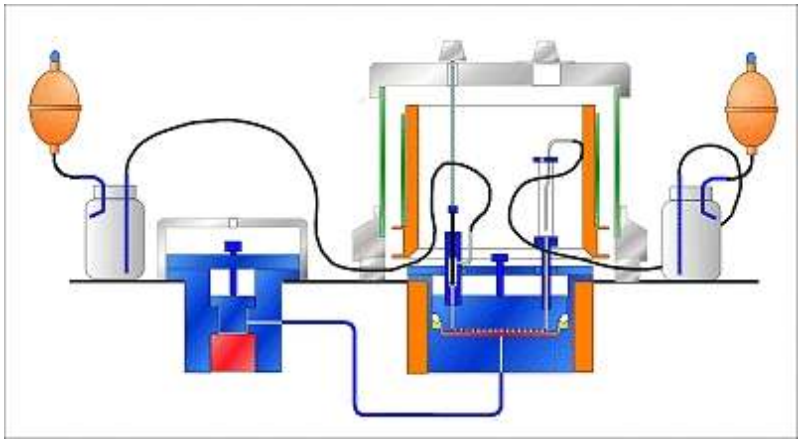

Figure 4.5: *Illustration of the membrane osmometer (Gonotec Osmomat 090) at the UOI Polymers Laboratory.*

In membrane osmometry, the solvent is separated from the polymer solution by a semi-permeable membrane which is tightly held between two chambers as exhibited in Figure 4.5. One chamber is sealed by a valve with a transducer attached to a thin stainless steel diaphragm which permits the measurement of pressure in the chamber continuously. The solvent chamber is filled with pure solvent and is isolated from the atmosphere except from the solvent passage through the membrane while the solution chamber is left open to the atmosphere. The solution cannot flow towards the pure solvent in this case but the solvent can flow through the membrane (that is the reason to use semi-permeable membrane). The chemical potential of the solvent is much higher than that of the solution and therefore there is a tendency for flow to occur from the solvent through the membrane to the polymer solution. Since the solvent is permitted to flow through the membrane, a change in concentration causes the solvent to diffuse to the solution side of the chamber. As this occurs, the pressure of the solvent decreases until the pressure difference across the membrane just counteracts the chemical potential difference caused by the solution. This pressure reduction which is required in order to equilibrate the chemical potential on both sides of the membrane is considered as the osmotic pressure. The osmotic pressure is related to the change in chemical potential by the following equation:

$$(m_1 - m_1^0) = V_1\, p \qquad (4.4)$$

where m_1^0 is the chemical potential of the pure solvent, m_1 the chemical potential of the solvent in solution, V_1 the molar volume of solvent in solution and p the osmotic pressure. Examining the osmotic pressure in terms of the free energy of mixing phenomena, the change in chemical potential can be related to the polymer molecular weight by substitution of the above equation into the following:

$$(m_1-m_1^0) = R\,T\,[c_2\,V_1 / M_2 + n_2^2\,(1/2 - c_1)\,c_2^2] \qquad (4.5)$$

where M_2 is the molecular weight of the polymer, n_2 is the partial specific volume of the polymer, c_1 the interaction parameter and c_2 the solution concentration. The relationship between the molecular weight and the osmotic pressure is then given by the following equation:

$$p / c_2 = R\,T / M_2 + R\,T\,n_2^2 / V_1\,(1/2 - c_1)\,c_2 \qquad (4.6)$$

The first term of this equation is the Van't Hoff expression for osmotic pressure at infinite dilution. The second term is the deviation from ideal behavior of the polymer solution and is related to the second Virial coefficient. The relationship between the second Virial coefficient and the interaction parameter c_1 is illustrated by:

$$A_2 = R\,T\,n_2^2 / V_1\,(1/2 - c_1) \qquad (4.7)$$

When the interaction parameter c_1 is equal to 1/2 and the second Virial coefficient is zero, then the osmotic pressure is governed by the ideal solution law. Experimentally, in calculating the molecular weight, osmotic pressure must be measured at several different concentrations. The factor p/c_2 is determined for each concentration and plotted p/c_2 versus c_2, extrapolating the concentration to zero. The slope of the resulting graph is the second virial coefficient and the molecular weight is calculated by the intercept.

4.4 Differential Scanning Calorimetry (DSC)

Differential scanning calorimetry or DSC is a thermo-analytical technique in which a physical property of the sample is monitored as a function of temperature, while the sample and the reference undergo a thermal treatment, heating or cooling. It is widely used in laboratory and industrial scale as a quality control instrument due to its applicability in evaluating sample curing and also for polymer curing.

In differential scanning calorimetry two capsules made by Al_3O_2 are placed in a thermal insulated cell of the instrument. The reference capsule remains unchanged during thermal treatment since it is empty, which means that the reference compound is air. The second capsule contains the sample. Both capsules are thermally treated, independently, in order for the temperature to be exactly the same. When a physical transformation occurs,

more or less heat flow will need to flow in the sample than the reference in order to maintain both at the same temperature. Whether less or more heat must flow in the sample depends on whether the process is exothermic or endothermic. When the sample undergoes an endothermic phase transition (e.g. melting), it absorbs heat and as a result more heat flow is required to the sample to increase its temperature at the same rate as the reference. Likewise, when the sample undergoes an exothermic phase transition (e.g. crystallization), it releases heat and as a result less heat flow is required to increase its temperature at the same rate as the reference. By monitoring the difference in heat flow between the sample and the reference, differential scanning calorimeters are able to measure the amount of heat absorbed or released during such transitions. A typical thermograph is shown in Figure 4.6.

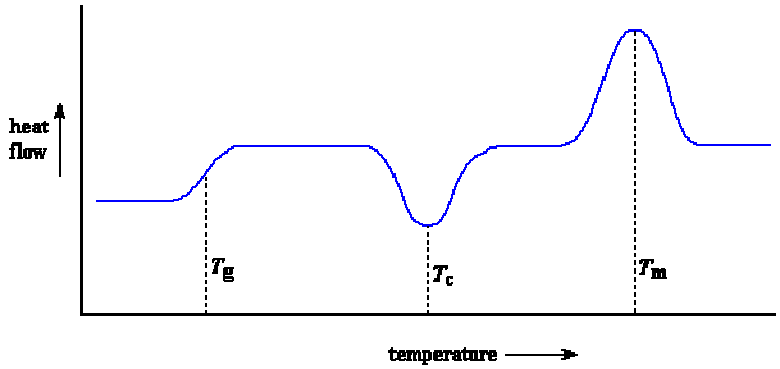

Figure 4.6: *DSC thermograph of a sample exhibiting three transformations, glass transition (T_g), crystallization (T_c) and melting (T_m).*

Each thermograph can provide information about the glass transition (T_g), the melting temperature (T_m) and the crystallization temperature (T_c) of a material. Melting and glass transition are endothermic transitions and crystallization is an exothermic transition.

The glass transition temperature is referred to amorphous polymers or semicrystaline polymers with amorphous regions and is the temperature where a reversible transition occurs from an amorphous, hard and relatively brittle state into an elastomeric, rubber-like state. The transition from the glassy state to the elastomeric state is endothermic and it is not considered a phase transition. Glass transition is still under continuous research whether some phase transition is underlied within. In the amorphous state, partial movements of parts of the polymer chains in a large scale are difficult to occur. By heating the amorphous material up to the glass transition temperature, the sectional movements of the polymer chains are activated and this transition is monitored and expressed via a characteristic curve in the DSC thermograph (Figure 4.5).

Differential scanning calorimetry may provide useful information about the glass transition temperature of block copolymers also. For a diblock copolymer, if two glass

transition temperatures exist, similar to the glass transition temperatures of the corresponding homopolymers, then the two different blocks are considered well separated. If three different glass transition temperatures exist (two close in value with the corresponding homopolymers and one somewhere in between), then the two phases are weakly separated due to partial mixing. Finally, when only one glass transition temperature appears between the glass transition temperatures of the two blocks, it normally means that there is a homogenous mixture of these two components with no phase separation or that the two blocks exhibit glass transition at identical temperatures as in this study (e.g. PS-PCHD diblocks).

CHAPTER 5

Instrumentation and Theory of Morphological Characterization

5.1 Transmission Electron Microscopy (TEM)

Transmission electron microscopy (TEM)[129-130] is a technique where an electron beam is used in order to magnify sample images. This requires operation in vacuum since air scatters electrons. The main advantage of using electrons instead of light is that they provide at least three (3) orders of magnitude increased resolution since they are smaller than atoms. The resolution provided by a visible-light microscope is approximately 200nm, while for an electron microscope it can go down as low as 0.1nm or lower. Many of the features that control the properties of materials are on a scale well below 200nm, therefore, there is a need in nano/materials science and engineering to image details, all the way down to the atomic level, in order to understand and ultimately control the properties of materials. In electron microscopy, the sample is exposed to an electron beam and through the interaction of the electrons with the sample, information for its structure are received. Electron microscopes are available for microscopic polymer analysis since 1940 where Knoll and Ruska first proposed the idea for which the latter received the Nobel Prize in Physics at 1986, shortly before his death in 1988.

Transmission electron microscope is a powerful instrument for studying the structure of biological and polymer materials. The potentials of this technique are not limited only to high resolution images, but also to the creation of small diameter domains for studying local changes of the chemical composition or the crystalline structure which can be verified via spectroscopy or scattering techniques respectively. Nevertheless, in order for the electron beam to penetrate the sample as well as to secure restricted inelastic scattering (resulting in better images), the sample is required to be quite thin regardless its type.

The operating principle of TEM is based on the fundamental principles of optics. According to De Broglie, the wavelength λ of electrons is equal to:

$$\lambda = h / m\, v \qquad (5.1)$$

where h is the Plank constant, m the electron mass and v its velocity. Observing equation 5.1, it is obvious that the wavelength of electrons can be decreased by increasing their velocity. It is easier to think of the image resolution for TEM studied in terms of the classic Rayleich criterion for visible-light microscope (VLM), which states that the smallest distance that can be resolved, δ, is given approximately by the equation:

$$\delta = 0.61\, \lambda / n\, sina \qquad (5.2)$$

where λ is the wavelength of the radiation, n the refractive index of the viewing medium and a the semi-angle of collection of the magnifying lens. For the sake of simplicity, $n\ sin\ a$ (which

is also called numerical aperture) can be approximated to unity resulting in a significant dependence of resolution with the wavelength of the radiation. Combining equations 5.1 and 5.2 and the above approximation, the following equation is concluded:

$$\lambda = 1.22 / E^{1/2} \qquad (5.3)$$

where E is the electron energy in electron volts (eV). The wavelength of light is approximately 0.4nm-0.7μm while for an electron with E = 100kV it is almost 0.004nm, which is much smaller than the diameter of an atom.

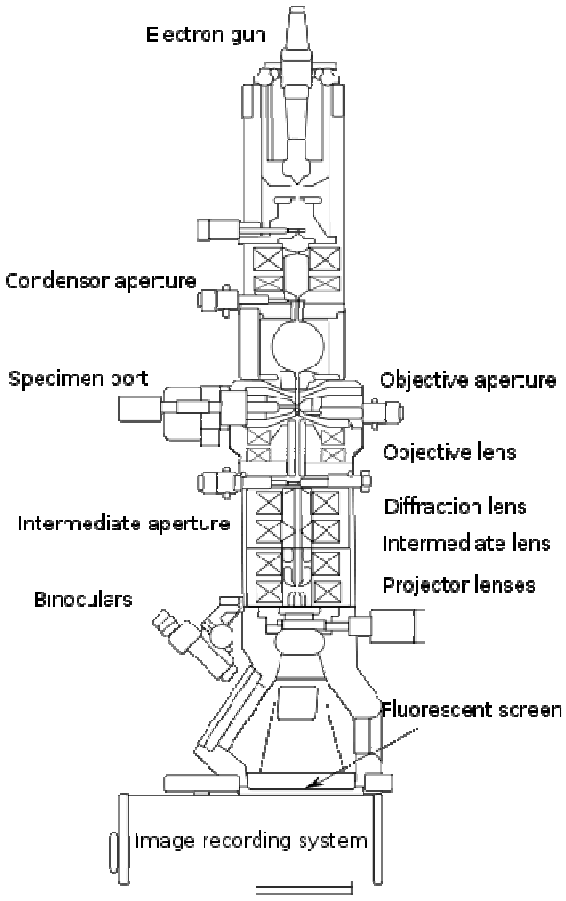

Figure 5.1: *Cross section scheme of a typical TEM instrument.*

In reality, the resolution of TEM is limited due to the spherical aberration of electron lenses but a new generation of aberration correctors has been able to partially overcome this drawback in order to increase resolution. Hardware correction of spherical aberration for the high-resolution transmission electron microscopy (HRTEM) has allowed the production of images with resolution below 0.5 angstrom (50 picometers) and magnification above 50 million times. The general set up of a TEM is similar to that of a VLM. The only difference is that the lenses are coils. A cross section of a TEM is given in Figure 5.1.

The transmission electron microscope consists of two basic parts, the illumination (Figure 5.2) and the image projection systems (Figure 5.3). The illumination system

comprises from the gun and the condenser lenses and its role is to take the electrons from the source and transfer them into the specimen. The electron gun is normally fitted with a tungsten filament cathode as the electron source. The electron beam is accelerated by an anode typically at 100-200 keV, while advanced TEMs can reach up to 1MeV which provides better examination of thicker specimens. The image projection system comprises from the objective lens, the intermediate lens, the diffraction lens, the projection lens, the viewing luminous screen for the observation of the specimen and the photographic camera. The first and most important magnification of the sample is performed by the objective lens where the rest of the lenses create the final magnification.

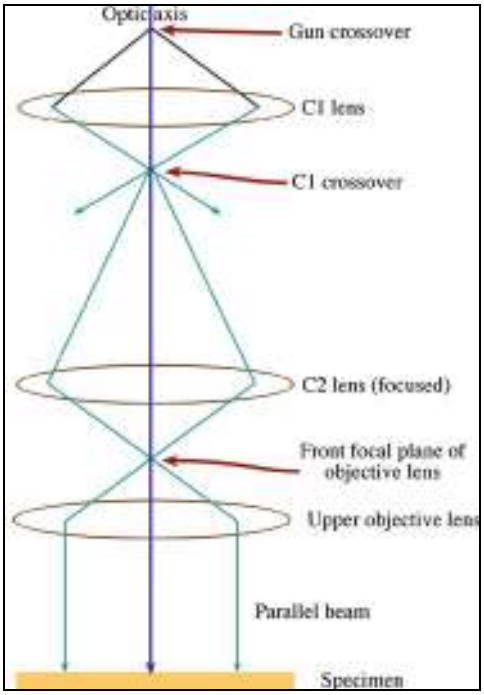

Figure 5.2: *The illumination system of typical TEMs using C1 and C2 lenses (condenser lenses) to image the source at the front focal plane (FFP) of the upper objective-condenser lens, thus creating a parallel beam*[129].

The transmission electron microscope can produce the image of the specimen by either the bright-field or the dark-field imaging methods. In bright-field mode, by inserting an objective aperture into the back focal plane (BFP) of the objective lens, only the direct-beam electrons are collected, while the scattering electrons are excluded. In this manner, the areas of the specimen that do not cause electron scattering appear bright, while those that cause electron scattering appear dark. In dark-field mode, by inserting a selected area diffraction (SAD) aperture into the image plane of the objective lens, only the scattering electrons from a specific diffracted beam are collected.

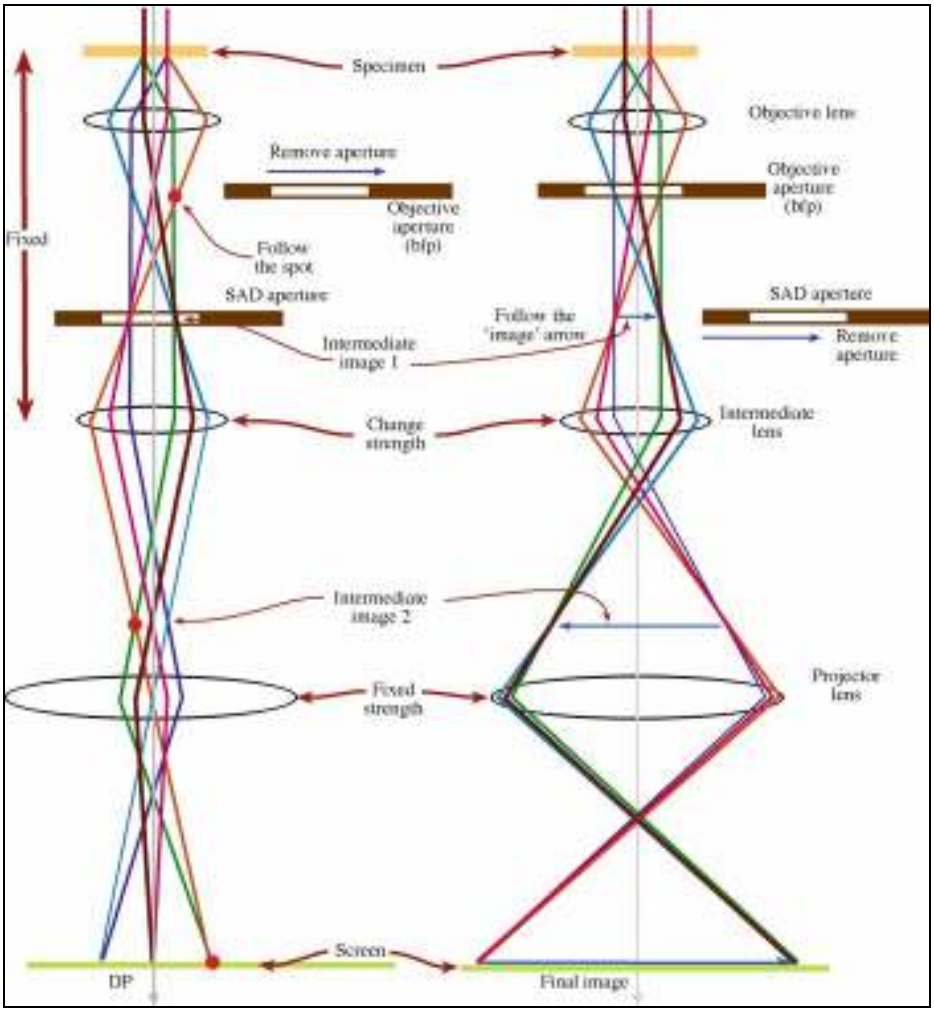

Figure 5.3: *The two basic operations of the TEM imaging system involve a) diffraction mode: projecting the diffraction pattern (DP) onto the viewing screen (showing on the left) and b) imaging mode: projecting the image onto the screen (showing on the right). In each case the intermediate lens selects either the back focal plane (BFP) (a) or the image plane (b) of the objective lens as its object*[129].

The creation of the image that appears on the viewing screen of a TEM depends on the image contrast. The electron wave can change both its amplitude and its phase as it goes through the specimen and both kinds of change lead to image contrast. Thus, a fundamental distinction that is made in the TEM is between amplitude contrast and phase contrast. In most cases, both kinds of contrast contribute to an image but there is a tendency to select conditions so that one will dominate. There are two principal types of amplitude contrast: mass-thickness and diffraction contrast. Mass-thickness contrast is resulted from variations in mass or thickness of the specimen or a combination of the two because the electrons interact, by incoherent elastic scattering, with more or less material which means more or less mass. Alternatively, diffraction contrast rises from coherent elastic scattering and can only vary locally since the specimen is not a perfect, uniformly thin film. Consequently, thicker or less crystallized areas of the specimen scatter electrons more and appear darker.

There are several ways to increase mass-thickness contrast by using smaller objective apertures, by alternating the beam accelerating voltage or by chemically staining the sample with heavy metal oxide compounds such as osmium tetroxide or ruthenium tetroxide. By decreasing the dimensions of the objective aperture, more scattered electrons are excluded. In contrast, by decreasing the objective aperture size, the radiation intensity is decreased, thus the intensity of projecting image is decreased. When the beam accelerating voltage is reduced, the beam energy is reduced also resulting in increased scattering and image contrast since in this case electrons remain more time in the structure of the sample. The disadvantage is the possible destruction of the specimen due to the increased remaining time of electrons in its structure leading to increased interactions between the electrons and the sample molecules.

The third method for increasing image contrast and most commonly used in polymer science is staining with heavy metal oxide compounds. Staining involves the incorporation of electron dense atoms into the polymer structure in order to increase the density and thus enhance image contrast. In block copolymers where one of the blocks is a polyiene, the most commonly used staining compound are diluted vapors of osmium tetroxide (OsO_4) in an aqueous solution which react with the carbon-carbon double bonds enhancing the image contrast due to cross-linking and the electron scattering due to the heavy metal. This cross-linking or bridging is a chemical reaction which causes hardening and increased density. The high vapor pressure of OsO_4 is beneficial, making vapor staining of sample sections possible. However, this vapor pressure, along with the toxicity of the compound and the limited exposure time, makes it extremely dangerous to use and appropriate care must be taken by any means. The reaction that takes place is shown in Scheme 5.1:

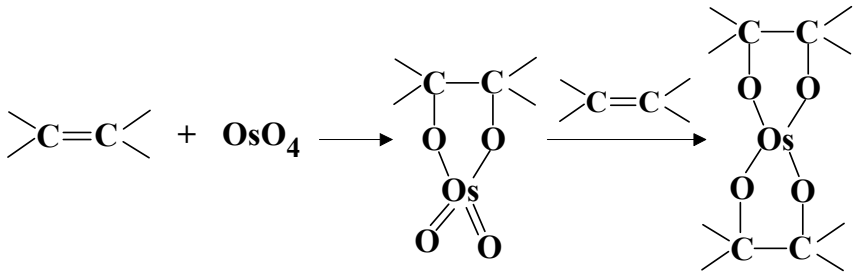

Scheme 5.1: *Reaction of osmium tetroxide (OsO_4) with the double C-C bonds of a polydiene.*

The result of this staining is that the polydiene phases appear darker while the phases of the other blocks appear brighter. This method is commonly used in polystyrene-polydiene copolymers as OsO_4 does not react with polystyrene. Similar results also are provided with ruthenium tetroxide (RuO_4) which reacts with polystyrene and it is primarily used for staining copolymers of polystyrene with polyolefines. There are also other types of staining compounds such as chlorosulfonic acid with uranyl acetate, phosphotungstic acid etc.

5.2 Small Angle X-Ray Scattering (SAXS)

Small angle X-ray scattering (SAXS)[131] is one of the most important techniques of molecular characterization of polymers and it is complimentary with transmission electron microscopy. The method is accurate, non-destructive and usually requires a minimum of sample preparation. The particle or structure sizes that can be analyzed range from 1-50 nm in a typical set-up but can be extended on both sides by measuring smaller angles (Ultra Small X-Ray Scattering, USAXS) or larger angles (Wide Angle X-Ray Scattering, WAXS) between the typical 0.1^0 and 10^0 of SAXS.

In SAXS, X-rays are produced by a source irradiating a sample. Usually the source is an X-ray tube but there are cases where the source can be also a synchrotron, especially when high beam intensities or unusual wavelengths are required. X-rays are electromagnetic waves just like visible light, but with shorter wavelength (~0.1nm). Sometimes, X-rays are described as particles which are called photons, therefore, every interaction between X-rays and matter can be described by two models, the oscillation model (wave) and the impulse-transfer model (photon).

Scattering can occur with or without energy loss. This means that the scattered radiation can have a different wavelength than the incident radiation, as in Compton scattering (incoherent scattering),[132] or it can have the same wavelength with the incident radiation, as in Rayleigh scattering (coherent scattering).[133] Compton scattering is produced when a photon hits an electron and is bounced away. The scattering radiation has different wavelength from the incident one and it cannot produce interference phenomena, therefore, it does not provide any structural information and it is part of the background radiation. Rayleigh scattering is produced when photons collide with strongly bound electrons. The electrons start to oscillate emitting radiation with the same frequency as the incident radiation. The waves produced are coherent which have the capability to interfere at the detector and therefore, these interference patterns contain information concerning the particle structure of the sample. This interference can be constructive or destructive depending on the orientation of the particles, the observation angle 2θ and the distance r of the light-emitting atoms from each other (Figure 5.4). In constructive scattering the interference causes a bright spot at the detector while in destructive scattering interference causes a dark spot at the detector since the waves extinguish each other. The result is a 2D interference pattern, where the intensity varies from position to position. The interference pattern is characteristic for the internal structure of a material, which means the orientation of the particles and the distances between them are very significant.

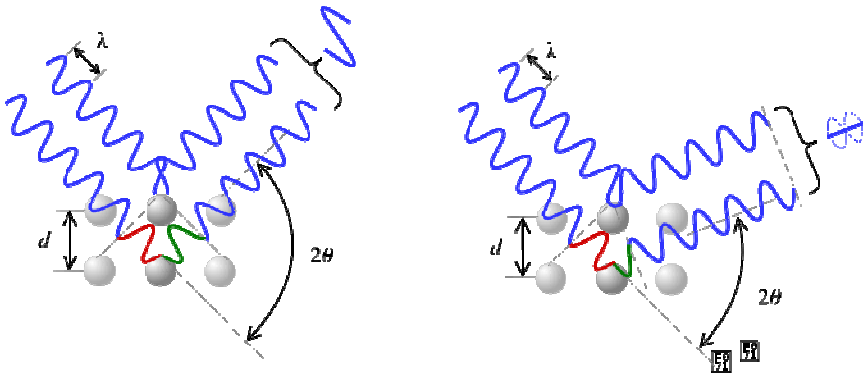

Figure 5.4: *Constructive (left figure) and destructive (right figure) scattering. When the wave is parallel, the detector receives brightness and when the wave is anti-parallel the detector receives darkness*[132].

Scattering patterns are usually presented as a function of q which is called either length of the scattering vector or momentum transfer and is given by the following equation:

$$q = 4\pi \sin\theta / \lambda \qquad (5.4)$$

The form factor is a significant feature of scattering patterns. The scattering from one particle, which includes many electrons/atoms, can be explained as the interference pattern produced by the emitting waves that are sent to the detector from each one of these electrons/atoms of the particle. By summing up all the wave amplitudes at the detector and making the square of this sum, results in an interference (scattering) pattern which oscillates in a fashion which is characteristic of the shape (form) of the particle and it is called form factor. There is also an additional interference pattern which is called structure factor and it is created when very densely packed particle systems (i.e. concentrated samples) are examined, where the distances between the particles are so short that come into the same order of magnitude with the distances inside the particles. As a result, the interference pattern of these particles will contain coherent contributions of the neighboring particles as well. In SAXS curves, concentration effects become visible by the formation of a descent in intensity and a small overshoot at the edge. Eventually, this overshoot can be transformed into a peak when the particles are well aligned and periodically oriented. This peak is called Bragg peak and the position of its maximum (q) indicates the distance (d) between the aligned particles using Bragg's law:

$$d = 2\pi / q \qquad (5.5)$$

By combining equations 5.4 and 5.5, the following equation is generated:

$$n\lambda = 2d \sin\theta \qquad (5.6)$$

where n is an integral number, λ the wavelength of the incident radiation, d the distance between the lattices and θ the observation angle between the radiation and the lattices (Figure 5.5).

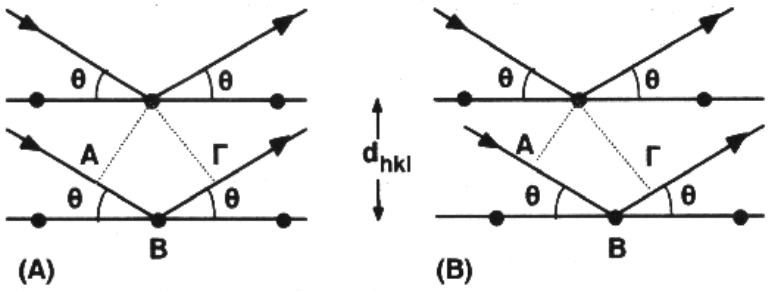

Figure 5.5: *Bragg's law for a rectangular unit cell. In case (A) AB=B=d sinθ and the wavelength distance is AB+BΓ=2 d sin θ. In case (B), which is more common, AB#BΓ but the wavelength distance is the same as well.*

Everything that is inserted inside an X-ray beam, even air, produces scattering, therefore, the use of vacuum in the sample-to-detector distance is very crucial. Furthermore, special sample holders are employed in order to fulfill the requirements of each sample (e.g. heating measurements). Typical sample sizes for solids are 1x1 mm^2 to 1x20 mm^2 while the sample thickness should be approximately smaller than or equal to 1mm.

The basic parts of a SAXS instrument are the source, the collimation system, the beam stop and the detector. In most cases, the source is an X-ray tube or a rotating anode and alternatively synchrotron facilities are employed for higher photon flux or to cover more wavelength requirements.

The most challenging part, is to separate the incoming beam from the scattered radiation at small angles (0.1^0). If the incoming beam has a larger divergence than this 0.1^0 requirement, then it is difficult to distinguish the relatively weak intensity of the scattering pattern of the sample from the much higher intensity of the direct beam. Therefore, the divergence of the direct beam must be kept very small. Hence, a collimation system is required. This is basically a system of pinholes or slits where the beam has to pass through them. In order to reduce the beam intensity considerably, these pinholes/slits must be narrow and/or somehow far away from each other. Additionally, the X-rays that come directly from the source are polychromatic, which means that they produce photons with different wavelengths. These photons are scattered into different directions, depending on their wavelength, resulting in the broadening of the scattering curves (wavelength smearing). In order to prevent this broadening, multi-layer optics can be inserted into the collimation system. These optics diffract only one particular wavelength and this wavelength can be selected by rotating the optics with respect to the direction of the incident beam. The

collimation systems that are employed for SAXS instruments are two, the point collimation system and the line collimation system (Figure 5.6).

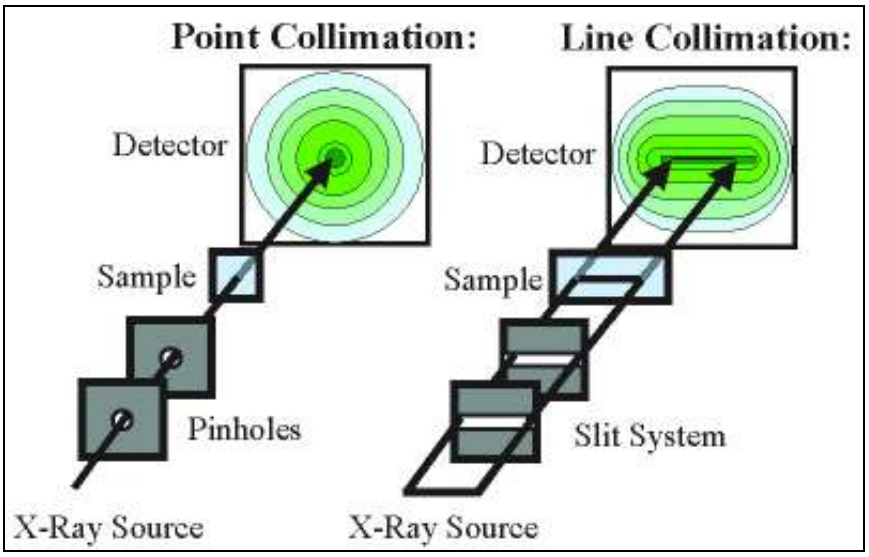

Figure 5.6: *The two collimation systems generally used in SAXS instruments*[132].

The point-collimation system: This system has pinholes that shape the beam to a small circular or elliptical spot which means that only a small domain of the sample is illuminated. The beam dimensions on the sample are usually 0.3 x 0.3 mm^2. The scattering is therefore centro-symmetrically distributed around the illuminated spot and the 2D pattern in the detection plane consists of concentric circles around the primary beam (Figure 5.6). An advantage of this system is that the scattering patterns have only minor instrumental broadening which is neglected in data evaluations. A disadvantage is that due to the small illumination volume, the scattered intensity is relatively weak. Furthermore, it is quite difficult to obtain a very narrow and clean beam, which generally results in poor resolution. In order to overcome this, usually the distance between the sample and the detector is increased. But this makes the instrument large and decreases the intensity at the detector. Consequently, the time measurement with point-collimation systems is in the order of hours or sometimes days.

The line-collimation system: In this system, the beam is confined only in one direction, so that the beam profile is a long and narrow line with dimensions approximately 20 x 0.3 mm^2 (Figure 5.6). The illuminated sample volume is approximately 50 to 100 times bigger than in point-collimation systems and the scattered intensity is, therefore, equally bigger. The beam profile can be made narrow enough and much cleaner than in the point-collimation system which results in smaller sample-to-detector distance. Consequently, the intensity is approximately 10 times higher and the measurement time is 500 to 1000 times shorter than in point collimation system. The large illumination volume of the sample however causes

broadening of the scattering pattern. This broadening effect can be eliminated by an additional mathematical treatment which is called desmearing and can be performed by several software programs.

The beam stop is used in order to prevent the direct beam from hitting the detector. Although some detectors are not necessarily destroyed from the direct beam, the intensive back scattering from the detector material overshadows the relatively weak signal from the sample. Two different types of materials are used as beam stops. One type consists of dense materials such as lead or tungsten, that block off the direct beam completely. The other type consists of transparent materials which attenuate the beam into an intensity that can be handled safely by the detector.

Three different types of detectors are used in SAXS, the wire detectors, the CCD (Charged-Couple Device) cameras and the imaging plates.

The wire detectors: These detectors have thin parallel wires inside an absorbing gas atmosphere. They usually provide large pixel sizes (around 100μm) and therefore have a poor spatial resolution. In order to cure this, larger sample-to-detector distances are employed at the cost of decreased angular range and reduced intensity. Wire detectors can be easily damaged by overexposure and they are costly to maintain.

The CCD cameras: They either detect X-ray photons directly (solid state detectors) by counting the secondary electrons that are produced inside a semiconductor material or they detect visible light that is produced by a fluorescent screen attached to a semiconductor chip. Usually they suffer from high dark-count rate which depends on the chip temperature and the acquisition time. Fortunately, these detectors are equipped with on-chip binning in order to connect neighboring pixels and increase the sensitivity. The chip sizes are relatively small though, which limits the angular range, but the pixel size is also small (around 25μm) which provides high resolution results. The prices of CCD cameras are relatively high and depend on the chip quality which is measured by number of failing pixels.

The imaging plates: These detectors are flexible sheets which are exposed like photographic films and scanned by a separate device in a second step. They have the highest linear dynamic range of all known detectors and they can be produced in any shape and size. But they need to be scanned by an external device, which makes automated experiments difficult. The dark-count rate depends on this scanner device but is usually small and easy to subtract. Also the pixel size is depended on the scanner device and lies between 25 and 100μm. The maintenance cost of the imaging plates is relatively low and they are not easily damaged by overexposure.

The scattering pattern produced by a well-organized sample, such as block copolymers, has similarities with the scattering of a crystalline material. The only significant difference is that the Bragg scattering occurs in smaller angles which correspond to larger

repeating distances than those of the dimensions of a crystal unit cell. In the case of copolymers that exhibit microphase separation in weak or intermediate segregation limit, sometimes different phases are created with varying interface thickness depending on the degree of separation. The existence of different phases in the unit cell structure results in a significant decrease of the structure factor as a function of q and the appearance of low scattering patterns (absence of peaks in the lnI (q) = f(q) diagram).

The scattering patterns received from small angle X-ray scattering are characteristic for the structure of an equilibrium morphology for a block copolymer. For lamellar morphology, a scattering pattern is expected where the q ratio in regard with the first scattering exhibits 1:2:3:4… values. This morphology is periodic in one dimension, while in the case where $\varphi = 0.5$ the even order reflections are eliminated. For cylindrical morphology, the hexagonal lattice of the cylinders is two dimensional and the corresponding group symmetry allows only restricted number of reflections which are in agreement with the $1:\sqrt{3}:\sqrt{4}:\sqrt{7}:\sqrt{9}\ldots$ ratio. For spherical morphology, the lattice is periodic in three dimensions and the allowed reflections for a body centered cubic lattice are in agreement with the $\sqrt{2}:\sqrt{4}:\sqrt{6}:\sqrt{8}:\sqrt{10}:\sqrt{12}\ldots$ ratio or simply the $1:\sqrt{2}:\sqrt{3}:\sqrt{4}:\sqrt{5}:\sqrt{6}\ldots$ ratio. Generally, samples with spherical morphology exhibit relatively low order which results in a small number of peaks in the scattering pattern. Finally, in cubic morphologies, such as the gyroid*, the unit cell exhibits a cubic symmetry and the periodicity applies in three dimensions. This morphology belongs in the $la\overline{3}d$ space group and the allowed reflections are in agreement with the $\sqrt{6}:\sqrt{8}:\sqrt{14}:\sqrt{16}:\sqrt{20}:\sqrt{22}\ldots$ ratio or more simply with the $\sqrt{3}:\sqrt{4}:\sqrt{7}:\sqrt{8}:\sqrt{10}:\sqrt{11}\ldots$ ratio if the initial ratio is divided with $\sqrt{2}$.

CHAPTER 6

Experimental Part

6.1 The High Vacuum Technique

The synthesis of the linear diblock copolymers and the complex architecture copolymers was accomplished via anionic polymerization by combining the high vacuum technique and well-known purifying procedures for all reagents and solvents[69,70]. This technique is used in order to remove impurities such as oxygen, carbon dioxide and moisture from the reagents. These impurities, during the polymerization, can react rapidly with the initiator or with the living anionic centers, according to the following reactions (Scheme 6.1), leading to undesirable termination or/and transfer reactions.

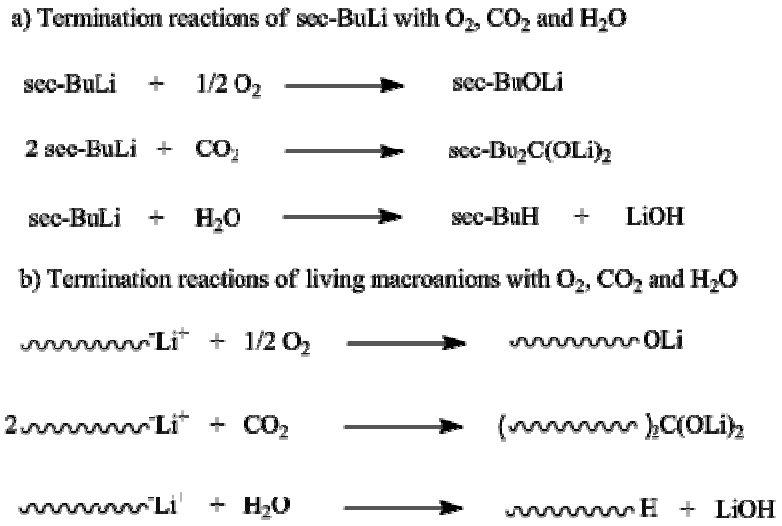

Scheme 6.1: *Termination reactions of the initiator sec-BuLi as well as of the living macroanions with O_2, CO_2 and H_2O.*

The purification procedures of all reagents (monomers, solvents, initiators, linking reagents, termination reagent) as well as the polymer synthesis procedures were performed on the high vacuum line, which is exhibited in Figure 6.1.

Figure 6.1: *Image of a high vacuum line in UOI Polymers Laboratory.*

The high vacuum line consists of an oil pump which is capable of producing vacuum at an order of 10^{-2} mm Hg. Furthermore, by using a mercury diffusion pump and a thermomandle, the distillation of mercury is possible, creating high vacuum (~ 10^{-6} mm Hg). The operation of the diffusion pump is based upon the diffusion of mercury vapors through a very narrow section which creates an increase in the speed of mercury molecules and according to Bernoulli's law, sub pressure, leading to a vacuum of the order of 10^{-6} mm Hg (Figure 6.2).

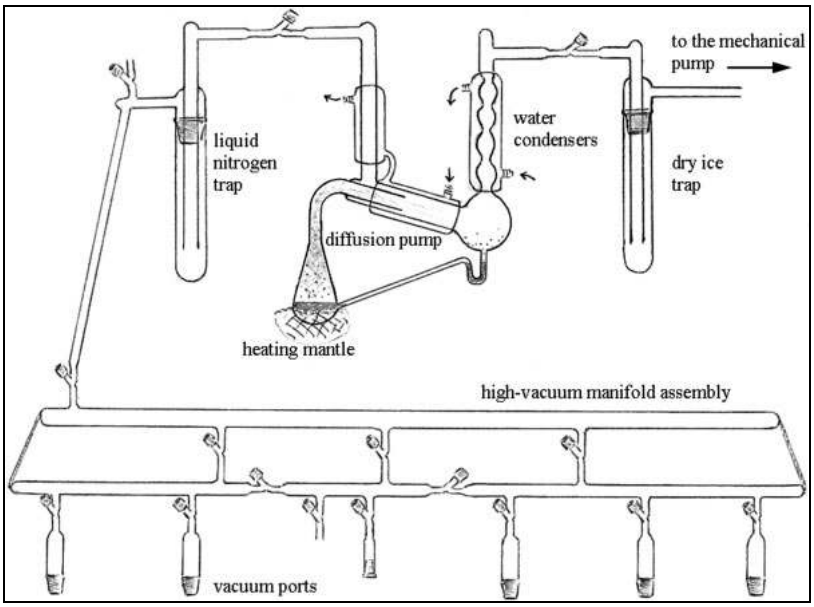

Figure 6.2: *Schematic illustration of a high vacuum line*[70].

The expression of this law is as follows: "When an uncompressible liquid flows through a pipe with variable dimensions, its velocity changes. When a part of the uncompressible fluid is accelerated, its movement should be performed from a high pressure area to a low pressure area in order to create the total force which accelerates the fluid. Consequently, when the dimensions of the pipes are variable, the pressure changes too, independently of the corresponding height difference". During the contact of mercury with the condenser walls, it condenses and returns in the heating glass vessel where the procedure is repeated. There are two traps for the protection of the oil pump, one of them with liquid nitrogen, which collects the volatile components from the reagents. The diffusion pump is connected through glass tubes (pyrex) with the main part of the high vacuum line. In order to manipulate the vacuum into the high vacuum line, Teflon high vacuum stopcocks are used (their main parts are made of pyrex) which also help to isolate parts of the high vacuum line when necessary. The connection with the vacuum line is performed through ground joints and depending on the procedure (solvent purification, monomer distillation etc.), properly made glass apparatuses are adjusted on these ground joints. Special safety features must be taken

into account while working on the high vacuum line (safety glasses, lab robe etc.) as well as great care must be taken during its use when specific reactions are taking place.

6.2 Solvent Purification

Benzene

Benzene is usually purified by transferring a proper amount, from the as commercially received, in a round bottom flask containing fresh finely grounded CaH_2 and a magnetic stir bar. Then it is attached carefully to the vacuum line, degassed and left for reaction of moisture with CaH_2 overnight. All gasses in the flask (like O_2, CO_2 and CO) are removed via degassing. Then it is degassed again twice and distilled in a calibrated cylinder containing n-BuLi and styrene in a 7:1 ratio which simultaneously react under vacuum creating $PS^{(-)}Li^{(+)}$ living ends. The persistence of the bright orange color of $PS^{(-)}Li^{(+)}$ indicates the purity of the solvent (Figure 6.3). Various quantities of the purified benzene are distilled into the polymerization or initiator or other type apparatuses when necessary.

Figure 6.3: *Picture of a cylinder with (polystyryl)lithium living ends in benzene attached on the vacuum line.*

Tetrahydrofuran (THF)

Tetrahydrofuran is usually refluxed over dispersed sodium (Na) for approximately 4 hours and it is collected in a round bottom flask containing fresh finely grounded CaH_2. Then, this flask is attached on the vacuum line, degassed and left for reaction of moisture with CaH_2 overnight. The next day, THF is degassed again 2-3 times, distilled in a flask containing sodium/potassium (Na/K) reactive alloy in a 1:3 ratio and stirred rapidly. The bright blue color which develops due to the existence of free potassium electrons after stirring for some time indicates that the solvent is free from impurities and especially humidity (Figure 6.4).

Figure 6.4: *Picture of the flask with THF in Na/K alloy attached on the vacuum line.*

6.3 Monomer Purification

Styrene (St)

Proper amount of styrene as commercially received is transferred in a round bottom flask containing fresh finely grounded CaH_2 which is attached on the vacuum line through a short path distillation apparatus. It is degassed once and stirred overnight in order for the CaH_2 to react with moisture. Then it is degassed again twice and distilled in a round bottom flask containing an appropriate amount of dibutylmagnesium (Bu_2Mg) in heptane ([monomer]/[Bu_2Mg] = 25/1) which has been introduced via a pyrex attachment through an elastic septum. Styrene is left to react with Bu_2Mg for at least 3 hours over stirring, it is degassed once more and it is finally distilled in calibrated ampoules and kept at -20^0C. The compound Bu_2Mg for the final purification step is preferred due to its higher solubility in hydrocarbon solvents. It is also important to mention that styrene should not remain in the Bu_2Mg solution additional time because since it will start to polymerize rapidly. Furthermore, other organometallic compounds cannot be used as in the case of dienes (ex. n-BuLi) since styrene is polymerized rapidly (in less than 30 minutes) and the reaction is highly exothermic.

1,3-Cyclohexadiene (CHD)

Initially, proper amount of as commercially received 1,3-cyclohexadiene is transferred in a round bottom flask containing fresh finely grounded CaH_2, attached on the vacuum line, degassed and left for reaction of moisture with CaH_2 overnight. The next day it is degassed again, distilled in a flask containing a sodium mirror and is left under stirring overnight. Then, cyclohexadiene is degassed and distilled in two more flasks containing sodium mirrors remaining at least one hour in each one. Afterwards, CHD is distilled in a flask containing n-BuLi in hexane (the solvent is removed in the vacuum line) and left over

stirring for half an hour at 0^0C. Finally it is distilled in calibrated ampoules and kept at -20^0C for a short period of time (less than 10 days) (Figure 6.5).

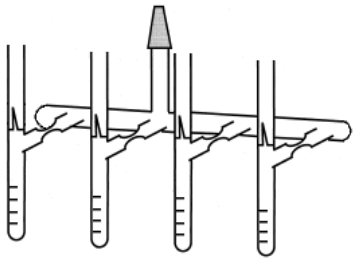

Figure 6.5: *Apparatus with calibrated ampoules for the distillation of the purified 1,3-cyclohexadiene. The same apparatus is used for the case of styrene as well.*

6.4 Dilution of the Initiator sec-Butyllithium

For the synthesis of the homopolymers and the linear diblock copolymers of this thesis, sec-BuLi was used as the initiator. This organometallic compound is very reactive, especially with air components such as CO_2, O_2 and H_2O. These undesirable reagents can lead to deactivation of the initiator, and therefore, uncontrolled polymerization might take place leading to non-monomodal samples as well as to increased molecular weights and polydispersities. The initiator sec-BuLi, as commercially received, is in high concentration (1.4M in hexane solution) and a dilute solution is needed in order to be used sufficiently for the required experiments. The dilution of the initiator is accomplished in a suitable apparatus with pre-calibrated ampules as shown in Figure 6.6:

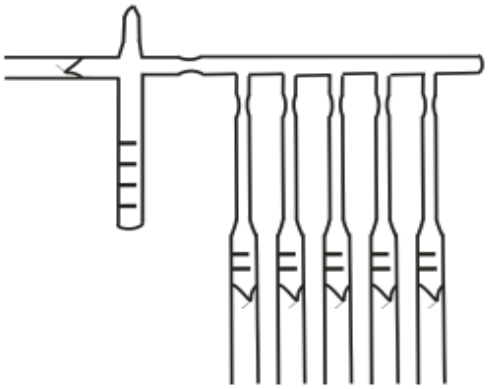

Figure 6.6: *Schematic of the apparatus used for the dilution of concentrated sec-BuLi with benzene or hexane to the needed concentration.*

First, the apparatus is connected on the vacuum line in order to achieve high vacuum. An amount of sec-BuLi (1.4M) is injected into the apparatus and the hexane is removed. Then, the necessary amount of benzene or hexane is distilled, the mixture is degassed and the apparatus is removed from the vacuum line through sealing off at the appropriate constriction

of the apparatus. The amount of benzene or hexane needed for the desirable concentration is calculated through the following equation:

$$C_1 V_1 = C_2 V_2 \qquad (6.1)$$

where C_1 is the initial concentration of sec-BuLi (usually 1.4M), V_1 the initial amount of sec-BuLi injected in the apparatus, C_2 the final concentration needed and V_2 the appropriate amount of benzene in order to achieve this concentration.

6.5 Purification of the Polar Additive DABCO (1,4-diazabicyclo[2.2.2]octane)

DABCO (molar mass = 112.2 g/mol) is a solid reagent (T_m = 158 - 160^{0}C) and is purified by triple sublimation via the apparatus shown in Figure 6.7. The appropriate quantity of DABCO is inserted in area B through the ground joint A. The apparatus is attached on the vacuum line through A and degassed. Then, DABCO is sublimated to location C using liquid nitrogen while heating location B with warm water or oil bath. After the first sublimation, two more are carried out transferring DABCO to areas D and E respectively. Afterwards, DABCO is diluted with benzene into the calibrated ampoule (E) and removed from the apparatus by heat-sealing on F, after degassing. This ampoule is adjusted to another apparatus and is diluted again with benzene until the desirable concentration is reached.

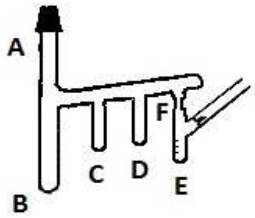

Figure 6.7: *Triple sublimation apparatus for the purification of DABCO.*

6.6 Purification of Naphthalene

Figure 6.8: *Photo of the apparatus for the purification of naphthalene, attached on the vacuum line.*

Naphthalene (molar mass = 128.17 g/mol, d = 1.14 g/cm^3) is an organic compound with molecular formula $C_{10}H_8$. It is the simplest polycyclic aromatic hydrocarbon and is a white crystalline solid (T_m = 80^{0}C) with a characteristic odor that is detectable even at concentrations as low as 0.08 ppm. The purification procedure (Figure 6.8) is the same as the purification procedure of DABCO.

6.7 Purification of the Linking Agents Dichlorodimethylsilane [$(CH_3)_2SiCl_2$], Trichloromethylsilane (CH_3SiCl_3) and Tetrachlorosilane ($SiCl_4$)

The purification procedure is the same for all these three linking reagents. Initially each one of them is transferred into a round bottom flask containing fresh finely grounded CaH_2. Then, it is attached on the vacuum line, degassed and left for reaction of moisture with CaH_2 overnight. The next day the round bottom flask is degassed again three to four times and a small amount is distilled into the whole apparatus with the calibrated ampoules in order for the corresponding silane to react with any possible impurities that may exist in the glass ampoule apparatus and to deactivate them. The remaining amount which has already reacted is distilled in the nitrogen trap through the vacuum line. After the completion of this procedure, the proper amount of silane is distilled into the calibrated ampoules and kept at -20^{0}C for significant time (~ 6 months).

6.8 Purification of Methanol (MeOH)

Methanol is transferred in a round bottom flask containing fresh finely grounded CaH_2, attached in the vacuum line, degassed and left for reaction of moisture with CaH_2 overnight. The next day is degassed again 3-4 times and distilled in small quantities into the necessary ampoules (Figure 6.9).

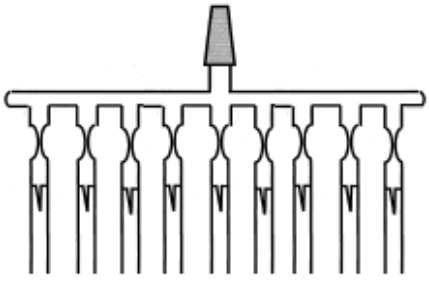

Figure 6.9: *Apparatus for the distillation of purified methanol into ampoules.*

Methanol is used as a termination reagent for anionic polymerization due to the following reaction (Scheme 6.2):

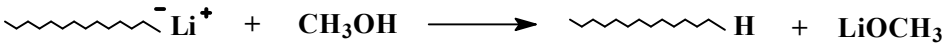

Scheme 6.2: *Termination reaction of macroanions with MeOH.*

6.9 Synthesis of Linear Diblock Copolymers

The synthesis of the linear diblock copolymers of polystyrene-b-poly(cyclohexadiene) (PS-b-PCHD) or poly(cyclohexadiene)-b-polystyrene (PCHD-b-PS) type was accomplished by the use of anionic polymerization and high vacuum techniques via sequential monomer addition. The main scope of the synthetic route adopted, was to synthesize diblock copolymers with narrow molecular weight distributions, predictable molecular weights and high 1,4-microstructure (~90%) for the PCHS segments. Seventeen (17) diblock copolymers were synthesized with varying molecular weights and volume fractions of the corresponding components. All polymerizations were accomplished by using benzene as solvent, sec-BuLi as the initiator and methanol as the termination reagent. For the successful polymerization of 1,3-cyclohexadiene in order for the final PCHD to exhibit high 1,4-microstructure (> 90%), the polar additive DABCO was used. The synthetic route that was adopted for both PS-b-PCHD and PCHD-b-PS diblock copolymers is shown in Scheme 6.3 and Scheme 6.4 respectively.

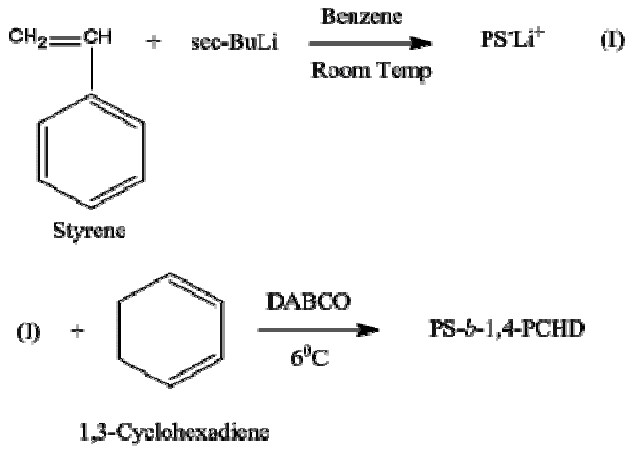

Scheme 6.3: *Synthetic route for the synthesis of the PS-b-PCHD diblock copolymers.*

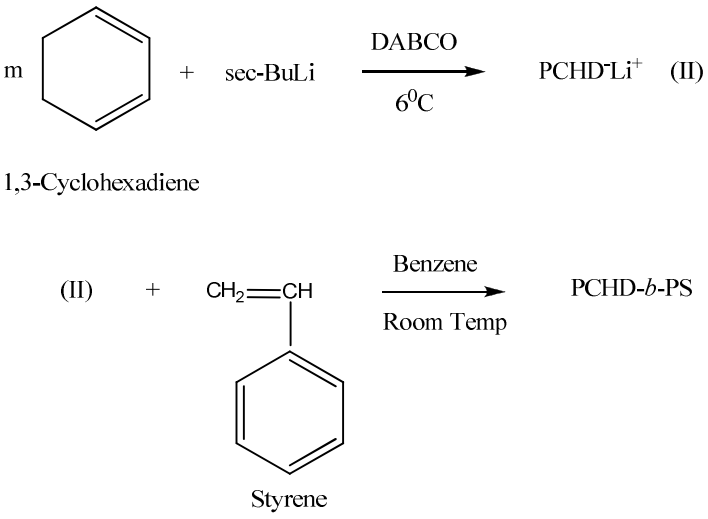

Scheme 6.4: *Synthetic route for the synthesis of the PCHD-b-PS diblock copolymers.*

The synthesis of the diblock copolymers was accomplished in the following apparatus (Figure 6.10):

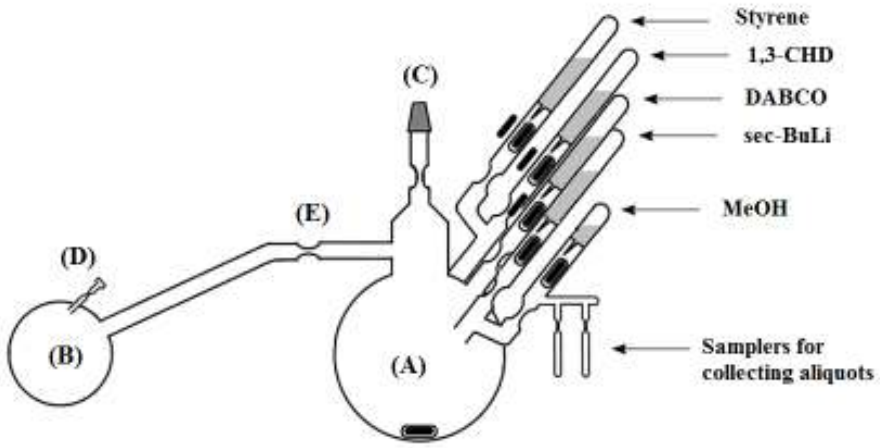

Figure 6.10: *Initial apparatus used for the synthesis of the PS-b-PCHD or PCHD-b-PS linear diblock copolymers.*

Initially, the appropriate glassblowing is performed and the ampoules of the monomers, the initiator, the polar additive and the termination reagent are attached on the apparatus. Then, the apparatus is attached to the vacuum line through the ground joint C, checked for pinholes by use of the Tesla coil and degassed. At this point, flame drying with a hand torch in order to accelerate degassing and remove any moisture traces is very useful. After the completion of degassing, a small amount (2-3 ml, depending on the solvent volume) of n-BuLi in hexanes is added with a syringe through the elastic septum at the side arm (small extinction in flask (B) at Figure 6.10. The elastic septum is rinsed and detached afterwards by sealing the constriction at (D) point and the small amount of hexane is distilled away into the nitrogen trap. The appropriate amount of benzene (solvent) is distilled from a purified reservoir, by using liquid nitrogen, into the spherical flask B through the vacuum line and as soon as the mixture is degassed, it is detached from the vacuum line by sealing off the constriction at area (C). The solution of n-BuLi and benzene is thawed and transferred 2-3 times to all the inner glass surface of the apparatus by carefully tumbling it. In this way, n-BuLi reacts with impurities that might exist in the apparatus and were not removed during its purification at ambient conditions. Then, the solution is collected at the purge recovery flask (B) which is placed into a hot bath of water (~45^0C) in order to rinse the apparatus and condense the solvent throughout it. This solvent is collected in the reactor flask and poured back into the purge recovery flask by carefully tilting the apparatus. Repeating this procedure periodically 10-15 times allows the collection of the remaining n-BuLi, along with its reaction products with impurities on the surface of the glass, back to the recovery flask (B). Then, the solution is collected in the purge recovery flask (B) and the pure solvent is gently distilled to the reactor flask (A) (Figure 6.11). The purge recovery flask (B) is immersed in a water bath

(~40^{0}C) while the reactor flask (A) following a procedure as exhibited in Figure 6.11 in an ice bath (~0^{0}C).

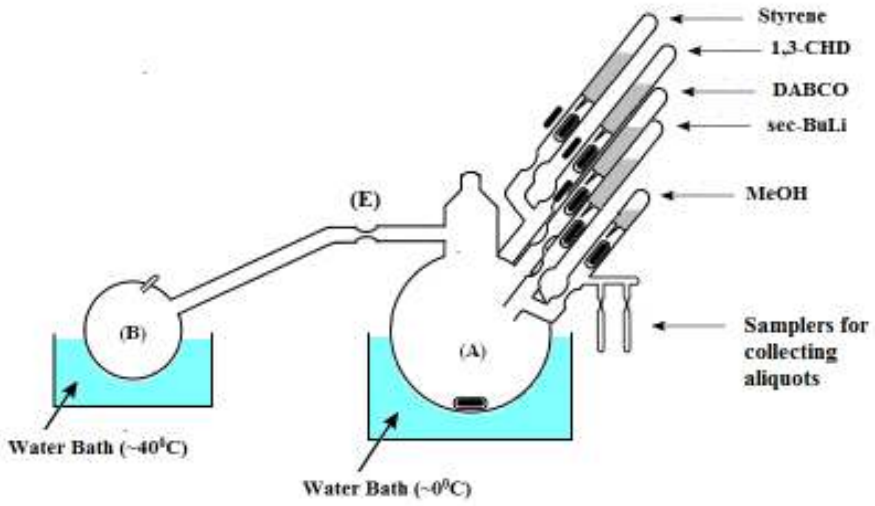

Figure 6.11: *Procedure adopted for distilling the pure solvent in the major polymerization flask (A).*

After the complete distillation of the solvent, the purge recovery flask is detached from the apparatus by sealing the constriction at point (E). The final polymerization reactor is shown in Figure 6.12.

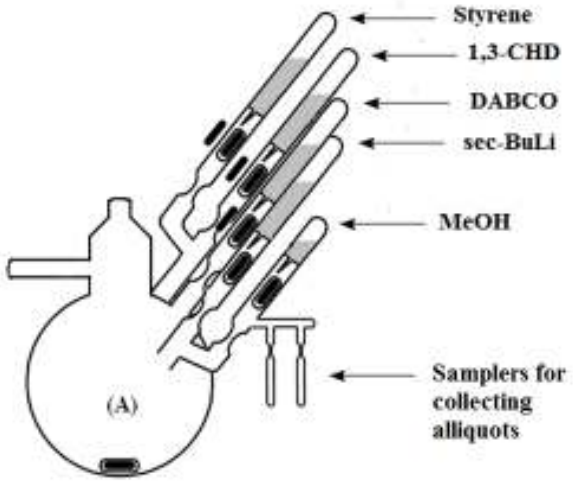

Figure 6.12: *The final polymerization reactor for the PS-b-PCHD or PCHD-b-PS linear diblock copolymers.*

When the solvent is warmed to room temperature, the break seals of the necessary reagents are ruptured through magnets sealed in pyrex glass and controlled by outside magnetic rods.

In a typical experiment for the synthesis of a PS-b-PCHD copolymer, 4 g of styrene (38.4 mmol) are added to the solution followed by the insertion of an appropriate amount of 2.85 ml of sec-BuLi solution (concentration of the initiator was 0.4M). In order to synthesize

PS chains of approximately $\overline{M}_n$ = 35.000 g/mol, the characteristic orange-red color is obtained immediately indicating the initiation of polymerization. In order to accomplish the mixing of the contents, one should carefully tumble the apparatus, rinse the ampoules well and collect all contents back to the reactor flask (A). Depending on the targeted molecular weight, the reaction is left to proceed between 12 to 24 hours. After the complete polymerization of styrene, a small aliquot for molecular characterization via SEC is obtained inside one of the attached samplers. Then, a 2.05 ml aliquot of the polar additive DABCO (0.111 mmol/ml in benzene) is introduced into the solution and is left to react for approximately 10 minutes. Prior to the addition of 1,3-cyclohexadiene, the solution is gently cooled down to ~6-7^{0}C. After the introduction of 2.69 g of 1,3-cyclohexadiene (33.6 mmol) into the reactor flask, the color of the solution changes into light-yellow which indicates the initiation of polymerization of the second monomer. The polymerization of 1,3-cyclohexadiene is left to proceed for 6 hours under stirring at constant low temperature and equal to 6-7^{0}C. Finally, the active copolymer is deactivated by rupturing the seal of the methanol, precipitated into methanol stabilized with proper antioxidant reagent, dried under vacuum at room temperature and finally stored at -20^{0}C for future use.

In the case of PCHD-b-PS copolymers, the initiator is first introduced into the reactor flask (A) followed by the addition of the polar reagent DABCO which is left to react for 10 minutes. Afterwards, 1,3-CHD is added in the mixture and left for polymerization for 6 hours under stirring at constant low temperature and equal to 6-7^{0}C. After the complete polymerization of the first block a small aliquot of the solution is obtained inside the attached samplers, as previously, for molecular characterization. At the final step, styrene is introduced in the solution and left to react until completion. In this case, the polymerization of styrene lasts shorter period of time due to the existence of the polar additive DABCO which changes the polymerization environment from non-polar to polar and therefore the aggregation degree is lower leading to faster kinetics. The rest of the synthesis steps are identical as in the PS-b-PCHD case. The PCHD-b-PS copolymers were synthesized in order to obtain higher molecular weights and volume fractions for the PCHD blocks. This occurs due to the fact that when 1,3-CHD is polymerized as the second monomer, termination and transfer reactions prevent the attainable molecular weight to reach high values in most cases.

One point that needs to be highlighted during these procedures is when rupturing the breaking seals of the ampoules. One should be aware of the vapor pressures of both sides and high volatile reagents (e.g. dienes, polar additives) should be cooled before the seal is broken in order to avoid moving the breaker (magnet inside pyrex glass) too forcefully and risking shattering it. A crucial point that needs attention is during the final rinsing of the polymerization reactor and during the final distillation of the solvent to the polymerization

reactor. It is very important to prevent the reacted n-BuLi solution to go through from the purge flask into the polymerization reactor. This unwanted procedure is avoided easily with a lower temperature differential than the motive of distillation making through the distillation of the pure solvent to last much longer.

Another important aspect is that for these diblock copolymers, fractionation in a solvent/non-solvent system was sometimes necessary. This occurred especially for higher molecular weights for the PCHD block where the termination and transfer reactions are stronger, leading to the broadening of the molecular weight distribution and to the termination of several anionic centers of either 1,3-CHD or styrene, depending on which monomer is polymerized first. For the fractionation of PS-b-PCHD copolymers, where needed, toluene was used as a solvent and methanol as non-solvent. For the fractionation of PCHD-b-PS copolymers, where needed again, toluene or chloroform was used as a solvent and a mixture of hexane/methanol as non-solvent.

Fractionation Procedure: Fractionation is the separation process in which a certain quantity of a mixture (solid/liquid) is divided up in a number of smaller quantities (fractions) in which the compositions change. In this case, the mixture comprises of the corresponding copolymer with the unwanted byproducts (which need to be removed), a solvent and a non-solvent. Depending on the polymer blocks that a copolymer comprises of, various systems of solvent/non-solvent can be adopted. Fractionation is performed in a separation flask equipped with a stopcock. Initially, the polymer mixture that needs fractionation is diluted in the chosen solvent under soft stirring, creating usually a solution of 2% wt or less, depending on the molecular characteristics of the mixture. The separation flask, without the stopcock, is placed in an annealing oven at approximately 150^0C and remains there until the following procedure is completed. The non-solvent (usually methanol) is added carefully to the diluted polymer mixture until the solution becomes cloudy, a procedure which depends exclusively on what are the molecular characteristics of the unwanted byproducts. If homopolymer exists, for example, the solution needs to become very cloudy in order to have in the lower phase the higher in molecular weight diblock copolymers. Then, the mixture is warmed up until it becomes transparent again, the separation flask is removed from the annealing oven, the stopcock is placed back again and closed, the mixture is transferred to the warm separation flask and is left to cool slowly down to ambient temperatures. During the introduction into the separation flask, the mixture should not touch the walls of the flask in order to maintain its homogeneity. It is of critical importance that the temperature of the mixture and the separation flask should be approximately the same during the introduction of the mixture into the separation flask. In this manner, the higher molecular weight macromolecules (higher fractions) will precipitate first by forming a lower layer of a more concentrated phase, while

the lower molecular weight macromolecules will form an upper phase. The two phases are described as the polymer rich phase and the polymer poor phase. The percentage of the wanted polymer in each phase depends on the molecular weight and the chemical composition. This type of fractionation is called "successive precipitation fractionation" and its success is monitored by usually taking small aliquots of the lower and upper phase for molecular characterization via SEC. If the results are not satisfying, the lower phase is collected and fractionated again until the complete elimination of the undesirable products.

6.10 Synthesis of the Linear ABA Triblock Copolymer

For the synthesis of the linear ABA triblock copolymer, where A is poly(cyclohexadiene) and B is polystyrene, sodium naphthalenide[134] was used initially as the difunctional initiator for the polymerization of styrene as the middle block. For the conjugation with the living $PCHD^{-}Li^{+}$ macroanions, the linking agent dimethyldichlorosilane was added to the difunctional polystyrene, followed by the addition of the PCHD as the outer blocks, forming the final PCHD-b-PS-b-PCHD triblock copolymer. The main purpose for the synthesis of this linear ABA triblock copolymer was to exhibit low molecular weight distribution, predictable molecular weight, appropriate microstructure for the polydiene and to successfully link the living outer blocks of poly(cyclohexadiene) with the difunctional polystyrene.

Synthesis of the Difunctional Initiator Sodium Naphthalenide

The initiation of the polymerization of styrene and dienes form sodium naphthalenide is very fast due to the electron transfer that occurs. The formation of this initiator depends on the nature of the polar and the hydrocarbon solvent mixture used. The polar/non-polar solvent mixture helps the electron transfer from sodium to naphthalene leading to stabilization of the forming compound through intramolecular exchanges with available electrons. The mechanism of the reaction relies on the electron transfer that occurs, leading to the formation of radical-anions of styrene that react rapidly with each other forming di-anions which are able to react with the remaining monomer units. In this way the propagation of the polymerization occurs leading to the formation of the α,ω-difunctional polystyrene.

For the synthesis of the difunctional initiator sodium naphthalenide, special procedures are followed. It is important to mention that the synthesis was performed under a polar environment and under controlled conditions while the concentration never exceeded 0.03 g/ml due to its pure solubility in higher concentrations. Initially, an appropriate glass apparatus (Figure 6.13) consisting of a purge section (A) which is also the main reactor and a collection flask (B) is made. It should be noted that this initiator is very sensitive in

impurities, therefore, special care is given on the purification of the polar solvent THF by adding purification steps as described below.

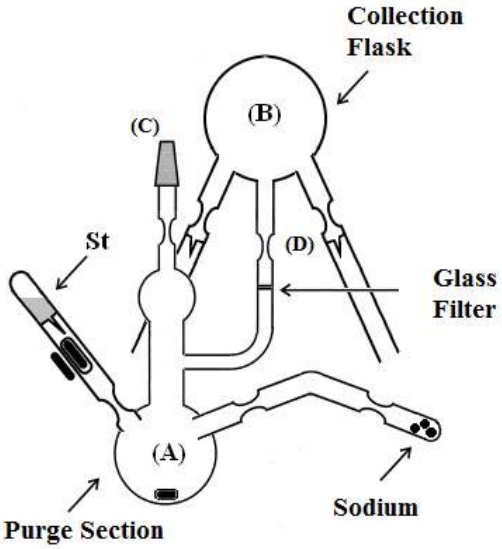

Figure 6.13: *Apparatus for the purification of THF.*

One ampoule containing a small amount of styrene (~1ml) and one properly formed side arm containing 3-4 small cubes of sodium, which will be used for the formation of a sodium mirror, are adjusted on the purge section (A). The collection flask (B) is connected with the purge recovery flask via a glass filter with an appropriate porous size in order to prevent sodium pieces from transferring into the collection flask. The apparatus is attached to the vacuum line, flame dried for any moisture traces and degassed. Then, with a soft-annealing flame, the formation of the sodium mirror is performed very carefully. When this procedure is completed, the appropriate amount (~80 mL) of the polar solvent THF is distilled into the main reactor and the apparatus is degassed again. It is detached from the vacuum line by sealing the constriction (C) and thawed to room temperature with tepid water. THF is transferred in the inner glass surface of the purge section and checked for its purity, since there will be deactivation of the sodium mirror if there are any impurities or moisture. Then, the styrene is introduced into the reactor and the orange-red color of the $PS^{-}Na^{+}$ anions is obtained which is characteristic of the reactivity and the purity of the solution. Polystyryl sodium in THF is left to react under stirring for one hour and then is transferred to the inner glass surface of the apparatus 2-3 times. In this way, polystyryl sodium reacts with any impurities that might exist. The solution is collected back to the reactor which is placed into warm water (~40^{0}C) in order to rinse the apparatus and condense the solvent throughout it. The solvent is collected in the collection flask and poured back into the main reactor (which is also the purge recovery flask) by carefully tilting the apparatus. Repeating this procedure

periodically 10-15 times allows the collection of the remaining polystyryl sodium, along with its reaction products with impurities on the surface of the glass, back to the main reactor. Then, the solution is gently distilled to the collection flask by immersing the purge section in a water bath (~25^{0}C) and the collection flask in an ice bath (~0^{0}C). Prior to the removal of the collection flask with the purified solvent (THF) by sealing the constriction above the glass filter (constriction D), the solution needs to be frozen since THF is very sensitive to thermal treatment.

For the synthesis of the sodium naphthalenide difunctional initiator, the apparatus shown in Figure 6.14 is used.

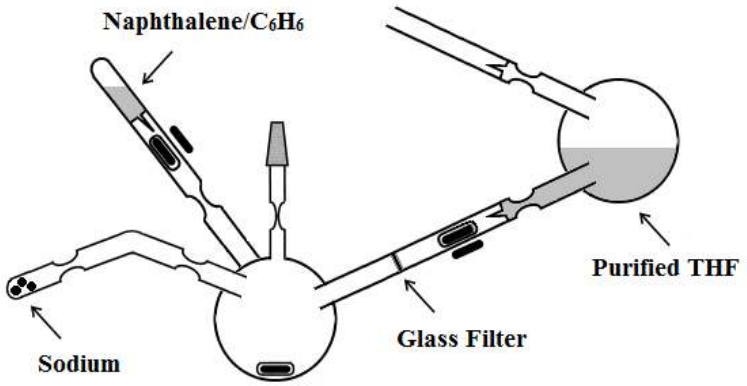

Figure 6.14: *Apparatus used for the synthesis of sodium naphthalenide.*

On the apparatus an ampoule of an appropriate amount of naphthalene (1 mL), properly diluted to the desired concentration in benzene (0.069 mmol/ml), the collection flask with the purified THF and a side arm which contains sodium are adjusted. The collection flask is again connected to the main reactor through a glass filter to prevent sodium pieces from transferring into it. The apparatus is attached on the vacuum line, degassed and the sodium mirror is created. It is detached from the vacuum line and the purified THF is introduced in the main reactor where it remains for several minutes in order to verify the purity of the solvent (otherwise the sodium mirror would have decomposed). Then, the naphthalene solution is introduced in the THF and the transparent solution turned into dark but clear green indicating the reaction of naphthalene with the sodium excess and the creation of the radical-anions of sodium naphthalenide. Then, the solution is left under stirring for at least two hours for the reaction to be completed, is transferred to the collection flask that initially contained purified THF, is cooled with liquid nitrogen and is removed from the apparatus by sealing the constriction above the glass filter. The difunctional initiator is ready to use and until the preparation of polymerization apparatus, it can be kept at -20^{0}C for approximately 12 hours. The reaction that takes place is shown in Scheme 6.5.

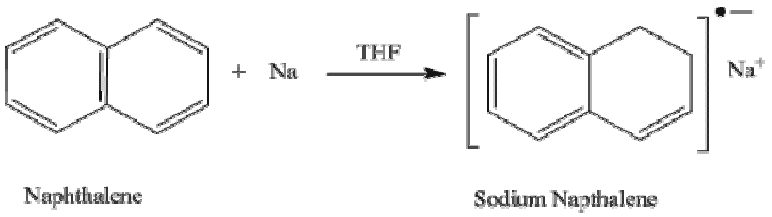

Scheme 6.5: *Synthesis reaction of the difunctional initiator sodium naphthalenide.*

An important aspect that needs to be mentioned is that the equation between the final molecular weight of the corresponding polymer (polystyrene in this case) and the difunctional initiator is the following:

$$\overline{M}_n = \frac{gr_{monomer}}{1/2 moles_{initiator}} \qquad (6.2)$$

Through equation 6.2, the concentration of the difunctional initiator is estimated in mmol/ml.

Synthesis of Difunctional Polystyrene and the Final PCHD-b-PS-b-PCHD Linear Triblock Copolymer

The apparatus that was used for the synthesis of the difunctional polystyrene is shown in Figure 6.15:

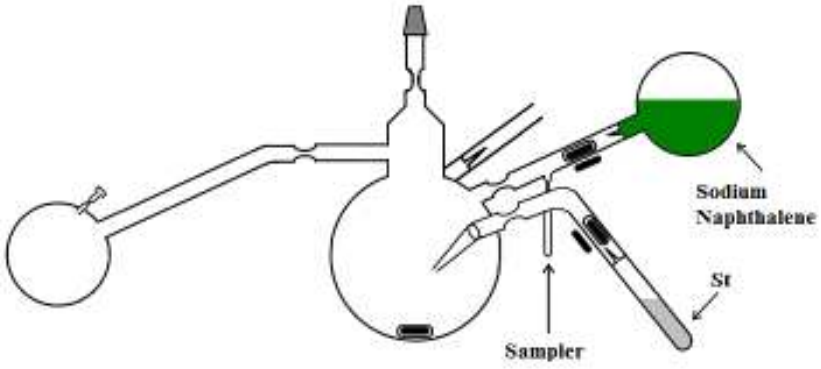

Figure 6.15: *Apparatus for the synthesis of the difunctional polystyrene.*

The ampoule containing styrene (1.6 g, 15.3 mmol) is connected with the polymerization reactor through a glass nozzle since styrene will be introduced in the reactor dropwise. The polymerization apparatus is attached on the vacuum line, degassed and 2-3ml of n-BuLi in hexane are injected. It is degassed again and the appropriate amount of benzene is distilled (100 ml), in order to adjust the ratio requirement of C_6H_6 : THF = 1.2:1. The system is degassed again and is detached from the vacuum line. The apparatus is rinsed by the same procedure described previously for the diblock copolymer synthesis and the purge section is removed. The polymerization procedure is different from the one previously

mentioned where manufactured initiators were used. Actually, through the double functionality, the polymerization initiates by synthesizing the middle block and then the outer blocks.

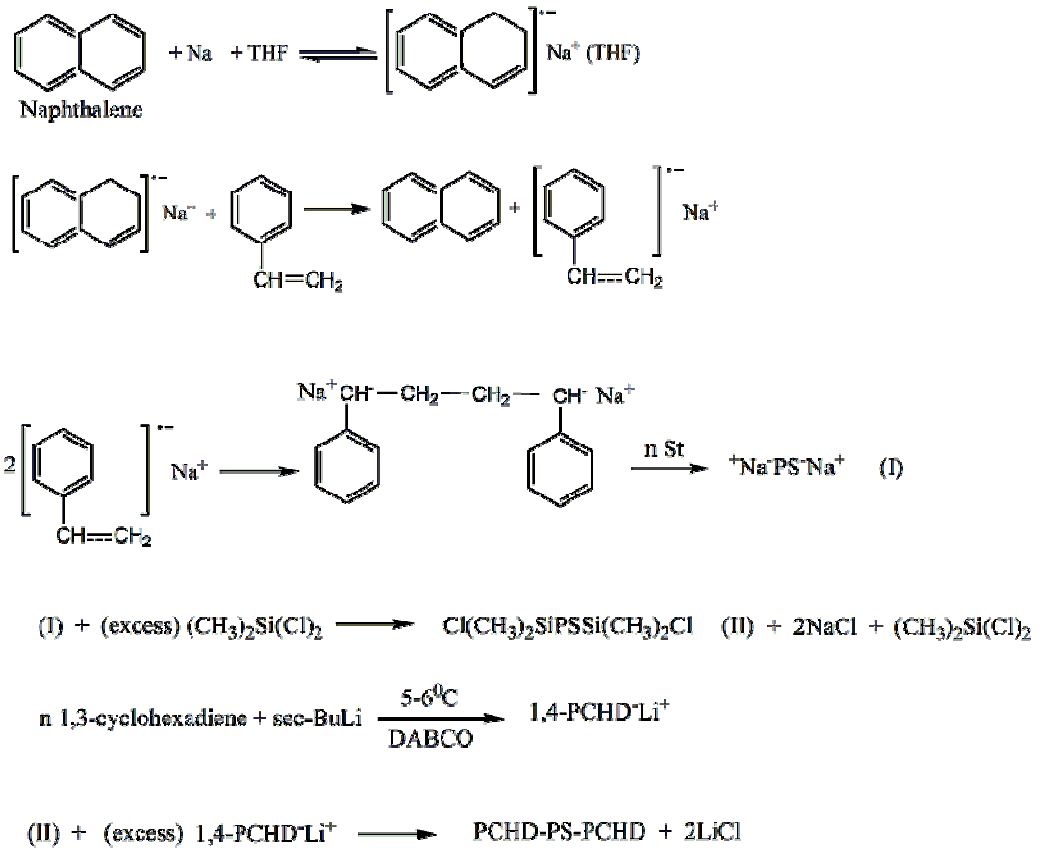

Scheme 6.6: *Synthesis reactions of the difunctional polystyrene, of the living poly(cyclohexadiene) arms and of the final PCHD-PS-PCHD linear triblock copolymer.*

The reactions that take place during the synthesis of the PCHD-b-PS-b-PCHD triblock copolymer are given is Scheme 6.6. Initially, benzene is mixed with sodium naphthalenide in THF. The solution must maintain its dark green color, which is an indication that the solution is very well purified, in order to proceed to the polymerization reaction. The solution is cooled down to -25^{0}C by using a mixture of isopropanol and nitrogen and is kept under stirring. Then, styrene is introduced dropwise into the polymerization reactor and the color changes immediately to red indicating the initiation of the polymerization. It is crucial to avoid local excess of styrene therefore the distillation from the ampoule to the main reactor is performed rather quickly and by using a warm water bath. The polymerization is left to complete for one hour by carefully keeping the temperature approximately at -25^{0}C and then a small aliquot is taken in the sampler for molecular characterization through SEC, while the rest of the solution is collected to the main reactor. Both the sampler and the main reactor of the apparatus are cooled down with liquid nitrogen in order to remove the sampler by sealing off. At the same time the empty ampoules of styrene and sodium naphthalenide are also

removed from the main reactor. It is very important to keep the living difunctional polystyrene frozen with liquid nitrogen in order to avoid deactivation of the living anions during thawing through decomposition of the polar media (THF).

For the linking reaction of dimethyldichlorosilane [$(CH_3)_2SiCl_2$] with the living difunctional polystyrene $Na^{(+)(-)}PS^{(-)(+)}Na$, the apparatus observed in Figure 6.16 is used.

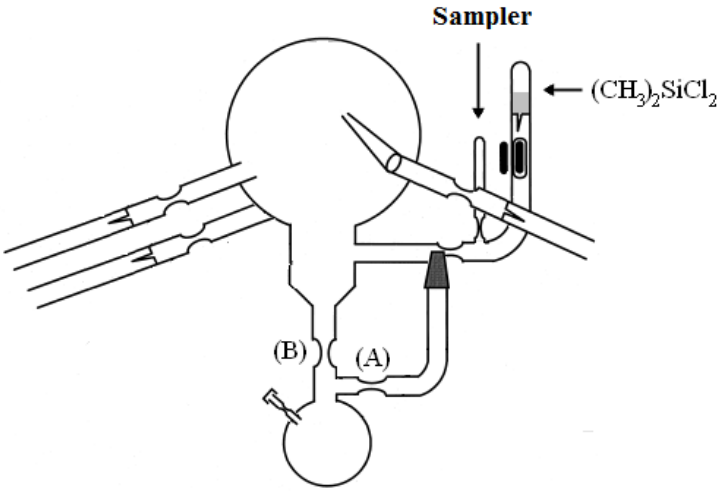

Figure 6.16: *Apparatus for the linking of the difunctional $Na^{(+)(-)}PS^{(-)(+)}Na$ with the dimethyldichlorosilane linking agent.*

This apparatus consists of the purge section and the main reactor which will be used for the linking reaction. Initially, the apparatus is attached on the vacuum line, degassed and a small amount of n-BuLi is introduced from the elastic septum, rinsed and sealed. The apparatus is degassed again and approximately 50 ml of benzene are distilled into the purge section, cooled with liquid nitrogen and degassed again. The apparatus is detached from the line by sealing off the constriction (A), the benzene solution is thawed and the solution of benzene and n-BuLi is transferred in the inner glass surface of the apparatus as described previously. Then, the apparatus is rinsed by continuous benzene reflux in order to remove traces of n-BuLi as well as its reaction products with impurities. Approximately half amount (25 ml) of the solvent is left in the main reactor in order to reduce the vapor pressure of the volatile linking agent during the introduction of the living anions of the difunctional polystyrene and the purge section is removed. The ampoule of the linking agent (5 ml, 41.1 mmol) is ruptured, the solution is homogenized and the empty ampoule of the silane is removed. The collection ampoule with the $Na^{(+)(-)}PS^{(-)(+)}Na$ is attached to the one side arm which is constricted with a glass nozzle as shown in Figure 6.17. The connection part is degassed very carefully on the vacuum line by flame drying 2-3 times, the apparatus is detached by sealing off constriction (A) and the apparatus is now ready in order to initiate the linking reaction.

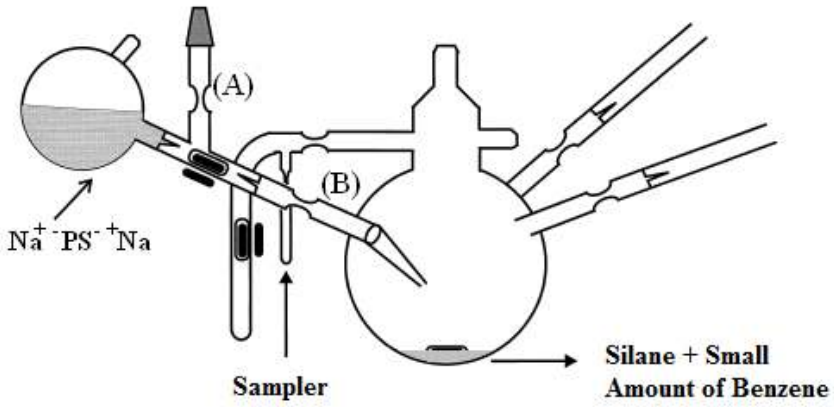

Figure 6.17: *The reactor for the linking reaction connected with the collection flask containing the difunctional polystyrene.*

The following procedure is the most crucial part of the synthetic route. Special care must be given in two parameters:

First, the amount of the chlorosilane linking agent must be a large excess when compared with the amount of the active polymer chains (at least 100 to 200-fold excess).

Second, the solution of the active polymer must be added to the chlorosilane as quickly as possible, without permitting the chlorosilane to transfer back to the connection part, or even worse, back to the flask with the difunctional polystyrene. For this reason the linking reactor with the linking agent in benzene is placed into an ice bath (0-5^{0}C) under soft stirring. The flask with the difunctional polystyrene is warmed and both break-seals are ruptured if possible simultaneously. The apparatus is tilted and a towel soaked in warm water is placed on the flask with the active difunctional polystyrene in order to help the insertion of the living polystyrene into the linking reactor. This procedure is pictured in Figure 6.18. The living polystyrene is, therefore, added in one continuous motion into the linking reactor where vigorous stirring is applied. After the addition is completed, the apparatus may be allowed to lie flat at room temperature. The most crucial aspect of this linking reaction is the reaction of the living polystyrene chain with only one chlorine atom of the linking agent leading to the intermediate product: $Cl(CH_2)Si\text{-}PS\text{-}Si\text{-}(CH_2)Cl$. This reaction is generally accomplished within only a few minutes. A visual indication is that as the red colored living anions are incorporated into the chlorosilane, their color completely fades and becomes colorless.

An important procedure for the successful synthesis of the final PCHD-b-PS-b-PCHD linear triblock copolymer is the removal of the linking agent [$Cl_2Si(CH_2)$] since even a small amount of unreacted chlorosilane could lead to undesirable products in the final material.

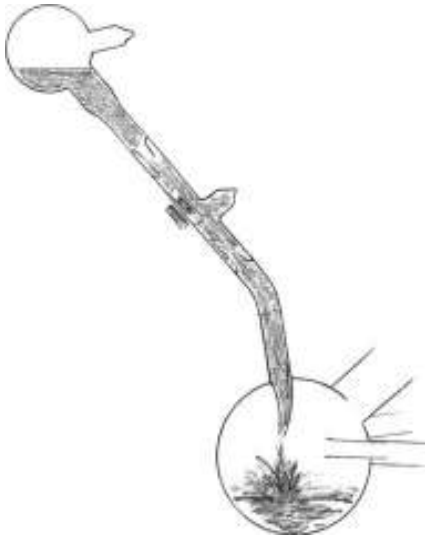

Figure 6.18: *Addition of the active difunctional polystyrene into the linking reactor*[70].

This volatile reagent is removed by adopting a specified procedure on the high vacuum line. The apparatus of Figure 6.19 is attached on the vacuum line through one of the two remaining break-seal entries (C).

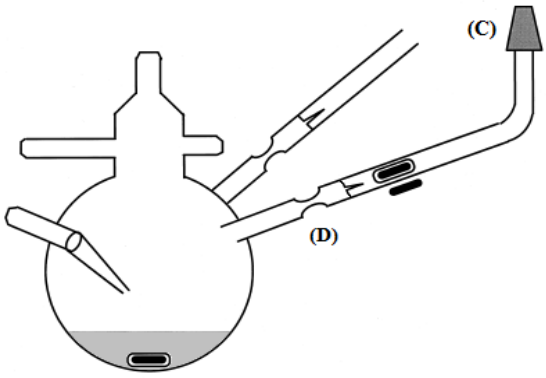

Figure 6.19: *Apparatus for the quantitative removal of the unreacted chlorosilane linking agent.*

The stopcock to the reactor for the linking reaction is opened and the glass part is degassed thoroughly. The seal is ruptured and the contents, benzene/THF and chlorosilane, are distilled to a waste collection flask attached on the high vacuum line until the solution becomes viscous to stir. Freshly purified benzene (~70ml) which is stirred on the vacuum line is distilled into the linking reactor and the contents are stirred for 30 minutes at approximately 30^0C in order to fully redilute the chlorofunctional polymer. In this manner the inner glass surface of the apparatus is rinsed from the remaining chlorosilane traces. The contents are again distilled to the waste collection flask and the procedure is repeated for at least two more times. After the third distillation of the contents to the waste collection flask, the reactor may be opened to the vacuum line for a period of time. Depending on the amount of chlorosilane and the attainable molecular weight of the polymer, this period of time can last from 5 days to

a couple of weeks. The reactor is usually warmed up to ~40^{0}C (depending on the polymer) for a slightly faster evacuation. The main liquid nitrogen trap must be cleaned after the first day. It is important to fill the liquid nitrogen trap frequently (4-5 times per 24 hours).

Another significant aspect that needs extreme care is the distillation process of the freshly purified benzene into the reactor. During this process, it is extremely dangerous to use liquid nitrogen for the distillation procedure since the system freezes in an inhomogeneous manner, meaning that two layers of the substances are created, one of the concentrated polymer solution and one of the incoming solvent. The result is that a lot of stress is placed on the flask and the glass might create cracks since the mechanical failure cannot be prevented.

The existence of high vacuum is an indication that all the chlorosilane amount has been removed from the apparatus. Purified benzene is again distilled into the reactor and the apparatus is detached from the vacuum line by sealing off constriction (D). Then, the reactor is connected, through the last break-seal entry, with the polymerization reactor of the living PCHD$^-$Li$^+$ forming the apparatus which is observed in Figure 6.20. A very important detail is that the poly(cyclohexadiene) living ends should exhibit a 20% molar excess in relation to the Si-Cl living ends of the linked polystyrene. In this way, it is certified that the corresponding Si-Cl ends will fully react with the living ends of PCHD$^-$Li$^+$.

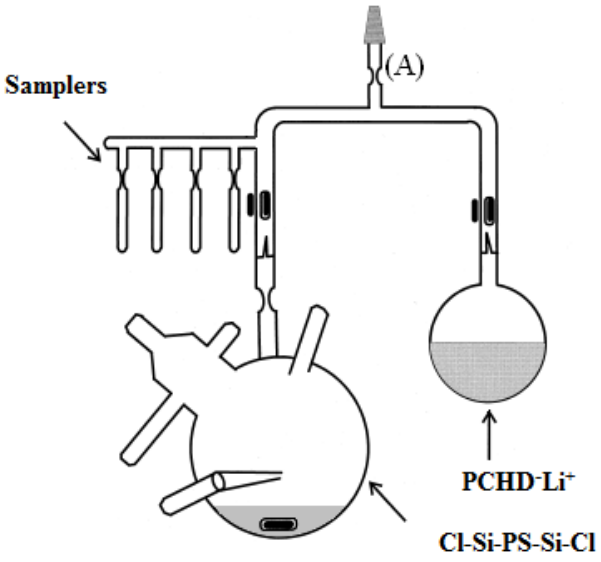

Figure 6.20: *Apparatus for the linking of the living PCHD$^-$Li$^+$ with Cl(CH$_2$)Si-PS-Si(CH$_2$)Cl and the formation of the final linear triblock copolymer of the PCHD-b-PS-b-PCHD type.*

The apparatus is attached carefully on the vacuum line, degassed thoroughly by flame drying 3-4 times or until high vacuum is achieved and is detached from the vacuum line by sealing off constriction (A). Then, the break seal of the living PCHD arm, which is in excess, is ruptured and the solution is transferred to the inner glass surface of the apparatus. In this way, the excess of the living anions reacts with any impurities and deactivates them.

Following this procedure, the break seal of the linked difunctional polystyrene is ruptured and the two solutions are mixed thoroughly. An indication of the linking reaction is the change of the color of the living arms from light yellow-green to an almost colorless solution. The final mixture is collected to the reactor of the linked difunctional polystyrene and the final linking reaction is left to proceed for a long period of time. Depending on the number of arms that are going to react, this period of time varies from one month to approximately two months. During this linking procedure, small aliquots of the mixture for molecular characterization via SEC are taken in order to monitor the progress of the linking reaction. After completion of the linking reaction, the material is precipitated in stabilized methanol, dried under vacuum and fractionated in a solvent/non-solvent mixture at approximately 3:1 ratio. The solvent used was a mixture of chloroform, which provides good solubility especially for the PCHD blocks, and toluene, which provides good solubility for the PS blocks and average solubility for PCHD. A mixture of methanol and hexane was used as non-solvent. The fractionation of the PCHD-b-PS-b-PCHD triblock copolymer was quite difficult due to the existence of PCHD homopolymer in the final material.

6.11 Synthesis of the (PS-b-PCHD)-PS´-(PCHD-b-PS) Linear Pentablock Copolymer

For the synthesis of the ABA´BA linear pentablock copolymer of the (PS-b-PCHD)-PS´-(PCHD-b-PS) type, the same procedures where used as in the case of the PCHD-b-PS-b-PCHD linear triblock copolymer. The difunctional initiator sodium naphthalenide was used for the polymerization of the middle PS´ block and the chlorosilane linking agent dichlorodimethylsilane [$(CH_3)_2SiCl_2$] was used for the linking reaction with the active arms. In this case the active arms were not of the $PCHD^-Li^+$ type but of the PS-b-$PCHD^-Li^+$ type (in 20% excess). The synthesis reactions are shown in Scheme 6.7.

It is important to mention that the middle PS block has totally different molecular characteristics from the PS block of the linear diblock copolymer used for the arms of the final product. The fractionation of this sample was easier due to the fact that in this case the final copolymer comprises of PS as the outer blocks. Consequently, by using toluene/methanol-hexane as solvent/non-solvent mixture, fractionation of the final linear pentablock copolymer was accomplished.

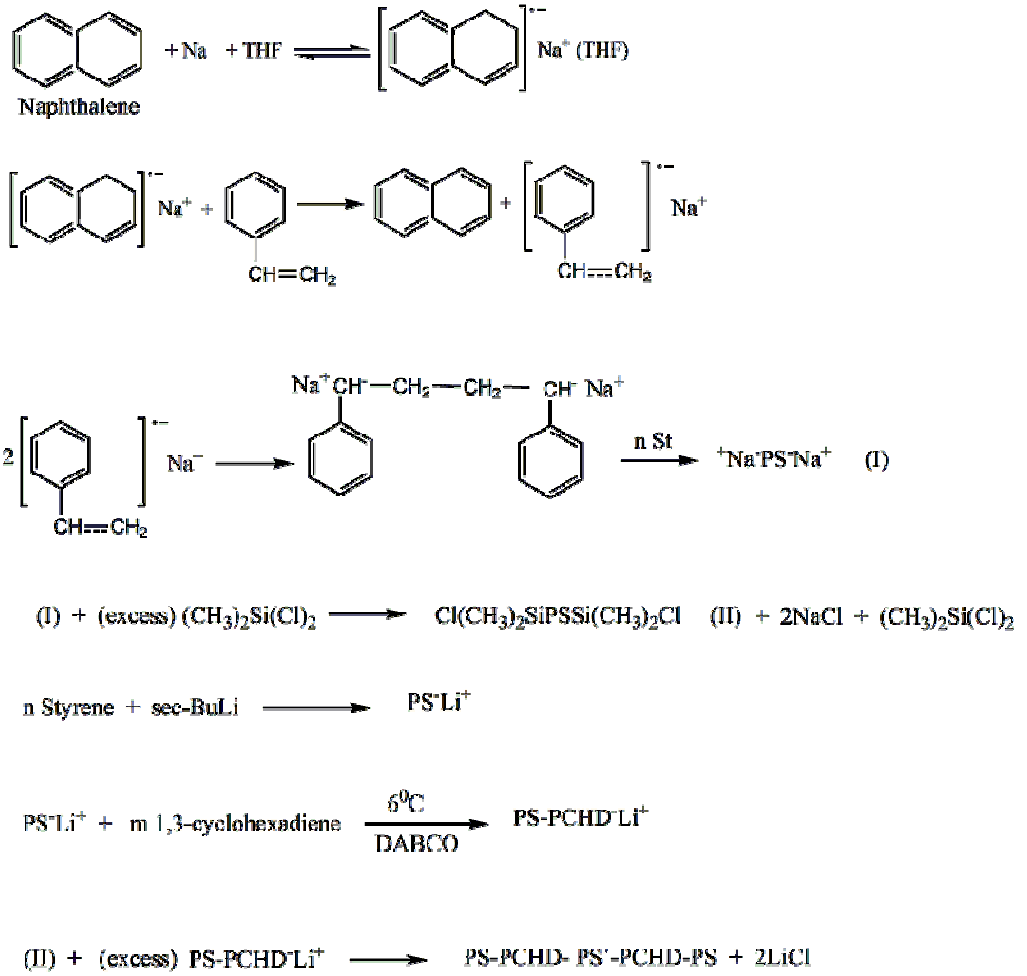

Scheme 6.7: *Synthetic route for the synthesis of the (PS-b-PCHD)-b-PS′-b-(PCHD-b-PS) linear pentablock copolymer.*

6.12 Synthesis of the $(PCHD)_2$-g-PS-g-$(PCHD)_2$ H-Type Copolymer

For the synthesis of the $(PCHD)_2$-g-PS-g-$(PCHD)_2$ H-type copolymer, the same procedures were established as described previously for the case of PCHD-b-PS-b-PCHD linear triblock copolymer. Sodium naphthalenide was used as the difunctional initiator and a 20% excess of living $PCHD^-Li^+$ was used as the outer block. The only significant difference was that instead of the dichlorodimethylsilane linking agent, the trichloromethylsilane (CH_3SiCl_3) linking agent was used for the linking reaction with the difunctional polystyrene. The alternation of the linking agent led to the synthesis of an H-type copolymer (Scheme 6.8). The fractionation of this sample was performed by using a mixture of toluene-chloroform/methanol-hexane as solvent/non-solvent, but it was more difficult to obtain the final pure H-type copolymer comparing to the PCHD-b-PS-b-PCHD copolymer due to the higher number of the outer blocks and there being PCHD.

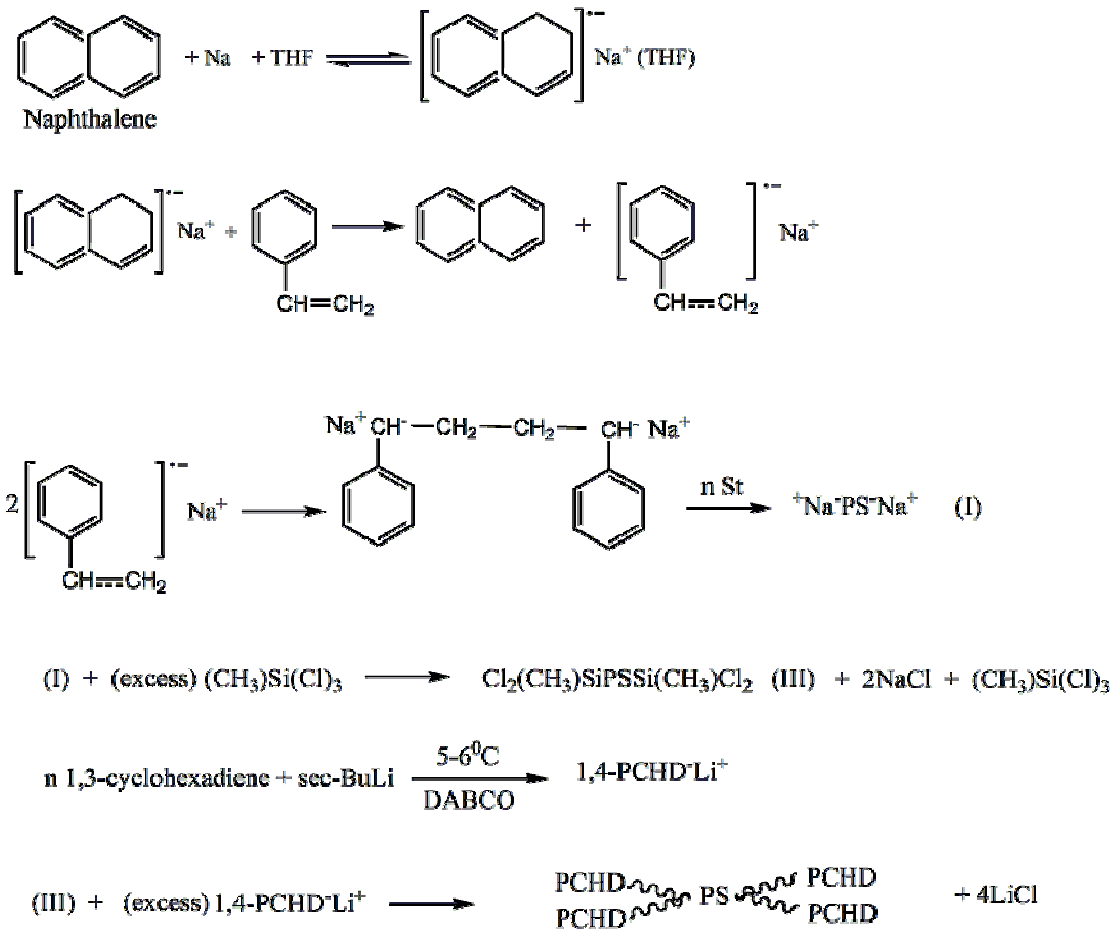

Scheme 6.8: *Synthetic route for the $(PCHD)_2$-PS-$(PCHD)_2$ H-type copolymer.*

6.13 Synthesis of the $(PCHD)_3$-g-PS-g-$(PCHD)_3$ Super H-Type Copolymer

The synthesis of the $(PCHD)_3$-g-PS-g-$(PCHD)_3$ super H-type copolymer was accomplished by using the same procedure performed for the synthesis of the PCHD-b-PS-b-PCHD linear triblock copolymer. The procedure has already been described thoroughly. The difunctional initiator sodium naphthalenide was used for the synthesis of the PS middle block and the linking agent tetrachlorosilane ($SiCl_4$) was used for the linking reaction with the excess of the active $PCHD^-Li^+$ arms. The synthesis reactions are shown in Scheme 6.9. For the fractionation of this sample, a mixture of toluene-chloroform/methanol-hexane was used as the solvent/non-solvent system, similar to the ABA copolymer and A_2BA_2 H-type copolymers.

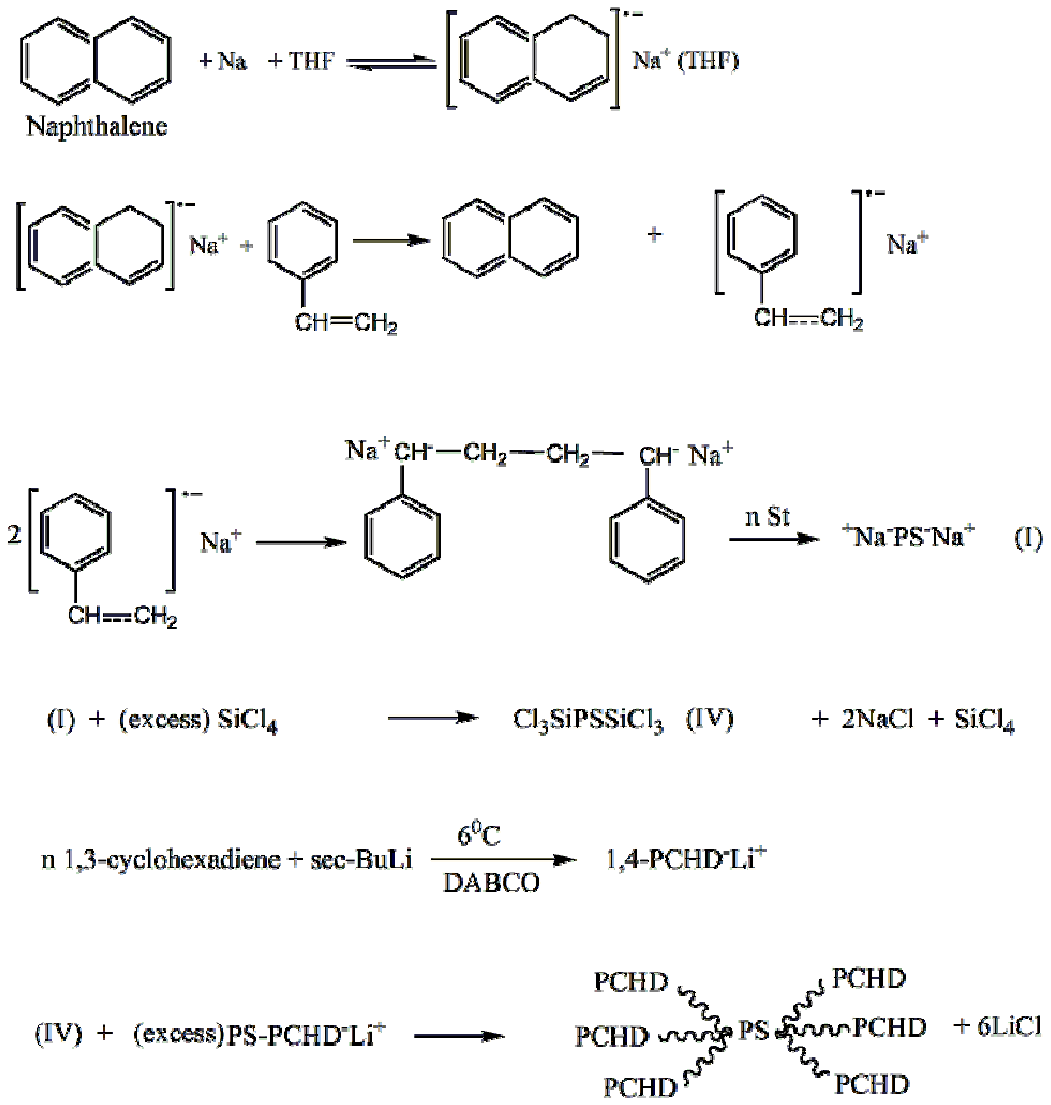

Scheme 6.9: *Synthetic route for the $(PCHD)_3$-PS-$(PCHD)_3$ super H-type copolymer*.

6.14 Synthesis of the $(PS\text{-}b\text{-}PCHD)_3$-g-PS′-g-$(PCHD\text{-}b\text{-}PS)_3$ Super H-Type Copolymer

Again for the synthesis of the $(PS\text{-}b\text{-}PCHD)_3$-g-PS′-g-$(PCHD\text{-}b\text{-}PS)_3$ super H-type copolymer, the procedure described previously was adopted. The difunctional initiator used for the polymerization of the middle block was sodium naphthalenide while for the linking reaction with the excess of PS-PCHD$^-$Li$^+$ arms, $SiCl_4$ was used. The synthesis reactions are represented in Scheme 6.10. The fractionation of this type of copolymer was somehow easier to perform, since the outer blocks were PS, and the toluene/methanol-hexane mixture was adopted as a solvent/non-solvent system

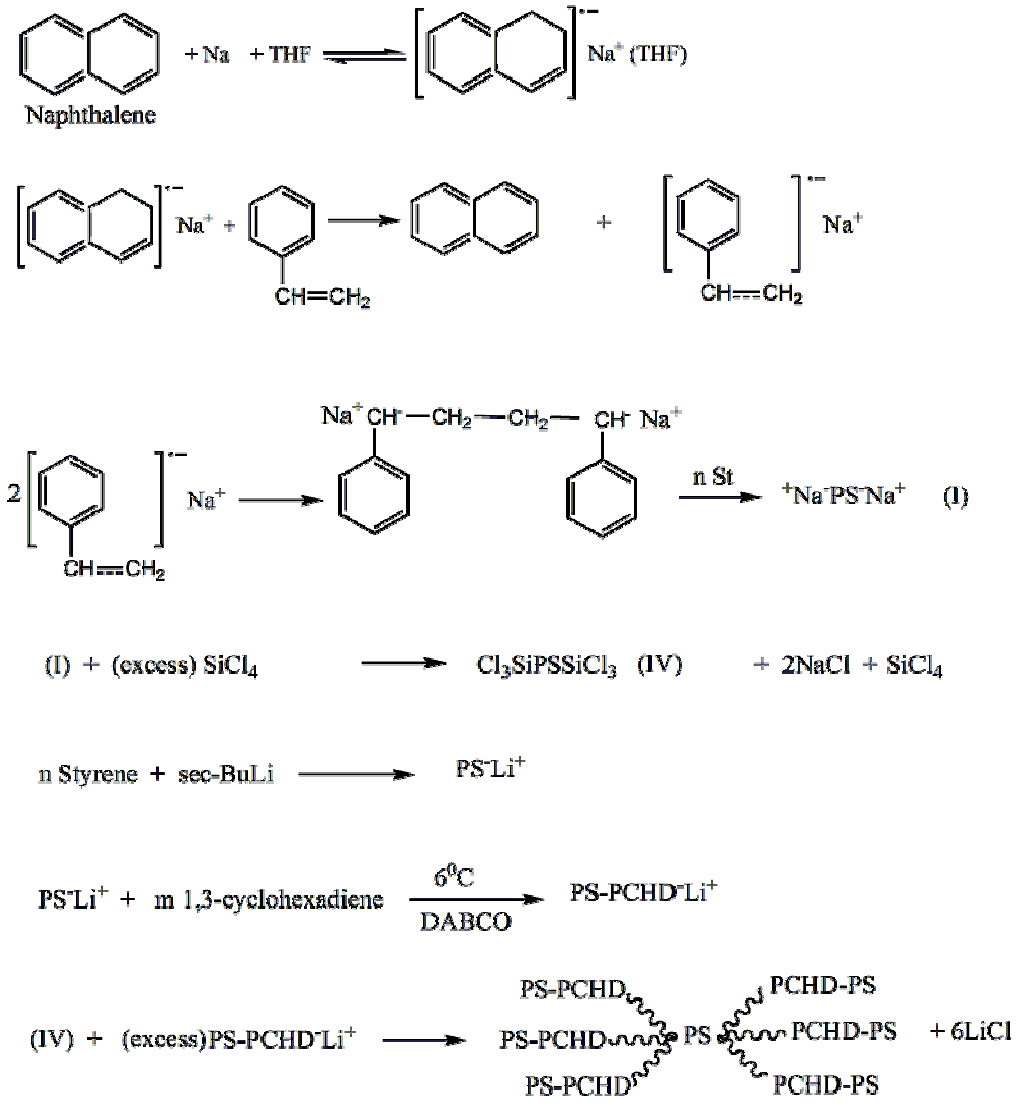

Scheme 6.10: *Synthetic route for the (PS-PCHD)$_3$- PS′-(PCHD-PS)$_3$ super H-type copolymers.*

6.15 Molecular Characterization

6.15.1 Size Exclusion Chromatography (SEC)

A size exclusion chromatograph (SEC), equipped with an isocratic pump (SpectraSystem P1000), column oven (LabAlliance) heated at 30^{0}C, three columns in series (PLgel 5 mm Mixed-C, 300× 7.5 mm), refractive index (RI, Shodex RI-101) and ultraviolet absorbance (UV, SpectraSystem UV1000) detectors, and tetrahydrofuran (THF) as the eluent, was calibrated with eight PS standards (M_p: 4.300 to 3.000.000 g/mol). In every case, prior to calculating the polydispersity indices (PDI) of the synthesized polymers as well as prior to making an estimation on the average molecular weights ($\overline{M}_n$ and $\overline{M}_w$), a series of standard PS solutions were always tested in order to examine the accuracy of the measurements. All measurements were performed at the Polymers Laboratory of the Department of Materials Science Engineering in the University of Ioannina.

6.15.2 Proton Nuclear Magnetic Resonance (^{1}H-NMR) Spectroscopy

Proton nuclear magnetic resonance (^{1}H-NMR) spectroscopy was used for determining the composition and the isomeric microstructures of poly(cyclohexadiene) blocks and was carried out in $CDCl_3$ at 30^0C using a Bruker AVANCE II spectrometer, located at the Chemistry Department in the University of Ioannina. Data were processed using UXNMR (Bruker) software.

6.15.3 Membrane Osmometry

Membrane osmometry (MO) was adopted to determine the number average molecular weight $\overline{M}_n$ by using a Gonotec Osmomat 090 in 35^0C. The solvent used was toluene, distilled from CaH_2, while the membrane was from regenerated cellulose. The number average molecular weight was estimated by creating a graph of $(p/c)^{1/2}$ as a function of c, where π is the osmotic pressure and c the concentration of the corresponding solution in g/ml.

6.16 Thermal Analysis

6.16.1 Differential Scanning Calorimetry (DSC)

For the glass transition temperatures and the melt temperatures of the materials, differential scanning calorimetry (DSC) was employed. The measurements were accomplished with a *Q*20 TA instrument, property of the Center for Nanophase Materials Science (CNMS) of Oak Ridge National Laboratory at Oak Ridge, Tennessee, USA. The heating ramp was 10^0C/min and the temperature range from 25^0C (room temperature) to 250^0C. A small amount of 2-5 mg was used from each sample and placed in an aluminum pan, which was sealed properly and introduced into the sample holder of the instrument. Two heating and one cooling procedures were performed and the results of the second heating were reported and analyzed using Advantage v5.4.0 (TA instruments) software.

6.17 Morphological Characterization

6.17.1 Transmission Electron Microscopy (TEM)

The observation of the samples was performed in a Zeiss Libra 120 energy filter transmission electron microscope (EFTEM) operating at 120 kV in bright field mode. The Zeiss Libra 120 EFTEM is equipped with Kohler illumination system, which is suitable for high resolution since it provides parallel beams to the optical axis resulting in aberration-free, homogeneous illumination and higher depth of field. Furthermore, it is equipped with an in-column OMEGA filter which prevents inelastically scattered electrons from hitting the sample improving therefore the contrast, and with an oil-free pumping system. In order to study the morphology of the seventeen (17) synthesized linear diblock copolymers, the

preparation of thin films that exhibit microphase separation was required. Thermodynamic equilibrium ensures enhanced self-assembly of the sample, leading eventually to distinguishable microphase separation. The preparation of the samples and the observation via EFTEM of the equilibrium morphologies were performed in the Center of Nanophase Materials Science (CNMS) of Oak Ridge National Lab at Oak Ridge, Tennessee, USA.

Casting-Annealing: Initially, for the preparation of the thin films, a 5% w/v solution of each sample in toluene was prepared. For one sample exhibiting PCHD majority, chloroform was used instead of toluene. The solvents should be non-selective for both blocks of the copolymer. The samples were casted for approximately 5 days in a properly established saturated environment under a beaker in a hood. In this way, the solvent is evaporated slowly from the solution. Thin films with thickness approximately 1 mm were formed and half parts of them were placed in an oven for annealing. Initially, the films were kept at 50^0C for twelve (12) hours, at 90^0C for other twelve hours and finally the temperature was adjusted at 120^0C, which is above the glass transition temperature of both polystyrene and poly(cyclohexadiene) (100-110^0C), and remained there for 5 days. Then, each film was removed from the annealing oven and immersed in liquid nitrogen for a few seconds (quenching). This procedure was adopted since there is a possibility that the formed morphology might alter, if the sample is cooled slowly to room temperature.

Ultramicrotomy: Ultramicrotoming can be defined as the technique of cutting ultra-thin sections suitable of polymers, biological and biomedical objects for transmission electron microscopy (TEM), scanning electron microscopy (SEM) or atomic force microscopy (AFM). As a result of developments in the design of electron microscopes it is now possible to examine much thicker sections (ultrathin) up to approximately 30 nm thick or less. Improvements in preparation techniques over the last few decades have demonstrated that thin sections of different materials that are free from artifacts can be successfully prepared for electron microscopic investigations. Therefore, successful sectioning now depends primarily on the experience of the experimentalist rather than on the instrumentation used. In order to avoid sectioning-induced errors and to fully exploit the capability of an ultramicrotome, one must master the optimum specimen preparation technique. The traditional application of ultra- and cryoultramicrotomy involves the sectioning of soft materials such as the aforementioned biological and biomedical substances and polymers. Recent experiences demonstrate that even hard materials can be successfully ultramicrotomed. In addition to soft materials such as aluminum or copper, materials as hard as steel, ceramics or even very hard substances like sapphires and carbides have been successfully sectioned by ultramicrotomy. These developments show that the technique of ultramicrotomy can be expected to extend to other sectors of materials science, supplementing existing preparation techniques.

For the research work involved in this thesis, environmental ultramicrotoming was performed in a Leica Ultracut UCT ultramicrotome (Figure 6.21), located in the High Temperature Materials Laboratory (HTML) of the Oak Ridge National Laboratory at Oak Ridge, Tennessee, USA. Cryogenic conditions were not employed for two main reasons: the hardness of each sample was improved even more by embedding in a suitable media and the glass transition temperatures of both polystyrene and poly(cyclohexadiene) are approximately 100-110^{0}C.

Figure 6.21: *The Leica Ultracut UCT ultramicrotome used for ultra-sectioning of the samples.*

Embedding Media:[135] There are three media for general use: epoxy, polyester and acrylic resins. The ease of sectioning and stability in the vacuum and the electron beam are important, with the epoxy resins being more stable. Variations can be made to each procedure for the appropriate medium to change its hardness. In the case of the synthesized copolymers, the araldite 502 kit by PELCO was employed. This epoxy resin was cured for one day at 50^{0}C.

Equipment: The ultramicrotome consists of a specimen-holder assembly and a knife support, which allows for any orientation of the sample via specimen rotation/tilt. This rotation and tilt are provided through a goniometer and 3D displacement movements of the knife (Figure 6.22).

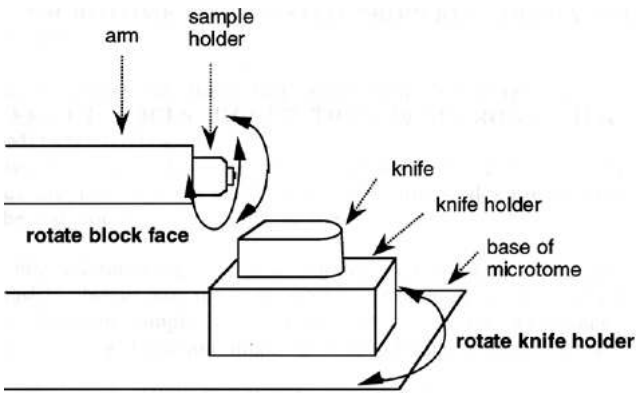

Figure 6.22: *Ultramicrotome arm/specimen holder and knife assemblies*[135].

The procedure consists of removing a small volume of the sample by trimming it into a pyramidal shape, with a very small surface area at one end, and placing it into a specimen holder. This assembly is then mounted on the ultramicrotome, against the knife, which is gently moved as close to the specimen as possible. The knife is fixed and the specimen is advanced on a precise path with an arranged cutting speed.

Trimming of the Specimen: Cutting the sample to make a pyramid is performed normally under a stereoscopic microscope so as to cut the specimen without damaging the sample. Using a razor blade or better still a specimen trimming device, the far end of the specimen is cut into a pyramid base a few millimeters tall. In the case of this research work, the Leica EM TRIM system was employed (Figure 6.23).

Figure 6.23: *The Leica EM TRIM model used for trimming the specimen blocks.*

The cutting surface will be reduced to a square or rectangular with sides between 0.5 and 2 mm. The edges of this surface must be perfectly clean and smooth. Two sides must be strictly parallel to each other and the other two can form a square or trapezoid (Figure 6.24).

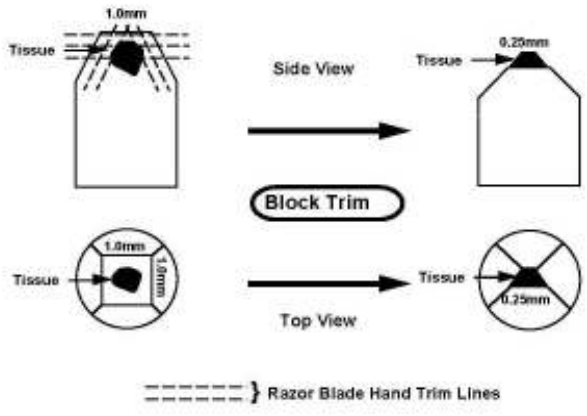

Figure 6.24: *Trimming the specimen block to the appropriate dimensions and shape*[135].

The pyramid should not be too sharp to prevent any vibration phenomena during cutting. It is better to prepare the sample a few hours earlier, allowing it to return to a stable state.

Glass and Diamond Knives: The knives used for sectioning are usually made of glass or diamond. Which type of knife will be used depends on the cutting thicknesses required, as well as on the sample ductility and brittleness. Glass knives are produced with a 45^0 angle and diamond knives are manufactured with angles of 35^0 and 45^0 (Figure 6.25).

Figure 6.25: *Diamond knives, 35^0 and 45^0 angle.*

Glass knives are sharp-edged glass prism manufactured from special glass strips free of reams. Strips 400mm long and 25mm wide with thickness of 6.4 mm, 8 mm or 10 mm are on the market. When selecting the thickness of a glass strip, it is important to take into consideration the requirements of the specimen (in terms of its nature and size) as well as the aim of the subsequent microscopic examination. The knife edges are formed at the narrow sides of the strip of glass and consequently these surfaces must be clean and relatively smooth, although a slight waviness is acceptable. Care should then be given on handling the glass so as not to get finger marks on the narrow sides of the strip. Special equipment (a knife maker) is necessary for the production of glass knives of high quality. The best results are obtained with the so-called balanced break method. This technique enables a standard

400mm-long strip of glass to be broken continuously into equal halves. The resulting flat-sided squares are broken in the next step into two glass knives.

Diamond knives are extremely delicate and expensive tools which can be really expensive based on the length of the edge. Simply touching the edge or cutting a section greater than 1 μm may permanently damage it. The benefits to using a diamond knife lie in its hardness. Proper care results in a knife that is sharp for years and can cut numerous sections. As the edge loses its sharpness, a progressive change in the quality of the sections slowly occurs. Regular cleaning of a diamond knife edge is very important to prevent a build-up of small fragments of embedding material which will cause scratches on the sections. These fragments may come from sections or parts of sections that have been allowed to dry out on the knife, or from fragments of resin torn out from soft material or partially-polymerized blocks. If this resin is not removed it may polymerize on the surface of the diamond knife and will then be impossible to remove. Diamonds knives are a great advantage when very long series of sections is required, since it is inconvenient to keep changing a glass knife with the constant realignment that is necessary. A good diamond will also be able to cut thinner sections (less than 30 nm) than the average glass knife. A common problem in using a diamond is that it is quite hydrophobic which prevents wetting of the knife edge. The remedy involves carefully running an eyelash along the inside edge of the diamond with the boat full. A recent addition to the types of knives used in ultrathin sectioning is the sapphire knife. As with the diamond knife, the sapphire is permanently mounted in a trough and is superior to the glass knife. It is however inferior in quality to the diamond knife and is incapable of cutting hard samples without damaging the edge.

Knife Orientation and Water-Level Adjustment: The knife is placed on a support that can be oriented so as to slightly tilt the diamond knife edge, in order to have a clearing angle between 3^0 and 9^0, most often 6^0. Usually the blade knife is equipped with a trough filled with purified water, upon which the sections will spread out. The water level in the trough must be precisely adjusted so as to form a low meniscus with the knife cutting edge. This can be verified by checking under the microscope whether a white shiny color over the surface of water has been produced (meniscus). Successive sections float on the surface of the water and thus can be easily picked up. The microscope is also used to align the sample with regard to the knife edge, as well as to make any adjustments and monitor operations during cutting.

Adjustments of the Specimen Block: The specimen block should be securely clamped in its holder and orientation head to prevent any movement during sectioning. Ideally the jaws of the holder should be parallel to each other and to the sides of the block to ensure adequate rigidity without squeezing the block out of the holder. A protrusion of approximately 3 mm is recommended for ultramicrotomy or else vibrations may occur during sectioning. The

specimen arm is set to the center of its vertical movement and to the same height with the knife edge. The specimen block face and the top edge of it is aligned to be parallel with the knife edge, so that the whole surface of the block is included in the first section and to ensure that the sections form a straight ribbon.

Adjustments of the Knife: To avoid damaging the knife it is advisable to attach the specimen holder to the specimen arm prior to fixing the knife. The knife height sets the cutting point and should ideally coincide with the mid-point of the specimen arm movement. The knife holder is tilted to set the clearance angle (4^0, 5^0 is suitable initial angle, if using a diamond knife the manufacturer's recommended clearance angle should be 6^0). Ensure that the screw on the knife holder is tightened. Initially, a coarse adjustment is performed by making the approach to the specimen block visually and by checking that the knife edge is far enough from the block. Then, a secondary adjustment is performed which is also the most important. Fine adjustment is performed under the microscope and the knife and specimen block are placed together at the stereoscopic field of view, at low magnification. The block is moved manually in front of the knife with a 2 μm step and when it is close enough, a reflection of the knife on the block is created (Figure 6.26).

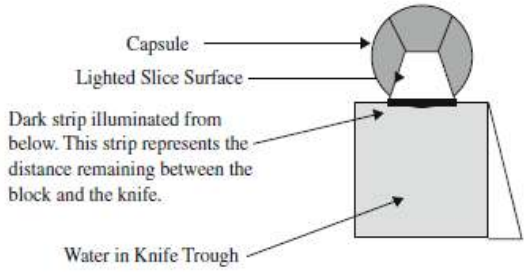

Figure 6.26: *Schematic representation of the reflection of the knife on the specimen block during the fine adjustment*[135].

A reverse image with illumination below the knife is produced, enabling the user to see the distance between the knife and the block, from the dark line visualized. The approach is completed by changing the step to 1 μm and by reducing the dark line as much as possible. Now the system is ready to begin sectioning.

Sectioning: Ultrathin sectioning can be disturbed by low-frequency vibrations which can emanate from rotating electrical machinery such as refrigerators or air-conditioners or from heavy vehicular traffic. It is essential that each ultramicrotome is placed on a separate table or bench as anyone else working on the same surface will certainly cause disturbances. The support table should be free-standing. The suitable equipment for sectioning is listed below:

- A small eyelash probe for manipulation of the sections (Figure 6.27a).
- A special "perfect loop" tool.

- A small bottle of clean trough liquid (usually water).
- A small syringe, pipette or trough-filling device.
- A small quantity of lens tissue and filter paper.
- A supply of specimen grids (300-600 mesh) (Figure 6.27b).
- A pair of fine tweezers, curved or straight, for handling the grids (Figure 6.27c).
- A Petri dish with 2 layers of filter paper for short-term storage of the grids with the collected sections
- A covered grid box or container for long-term storage of the grids
- A diamond knife with a cleaning stick and a small bottle of ethanol or detergent

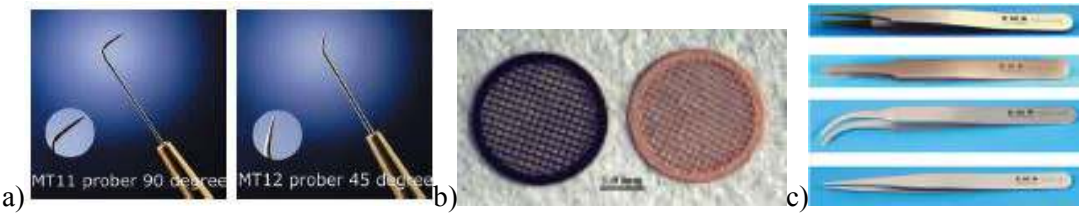

Figure 6.27: *a) Small eyelash probes, b) Specimen grids, c) Tweezers, curved or straight.*

After all the adjustments described previously are performed, the system is ready for cutting specimen sections. Initially, a first slice, as thin as possible (approximately 0.5-1 μm) is cut. This is the most delicate part of the sectioning procedure because the specimen block is very close to the knife and its very brittle edge must not be damaged.

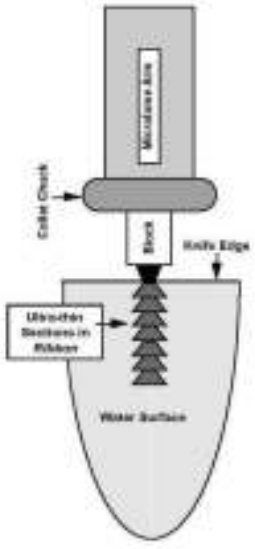

Figure 6.28: *Ultrathin sections forming ribbon during cutting*[135].

The cutting window, i.e. the slow-speed range, is adjusted with the control unit of the ultramicrotome, and then the automatic movement of the specimen block begins. Cutting speed (usually adjusted between 1 to 2 mm/sec) and thickness are selected. At the beginning,

a few semi-fine sections can be cut (200-500 nm) in order to produce a shiny, smooth cutting surface before moving on to thinner sections. Then, thin fine slices of 50-75 nm thickness are made. These sections are made in the form of ribbon if both faces of the block are well aligned and parallel to the knife edge (Figure 6.28).

Retrieval of Sections: The user must be very careful during the collection of sections from the trough. It is essential to avoid touching the knife blade with the edge of the grid. To do this, an eyelash whose end is first dipped into the water trough is used. The sections that are close to the knife edge are moved away and they are recovered on a grid (Figure 6.29).

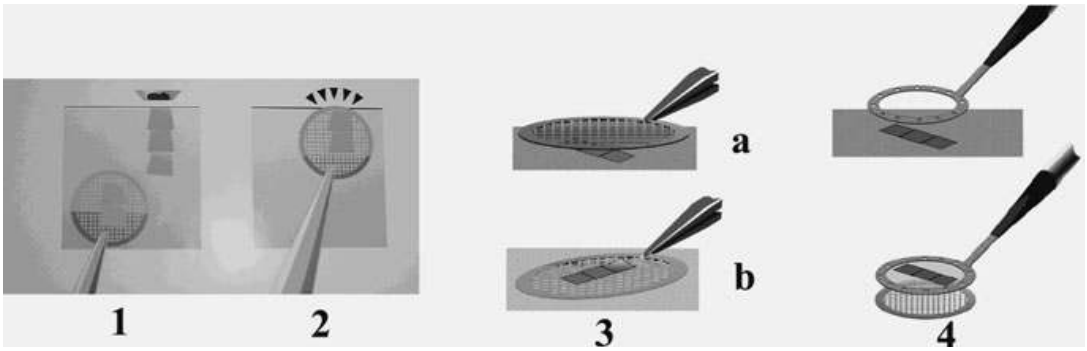

Figure 6.29: *Retrieving sections: 1) proper technique for retrieving slices far from the knife edge, 2) improper retrieval, too close to the knife edge, risk of damaging the knife edge, 3) section retrieval with a grid from above (a) or below (b) and 4) section retrieval with a special "perfect loop" tool.*[135]

Three methods are possible as illustrated in Figure 6.29. In the first method, if the grid has a support film, the section ribbon is retrieved by simply touching the grid to the surface of the water where the sections are located. In the second method, if the grid is bare, the sections are recovered by immersing the grid into the water trough and the sections are gathered by carefully raising the grid out of the water, while keeping the ribbon of slices over the grid using an eyelash. This method was employed for the retrieval of grids for this Diploma Thesis. For both methods, the excess water is removed by gently placing the grid vertical to the level of a filter paper. In the third method, the sections can be retrieved with a special "perfect loop". The sections are retrieved from above and then the water is removed using the corner of a filter paper. In all cases, the grids are stored in a grid holder.

Staining: Staining was performed in the Chemistry Department of the University of Tennessee (UT) at Knoxville, Tennessee, USA. All grids were exposed for approximately 45 minutes in fresh osmium tetroxide (OsO_4) vapors in an aqueous solution (2% OsO_4 in water) order to be stained (Figure 6.30).

Figure 6.30: *Staining of specimen grids in a covered Petri dish filled with OsO_4 vapors in an aqueous solution.*

The procedure was performed under high safety conditions in a Petri dish filled with OsO_4 vapors in a properly formed hood. In this way, the required contrast for TEM image observation is performed with the polydiene phase of the copolymers being stained and appearing darker in the TEM images. The polystyrene phase appears white since it does not react with OsO_4.

6.17.2 Small Angle X-Ray Scattering (SAXS)

Small angle X-ray scattering was performed with Anton Paar SAXSess mc^2 (Figure 6.31) in the Center of Nanophase Materials Science (CNMS) of Oak Ridge National Lab at Oak Ridge, Tennessee, USA.

Figure 6.31: *Anton Paar SAXSess mc^2 instrument for SAXS measurements*[131].

The X-ray source is a sealed-tube suitable for both point and/or line collimation mode. The temperature ranges from -150^{0}C to 300^{0}C enabling also thermal SAXS measurements. Various sample holders are available such as quartz capillaries for liquids, high temperature sample holder for solids, paste cell for viscous samples etc. The beam stop is transparent with precision drive for vertical and tilt alignment. It is also equipped with two types of detectors, either imaging plate detector (with 2D data acquisition) or CCD camera detector (with 2D data acquisition) while the accessible q-range is from 0.03 nm^{-1} (q_{min}) to 28 nm^{-1} (q_{max}) and the measurable d size from 0.1 nm to 200 nm. The data analysis was performed via SAXSquant™ data acquisition & analysis software.

CHAPTER 7

Experimental Results – Discussion - Conclusions

7.1 Molecular Characterization Results for the Linear Diblock Copolymers

The molecular characterization results are presented and discussed for the seventeen (17) linear diblock copolymers of the PS-b-PCHD and PCHD-b-PS type synthesized for this thesis. All samples, as already mentioned were synthesized via anionic polymerization by using the sequential monomer addition method and high vacuum techniques. High 1,4-microstructure was adopted for all PCHD blocks by using the polar additive DABCO. All polymerizations were performed by using sec-BuLi as initiator, in a sec-BuLi/DABCO:1/2 molar ratio, and benzene as the solvent.

As it was mentioned in previous chapters, several methods were adopted for the molecular characterization of these samples. Size exclusion chromatography (SEC) with THF as the eluent at 30^0C was used extensively in order to verify the narrow molecular weight distributions of the first blocks, as well as of the final linear diblock copolymers and to receive information concerning the number average molecular weights of the initial blocks and the final materials. As the instrument was always calibrated with PS standards, only the number average molecular weight values for the PS block were considered accurate, when styrene was polymerized first. In order to verify the total number average molecular weight values for each sample, as well as the values for each PCHD block, membrane osmometry (MO) with toluene at 35^0C was adopted. By combining the results from these two characterization methods and using them in the $I = \frac{\overline{M}_w}{\overline{M}_n}$ equation, information about the weight average molecular weight of the final materials were obtained. Furthermore, another method used for the molecular characterization of the samples, and especially to verify the high 1,4-microstructure for the PCHD blocks (~90%) as well as the chemical and compositional homogeneity of the samples, was proton nuclear magnetic resonance (^{1}H-NMR) spectroscopy.

In Table 7.1 the most significant molecular characteristics of the seventeen linear diblock copolymers are summarized. By using equation 3.8 ($f_A = \frac{\overline{M}_{n,A}}{\overline{M}_{n,A} + \overline{M}_{n,B}}$, with A corresponding to PS and B to PCHD block respectively), where the relationship between the number average molecular weight and the molecular composition f is given, the values of the two last columns in Table 7.1 were estimated (f_{PS} and f_{PCHD}).

Table 7.1: *Molecular characterization results for the linear diblock copolymers. The samples are sorted in descending values for f_{PS} (weight fraction of PS). The bolded samples are those in which 1,3-CHD was polymerized first.*

Samples	$\overline{M}_n$ 1st block (g/mol)	$\overline{M}_n$ 2nd block (g/mol)	$\overline{M}_n$ diblock (g/mol)	$\overline{M}_w$ diblock (g/mol)	$\frac{\overline{M}_w}{\overline{M}_n}$ diblock	f(wt%) PS block	f(wt%) PCHD block
PS-PCHD-10	43.470	2.100	45.570	47.850	1,05	95,40	4,6
PS-PCHD-8	37.600	2.400	40.000	42.800	1,07	94,0	6,0
PS-PCHD-2	41.820	4.520	46.340	48.200	1,04	90,2	9,8
PS-PCHD-1	44.750	6.020	50.770	52.800	1,04	88,1	11,9
PS-PCHD-5	30.200	6.400	36.600	38.800	1,06	82,5	17,5
PCHD-PS-15	12.300	45.000	57.300	64.200	1,12	78,0	22,0
PS-PCHD-17	21.700	7.300	29.000	31.030	1,07	75,0	25,0
PS-PCHD-14	28.100	15.600	43.700	50.700	1,16	64,3	35,7
PS-PCHD-3	11.200	6.600	17.800	19.050	1,07	62,9	37,1
PS-PCHD-12	24.500	15.500	40.000	43.600	1,09	61,2	38,8
PS-PCHD-18	10.700	6.900	17.600	19.360	1,10	60,8	39,2
PS-PCHD-11	24.500	16.100	40.600	44.660	1,10	60,3	39,7
PS-PCHD-16	19.600	13.400	33.000	34.300	1,04	59,4	40,6
PCHD-PS-9	22.000	29.200	51.200	61.400	1,20	57,1	42,9
PS-PCHD-19	18.400	21.100	39.500	42.260	1,07	46,6	53,4
PS-PCHD-4	15.500	20.100	35.600	39.900	1,12	43,5	56,5
PCHD-PS-13	34.700	13.000	47.700	58.670	1,23	27,2	72,8

*Molecular weight distribution results were estimated via SEC (THF in 30^0C) and number average molecular weight results via membrane osmometry (toluene in 35^0C).

As it can be observed, a variety of results can be concluded from Table 7.1. The lowest total molecular weight of the final materials is 17.600 g/mol while the highest is

57.300 g/mol. The molecular weight distributions are narrow implying that the samples exhibit chemical and compositional homogeneity. Furthermore, there is a large variety of compositions ranging from 95.4% down to 25% for PS block. Fourteen (14) of the samples synthesized are of PS majority, while three (3) are of PCHD majority. Additionally, three (3) are also the samples where 1,3-cyclohexadiene was polymerized first. The theoretical calculations for $\overline{M}_n$ values of PS block were always in accordance with the experimental results from SEC and MO, while some differences were observed between the theoretical calculations and experimental results for $\overline{M}_n$ values of several PCHD blocks. This phenomenon is due to the fact that termination and side reactions described in a previous Chapter may occur during 1,3-cyclohexadiene polymerization, especially when higher molecular weights are necessary, increasing in this way the molecular weight distribution and reducing the amount of monomer that reacts with the living anions. In all SEC chromatographs, the lines corresponding to the distributions of the final linear diblock copolymers (black ones) are displayed in higher molecular weights than the lines corresponding to the distribution of the first polymerized block (red ones), indicating the successful copolymerization for all synthesized samples. As it can be easily understood, the main challenge on synthesizing these linear diblock copolymers was to succeed in the formation of PCHD blocks with the desirable molecular characteristics and without any side or termination reactions. By using high vacuum techniques, which led to well-purified reagents, and the polar additive DABCO, these termination and side reactions were limited leading to the synthesis of well-defined final materials.

7.1.1 Size Exclusion Chromatography (SEC) Results

In Figures 7.1 to 7.17, the chromatograms for all seventeen linear diblock copolymers are represented, as well as for their first block precursors, following the pattern of Table 7.1 (i.e. from the sample with the highest PS majority to the sample with the lowest one). Prior to every measurement, the chromatogram was calibrated with PS standards with well-known molecular weights.

It is easily observed from the SEC chromatograms (Fig. 7.1, 7.2 and 7.3) of these three linear diblock copolymers (PS-b-PCHD-10, PS-b-PCHD-8 and PS-b-PCHD-2 respectively) that they exhibit very narrow and monomodal molecular weight distributions implying high chemical and compositional homogeneity. Additionally, the fact that they all exhibit a PS majority composition above 90% and very low molecular weights for the PCHD blocks, leads to the conclusion that any termination and/or side reactions during the polymerization of 1,3-cyclohexadiene were absent. In the cases of the PS-b-PCHD-1and PS-b-PCHD-2 samples, the difference between the peaks of the final material (black) and the first

block (red) is very low, which is something reasonable since the PCHD blocks for these two samples exhibit very low number average molecular weights.

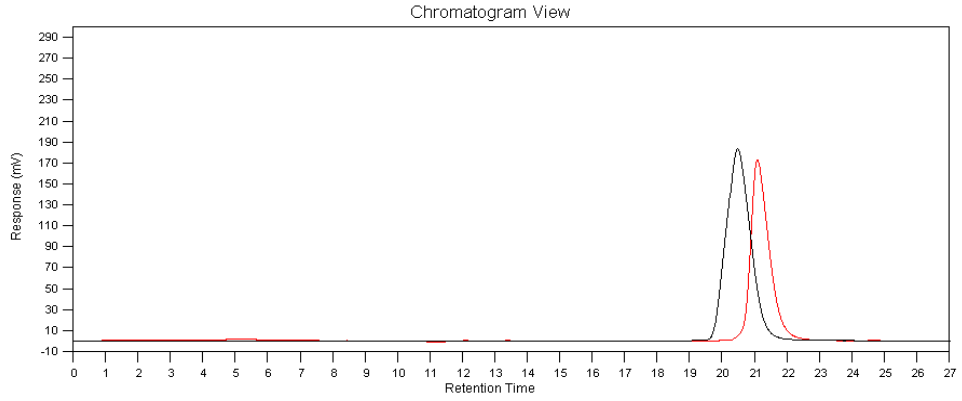

Figure 7.1: *SEC chromatograms of the PS block with* $\overline{M}_n^{PS}$ *= 43.470 g/mol and of the linear diblock copolymer PS-PCHD-10, with* $\overline{M}_{n,tot}$ *= 45.570 g/mol, I = 1,05 and* f_{PS} *= 95,4%.*

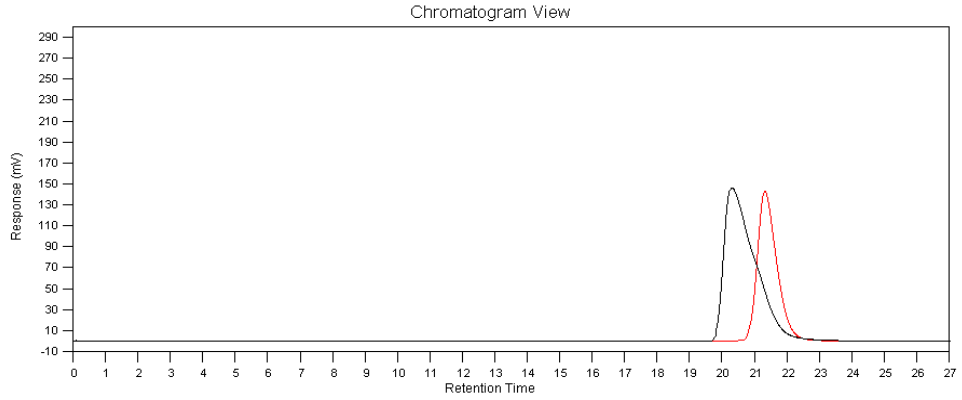

Figure 7.2: *SEC chromatograms of the PS block with* $\overline{M}_n^{PS}$ *= 37.600 g/mol and of the linear diblock copolymer PS-PCHD-8, with* $\overline{M}_{n,tot}$ *= 40.000 g/mol, I = 1,07 and* f_{PS} *= 94%.*

By observing the SEC chromatograms (Fig 7.4 and 7.5 respectively) of these two linear diblock copolymers (PS-PCHD-1 and PS-PCHD-5), it is clearly understood that their molecular weight distributions are monomodal. The presence of only one peak and their low polydispersity indices indicates their chemical and compositional homogeneity as well as the absence of any side and/or termination reactions during the polymerization of 1,3-cyclohexadiene.

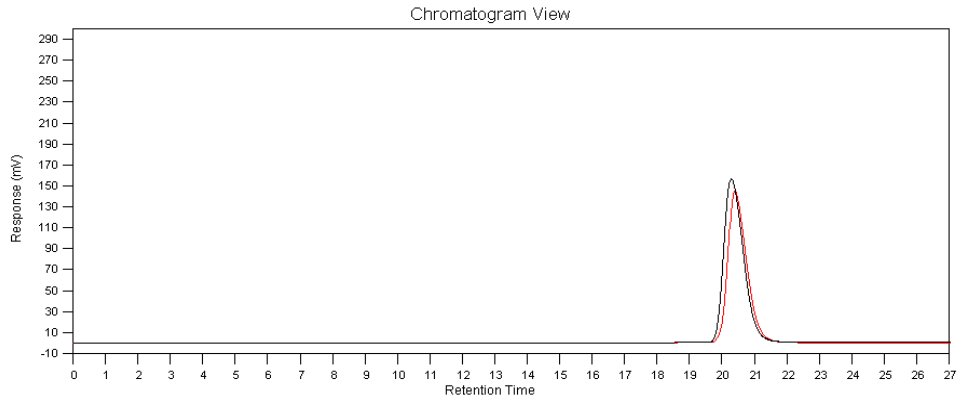

Figure 7.3: *SEC chromatograms of the PS block with* $\overline{M}_n^{PS}$ *= 41.280 g/mol and of the linear diblock copolymer PS-PCHD-2, with* $\overline{M}_{n,tot}$ *= 46.340 g/mol, I = 1,04 and* f_{PS} *= 90,25%.*

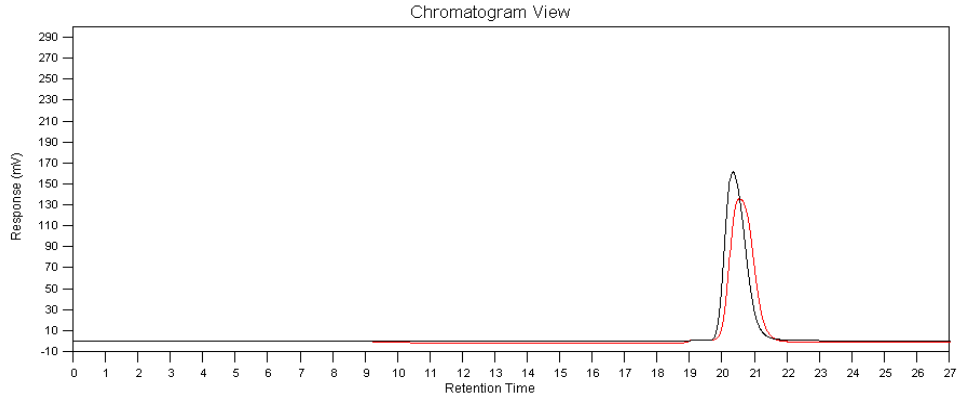

Figure 7.4: *SEC chromatograms of the PS block with* $\overline{M}_n^{PS}$ *= 44.750 g/mol and of the linear diblock copolymer PS-PCHD-1, with* $\overline{M}_{n,tot}$ *= 50.770 g/mol, I = 1,04 and* f_{PS} *= 88,1%.*

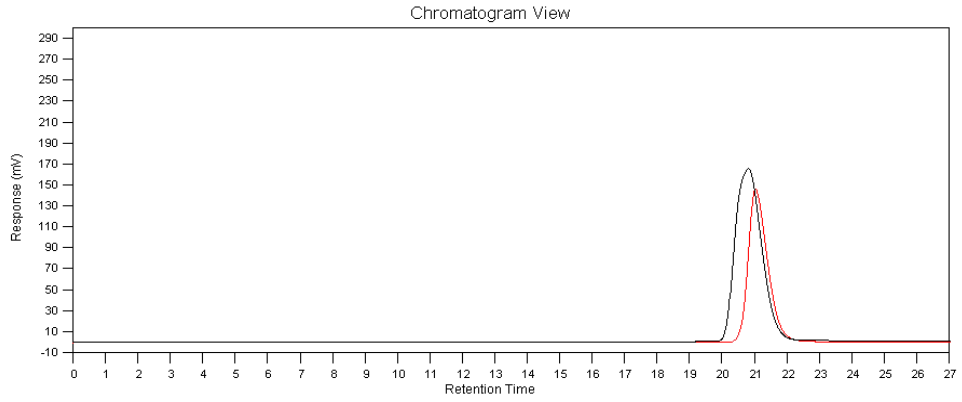

Figure 7.5: *SEC chromatograms of the PS block with* $\overline{M}_n^{PS}$ *= 30.200 g/mol and of the linear diblock copolymer PS-PCHD-5, with* $\overline{M}_{n,tot}$ *= 36.600 g/mol, I = 1,06 and* f_{PS} *= 82,5%.*

Furthermore, it is observed that as the volume fraction of the PS block decreases, the difference between the two corresponding peaks increases towards higher molecular weights, since the molecular weight of the second block increases as well.

The SEC chromatogram of Figure 7.6 represents the one of the three linear diblock copolymer cases where 1,3-cyclohexadiene was polymerized first (PCHD-PS-15). The aim of this change in the used monomer addition sequence was primarily the increase of the PCHD block composition in order to synthesize a final material exhibiting PCHD majority.

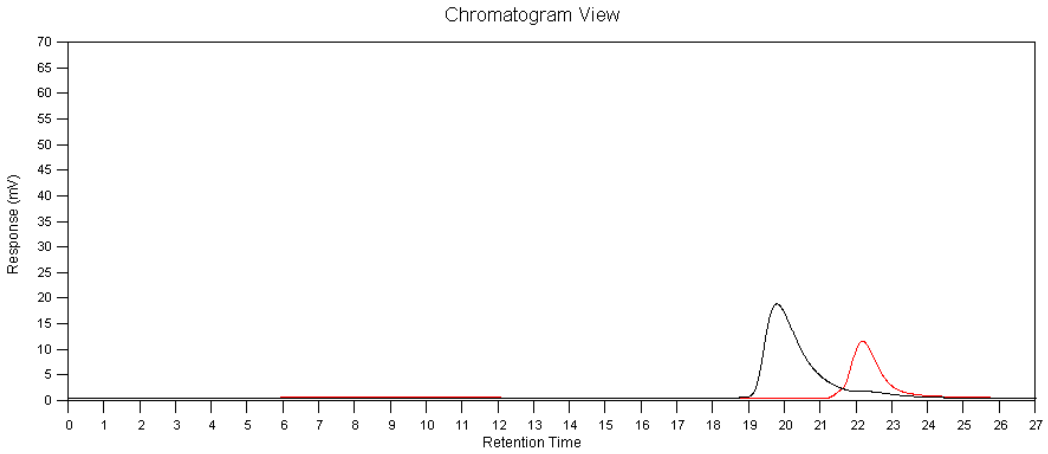

Figure 7.6: *SEC chromatograms of the PCHD block with* $\overline{M}_n^{PCHD}$ *= 12.300 g/mol and of the linear diblock copolymer PCHD-PS-15, with* $\overline{M}_{n,tot}$ *= 57.300 g/mol, I = 1,12 and* f_{PS} *= 78%.*

Cyclohexadiene, when polymerized first, leads to higher molecular weights with very low traces of side and/or termination reactions, depending on the polar additive. Such behavior occurs during the propagation of the polymerization it can reach higher values when compared to the propagation through polystyrene anions. A disadvantage of polymerizing 1,3-cyclohexadiene first, is that the molecular weight distribution of the final copolymer is slightly increased. For this sample, the increase of the PCHD block composition in order to synthesize a final material with PCHD majority was not successful. This might be attributed to the fact that an amount of the monomer did not react with the initiator. However, the symmetric peak from SEC and the relatively low polydispersity index (I = 1,12) indicates that the final linear diblock copolymer exhibits relatively good chemical and compositional homogeneity. The polymerization of styrene as the second monomer from the macroinitiator composed of the PCHD living ends was successful and the propagation proceeded as expected. Additionally, it is important to mention that the existence of the polar additive DABCO, which is already introduced in the solution, changes the polarity and reduces the aggregation degree of polymerization. The polymerization of styrene as the second monomer, therefore, lasted shorter period of time which was approximately one hour. Finally, a large difference between the SEC peaks of the PCHD block (red line) and of the final material (black line) due to the high molecular weight of the second block (PS) is observed.

In Figures 7.7 and 7.8 the SEC chromatograms of samples PS-PCHD-17 and PS-PCHD-14 with f_{PS} = 75,0% and f_{PS} = 64,3% respectively are represented. Analyzing the SEC

chromatogram for the PS-PCHD-17 linear diblock copolymer, one monomodal peak with very narrow polydispersity index (I = 1,07) is observed, indicating high chemical and compositional homogeneity for this sample as well.

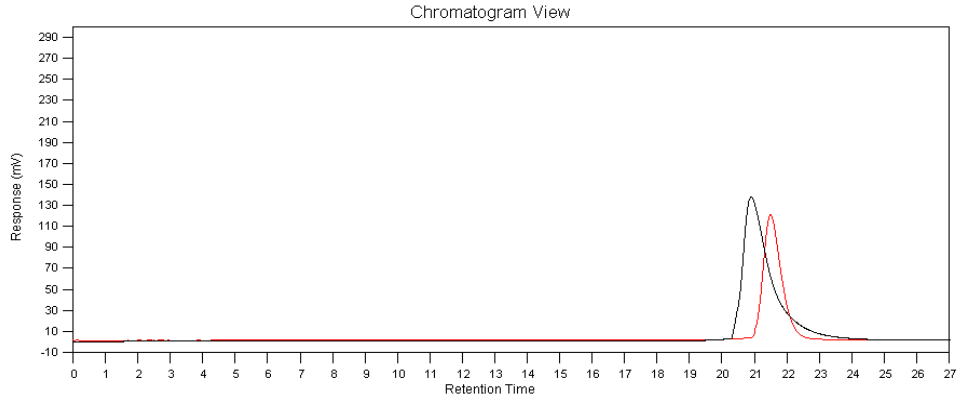

Figure 7.7: *SEC chromatograms of the PS block with* $\overline{M}_n^{PS}$ *= 21.700 g/mol and of the linear diblock copolymer PS-PCHD-17, with* $\overline{M}_{n,tot}$ *= 29.000 g/mol, I = 1,07 and* f_{PS} *= 75%.*

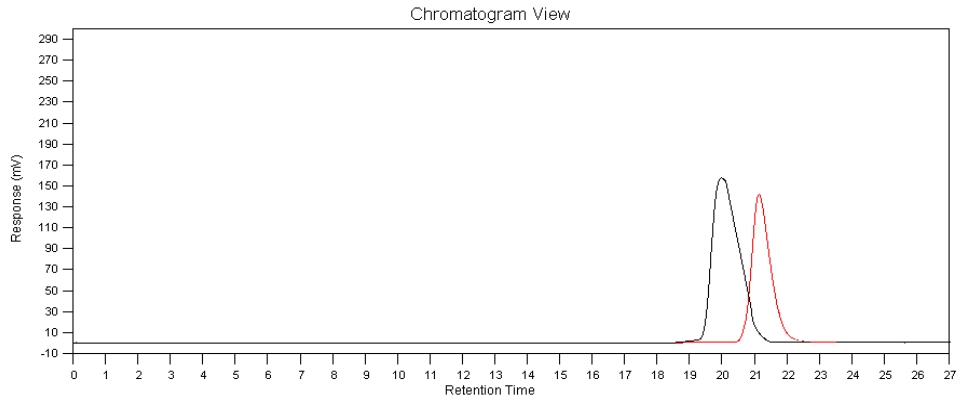

Figure 7.8: *SEC chromatograms of the PS block with* $\overline{M}_n^{PS}$ *= 28.100 g/mol and of the linear diblock copolymer PS-PCHD-14, with* $\overline{M}_{n,tot}$ *= 43.700 g/mol, I = 1,16 and* f_{PS} *= 64,3%.*

For the PS-PCHD-14 sample, it is the first of time that the molecular weight of PCHD block is relatively high ($\overline{M}_{n,PCHD}$ = 15.600 g/mol), if compared to the previous samples, leading to quite broad SEC peak and increased polydispersity (I = 1,16). The increase of the molecular weight for the PCHD block, and eventually for the final copolymer, concluded to broadening of the total molecular weight distribution. Nevertheless, the rather symmetric peak indicates that the degree of chemical and compositional homogeneity is high and any homopolymer is absent.

In the two following Figures (Figures 7.9 and 7.10) the SEC chromatograms are exhibited for the PS-PCHD-3 and PS-PCHD-12 samples respectively. Analyzing the SEC chromatograms of these two copolymers it is evident that their molecular weight distributions are narrow and monomodal indicating a high degree of chemical and compositional

homogeneity. Furthermore, in the case of the PS-PCHD-12 sample, a small broadening of the peak towards to lower molecular weights can be attributed to the increased molecular weight of PCHD block, as already mentioned for samplePS-PCHD-14.

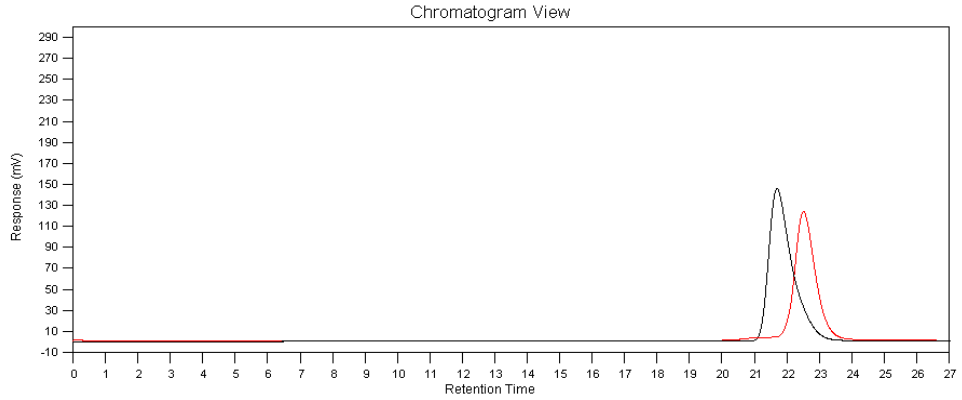

Figure 7.9: *SEC chromatograms of the PS block with* $\overline{M}_n^{PS}$ *= 11.200 g/mol and of the linear diblock copolymer PS-PCHD-3, with* $\overline{M}_{n,tot}$ *= 17.800 g/mol, I = 1,07 and* f_{PS} *= 62,9%.*

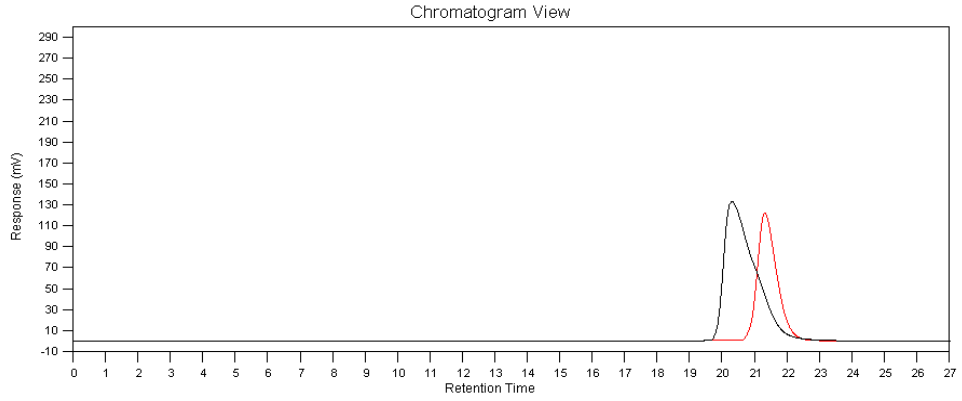

Figure 7.10: *SEC chromatograms of the PS block with* $\overline{M}_n^{PS}$ *= 24.500 g/mol and of the linear diblock copolymer PS-PCHD-12, with* $\overline{M}_{n,tot}$ *= 40.000 g/mol, I = 1,09 and* f_{PS} *= 61,25%.*

The next two SEC chromatographs correspond to samples PS-PCHD-18 and PS-PCHD-11 (Figures 7.11 and 7.12 respectively). Both samples (PS-PCHD-18 and PS-PCHD-11) exhibit narrow and monomodal molecular weight distributions indicating no traces of uncontrolled termination and/or side reactions during the synthesis of the first block (red line), thus high degree of chemical and compositional homogeneity can be concluded. In both samples it is evident that the polymerization of CHD was accomplished since the change in elution volume for the initial first block and the final material is straightforward.

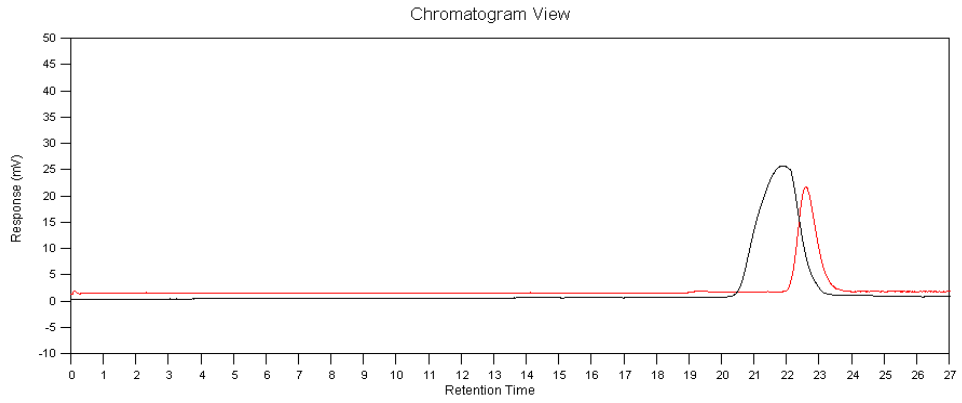

Figure 7.11: *SEC chromatograms of the PS block with* $\overline{M}_n^{PS}$ *= 10.700 g/mol and of the linear diblock copolymer PS-PCHD-18, with* $\overline{M}_{n,tot}$ *= 17.600 g/mol, I = 1,10 and* f_{PS} *= 60,8%.*

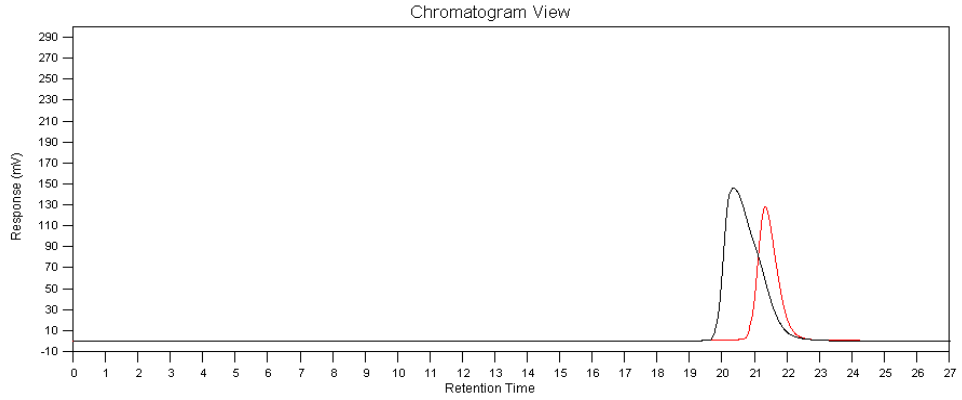

Figure 7.12: *SEC chromatograms of the PS block with* $\overline{M}_n^{PS}$ *= 24.500 g/mol and of the linear diblock copolymer PS-PCHD-11, with* $\overline{M}_{n,tot}$ *= 40.600 g/mol, I = 1,10 and* f_{PS} *= 60,3%.*

In Figures 7.13 and 7.14 the SEC chromatograms for the samples PS-PCHD-16 and PCHD-PS-9 are given. In the case of PS-PCHD-16 linear diblock copolymer, high chemical and compositional homogeneity can be concluded, since the molecular weight distribution is very narrow and monomodal (I = 1,04). Furthermore, one should expect higher values for the polydispersity index, since the molecular weight of the PCHD block is not so low (13.400 g/mol), but the well-purified reagents and the use of high vacuum techniques has lead to better kinetics for the synthesis of the necessary diblock.

Observing the SEC chromatogram corresponding to PCHD-PS-9, one can clearly understand that it is a similar case with the PCHD-PS-15 linear diblock copolymer which was discussed previously. The molecular weight distribution is monomodal but there is a broadening, especially at lower molecular weights, which is a result of the relatively high molecular weight for the PCHD block as well as for the final diblock.

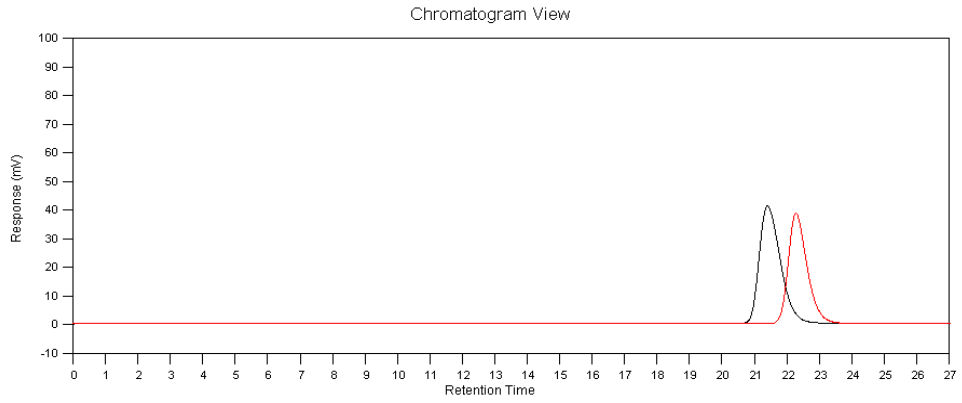

Figure 7.13: *SEC chromatograms of the PS block with* $\overline{M}_n^{PS}$ *= 19.600 g/mol and of the linear diblock copolymer* PS-PCHD-16*, with* $\overline{M}_{n,tot}$ *= 33.000 g/mol, I = 1,04 and* f_{PS} *= 59,4%.*

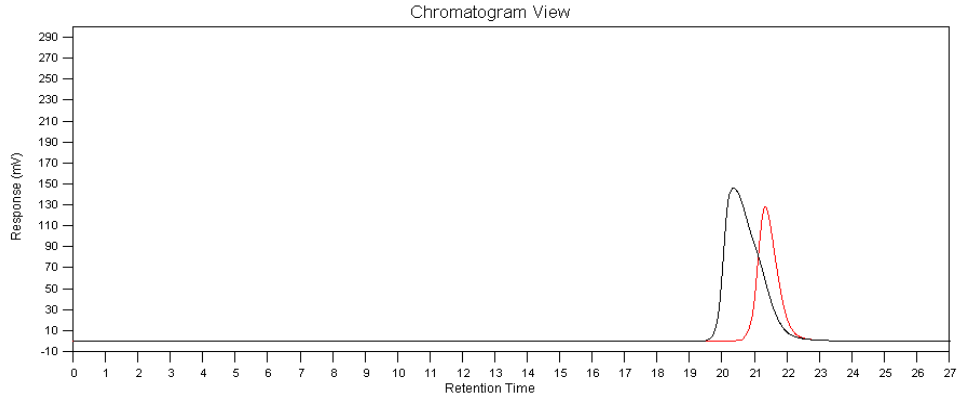

Figure 7.14: *SEC chromatograms of the PCHD block with* $\overline{M}_n^{PCHD}$ *= 22.000 g/mol and of the linear diblock copolymer* PCHD-PS-9*, with* $\overline{M}_{n,tot}$ *= 51.200 g/mol, I = 1,20 and* f_{PS} *= 57,1%.*

The aim of synthesizing a final diblock copolymer with PCHD majority was not accomplished again, probably due to an amount of 1,3-CHD monomer that did not react. However, the polymerization procedures for both monomers proceeded as expected and considering the satisfying molecular characterization results, it is safe to assume that this sample exhibits relatively high chemical and compositional homogeneity.

The three last linear diblock copolymers which will be discussed (PS-PCHD-19, PS-PCHD-4 and PCHD-PS-13) exhibit PCHD majority. Taking into account the weight fraction for the PS-PCHD-19 sample (f_{PS} = 46,6%), it is understood that corresponds to an almost symmetric linear diblock copolymer. Additionally, the fact that there are drawbacks for the synthesis of monomodal PS-PCHD copolymers with PCHD as the majority second block and relatively high molecular weight, reflects the slight difference between the weight fractions of the two blocks. Nevertheless, according to the SEC chromatogram of Figure 7.15, the molecular weight distribution is narrow (I = 1,07) and monomodal indicating high chemical and compositional homogeneity.

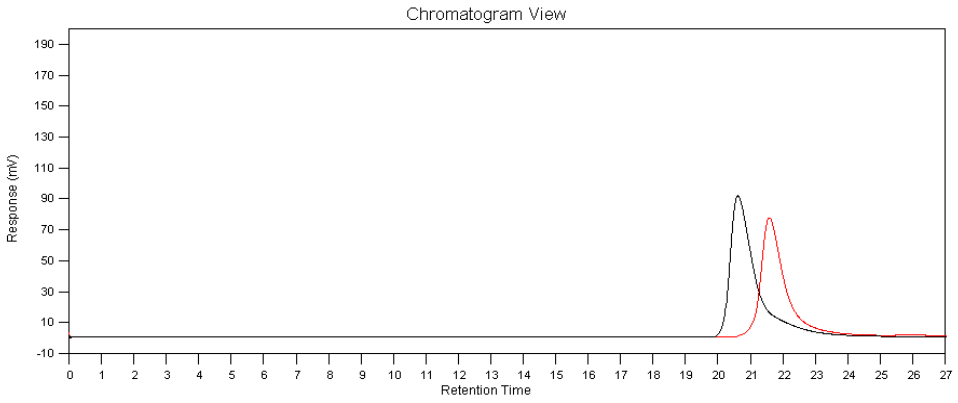

Figure 7.15: *SEC chromatogram of the PS block with* $\overline{M}_n^{PS}$ *= 18.400 g/mol and of the linear diblock copolymer PS-PCHD-19, with* $\overline{M}_{n,tot}$ *= 39.500 g/mol, I = 1,07 and* f_{PS} *= 46,6%.*

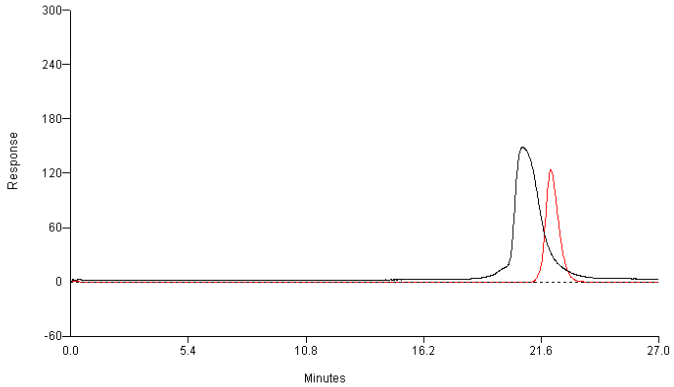

Figure 7.16: *SEC chromatogram of the PS block with* $\overline{M}_n^{PS}$ *= 15.500 g/mol and of the linear diblock copolymer PS-PCHD-4, with* $\overline{M}_{n,tot}$ *= 35.600 g/mol, I = 1,07 and* f_{PS} *= 43,5%.*

The case of sample PS-PCHD-4 is unique since initially the molecular weight distribution was bimodal, indicating the existence of PS homopolymer in the final material. Fractionation was necessary in a solvent/non-solvent mixture of toluene/methanol in order to separate the lower undesirable molecular weight fractions. As it can be observed from Figure 7.16, fractionation was successful and the final copolymer exhibited narrow (I = 1,12) and monomodal molecular weight distribution.

Finally, the SEC chromatogram for the PCHD-PS-13 linear diblock copolymer is observed in Figure 7.17. Analyzing the SEC chromatogram of this sample, it is evident that the molecular weight distribution is monomodal but quite broad.

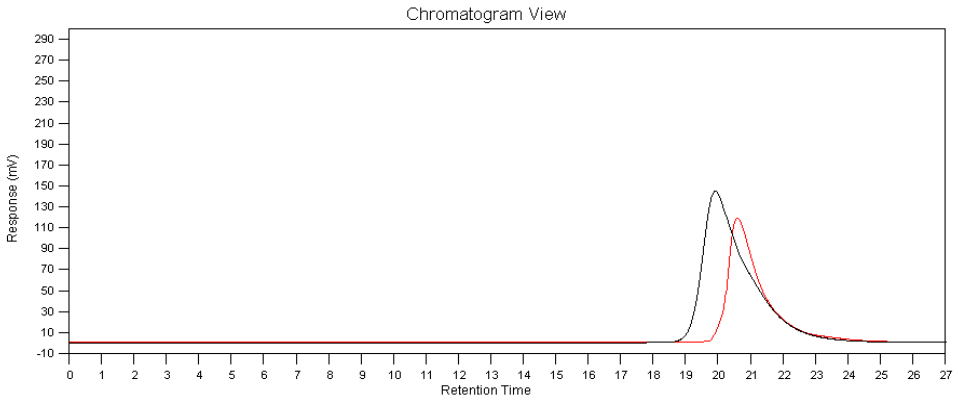

Figure 7.17: *SEC chromatograms of the PCHD block with* $\overline{M}_n^{PCHD}$ *= 34.700 g/mol and of the linear diblock copolymer PCHD-PS-13, with* $\overline{M}_{n,tot}$ *= 47.700 g/mol, I = 1,23 and* f_{PS} *= 27,25%.*

The polymerization of 1,3-cyclohexadiene as the first monomer led to this broadening and the polydispersity index was the highest among all synthesized samples (I = 1,23). This sample is the only one of these series that exhibits the highest volume fraction (f_{PCHD} = 72,75%) as well as the highest molecular weight (34.700 g/mol) for the PCHD block, which is the main reason of the increased polydispersity. However, no significant observation of any side and/or termination reactions appeared from the molecular characterization via SEC, indicating chemical and compositional homogeneity for this sample as well.

Concluding, it is clearly understood from the molecular characterization via SEC, that all seventeen (17) linear diblock copolymers synthesized can be considered as well-defined samples with monomodal molecular weight distributions. Several samples exhibit very narrow polydispersities while others slightly broadened, depending on how increased was the total molecular weight and the molecular weight of the PCHD block or on which monomer was polymerized first. It is possible that, for some samples, small scale termination and/or side reactions might have occurred in very small percentages, especially in those where the polydispersity indices are approximately or above 1,10. Nevertheless, the chemical and compositional homogeneity seems not to be affected.

7.1.2 Proton Nuclear Magnetic Resonance (^{1}H-NMR) Spectroscopy Results

The molecular characterization via proton nuclear magnetic resonance (^{1}H-NMR) spectroscopy was necessary in order to verify the molecular characterization results via SEC and membrane osmometry as well as to confirm the existence of the desirable 1,4-microstructure at high values (> 85%) for the PCHD segments of the linear diblock copolymers. The polymerization system sec-BuLi / DABCO / benzene was used for the synthesis of all linear diblock copolymers as it has already been mentioned, leading approximately to 85-90% 1,4-microstructure and 10-15% 1,2-microstructure for the PCHD block.

In the case of PCHD polymerization with organolithium initiators (e.g. n-BuLi) and no polar additives, the final materials exhibited almost 100% 1,4-microstructure, even though the initiation and propagation reactions were relatively slow.[41]This observation led to the conclusion that the negative charge is located on the a-carbon, thus 1,4-microstructure is favored. By using the polar additive TMEDA, which creates a complex with lithium, the initiation and propagation reactions are significantly increased and 1,2-microstructure is also increased due to the detachment of lithium from the main chain and the delocalization of the negative charge form a-carbon to c-carbon (Figure 7.18).

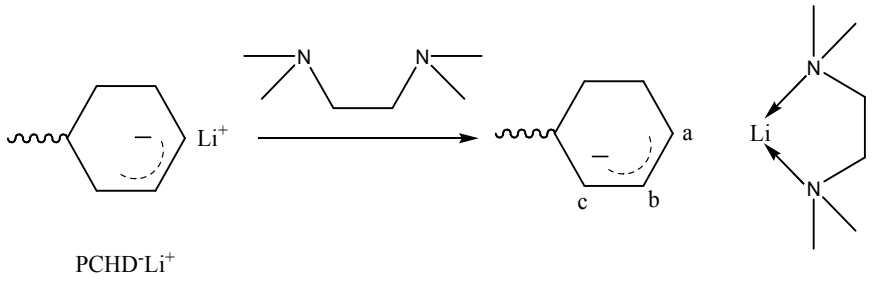

Figure 7.18: *Influence of the polar additive TMEDA on the microstructure of PCHD.*

On the other hand, the polar additive DABCO, which is bulkier than TMEDA and less polar, creates as well a complex with lithium by also removing it from the main chain and increasing the rate of propagation reaction (Figure 7.19). But in this case, lithium remains closer to the main chain and localization at a-carbon is most prominent, leading mainly to a high 1,4-microstructure.

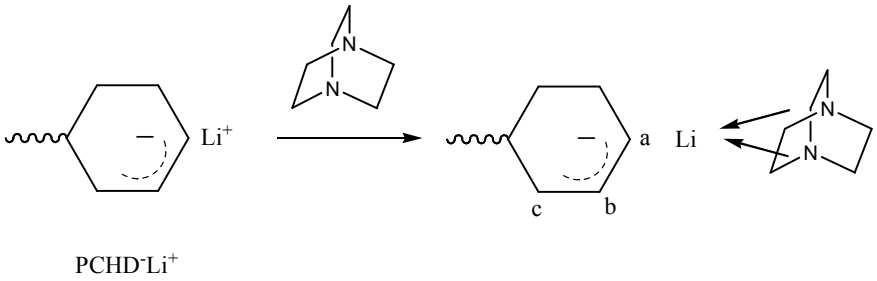

Figure 7.19: *Influence of the polar additive DABCO on the microstructure of PCHD.*

The most characteristic feature of a ^{1}H-NMR spectrum is its proton chemical shifts which correspond to specific protons mainly of the monomeric units. In Table 7.2 the proton chemical shifts for polystyrene and poly(cyclohexadiene) are given. As it can be understood, the ratio of each block can be estimated via ^{1}H-NMR spectroscopy since, according to Table 7.2, different protons generate different chemical shifts in a ^{1}H-NMR spectrum.

Table 7.2: *Category and number of protons with their corresponding chemical shifts for polystyrene and poly(cyclohexadiene).*

Polymer	Category-Number of Protons	Microstructure	Chemical Shift (ppm)
PS	Aromatics (5)	---	6,30-7,50
PCHD	Aromatics (2 double bond, 4 a-protons)	1,4	5,4-5,8 and 1,85-2,35[a]
	Aromatics (2 double bond, 3 a-protons)	1,2	5,4-5,8 and 1,85-2,35[a]

[a] Chemical shift range for α-protons (allylic) of PCHD.

More specifically, olefinic and aromatic protn chemical shifts appear above 4 ppm while the aliphatic appear at lower chemical shifts (> 2,5 ppm). Olefinic proton chemical shifts usually attract greater interest since they correspond to double bond protons of polydienes. For the PS-PCHD diblock samples, the proton chemical shifts of the aromatic hydrogen atoms of polystyrene at 6,3-7,5 ppm are very distinguished. In addition, the proton chemical shifts at 5,4-5,8 ppm of hydrogen atoms connected to carbons which form the double bond in the ring of PCHD are also very significant.

The ratios of the different microstructures for polydienes can be also calculated via ^{1}H-NMR spectroscopy, providing very useful information concerning the synthetic route and the kinetics of the propagation reactions. More specifically, in the case of poly(cyclohexadiene), the corresponding peaks for 1,4- and 1,2- microstructures are confirmed through the chemical shifts of allylic protons (a-protons, H_α) of the aromatic ring at 1,85-2,35 ppm, while the aliphatic protons (β-protons) appear at 1,25-1,85 ppm. As Natori et al. first noticed[41] there is a difference between 1,2-units and 1,4-units due to the different number of hydrogen atoms (H_α) on the carbons adjacent to the double bond. By performing several experiments, Natori concluded that 1,2-units satisfy the equation H_α / H_a + H_β = 1/2, while 1,4-units satisfy the equation H_α / H_α + H_β = 1/3. This means that allylic protons (H_α) and aliphatic protons (H_β) for the 1,2-microstructure are in both cases three (3), while for the 1,4-microstructure H_α are two (2) and H_β four (4) (Figure 7.20).

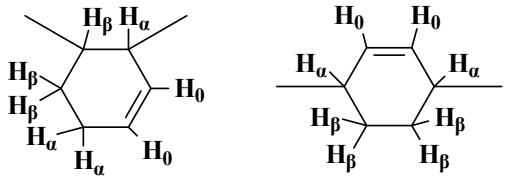

1,2- **1,4-**

Figure 7.20: Allylic and aliphatic protons (H_α and H_β respectively) of 1,2- and 1,4-units of poly(cyclohexadiene). H_a appear at 1,85-2,35 ppm, H_β appear at 1,25-1,85 ppm and H_0 (hydrogens attached to carbons of the double bond) appear at 5,4-5,8 ppm.[41]

Furthermore, a method referred by Quirk et al.[136] was utilized for the calculation of the 1,2- and 1,4-microstructure ratios for each sample. In this method, the integration of the olephinic resonances (5,4-5,8 ppm) is compared with the integration of the allylic resonances (1,85-2,35 ppm). The olefinic protons in the 1,2-microstructure are two (2) and the allylic protons are three (3), as previously reported, while in the 1,4-microstructure there are two (2) olefinic protons and two (2) allylic protons. Based on the aforementioned facts, the following equations were used to determine the ratio of the 1,2- and 1,4- microstructures for PCHD block:

$$\frac{Area_{olephinic}}{Area_{allylic}} = \frac{(2f_{1,2} + 2f_{1,4})}{(3f_{1,2} + 2f_{1,4})} \qquad (7.1)$$

$$f_{1,2} + f_{1,4} = 1 \qquad (7.2)$$

where $f_{1,2}$ is the relative amount of the 1,2-microstructure and $f_{1,4}$ is the relative amount of the 1,4-microstructure. Based on the above two equations and the information given from the ^{1}H-NMR spectra obtained for all seventeen linear diblock copolymer samples the 1,4- and 1,2-microstructure percentages were calculated and the results are stated on Table 7.3.

A ^{1}H-NMR spectrum, except from the molar ratio of the microstructure, can also provide information for the number average molecular weight of each sample. In this manner, it is possible to verify the results from size exclusion chromatography and membrane osmometry, even though in many cases it is not a direct method for measuring the number average molecular weight. Nevertheless, such a procedure is possible by calculating the molar ratio (% moles) of each block through the following equation:

$$X_A = \frac{a_A}{\beta} \qquad (7.3)$$

where X_A is the molar ratio (% moles) of A block, α_A is the area of the peaks in the ^{1}H-NMR spectrum for A block and β is the number of protons that cause the particular chemical shift. By using the data from Table 7.2 in equation 7.3, one can conclude at the following two equations:

$$X_{PS} = \frac{a_{6,3-7,2}}{5} \qquad (7.4)$$

$$X_{PCHD} = \frac{a_{5,2-5,4}}{2} \qquad (7.5)$$

Table 7.3: *Weight fractions calculated from SEC and ^{1}H-NMR. Also the percentage ration between 1,2- and 1,4 microstructure for the PCHD segments as calculated by ^{1}H-NMR are also given.*

Samples	f(wt%) PS block (SEC)	f(wt%) PCHD block (SEC)	f(wt%) PS block (NMR)	f(wt%) PCHD block (NMR)	% 1,2-PCHD (NMR)	% 1,4-PCHD (NMR)
PS-PCHD-10	95,4	4,6	91,7	7,3	4	96
PS-PCHD-8	94,0	6,0	90,0	10,0	3	97
PS-PCHD-2	90,2	9,8	91,9	8,1	5	95
PS-PCHD-1	88,1	11,9	92,8	7,2	8	92
PS-PCHD-5	82,5	17,5	83,5	16,5	7	93
PCHD-PS-15	78,0	22,0	75,5	24,5	9	91
PS-PCHD-17	75,0	25,0	76,0	24,0	6	94
PS-PCHD-14	64,3	35,7	61,3	38,7	10	90
PS-PCHD-3	62,9	37,1	65,9	34,1	8	92
PS-PCHD-12	61,2	38,8	62,9	37,1	6	94
PS-PCHD-18	60,8	39,2	62,8	37,2	10	90
PS-PCHD-11	60,3	39,7	62,0	38,0	11	89
PS-PCHD-16	59,4	40,6	62,0	38,0	7	93
PCHD-PS-9	57,1	42,9	53,5	46,5	8	92
PS-PCHD-19	46,6	53,4	45,5	54,5	12	88
PS-PCHD-4	43,5	56,5	40,0	60,0	7	93
PCHD-PS-13	27,2	72,8	23,3	76,7	9	91

Then, the determination of the weight ratio (%wt) is possible, by multiplying each X value with the molecular weight of the corresponding monomer unit according to the equation:

$$\%wt = \frac{X_A \times MW_A}{B} \qquad (7.6)$$

where MW_A is the molecular weight of the monomer unit for A block and parameter B is given by $B = X_{PS} \times MW_{PS} + X_{PCHD} \times MW_{PCHD}$, with MW_{PS} = 104 g/mol and MW_{PCHD} = 80 g/mol. The weight fractions of PS and PCHD as calculated by ^{1}H-NMR are also given together with the relative values as obtained from SEC at Table 7.3. It can be observed that there is an excellent consistency between the values as calculated by the two different techniques, which indicates the compositional and molecular homogeneity.

In the Figures 7.21-7.37 the ^{1}H-NMR spectra of the seventeen (17) PS-PCHD or PCHD-PS linear diblock copolymers synthesized for this research work are presented. The intensity of the ^{1}H-NMR signals is displayed along the vertical axis of a spectrum and is proportional to the molar concentration of the sample. It is very important to refer that all proton chemical shifts in the following spectra appear shifted at approximately 0,2 – 0,5 ppm towards the left side of each spectrum due to different experimental conditions (temperature, magnetic field etc.) each measurement was performed, with regard to the reference proton chemical shifts, when compared to the theoretically predicted spectra.

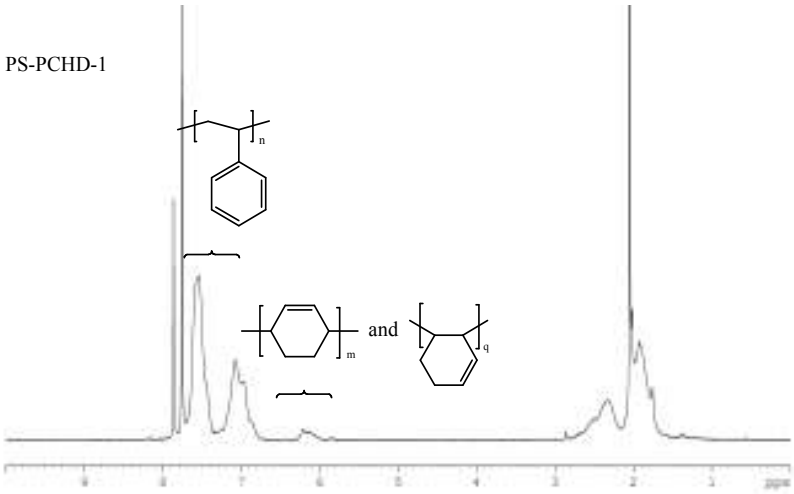

Figure 7.21: *^{1}H-NMR spectrum of the PS-PCHD-1 linear diblock copolymer.*

As it can be easily observed, in the ^{1}H-NMR spectrum of PS-PCHD-1 copolymer, chemical shifts at 6,8 – 7,7 ppm which correspond to aromatic hydrogen atoms of polystyrene and at 5,8 – 6,3 ppm corresponding to hydrogen atoms bounded to carbons of the double bond of PCHD. Also, a chemical shift at 2,85 ppm corresponding to the hydrogen atom bounded to one of the carbons of polystyrene (Ar-C-**H**), several proton chemical shifts at 1,65 – 2,7 ppm corresponding to α- (aliphatic) and β- (allylic) protons of the PCHD aromatic ring and a chemical shift at 1,35 ppm corresponding to hydrogen atoms bounded to the b-carbon of polystyrene (R-C**H$_2$**) can be observed. The proton chemical shifts appearing at approximately 8 ppm correspond to the deuterated chloroform ($CDCl_3$) which is the solvent used to dilute each sample. All the above are characteristic proton chemical shifts which confirm the high

purity and homogeneity of the final materials as well as the existence of polystyrene and poly(cyclohexadiene) units and appear at the ^{1}H-NMR spectra for all seventeen samples.

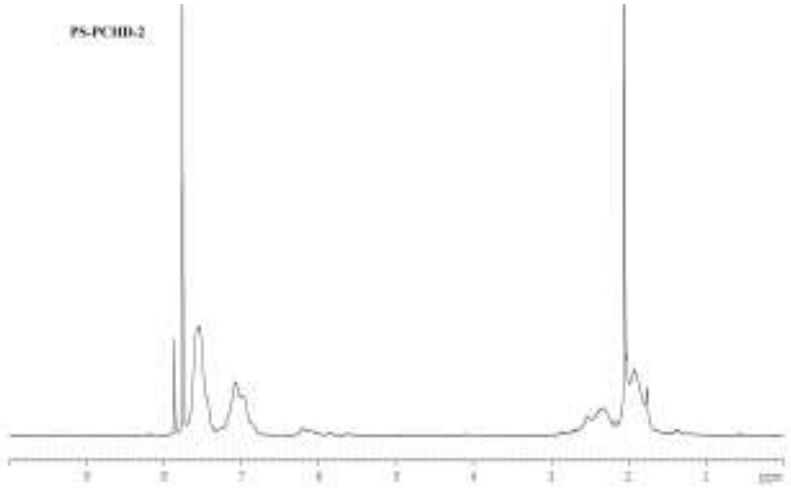

Figure 7.22: *^{1}H-NMR spectrum of the PS-PCHD-2 linear diblock copolymer.*

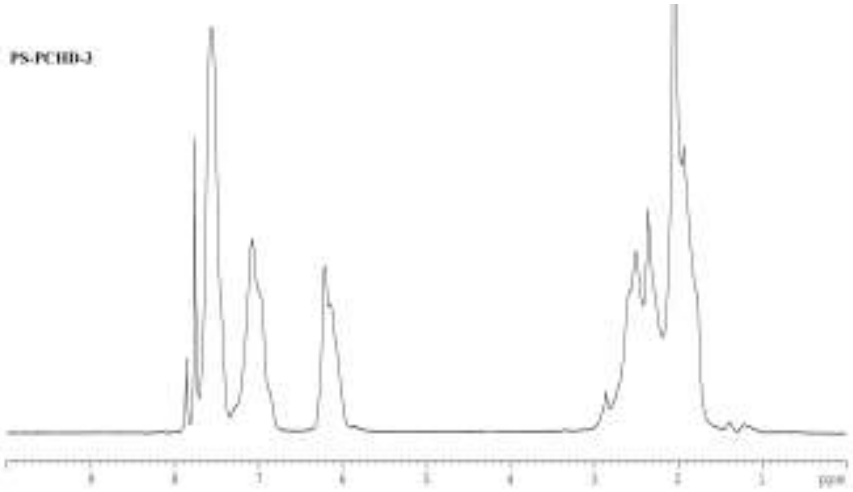

Figure 7.23: *^{1}H-NMR spectrum of the PS-PCHD-3 linear diblock copolymer.*

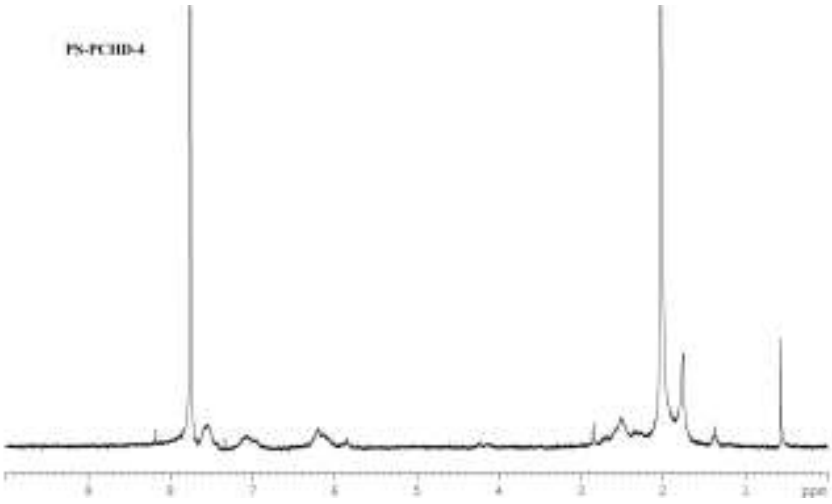

Figure 7.24: *^{1}H-NMR spectrum of the PS-PCHD-4 linear diblock copolymer.*

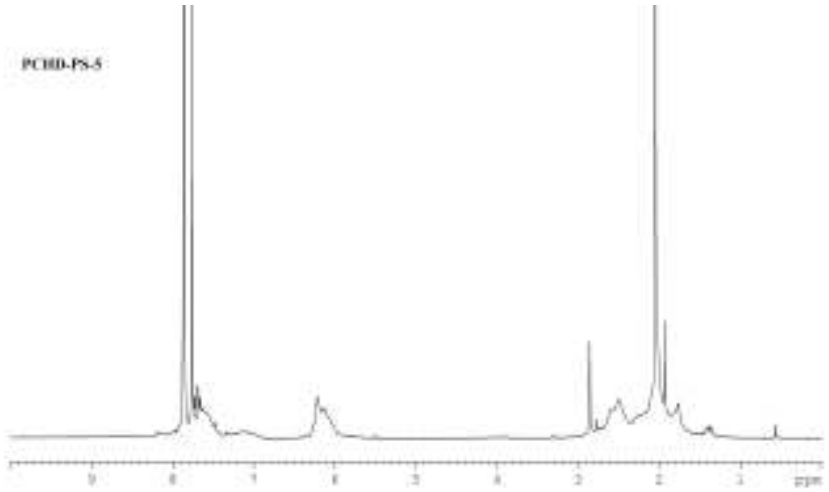

Figure 7.25: *^{1}H-NMR spectrum of the PS-PCHD-5 linear diblock copolymer.*

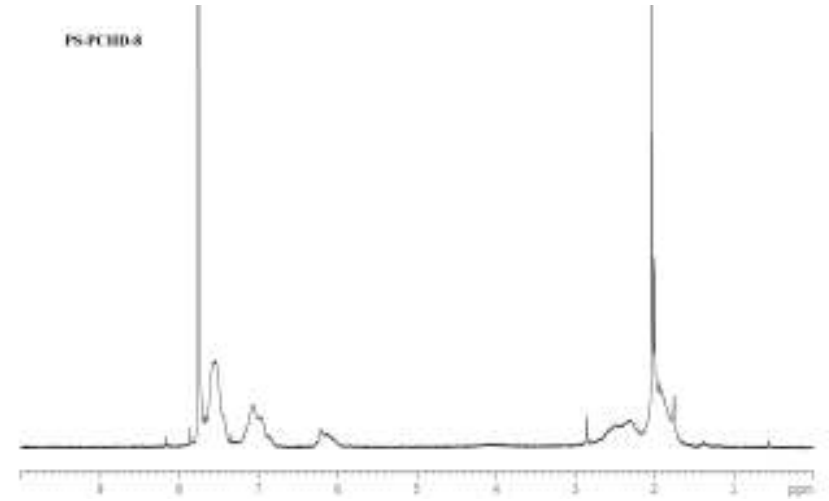

Figure 7.26: *^{1}H-NMR spectrum of the PS-PCHD-8 linear diblock copolymer.*

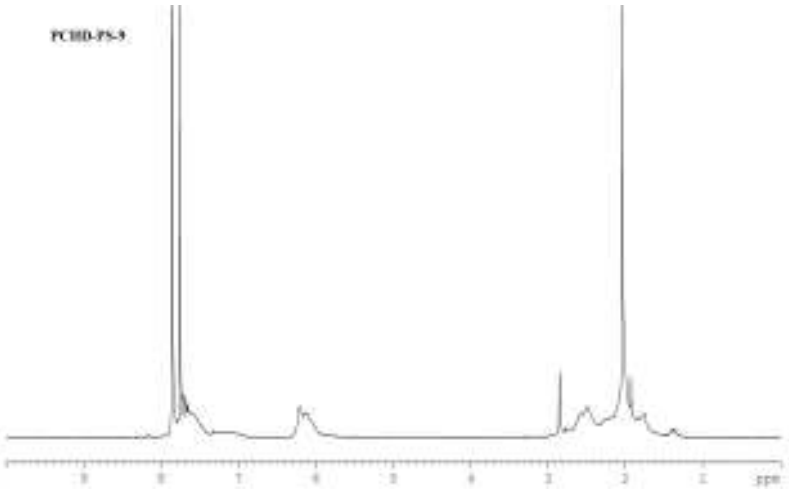

Figure 7.27: *^{1}H-NMR spectrum of the PCHD-PS-9 linear diblock copolymer.*

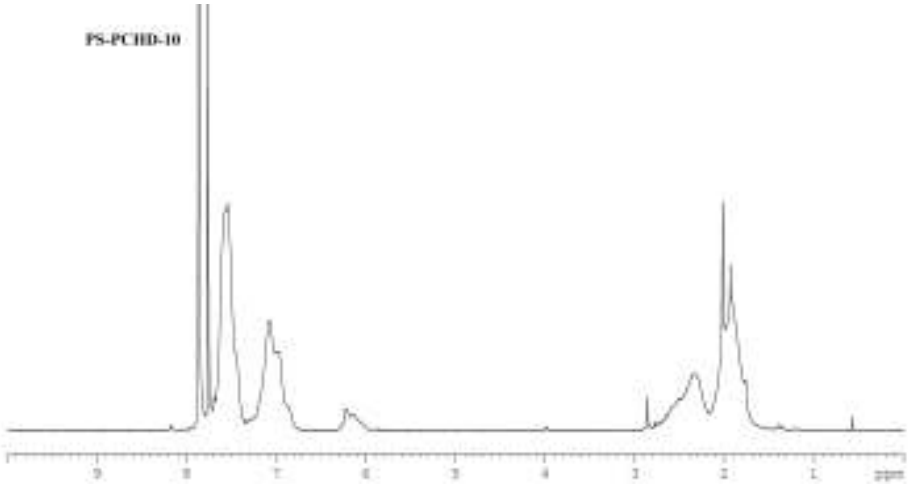

Figure 7.28: *^{1}H-NMR spectrum of the PS-PCHD-10 linear diblock copolymer.*

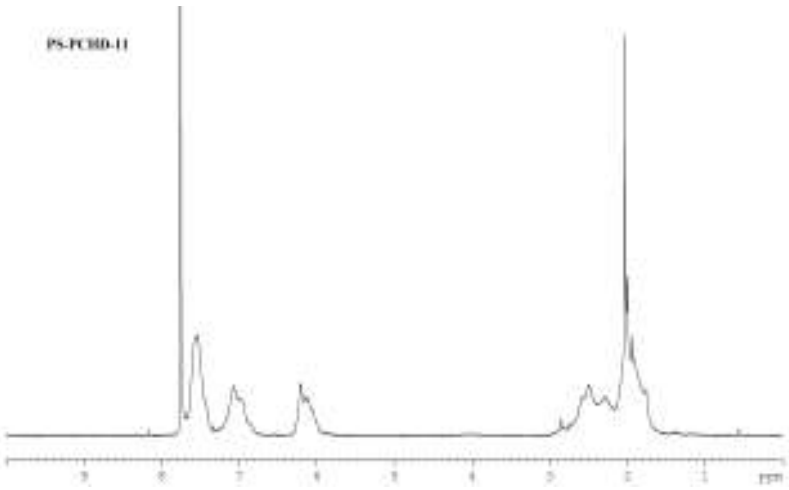

Figure 7.29: *^{1}H-NMR spectrum of the PS-PCHD-11 linear diblock copolymer.*

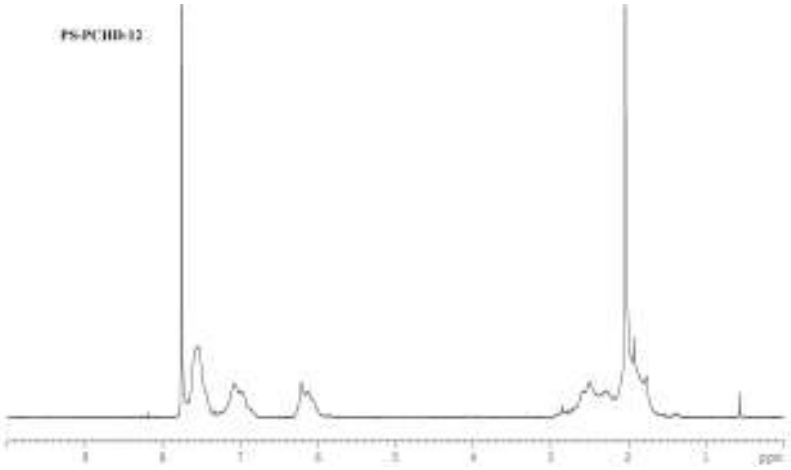

Figure 7.30: *^{1}H-NMR spectrum of the PS-PCHD-12 linear diblock copolymer.*

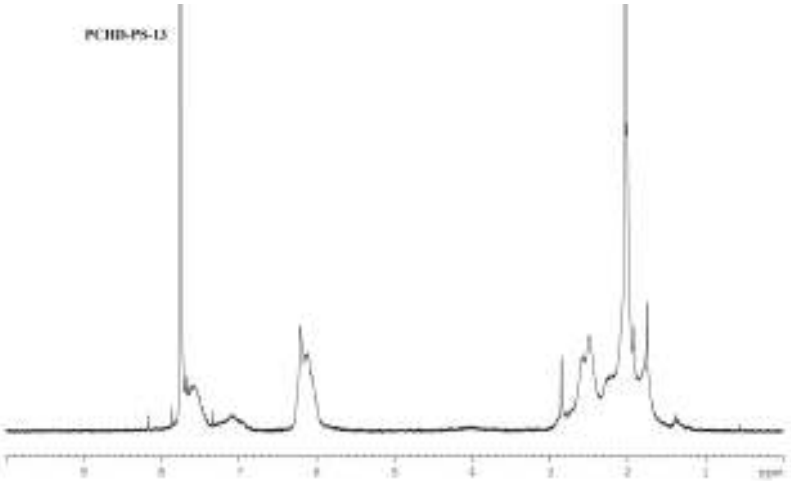

Figure 7.31: *^{1}H-NMR spectrum of the PCHD-PS-13 linear diblock copolymer.*

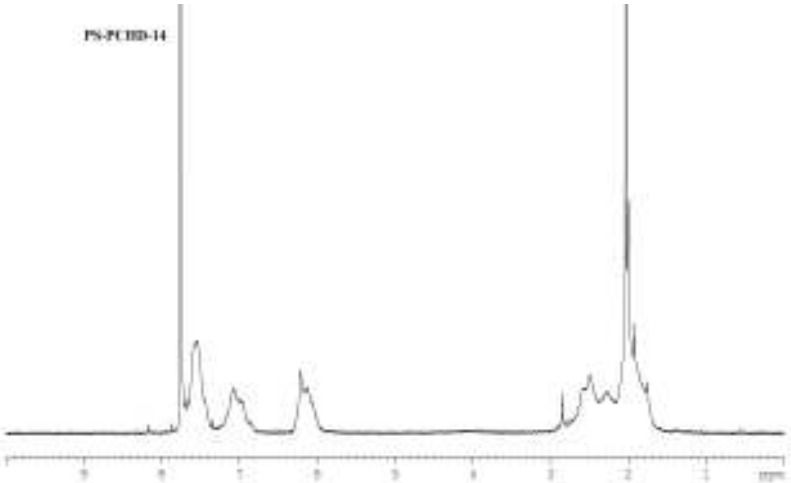

Figure 7.32: *^{1}H-NMR spectrum of the PS-PCHD-14 linear diblock copolymer.*

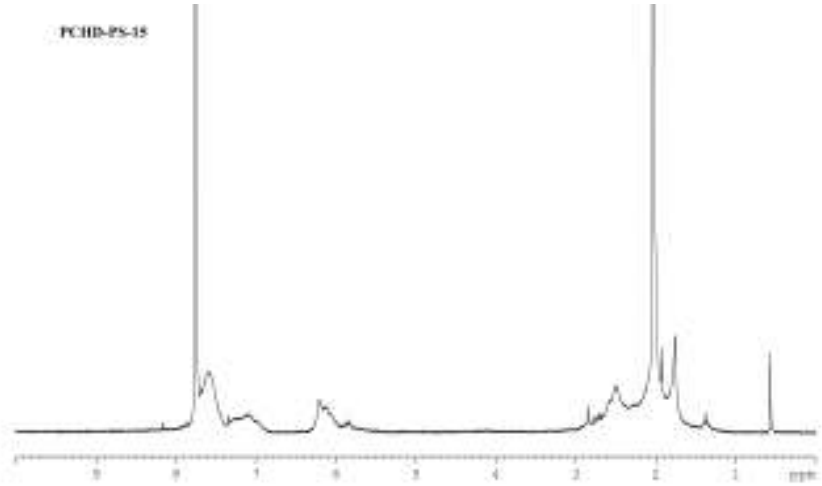

Figure 7.33: *^{1}H-NMR spectrum of the PCHD-PS-15 linear diblock copolymer.*

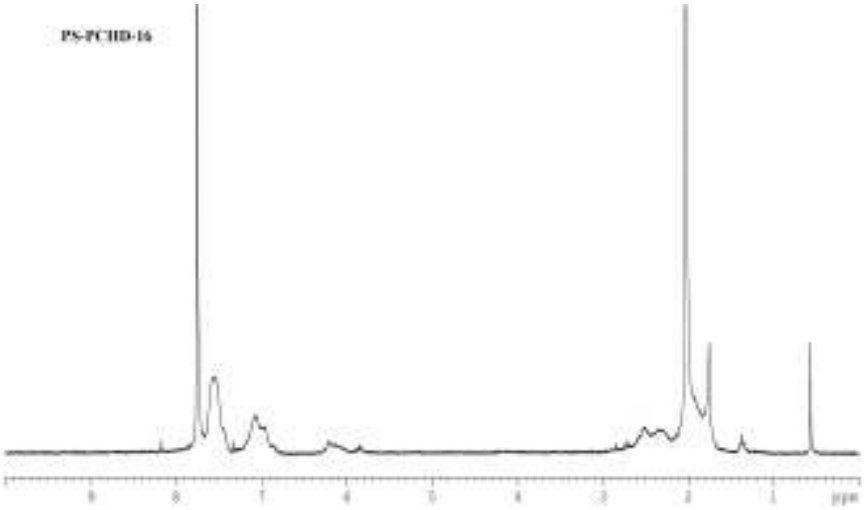

Figure 7.34: *^{1}H-NMR spectrum of the PS-PCHD-16 linear diblock copolymer.*

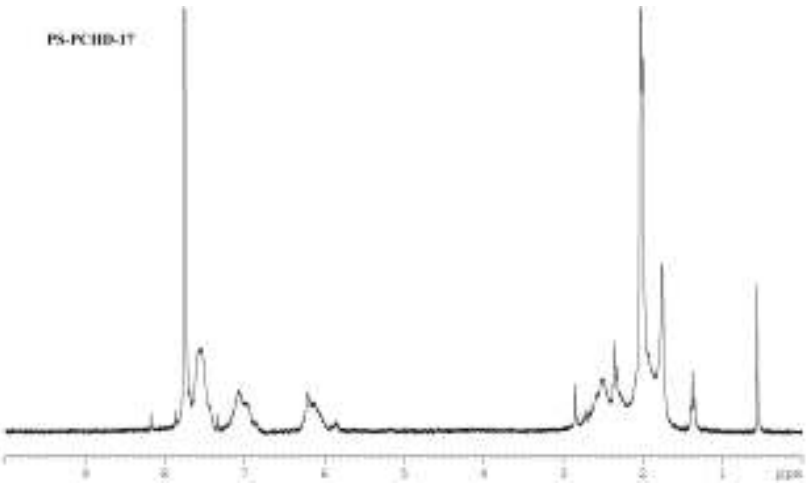

Figure 7.35: *^{1}H-NMR spectrum of the PS-PCHD-17 linear diblock copolymer.*

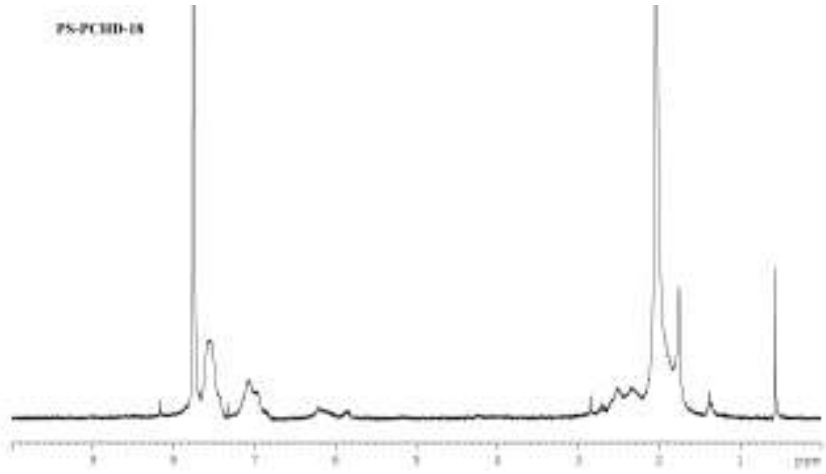

Figure 7.36: *^{1}H-NMR spectrum of the PS-PCHD-18 linear diblock copolymer.*

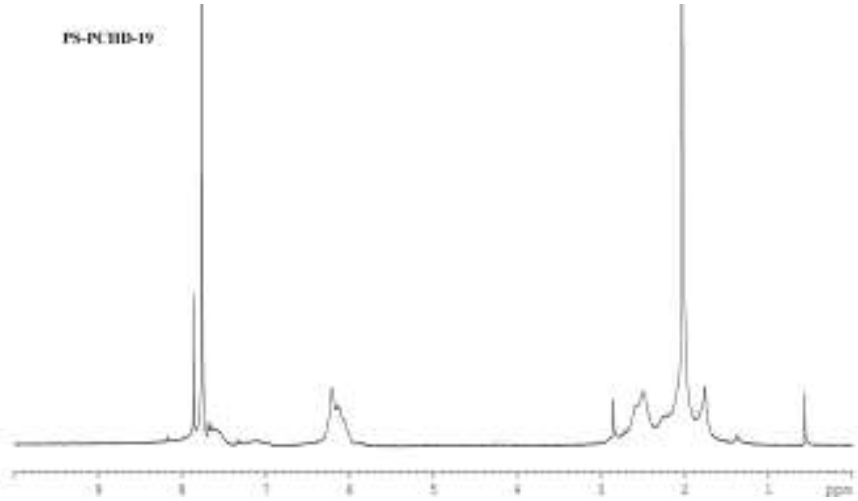

Figure 7.37: *^{1}H-NMR spectrum of the PS-PCHD-19 linear diblock copolymer.*

It is important to mention that by using equations 7.3-7.6, the ratios for PS and PCHD blocks for each of the synthesized linear diblock copolymers were calculated, leading to verification of the molecular characterization results via size exclusion chromatography and membrane osmometry. Only minor differences within the experimental error of the techniques were recorded. Furthermore, by using equations 7.1 and 7.2, the ratios of the 1,2- and the 1,4-microstructures were calculated (Table 7.3) leading to the conclusion that they exhibit high 1,4-microstructure (88%-97% for all samples).

7.2 Thermal Analysis Results

The thermal analysis results via differential scanning calorimetry (DSC) for the seventeen (17) linear diblock copolymers are given and discussed in the following pages. DSC can provide very useful information concerning the glass transition temperature, melting point and the crystallization of a polymeric material. The glass transition temperature (T_g) of

polystyrene is approximately 100^0C, depending on the molecular weight. Polystyrene is an amorphous thermoplastic polymer, which means that it can be heated above its glass transition temperature and can be cooled by returning to its initial form without any changes to the chemical structure and properties. This phenomenon is reversible, can be repeated theoretically innumerous times and it occurs mainly due to chain association through stacking of the aromatic rings. The glass transition temperature of PCHD, which is approximately 100^0C – 110^0C, and its increased thermal and mechanical properties are considered the most important factors leading to its behavior as an amorphous thermoplastic elastomer.

In Figures 7.38 – 7.54 are the DSC curves for all linear diblock copolymers synthesized for this thesis are given. All thermographs displayed correspond to the second heating procedure of each measurement. The first heating was performed in order to erase all the history of the sample at a specific rate (commonly 10^0C/min) and the cooling occurred at ambient conditions.

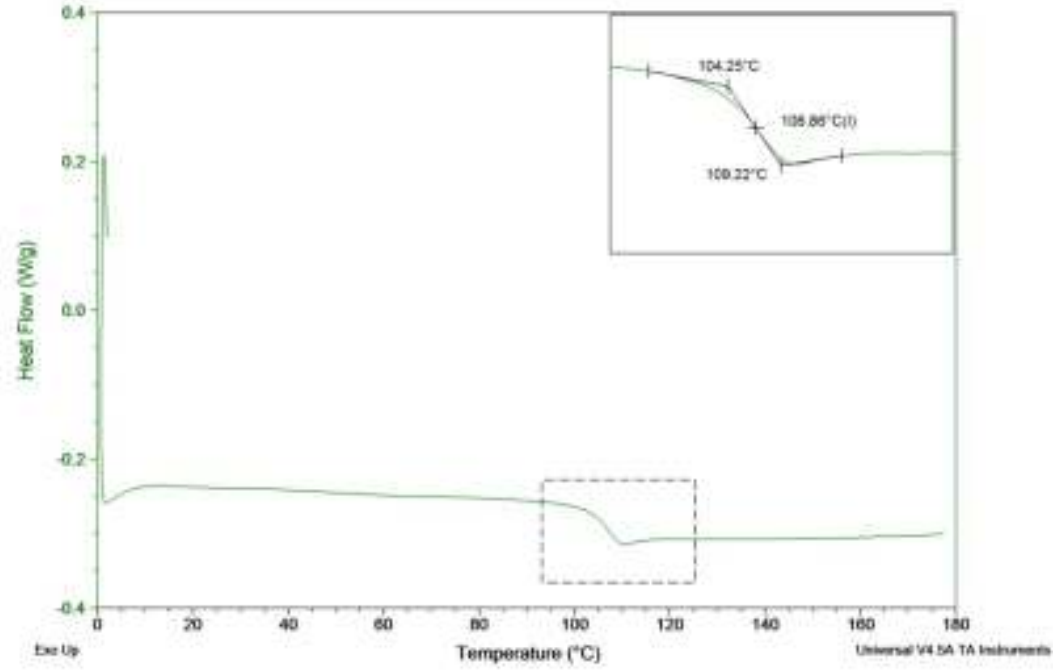

Figure 7.38: *DSC curve of the PS-PCHD-1 linear diblock copolymer with T_g = 106.86^{0}C and $\overline{M}_n$ =50.770 g/mol.*

Analyzing the DSC curve for the PS-PCHD-1 linear diblock copolymer (Figure 7.38) an endothermic transition at approximately 107^0C is observed which is corresponding to glass transition temperature. No crystallization occurs below 180^0C but also no melting temperature (T_m) is observed. Such behavior is attributed to the fact that the melting temperature of 1,4-poly(cyclohexadiene) is around 200^0C while anionically synthesized PS is considered amorphous and no T_m is observed (since it is almost 100% atactic). A new series of DSC measurements were performed to all samples up to 250^0C, but again no crystallization (as

expected) or melting occurred. This implies that the copolymerization of styrene with 1,3-CHD also increased significantly the T_m of the PCHD block. Furthermore, due to the similar glass transition temperatures of the two blocks, the system exhibits only one glass transition temperature. The step used to perform the thermal studies was 10^0C/min in all cycles.

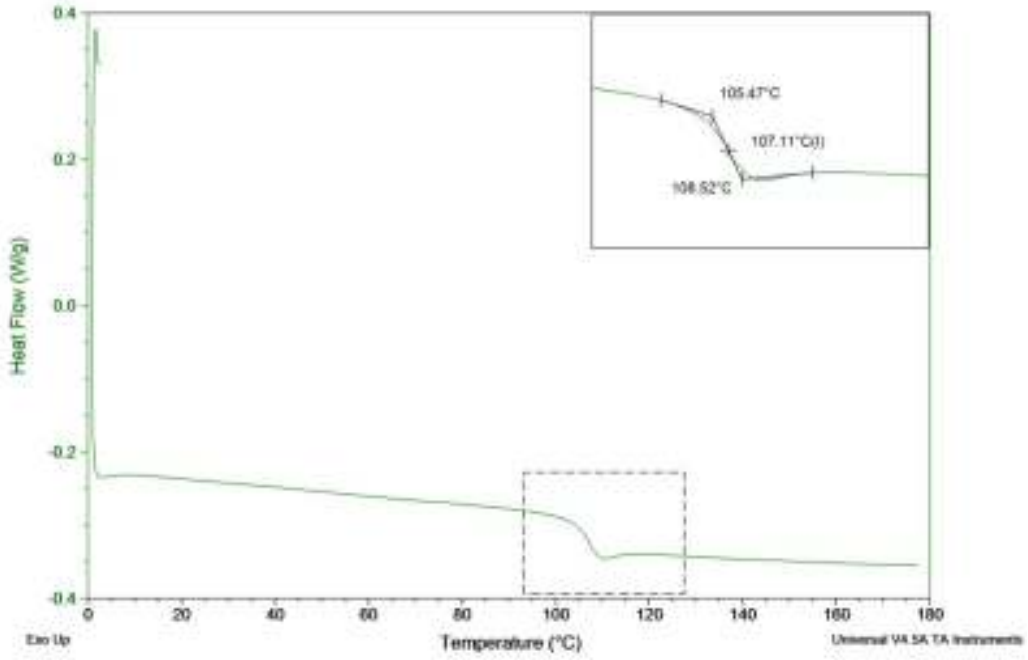

Figure 7.39: *DSC curve of the PS-PCHD-2 linear diblock copolymer with T_g = 107.11^{0}C and $\overline{M}_n$ =46.340 g/mol.*

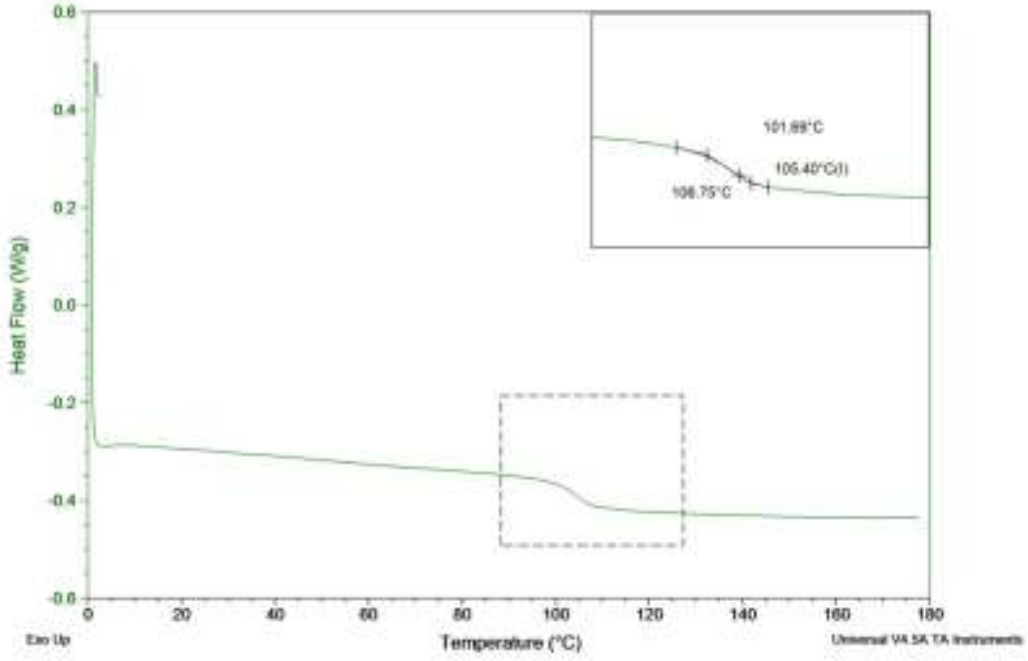

Figure 7.40: *DSC curve of the PS-PCHD-3 linear diblock copolymer with T_g = 105.4^{0}C and $\overline{M}_n$ =17.800 g/mol.*

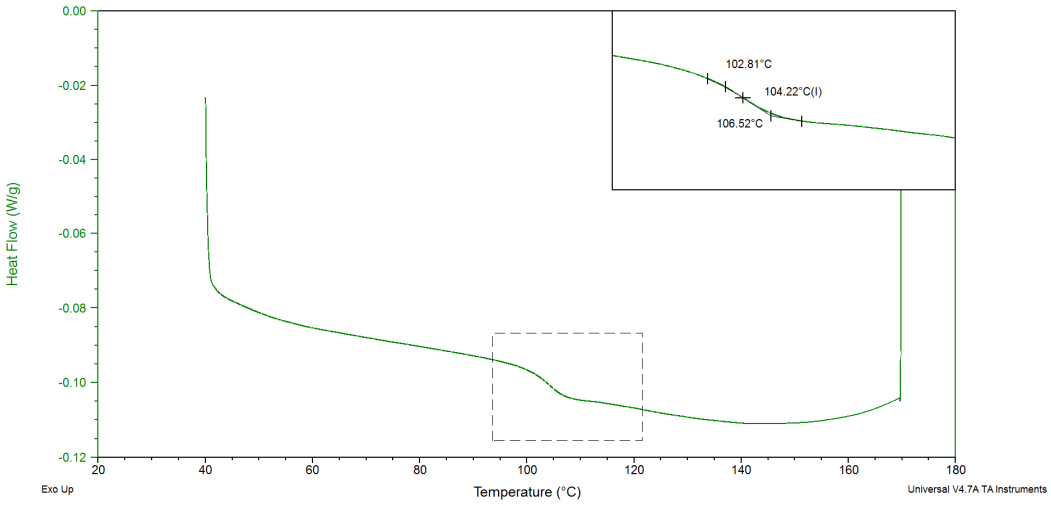

Figure 7.41: *DSC curve of the PS-PCHD-4 linear diblock copolymer with T_g = 104.22^{0}C and $\overline{M}_n$ =35.600 g/mol.*

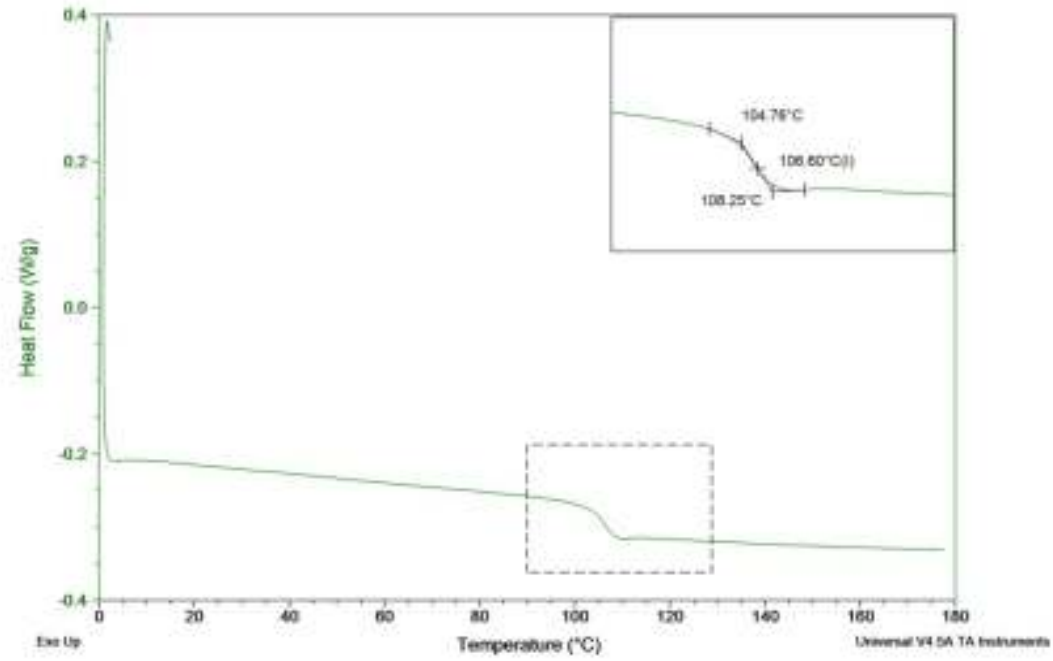

Figure 7.42: *DSC curve of the PS-PCHD-5 linear diblock copolymer with T_g = 106.6^{0}C and $\overline{M}_n$ =36.600 g/mol.*

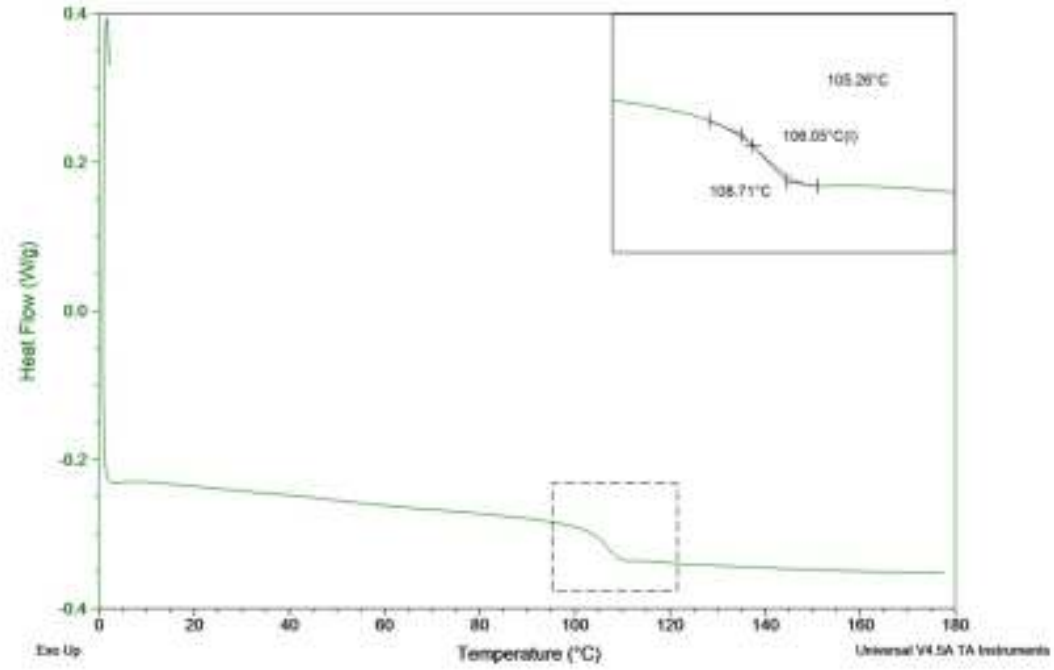

Figure 7.43: *DSC curve of the PS-PCHD-8 linear diblock copolymer with T_g = 106.05^{0}C and $\overline{M}_n$ =40.000 g/mol.*

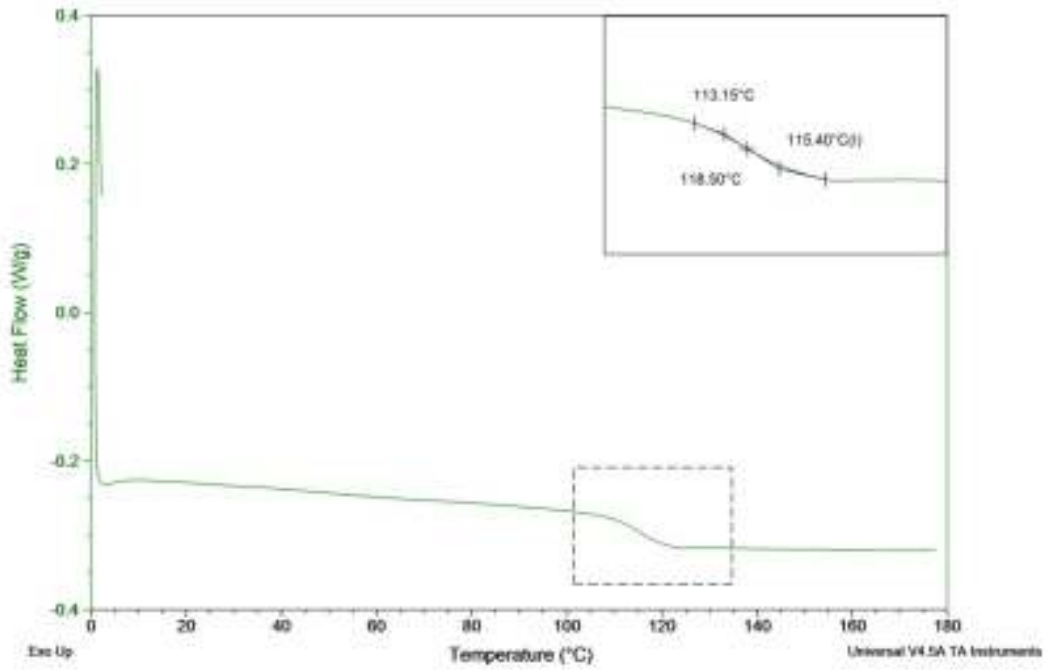

Figure 7.44: *DSC curve of the PCHD-PS-9 linear diblock copolymer with T_g = 115.4^{0}C and $\overline{M}_n$ =51.200 g/mol.*

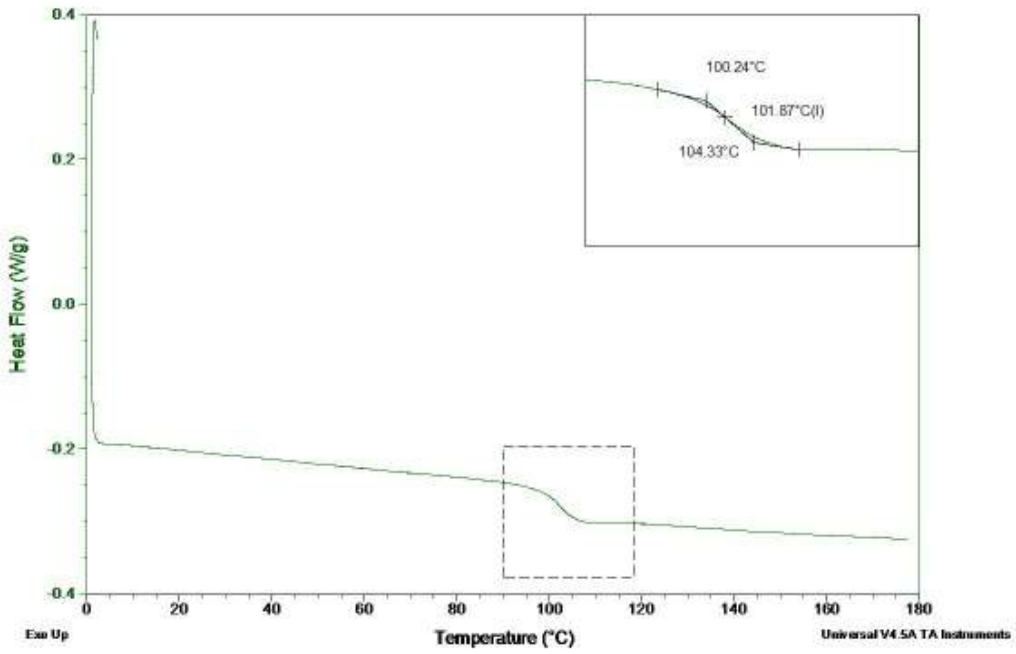

Figure 7.45: *DSC curve of the PS-PCHD-10 linear diblock copolymer with* T_g *= 101.87*^{0}*C and* $\overline{M}_n$ *=45.570 g/mol.*

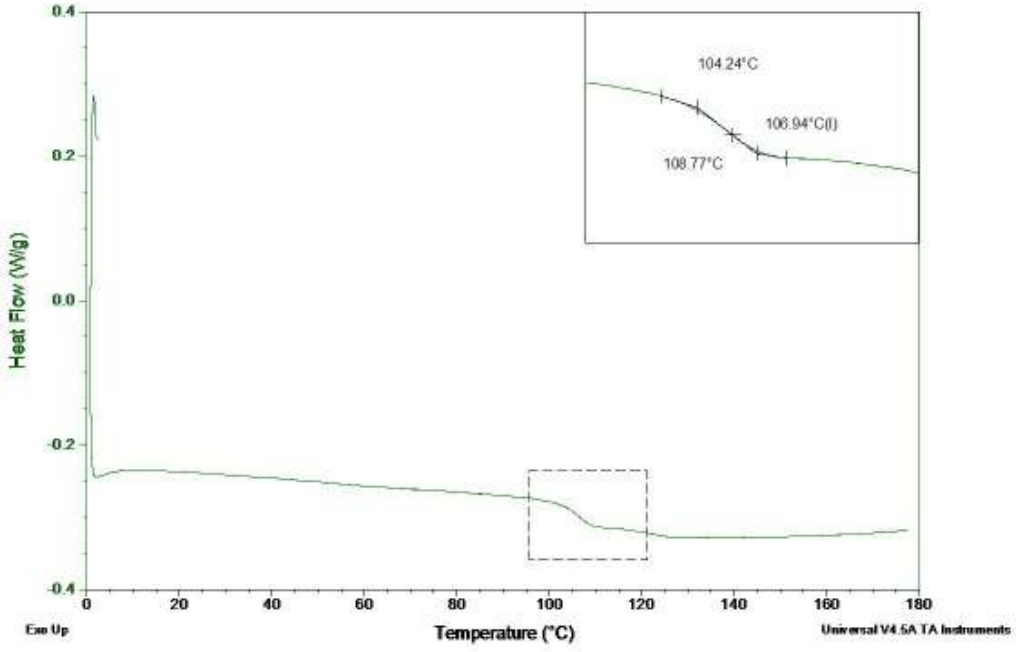

Figure 7.46: *DSC curve of the PS-PCHD-11 linear diblock copolymer with* T_g *= 106.99*^{0}*C and* $\overline{M}_n$ *=40.600 g/mol.*

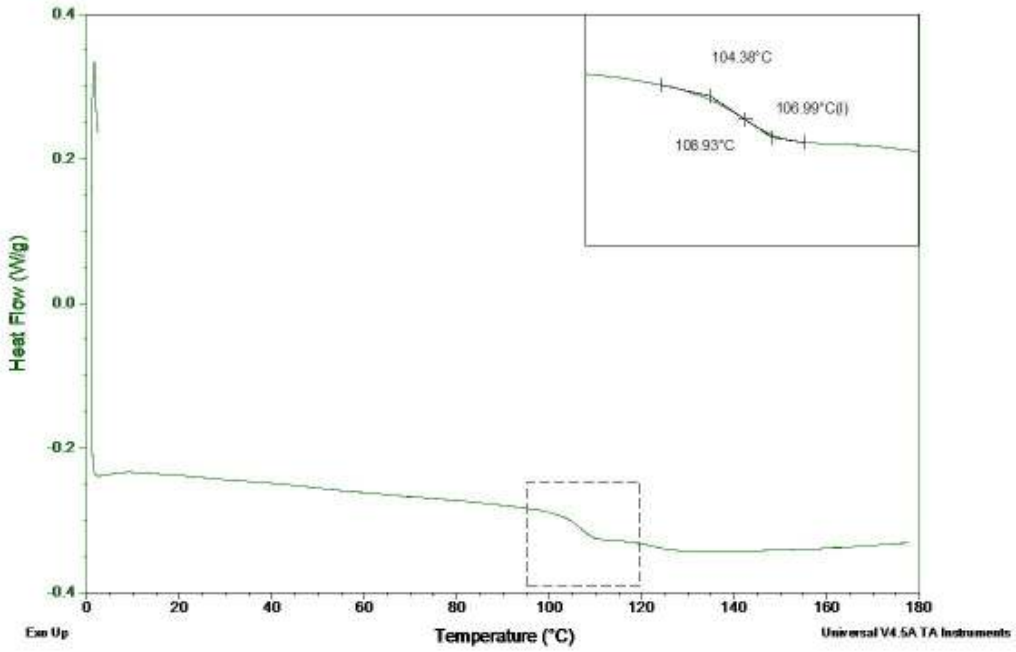

Figure 7.47: *DSC curve of the PS-PCHD-12 linear diblock copolymer with* T_g *= 106.96*^{0}*C and* $\overline{M}_n$ *=40.000 g/mol.*

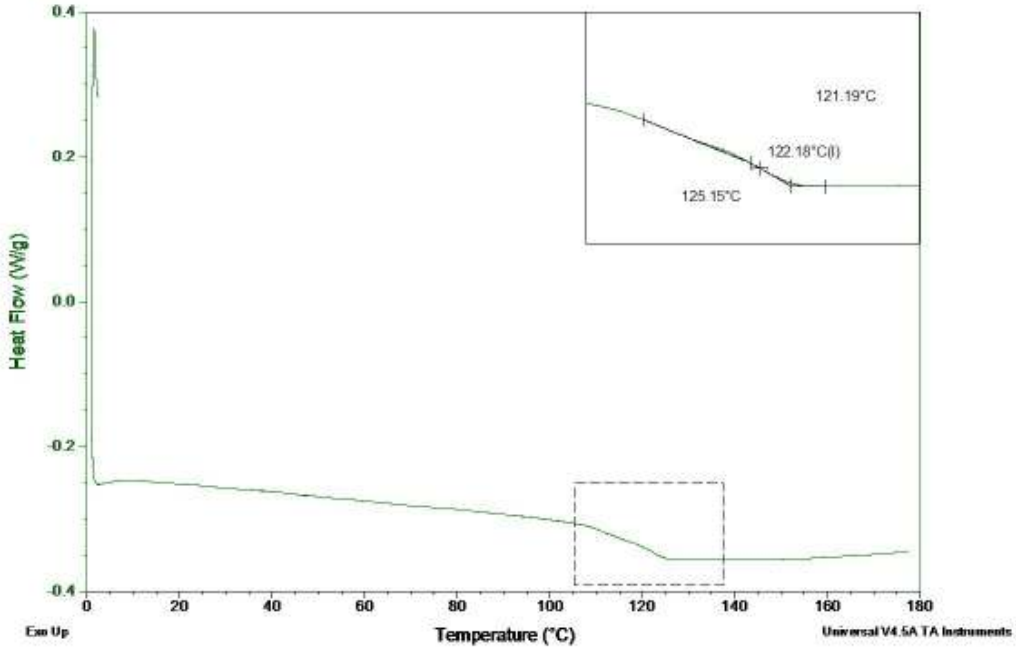

Figure 7.48: *DSC curve of the PCHD-PS-13 linear diblock copolymer with* T_g *= 122.18*^{0}*C and* $\overline{M}_n$ *=47.700 g/mol.*

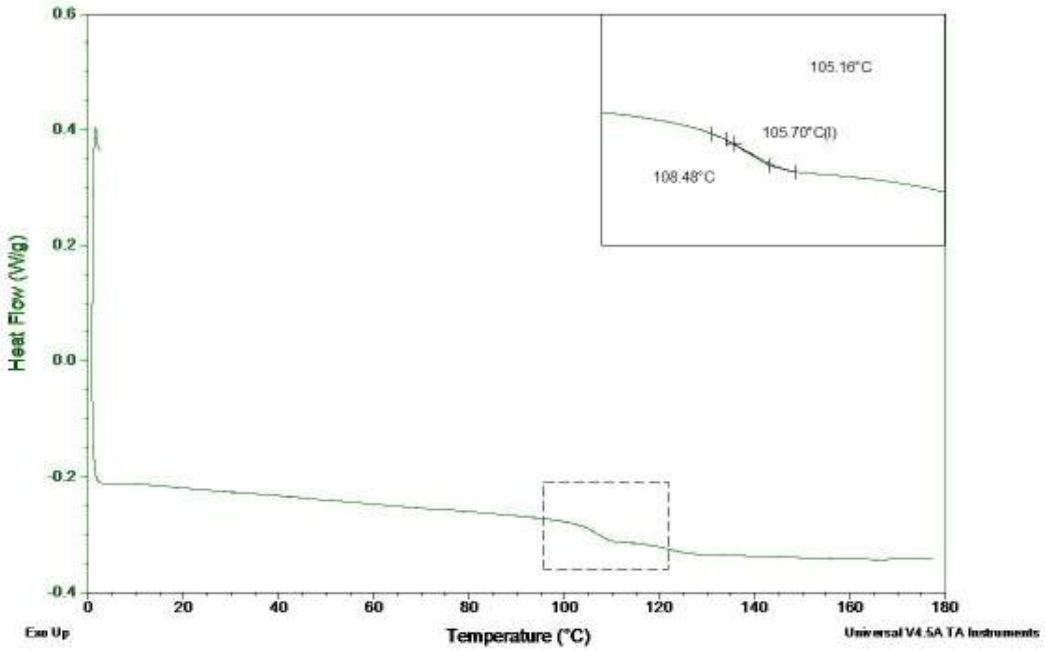

Figure 7.49: *DSC curve of the PS-PCHD-14 linear diblock copolymer with* T_g *= 105.7*^{0}*C and* $\overline{M}_n$ *=43.700 g/mol.*

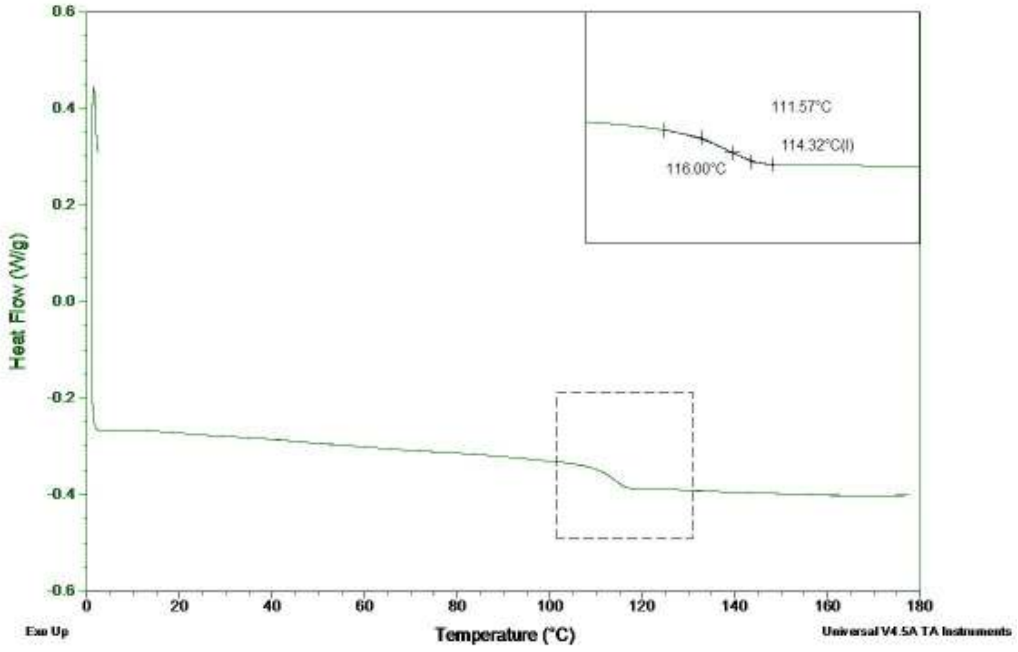

Figure 7.50: *DSC curve of the PCHD-PS-15 linear diblock copolymer with* T_g *= 114.32*^{0}*C and* $\overline{M}_n$ *=57.300 g/mol.*

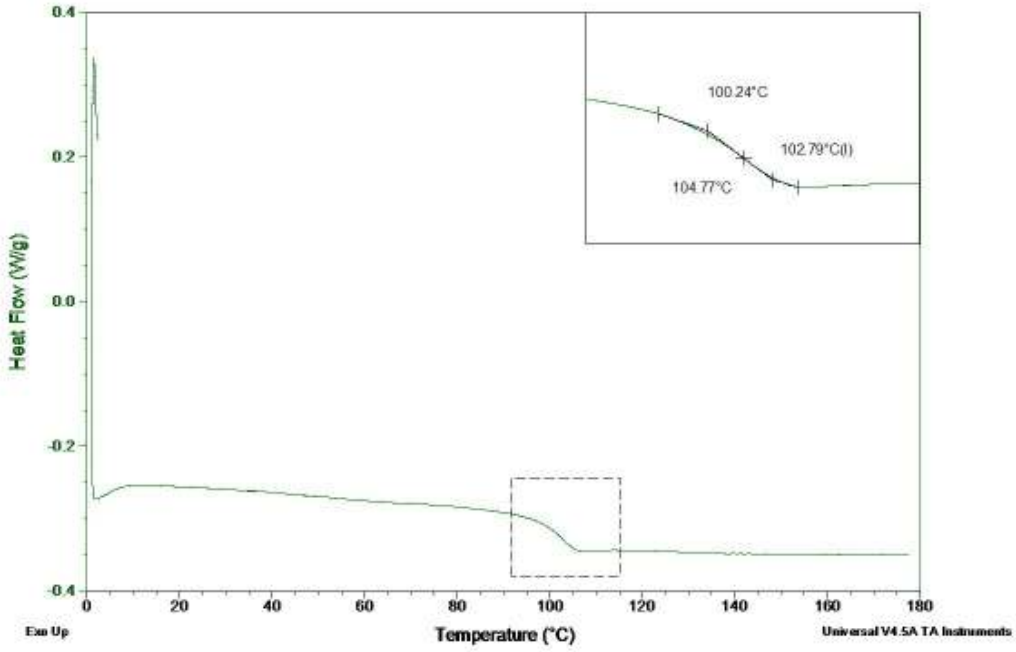

Figure 7.51: *DSC curve of the PS-PCHD-16 linear diblock copolymer with T_g = 102.79^{0}C and $\overline{M}_n$ =33.000 g/mol.*

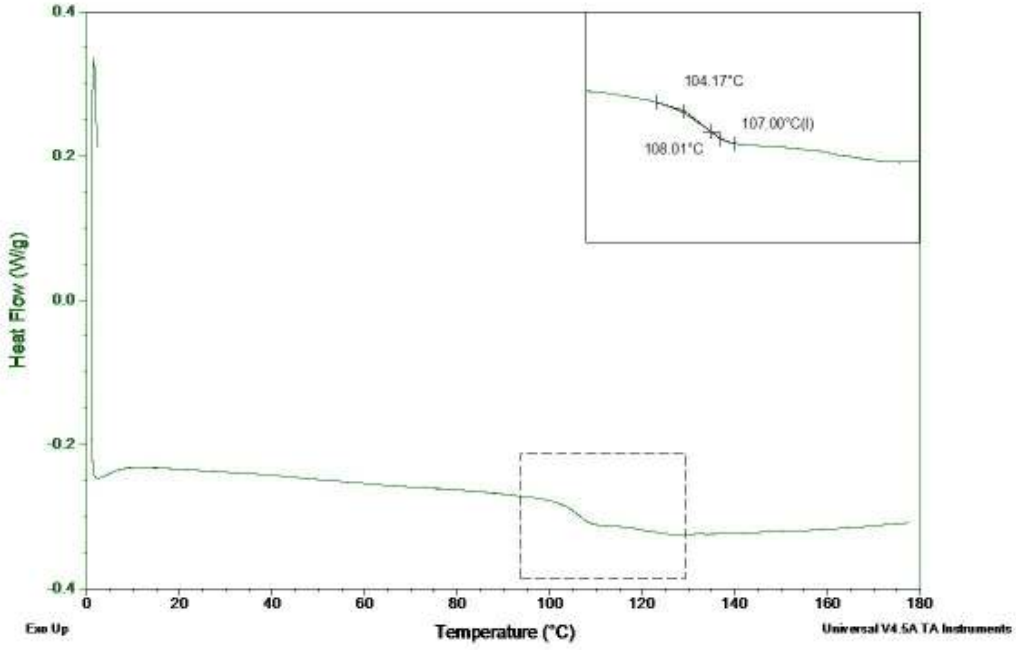

Figure 7.52: *DSC curve of the PS-PCHD-17 linear diblock copolymer with T_g = 107^{0}C and $\overline{M}_n$ =29.000 g/mol.*

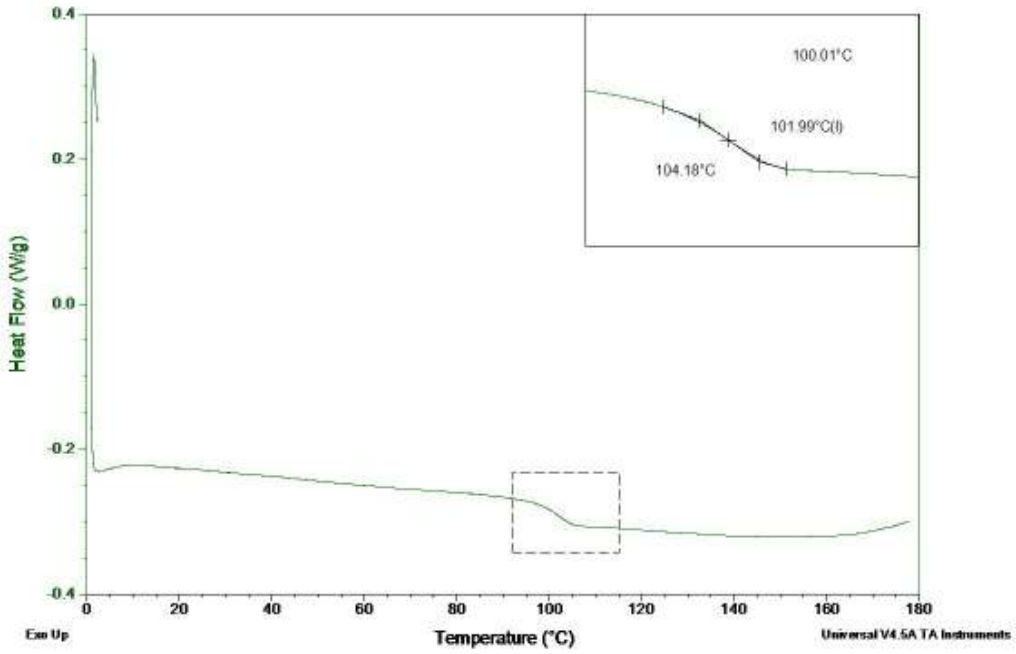

Figure 7.53: *DSC curve of the PS-PCHD-18 linear diblock copolymer with T_g = 101.99^{0}C and $\overline{M}_n$ =17.600 g/mol.*

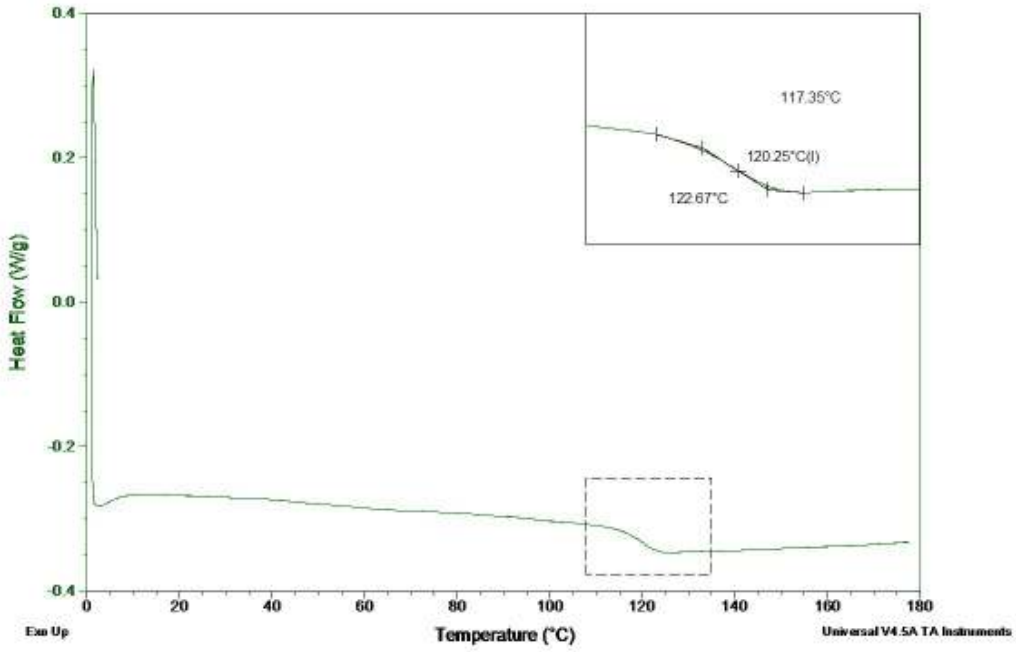

Figure 7.54: *DSC curve of the PS-PCHD-19 linear diblock copolymer with T_g = 120.25^{0}C and $\overline{M}_n$ =39.500 g/mol.*

In Table 7.4 the glass transition temperatures for all linear diblock copolymers synthesized are given. It is evident that most of the synthesized materials, with PS majority, exhibit T_g ranging from ~102^{0}C up to 107^{0}C. Furthermore, such a T_g range is observed only for samples with PS as the first block.

Table 7.4: *Glass transition temperatures (T_g) of the linear diblock copolymers in comparison with their molecular characteristics. The samples are sorted by descending f_{PS} values. The bolded samples are those for which 1,3-CHD was polymerized first.*

Samples	$\overline{M}_n$ 1st block (Kg/mol)	$\overline{M}_n$ 2nd block (Kg/mol)	$\overline{M}_n$ diblock (Kg/mol)	$\overline{M}_w$ diblock (Kg/mol)	f(wt%) PS block	f(wt%) PCHD block	T_g (^{0}C)
PS-PCHD-10	43.470	2.100	45.570	47.850	95,4	4,6	101,9
PS-PCHD-8	37.600	2.400	40.000	42.800	94,0	6,0	106,0
PS-PCHD-2	41.820	4.520	46.340	48.200	90,2	9,8	107,1
PS-PCHD-1	44.750	6.020	50.770	52.800	88,1	11,9	106,9
PS-PCHD-5	30.200	6.400	36.600	38.800	82,5	17,5	106,5
PCHD-PS-15	12.300	45.000	57.300	64.200	78,0	22,0	114,3
PS-PCHD-17	21.700	7.300	29.000	31.030	75,0	25,0	107,0
PS-PCHD-14	28.100	15.600	43.700	50.700	64,3	35,7	105,7
PS-PCHD-3	11.200	6.600	17.800	19.050	62,9	37,1	105,4
PS-PCHD-12	24.500	15.500	40.000	43.600	61,2	38,75	107,0
PS-PCHD-18	10.700	6.900	17.600	19.360	60,8	39,2	102,0
PS-PCHD-11	24.500	16.100	40.600	44.660	60,3	39,7	107,0
PS-PCHD-16	19.600	13.400	33.000	34.300	59,4	40,6	102,8
PCHD-PS-9	22.000	29.200	51.200	61.400	57,1	42,9	115,4
PS-PCHD-19	18.400	21.100	39.500	42.260	46,6	53,4	120,2
PS-PCHD-4	15.500	20.100	35.600	39.900	43,5	56,5	104,2
PCHD-PS-13	34.700	13.000	47.700	58.670	27,2	72,8	122,1

Another important observation which can be concluded from the DSC experimental results is that the linear diblock copolymers with PCHD majority exhibit increased glass transition temperatures in comparison with the linear diblock copolymers of PS majority. Such behavior indicates that the chemical structure of 1,4-PCHD affects the T_g of the final

materials, by increasing it by several degrees (114 up to 122^0C instead of 102^0C up to 107^0C). The reason lies on the covalent bonding of aromatic rings in the main chain of PCHD block, which provide increased thermal stability. According to the literature[3] if 1,2-microstructured PCHD block of a PS-b-PCHD linear diblock copolymer is increased up to 52%, the thermal stability and properties are improved even more, reaching higher values for T_g (~ 145^0C). Minor impact on the glass transition temperatures seems to create the molecular weight (increase or decrease), in contrast with Natori's results who showed that the T_g of PS-b-PCHD linear diblock copolymers with 52% 1,2-microstructure increases when the total molecular weight is also increased. It is also important to mention that the samples with PCHD as the first block (PCHD-PS-9 and PCHD-PS-15) exhibit also higher glass transition temperatures. This can be attributed to the fact that the polydispersity of PCHD before copolymerization with styrene was already increased, implying that several side and/or termination reactions occurred creating byproducts which might are able to increase the T_g of the copolymer. Unique is the case for the PS-b-PCHD-4 sample which exhibits PCHD majority but rather low glass transition temperature. This can be attributed to the fractionation procedure established only for this sample and the removal of any byproducts that might increase the T_g (as in the cases of PCHD-b-PS-9 and PCHD-PS-5 samples).

7.3 Molecular Characterization Results of the Copolymers Synthesized With the Difunctional Initiator Sodium/Naphthalenide

As described in detail at the experimental section, five (5) copolymers were synthesized by using sodium/naphthalene as the initiation system via anionic polymerization and high vacuum techniques. These copolymers are a linear triblock copolymer of PCHD-b-PS-b-PCHD type, a linear pentablock copolymer of (PS-b-PCHD)-b-PS΄-b-(PCHD-b-PS) type, an H-type copolymer of $(PCHD)_2$-g-PS-g-$(PCHD)_2$ type and two super H-type copolymers of $(PCHD)_3$-g-PS-g-$(PCHD)_3$ and $(PS\text{-}b\text{-}PCHD)_3$-g-PS΄-g-$(PCHD\text{-}b\text{-}PS)_3$ type. The molecular characterization results for these five (5) copolymers are presented and discussed in the following pages.

7.3.1 Size Exclusion Chromatography (SEC) Results

The synthesis of these copolymers was very difficult and time consuming, therefore, every procedure was performed according to the necessary standards for successful synthesis. Initially, an aliquot was taken for SEC characterization after the complete polymerization of styrene (middle block) with the difunctional initiator sodium/naphthalenide. As observed at Table 7.5 and the following Figures (Figures 7.55-7.57), this step for the synthesis of each of the five copolymers was successful. The difunctional polystyrene used for the synthesis of the linear triblock copolymer of the PCHD-b-PS-b-PCHD type and of the linear pentablock

copolymer of the (PS-b-PCHD)-b-PS′-b-(PCHD-b-PS) type was identical as well as the difunctional polystyrene used for the synthesis of the super-H copolymers of the $(PCHD)_3$-g-PS-g-$(PCHD)_3$ type and of the $(PS\text{-}b\text{-}PCHD)_3$-g-PS′-g-$(PCHD\text{-}b\text{-}PS)_3$ type.

Table 7.5: *Molecular characterization results for the difunctional polystyrenes.*

Samples	$\overline{M}_n$ Difunctional PS middle block (Kg/mol)	$\overline{M}_w$ Difunctional PS middle block (Kg/mol)	$\frac{\overline{M}_w}{\overline{M}_n}$
NaPSNa for PCHD-PS-PCHD	84.000	85.680	1,02
NaPSNa for (PS-PCHD)-PS′-(PCHD-PS)	84.000	85.680	1,02
NaPSNa for $(PCHD)_2$-PS-$(PCHD)_2$	80.000	81.600	1,02
NaPSNa for $(PCHD)_3$-PS-$(PCHD)_3$	48.500	50.440	1,06
NaPSNa for $(PS\text{-}PCHD)_3$-PS′-$(PCHD\text{-}PS)_3$	48.500	50.440	1,06

*Molecular weight distribution results were estimated via SEC (THF in 30^0C) and number average molecular weight results via membrane osmometry (toluene in 35^0C).

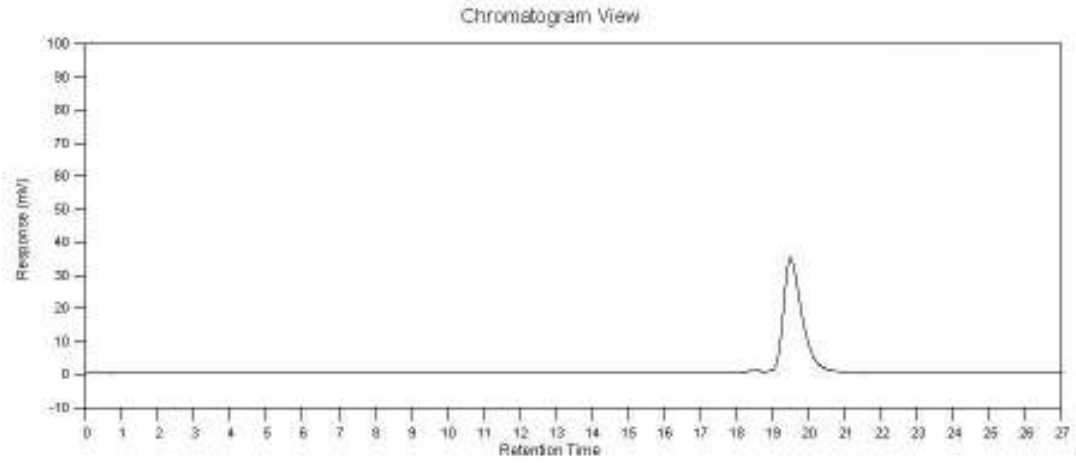

Figure 7.55: *SEC chromatogram of the difunctional $Na^{(+)(-)}PS^{(-)(+)}Na$ for the linear triblock copolymer of the PCHD-b-PS-b-PCHD type and for the linear pentablock copolymer of the (PS-b-PCHD)-b-PS′-b-(PCHD-b-PS) type with $\overline{M}_n$ = 84.000 g/mol and I = 1,02.*

The amount of the synthesized difunctional polystyrene was separated in two equal quantities in order to accomplish that. In the case of the PCHD-b-PS-b-PCHD and the (PS-b-PCHD)-b-PS′-b-(PCHD-b-PS) copolymers, each one of them was reacted with large excess of the linking agent $(CH_3)_2SiCl_2$ and, after the removal of this excess, was linked with the corresponding living arms ($PCHD^-Li^+$ and PS-b-$PCHD^-Li^+$ respectively). In the case of the $(PCHD)_3$-g-PS-g-$(PCHD)_3$ and $(PS\text{-}b\text{-}PCHD)_3$-g-PS′-g-$(PCHD\text{-}b\text{-}PS)_3$ copolymers, each one of them was reacted with large excess of the linking agent $SiCl_4$ and, after the removal of

excess, was linked with the corresponding living arms ($PCHD^-Li^+$ and PS-b-$PCHD^-Li^+$ respectively). For the H-type copolymer of the $(PCHD)_2$-g-PS-g-$(PCHD)_2$ type, the synthesized difunctional polystyrene was reacted with a large excess of the linking agent CH_3SiCl_3 and, after the removal of excess, was linked with PCHD living arms as mentioned already for the complex copolymers.

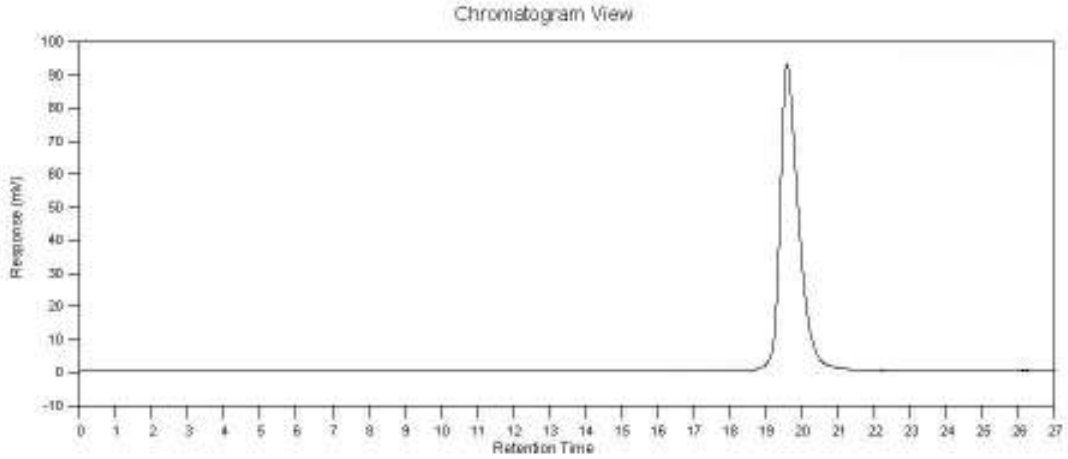

Figure 7.56: *SEC chromatogram of the difunctional $Na^{(+)(-)}PS^{(-)(+)}Na$ for the H-type copolymer of the* $(PCHD)_2$-g-PS-g-$(PCHD)_2$ *type with* $\overline{M}_n$ *= 80.000 g/mol and I = 1,04.*

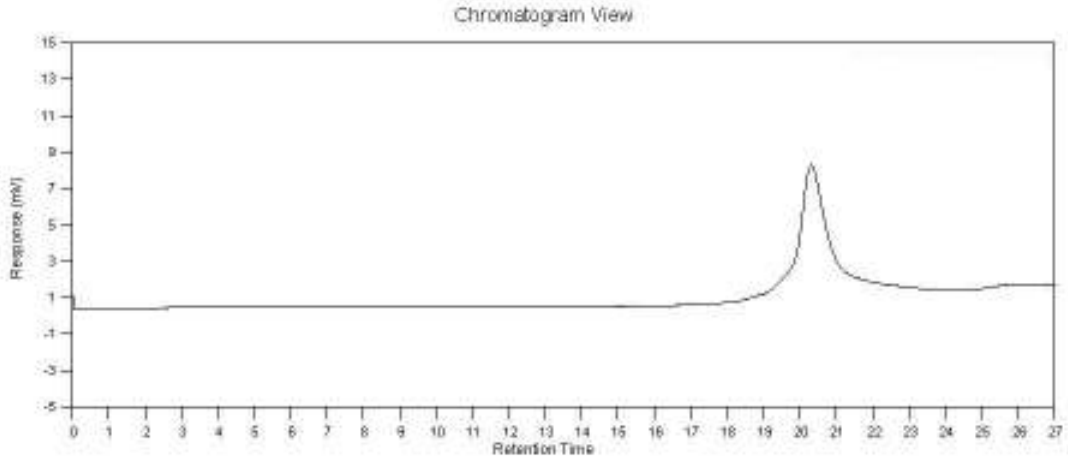

Figure 7.57: *SEC chromatogram of the difunctional $Na^{(+)(-)}PS^{(-)(+)}Na$ for the super H-type copolymers of the $(PCHD)_3$-g-PS-g-$(PCHD)_3$ type and of the $(PS\text{-}b\text{-}PCHD)_3$-g-PS´-g-$(PCHD\text{-}b\text{-}PS)_3$ type with* $\overline{M}_n$ *= 48.500 g/mol and I = 1,06.*

Observing all three chromatograms from figures 7.55-7.57 it is clearly evident that the difunctional polystyrenes used for the synthesis of the complex architecture copolymers exhibit monomodal peaks with very low polydispersity indices. Therefore, the reaction of the difunctional initiator sodium/naphthalene with styrene, in order to form the difunctional polystyrene, was successful and the carefully chosen molar ratios of sodium/naphthalene with

styrene, according to the theoretical calculations through equation 6.2 ($\overline{M}_n = \frac{gr_{monomer}}{1/2 moles_{initiator}}$), did not produce any unwanted monofunctional products.

The SEC chromatograms of the synthesized living arms which were linked with the difunctional polystyrene are given in Figures 7.58-7.62 and their molecular characteristics are presented in Table 7.6.

Table 7.6: *Molecular characterization results for the living arms linked with the difunctional polystyrenes.*

Samples	$\overline{M}_n$ of the corresponding living arm (Kg/mol)	$\overline{M}_w$ of the corresponding living arm (Kg/mol)	$\frac{\overline{M}_w}{\overline{M}_n}$
PCHD$^-$Li$^+$ for PCHD-PS-PCHD	6.500	6.760	1,04
PS-PCHD$^-$Li$^+$ for (PS-PCHD)-PS´-(PCHD-PS)	23.600	24.780	1,05
PCHD$^-$Li$^+$ for $(PCHD)_2$-PS-$(PCHD)_2$	15.500	16.275	1,05
PCHD$^-$Li$^+$ for $(PCHD)_3$-PS-$(PCHD)_3$	22.300	23.640	1,06
PS-PCHD$^-$Li$^+$ for $(PS\text{-}PCHD)_3$-PS´-$(PCHD\text{-}PS)_3$	29.000	31.030	1,07

*Molecular weight distribution results were estimated via SEC (THF in 30^0C) and number average molecular weight results via membrane osmometry (toluene in 35^0C).

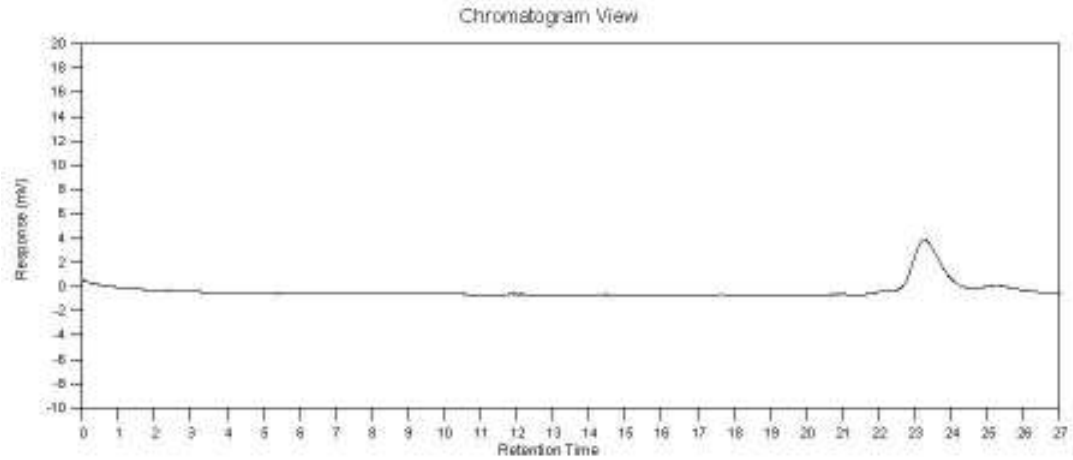

Figure 7.58: *SEC chromatogram of the PCHD$^-$Li$^+$ living arm which was linked with the Cl-Si-PS-Si-Cl difunctional precursor with, $\overline{M}_n$ = 6.500 g/mol and I = 1,04.*

Analyzing the observed SEC chromatograms of the living arms for each case, it is easily concluded that they exhibit monomodal peaks with low polydipsersity indices

indicating chemical and compositional homogeneity. It is essential for the success of the linking reaction that the molar ratio of the living arms will be in a 10-20% excess versus the free Si-Cl bonds of the difunctional backbone, in order for all Cl atoms to react with the corresponding living arms.

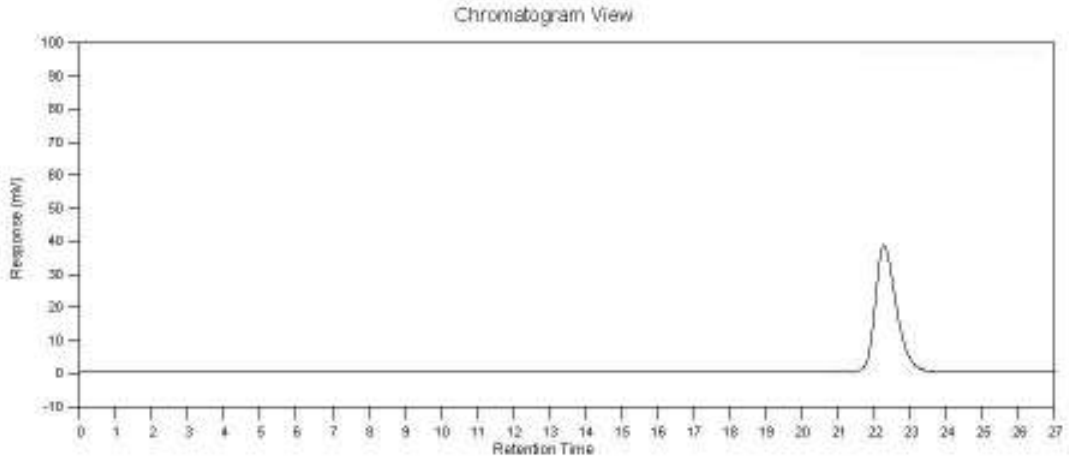

Figure 7.59: *SEC chromatogram of the PS-PCHD$^-$Li$^+$ living arm which was linked with the Cl-Si-PS-Si-Cl difunctional precursor with,* $\overline{M}_n$ *= 23.600 g/mol and I = 1,05.*

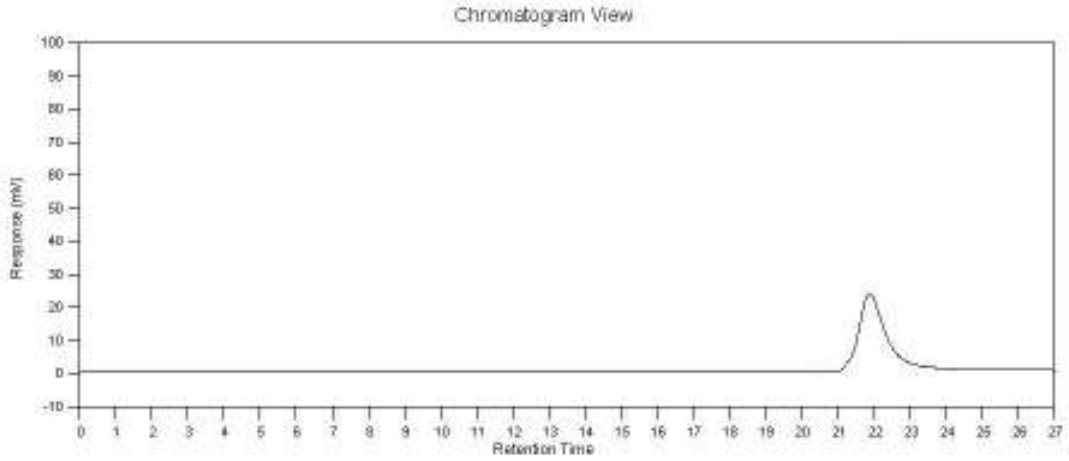

Figure 7.60: *SEC chromatogram of the PCHD$^-$Li$^+$ living arm which was linked with the Cl_2-Si-PS-Si-Cl_2 difunctional precursor with,* $\overline{M}_n$ *= 15.500 g/mol and I = 1,05.*

Additionally, the living arms must exhibit as high purity as the difunctional backbone in order to avoid any unwanted reactions that may occur during the linking procedure. It is certain though that an amount of the living arms will not react leading to bimodal final samples. After monitoring for several weeks via SEC the progress and completion of the linking reaction for each of the five copolymers, the final materials were precipitated in stabilized methanol and were fractionated in solvent/non-solvent systems in order to purify the desirable material from the byproducts and the precursors.

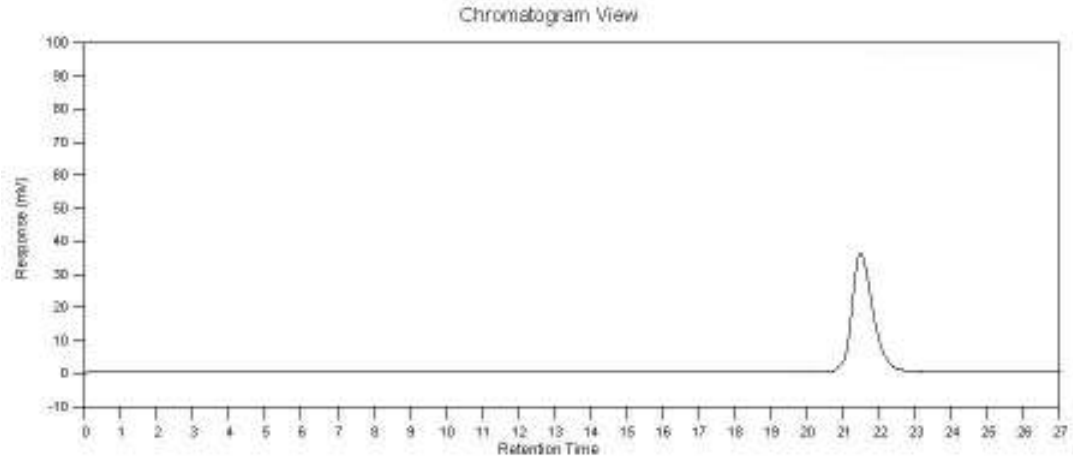

Figure 7.61: *SEC chromatogram of the PCHD$^-$Li$^+$ living arm which was linked with the Cl_3-Si-PS-Si-Cl_3 difunctional precursor, with $\overline{M}_n$ = 22.300 g/mol and I = 1,06.*

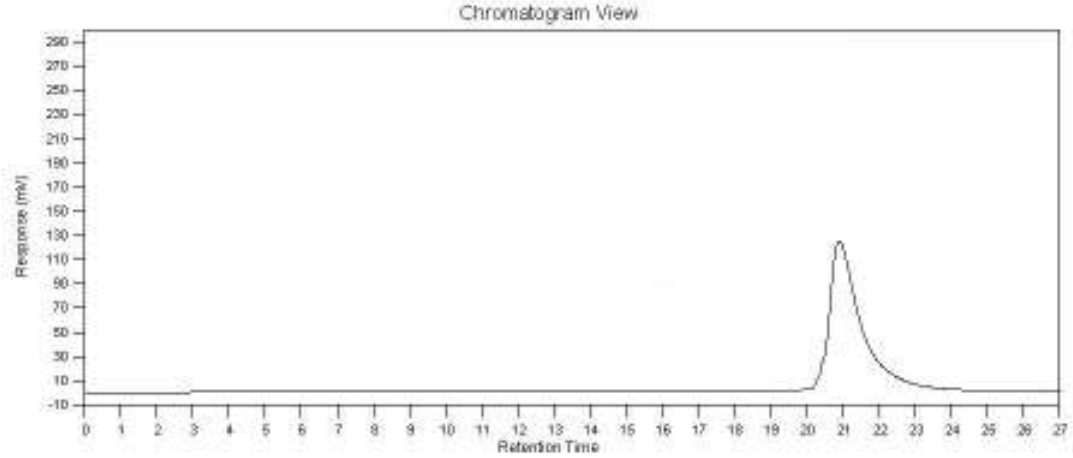

Figure 7.62: *SEC chromatogram of the PS-PCHD$^-$Li$^+$ living arm which was linked with the Cl_3-Si-PS-Si-Cl_3 difunctional precursor, with $\overline{M}_n$ = 29.000 g/mol and I = 1,07.*

In the following Figures (Figures 7.63-7.67) the SEC chromatograms of the fractionated (red line) and non-fractionated (black line) final copolymers are presented. Additionally, in Table 7.7, the molecular characterization results of the final fractionated materials are given. Observing initially the molecular characterization results of Table 7.7 and the SEC chromatographs of the five (5) final unfractionated copolymers (black lines) synthesized by using the difunctional initiator sodium/naphthalenide, it can be concluded that the linking reactions were successful and the molecular weight values are in close agreement with the theoretically predicted calculations. Furthermore, the existence of up to 25% unreacted amount of living arms is observed which is expected since, for each case, the living arms were introduced into the solution of the properly linked difunctional polystyrene in a 10-20% excess.

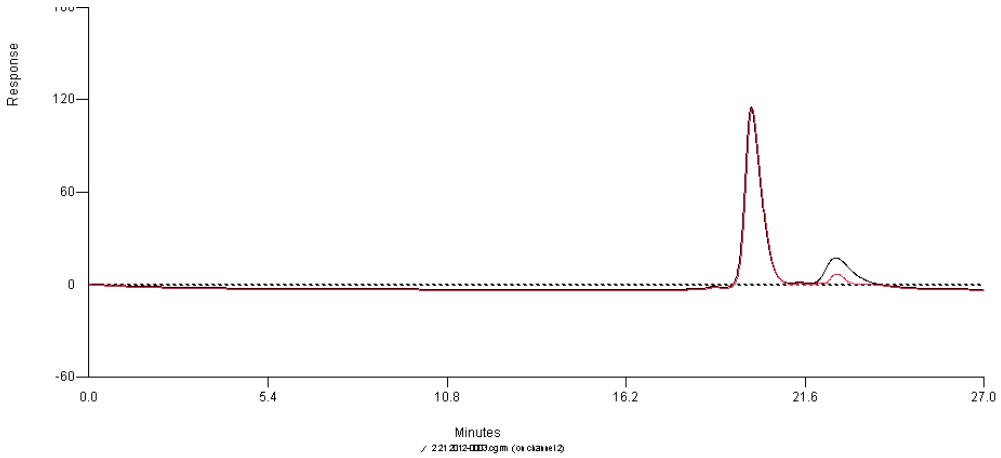

Figure 7.63: *SEC chromatograms of the fractionated (red line) and unfractionated (black line) final linear triblock copolymer of the PCHD-b-PS-b-PCHD type with* $\overline{M}_{n,tot}$ *= 98.200 g/mol and I = 1,02 and* $\overline{M}_{n}$ *= 6.800 g/mol with I = 1,04 for the second peak corresponding to non-reacted living arms of PCHD.*

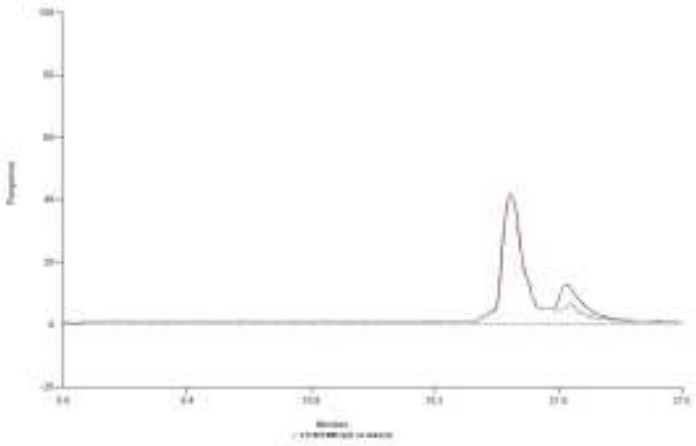

Figure 7.64: *SEC chromatograms of the fractionated (red line) and unfractionated (black line) final linear pentablock copolymer of the (PS-b-PCHD)-b-PS´-b-(PCHD-PS) type with* $\overline{M}_{n,tot}$ *= 130.500 g/mol and I = 1,03 and* $\overline{M}_{n}$ *= 24.500 g/mol with I = 1,04 for the second peak corresponding to non-reacted living arms of PS-PCHD.*

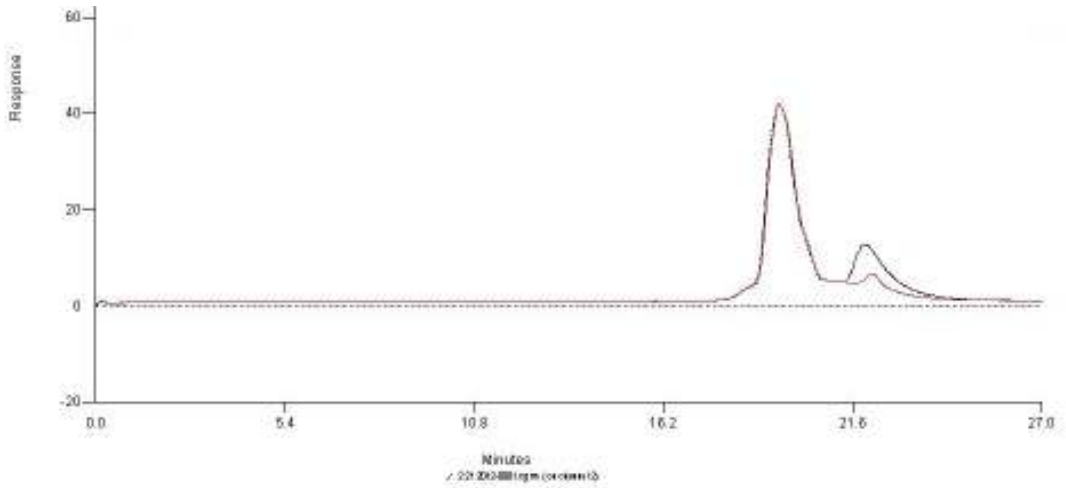

Figure 7.65: *SEC chromatograms of the fractionated (red line) and unfractionated (black line) final H-type copolymer of the $(PCHD)_2$-g-PS-g-$(PCHD)_2$ type with $\overline{M}_{n,tot}$ = 150.500 g/mol and I = 1,05 and $\overline{M}_n$ = 18.500 g/mol with I = 1,04 for the second peak corresponding to non-reacted living arms of PCHD.*

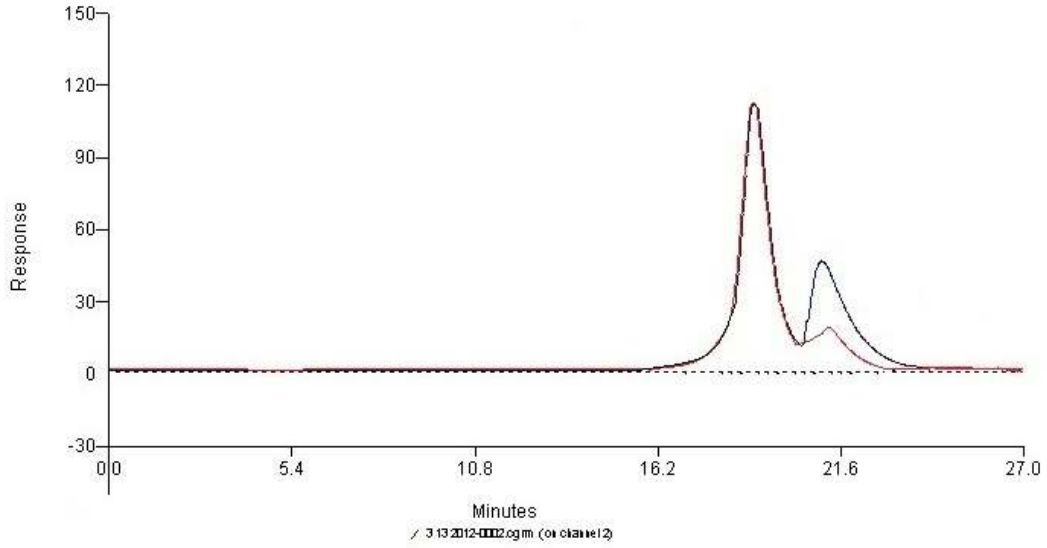

Figure 7.66: *SEC chromatograms of the fractionated (red line) and unfractionated (black line) final super H-type copolymer of the $(PCHD)_3$-g-PS-g-$(PCHD)_3$ type with $\overline{M}_{n,tot}$ = 180.300 g/mol and I = 1,07 and $\overline{M}_n$ = 22.300 g/mol with I = 1,06 for the second peak corresponding to non-reacted living arms of PCHD.*

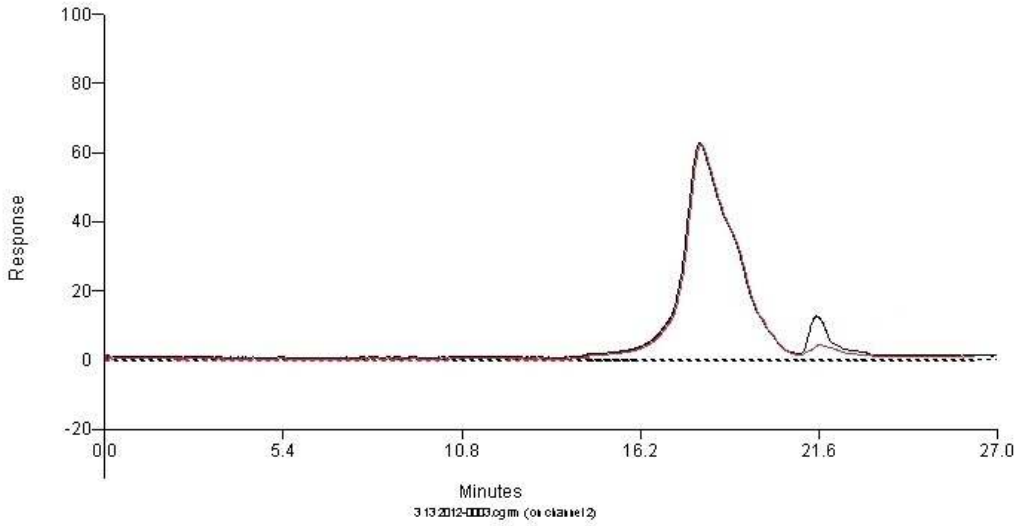

Figure 7.67: *SEC chromatograms of the fractionated (red line) and unfractionated (black line) final super H-type copolymer of the (PS-b-PCHD)$_3$-g-PS′-g-(PCHD-b-PS)$_3$ type with $\overline{M}_{n,tot}$ = 195.600 g/mol and I = 1,09 and $\overline{M}_n$ = 26.200 g/mol with I = 1,06 for the second peak corresponding to non-reacted living arms of PS-PCHD.*

Table 7.7: *Molecular characterization results for the final copolymers synthesized with the difunctional initiator sodium/naphthalene.*

Samples	$\overline{M}_n$ (Kg/mol)	$\overline{M}_w$ (Kg/mol)	$\frac{\overline{M}_w}{\overline{M}_n}$
PCHD-PS-PCHD	98.200	102.130	1,04
(PS-PCHD)-PS′-(PCHD-PS)	130.550	137.080	1,05
$(PCHD)_2$-PS-$(PCHD)_2$	150.500	158.020	1,05
$(PCHD)_3$-PS-$(PCHD)_3$	180.300	192.920	1,07
$(PS\text{-}PCHD)_3$-PS′-$(PCHD\text{-}PS)_3$	195.600	213.200	1,09

*Molecular weight distribution results were estimated via SEC (THF in 30^0C) and number average molecular weight results via membrane osmometry (toluene in 35^0C).

The fractionation procedure for each of the final copolymers synthesized with the difunctional initiator sodium/naphthalenide was a very crucial and difficult part. Several solvent/non-solvent systems, which will be discussed below, were used for each case in order to find the optimum one.

Initially, for the linear triblock copolymer case (PCHD-b-PS-b-PCHD), the commonly used solvent/non-solvent system of toluene/MeOH was used leading to

unsuccessful results due to the low solubility of PCHD chains in toluene. Then, a very low concentrated solution (< 0.1% wt) of the sample in chloroform/toluene (1:1 ratio) was created and hexane was introduced in a 1:3 (chloroform-toluene/hexane) ratio forming a new solvent/non-solvent system. After introducing also a relatively small amount of MeOH into the mixture, fractionation of the final material was possible. Chloroform provides good solubility for the PCHD block, while toluene provides good solubility for the PS block and average solubility for the PCHD block. The verification of the successful fractionation was performed through SEC and the results can be observed in Figure 7.63 (red line) where the second peak corresponding to the unreacted amount of the living PCHD arm has subsequently been decreased.

Similar fractionation procedure was performed also for the synthesized copolymers of the $(PCHD)_2$-g-PS-g-$(PCHD)_2$ and $(PCHD)_3$-g-PS-g-$(PCHD)_3$ types that exhibited PCHD outer blocks. The SEC chromatographs of the fractionated final materials are presented in Figures 7.64 and 7.65 respectively (red lines). These three already mentioned fractionations were more difficult than the two described below, due to the existence of the PCHD homopolymer in the final material and also due to the fact that the wanted architecture required PCHD being the outer block.

In the case of the (PS-b-PCHD)-b-PS´-b-(PCHD-b-PS) and $(PS\text{-}b\text{-}PCHD)_3$-g-PS´-g-$(PCHD\text{-}b\text{-}PS)_3$ copolymers, fractionation was performed with the system toluene/hexane/MeOH. A very low concentrated solution (> 0.1% wt) of the final unfractionated sample was created in toluene. Hexane was introduced in a 1:3 ratio (toluene/hexane) forming a solvent/non-solvent system. By the addition of several amount of MeOH, fractionation of the final material was feasible. In this case, PS-b-PCHD unreacted living excess was easier to be removed from the final product. By using hexane, which is a non-solvent for the PS block, the successful removal of the unreacted PS-b-PCHD living arms was possible. The verification was accomplished through SEC characterization as it is represented in Figures 7.66 and 7.67 (red lines).

7.3.2 Proton Nuclear Magnetic Resonance (^{1}H-NMR) Spectroscopy Results

Similarly to the linear diblock copolymers, the ^{1}H-NMR spectroscopy was utilized in order to verify the 1,2- and 1,4- microstructure of the PCHD block of the final materials as well as to verify the composition of the two different segments (PS and PCHD respectively). It was expected to observe the olefinic chemical shifts of the aromatic hydrogen atoms of polystyrene at 6,3-7,5 ppm, the olefinic hydrogen atoms of the poly(cyclohexadiene) ring at 5,4-5,8 ppm and the aliphatic protons and allylic protons of PCHD at 1,25-1,85 ppm and at 1,85-2,35 ppm respectively.

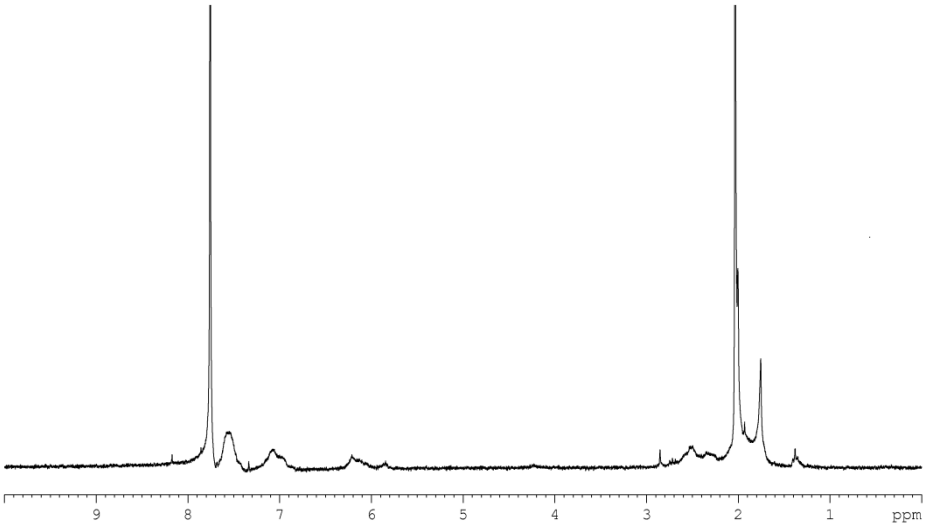

Figure 7.68: *^{1}H-NMR spectrum of the PCHD-b-PS-b-PCHD linear triblock copolymer.*

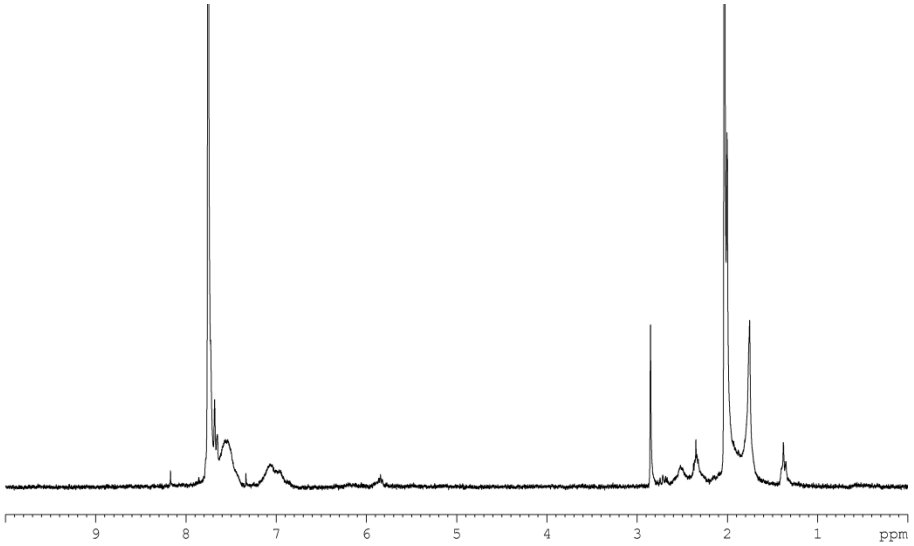

Figure 7.69: *^{1}H-NMR spectrum of the (PS-b-PCHD)-b-PS′-b-(PCHD-b-PS) linear pentablock copolymer.*

As it can be observed from the ^{1}H-NMR spectra (Figures 7.68-7.72), the existence of both polystyrene and poly(cyclohexadiene) blocks in the final materials is verified as well as the complete absence of any silane traces which correspond to a chemical shift at approximately 0,8 ppm. Furthermore, the calculated compositions of the two different segments are in good agreement with the molecular characterization results via SEC.

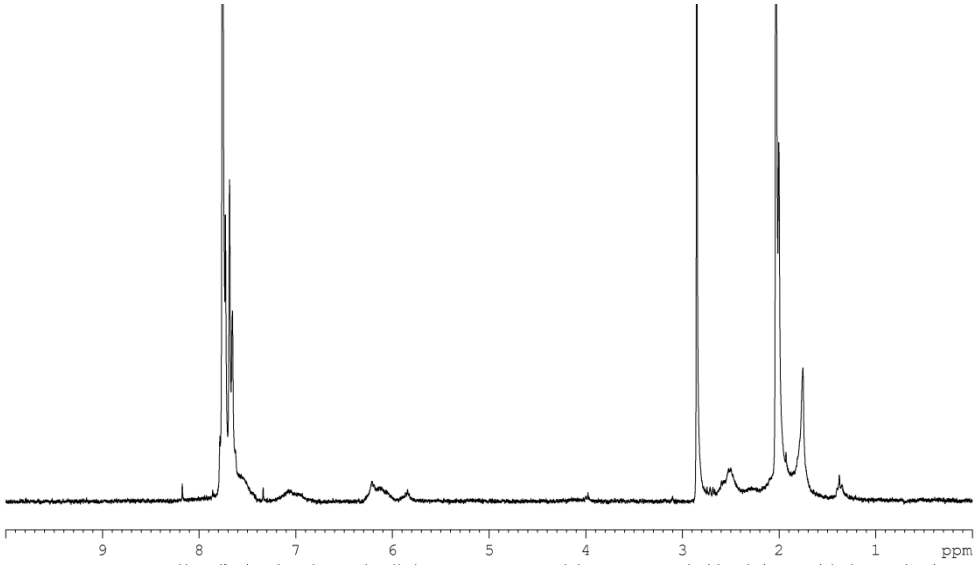

Figure 7.70: *^{1}H-NMR spectrum of the $(PCHD)_2$-g-PS-g-$(PCHD)_2$ H-type copolymer.*

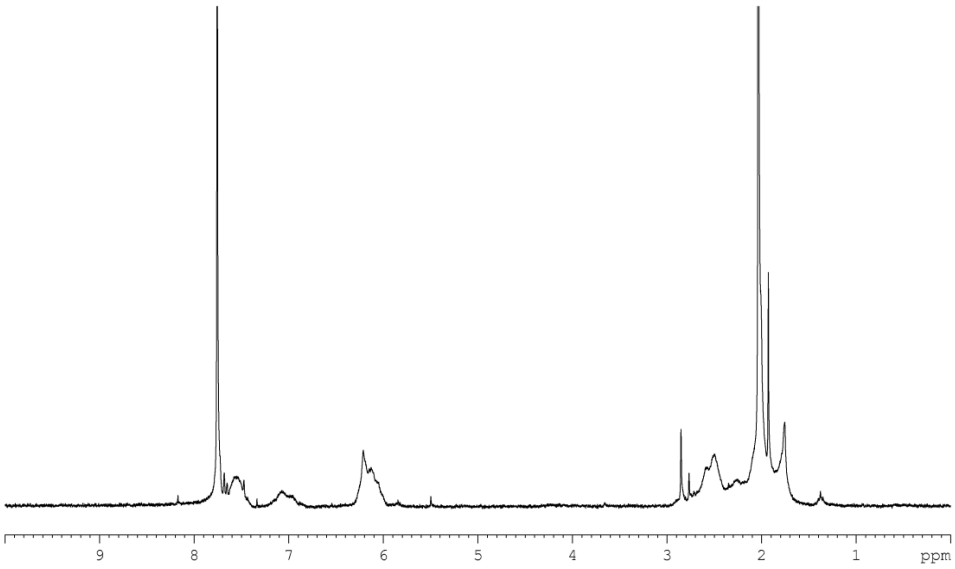

Figure 7.71: *^{1}H-NMR spectrum of the $(PCHD)_3$-g-PS-g-$(PCHD)_3$ super H-type copolymer.*

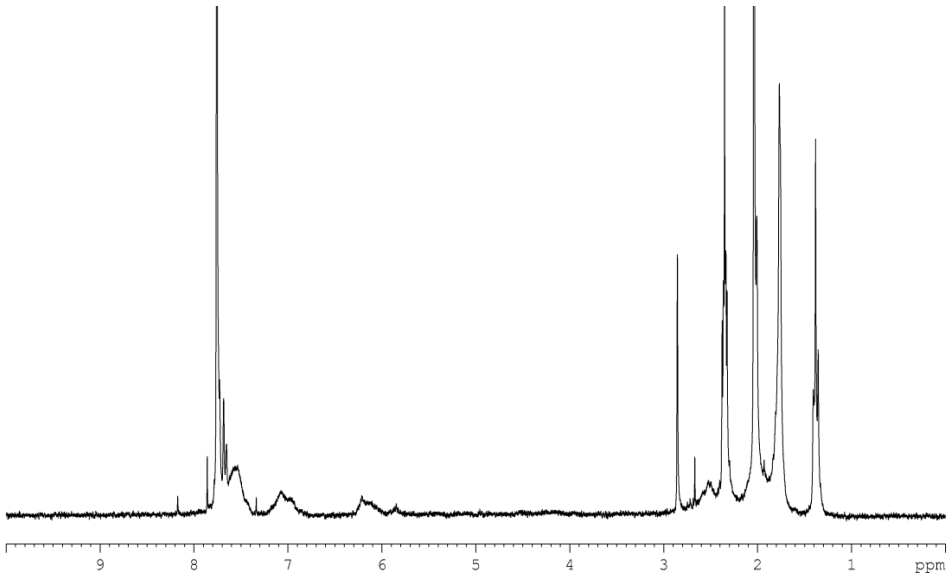

Figure 7.72: *^{1}H-NMR spectrum of the (PS-b-PCHD)$_3$-g-PS´-g-(PCHD-b-PS)$_3$ super H-type copolymer.*

7.4 Morphological Characterization Results for the Linear Diblock Copolymers

The morphological characterization of the linear diblock copolymers synthesized for this thesis was accomplished by using two methods which are complementary in cases where microphase separation of polymers is examined, transmission electron microscopy (TEM) and small angle X-ray scattering (SAXS) respectively. The measurements were performed in the Center for Nanophase Materials Science (CNMS) of Oak Ridge National Laboratory (ORNL) at Oak Ridge, Tennessee, USA. As described previously, both TEM images and SAXS plots can provide unique information concerning the microphase separation of linear diblock copolymers and their corresponding morphologies. For that reason, a wide variety of volume fractions was targeted and synthesized in order to study the alternations of microphase separation of PS-PCHD copolymers in regard with the different volume fractions, the interaction parameter χ and the variations of the degree of polymerization N, thus the molecular weight. The degree of polymerization N for a linear diblock copolymer can be easily calculated from the following equation:

$$N_{PS-b-PCHD} = N_{PS} + N_{PCHD} = \frac{\overline{M}_n^{PS}}{M_0^{St}} + \frac{\overline{M}_n^{PCHD}}{M_0^{CHD}} \qquad (7.1)$$

where M_0^{PS} = 104 g/mol is the molecular weight of polystyrene's monomer unit and M_0^{PCHD} = 80 g/mol is the corresponding molecular weight of poly(cyclohexadiene)'s monomer unit.

As reported previously, seventeen (17) samples were synthesized in an effort to understand the fundamentals of the microphase separation for this system as well as to create a possible phase diagram $\chi N = f(\varphi)$ where φ is the volume fraction of polystyrene, which has

not been reported in the literature even though there are several studies with very interesting morphological characterization results already published for such copolymers.[3,137] The volume fractions for all seventeen samples were calculated by using equation 3.7:

$$\phi_A = \frac{f_A d_A}{f_A d_B + f_B d_A}$$

where, A corresponds to polystyrene and B to poly(cyclohexadiene), while d_A = 1,05 g/ml is polystyrene's density and d_B = 1,10 g/ml is poly(cyclohexadiene)'s density. The volume fractions are presented in Table 7.8.

Another unique feature of the specific linear diblock copolymers is the different structure and properties adopted in comparison with other well-studied polystyrene/polydiene systems, due to the existence of the PCHD block. As reported in a previous section of this thesis, even though PCHD is a polydiene, it exhibits very different properties compared to other commonly used polydienes, such as poly(isoprene) and poly(butadiene), due to the existence of the cyclic ring in its main chain. Consequently, its morphological characterization is expected to provide also quite different results, when copolymerized with styrene and is considered rather challenging.

Another important aspect of the PS-b-PCHD copolymers system is that the interaction parameter χ is yet unknown. A few theoretical calculations have been performed[138] without any confirmed experimental yet. For that reason, a series of thermal SAXS measurements was performed also in an effort to calculate the interaction parameter χ since it is inversely proportional with temperature (equation 3.3, $\chi = \alpha T^{-1} + \beta$).

The sample preparation for the molecular characterization results, especially for TEM measurements, is essential and very important as described previously in another chapter. Casting must be performed in a non-selective solvent for several days in order to promote the formation of equilibrium morphologies. All linear diblock copolymers synthesized were cast from toluene, except from the PCHD-b-PS-13 sample which exhibits PCHD majority and was cast from chloroform since it was insoluble in toluene. Casting was accomplished in approximately 5-7 days depending on the solvent used. Then, each film that was made, was separated in two equal amounts in order to study morphologically the unannealed and annealed this sections. Annealing was performed in 6-7 days. For the first 12 hours the temperature was set at 50^0C, for the next 12 hours the temperature was set at 90^0C and for the next 5-6 days the temperature was set at 120^0C. Then, each film was removed from the annealing oven and quenched in liquid nitrogen in order to avoid any alternation of the formed morphology due to cooling slowly to room temperature. As long as casting and annealing are properly accomplished, the films of the samples can be used immediately for

SAXS measurements, while for TEM measurements further procedures must be adopted (embedding, ultramicrotoming, staining).

Table 7.8: *Volume fraction and degree of polymerization for the linear diblock copolymers.*

Samples	f(wt%) PS block	f(wt%) PCHD block	φ(PS)	φ(PCHD)	$N_{PS\text{-}b\text{-}PCHD}$
PS-PCHD-10	95,4	4,6	91,2	8,8	444
PS-PCHD-8	94,0	6,0	89,3	10,7	391
PS-PCHD-2	90,2	9,8	86,5	13,5	459
PS-PCHD-1	88,1	11,9	84,5	15,5	506
PS-PCHD-5	82,5	17,5	79,4	20,6	370
PCHD-PS-15	78,0	22,0	75,2	24,8	586
PS-PCHD-17	75,0	25,0	72,4	27,6	300
PS-PCHD-14	64,3	35,7	62,4	37,6	465
PS-PCHD-3	62,9	37,1	61,1	38,9	190
PS-PCHD-12	61,2	38,8	59,5	40,5	429
PS-PCHD-18	60,8	39,2	59,1	40,9	189
PS-PCHD-11	60,3	39,7	58,7	41,3	437
PS-PCHD-16	59,4	40,6	57,8	42,2	356
PCHD-PS-9	57,1	42,9	55,6	44,4	556
PS-PCHD-19	46,6	53,4	45,6	54,4	441
PS-PCHD-4	43,5	56,5	42,6	57,4	400
PCHD-PS-13	27,2	72,8	26,9	73,1	559

7.4.1 Transmission Electron Microscopy (TEM)

In the following pages the TEM images from the morphological characterization of the seventeen (17) linear diblock copolymers are presented. All samples were stained with

osmium tetroxide (OsO_4) in order to increase the contrast of the corresponding PCHD blocks since PS does not react with the specific stainer.

Figures 7.73a and 7.73b represent the TEM images from the annealed and the unannealed PS-b-PCHD-1 sections respectively.

a) 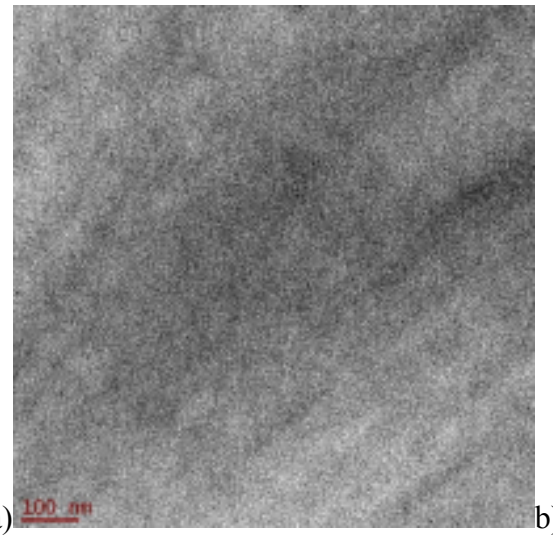 b) 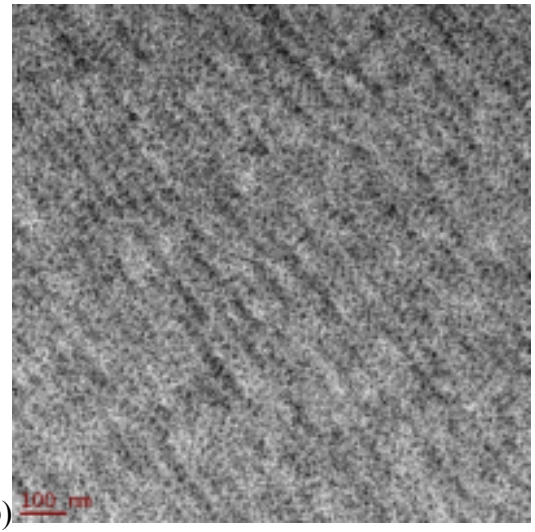

Figure 7.73: *a) TEM image of the annealed PS-b-PCHD-1 film b) TEM image of the unannealed PS-b-PCHD-1 film.*

It is easily observed by the two TEM images of the annealed and unannealed sample that they exhibit both differences and similarities as far as their morphology is concerned. The main similarity is that they both exhibit spheres of the minority component (PCHD) in a matrix of the majority component (PS) which is not something unexpected since the volume fraction of PS is high (φ_{PS} = 84,5%). The PCHD spheres are displayed darker, due to the staining with osmium tetroxide for 45 minutes, while the PS matrix appears white. The spheres are not oriented in a body centered cubic (BCC) structure as it is usually expected, but they exhibit a rather random orientation. The main difference of these two systems is that the PCHD spheres of the annealed sample appear much smaller than those of the unannealed sample. This could be attributed to the fact that PS-b-PCHD-1 sample exhibits a rather high degree of polymerization (N = 505,55) and by increasing the temperature, the χ parameter is decreased and the system might be very close to the order-disorder transition. This could happen only if the χ parameter is significantly decreased, which means that the entropic factors tend to become more prominent than the enthalpic factors. For the unannealed sample, PCHD spheres are more distinct and appear larger, which correlates with what is described above. Therefore, the sections are still in the equilibrium state where the need for the minimization of the local energy is fulfilled. Furthermore, it can be implied that, even though the χ parameter is yet unknown, the system is in the intermediate segregation regime, since the degree of polymerization is rather high (N = 506).

In Figures 7.74a and 7.74b the TEM images of the annealed and unannealed PS-b-PCHD-2 sections are exhibited respectively.

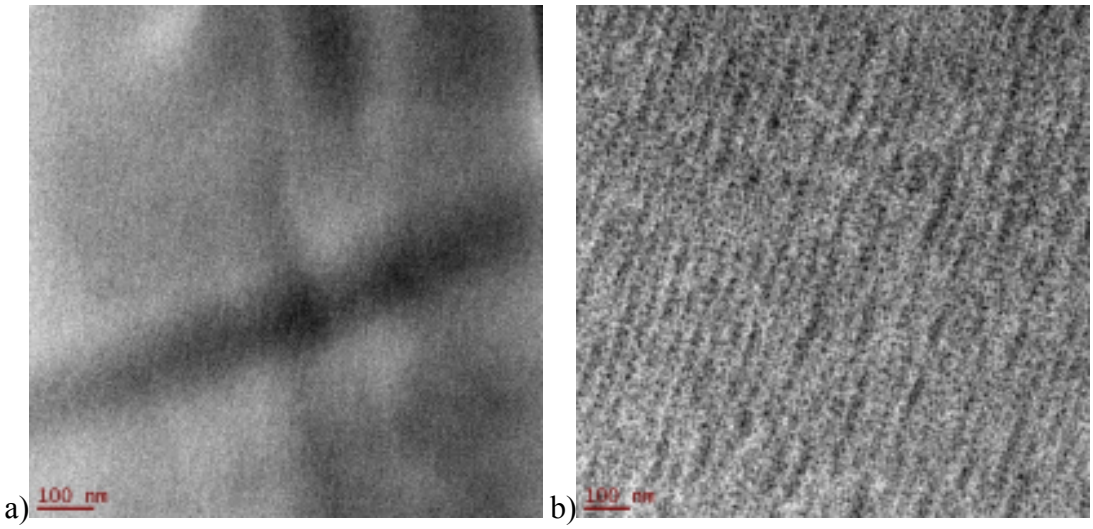

Figure 7.74: *a) TEM image of the annealed PS-b-PCHD-2 film b) TEM image of the unannealed PS-b-PCHD-2 film.*

In this case, the annealed film seems to exhibit no microphase separation while the unannealed one exhibits spheres of the minority component (PCHD) in a matrix of the majority component (PS). The PCHD spheres are displayed again darker, since the film has been stained with OsO_4, while the PS matrix appears white. The PCHD spheres are again not oriented in a BCC structure indicating poor microphase separation. The volume fraction of the majority component (PS) is very close to the one for the PS-b-PCHD-1 linear diblock copolymer (φ_{PS} = 86,5%) which is consistent with the identical morphology observed for the unannealed films of these two samples. The observation of no microphase separation for the annealed samples enhances the previously described assumptions for the PS-b-PCHD-1 annealed sections. This means that the temperature increase led to significant decrease of the χ parameter which resulted eventually to the transition from the somewhat ordered state to the disordered state. Since the degree of polymerization is relatively high again (N = 459) and is not affected by the temperature alternations, it can play a significant role as a constant factor for better understanding the microphase separation of each synthesized linear diblock copolymer. In order to verify the assumption that the system outcame the order-disorder transition, annealing procedures could be performed in several lower temperatures (e.g 50^0C, 70^0C, 90^0C etc.) than the selected one (120^0C) and observe approximately, by the corresponding TEM images, where the transition from randomly oriented spheres to disorder state occurs.

The TEM images for the annealed and unannealed films of the PS-b-PCHD-3 sample are presented in Figures 7.75a and 7.75b respectively.

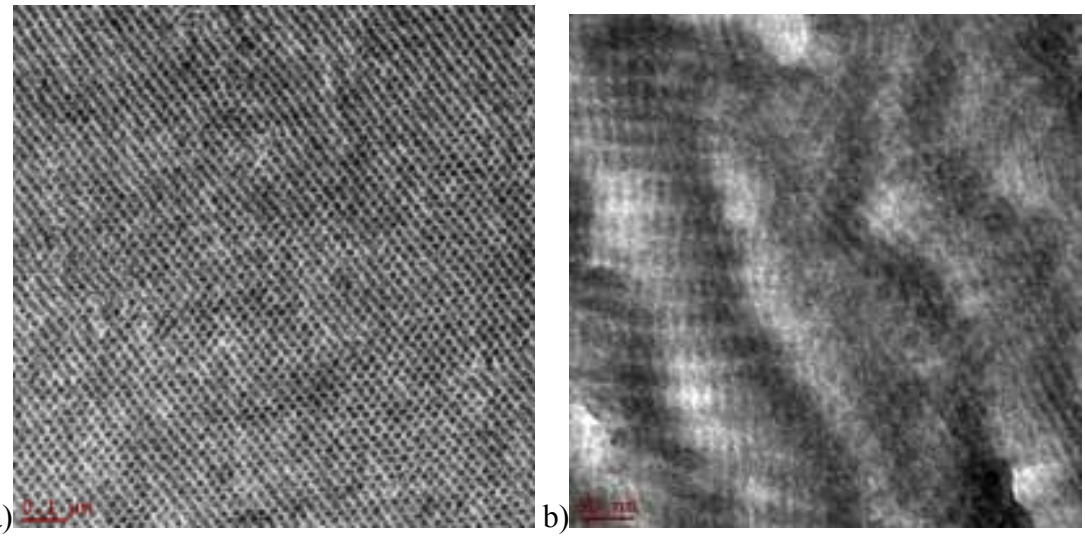

Figure 7.75: *a) TEM image of the annealed PS-b-PCHD-3 film b) TEM image of the unannealed PS-b-PCHD-3 film.*

From the TEM images of the annealed and unannealed sections of the PS-PCHD-3 linear diblock copolymer films is observed that significant differences occur. The annealed sections exhibit hexagonally packed cylinders of the minority component (PCHD), in a matrix of the majority component (PS) block. The hexagonally packed cylinders of the PCHD block are highly self-organized and appear darker, while the PS matrix appears white. It is also clear that this morphology is consistent and with great periodicity indicating the successful procedures that were established for the synthesis and the preparation (casting, annealing, ultramicrotoming, staining) for morphological characterization. The self-assembly and the appearance of highly self-organized morphology in an annealed sample is usually expected, especially if the degree of polymerization is rather low (N = 190). In the case of the annealed PS-b-PCHD-3 sections, the increase of the temperature up to 120^0C, which is above the glass transition temperature ($105,4^0$C) of the system, favors the sectional movements of the polymer chains where the thickness of the interface as well as the junction points are minimized and the hexagonally packed cylinders of the PCHD block are formed in a PS matrix. By quenching the sample in liquid nitrogen immediately after the removal from the annealing oven, the formed morphology is "captured" in order to avoid its alternation due to cooling slowly at room temperature. The volume fraction of φ_{PS} = 60,1% corresponds to hexagonally packed cylinder morphology for the well-studied PI-b-PS system by Fredrickson and Bates[126] . This experimental result is in good agreement with the aforementioned results which means that at least for φ_{PS} = 60,1%, the PS-b-PCHD system behaves as the PI-b-PS system. On the contrary, the unannealed film is not well-ordered, even though a formed structure is clearly observed. This structure though, does not correlate with any of the theoretically and experimentally known equilibrium morphologies from other well-studied systems (e.g. PI-b-PS). It seems like cylinders of the minority PCHD block in a matrix of the

majority PS block are going to be formed, but the microphase separation is relatively low. The rather large folds observed in Figure 7.75b were present in every domain of the sections studied, which implies that mechanical deformations occurred most likely during the trimming procedure. It is an assumption which proves what was described in the theoretical part concerning the great care needed during the trimming and ultramicrotoming procedures. Finally it is considered that rotate-tilt or/and double tilt experiments should be made in order to verify the structure formed.

In Figures 7.76a and 7.76b the TEM images from the annealed and unannealed PS-b-PCHD-4 sections respectively are given. For these two TEM images several differences as well as similarities can be observed. They both exhibit dark and light regions which are poorly organized but they can be distinguished from each other. Due to staining with OsO_4, the dark regimes correspond to PCHD segments, while the lighter ones to PS segments. Both TEM images exhibit significant dark domains, which is something that verifies the volume fraction calculated for the PCHD block from the molecular characterization results (φ_{PCHD} = 57,4%).

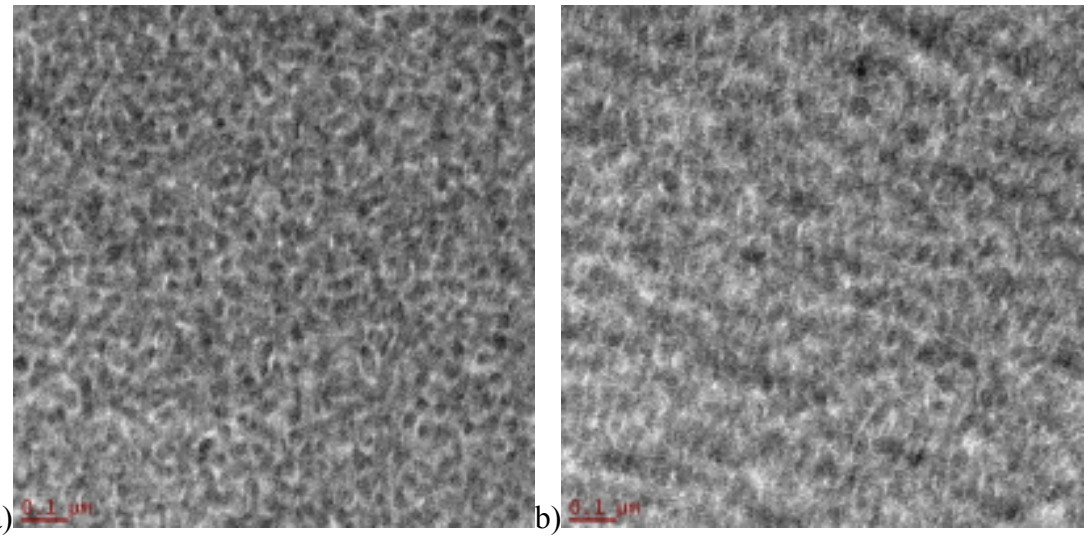

Figure 7.76: *a) TEM image of the annealed PS-b-PCHD-4 film b) TEM image of the unannealed PS-b-PCHD-4 film.*

For the annealed film, the microphase separated structure seems like cylinders of the PCHD block in a matrix of the PS block. The PCHD cylinders are rather large and apparently the size of the interface between the two blocks is not small. The asymmetry between the two blocks is also rather small (φ_{PS} = 42,6% and φ_{PCHD} = 57,4%) which means that the asymmetry between the chain sizes is minimal and curving of the interface towards the minority block occurs in a small scale. For the unannealed film, similar observations can be implied from the TEM image. Nevertheless, the PCHD cylinders seem to be smaller than those of the annealed sample as well as the interfaces between the two blocks. Furthermore, even though the PCHD

exhibits larger volume fraction, it seems that eventually forms cylinders propably due to the flexibility of the chains when compared with PS. Unfortunately, the poor-ordered structure is not able to provide any further significant information about the correlation between the increase of the temperature and the increased size of the PCHD domains of the annealed sample.

In Figures 7.77a and 7.77b the TEM images for the annealed and unannealed PS-b-PCHD-5 sections respectively are given. For both annealed and unannealed films, microphase separation of the corresponding blocks is observed. More specifically, for the annealed sample, hexagonally packed cylinders of the minority component (PCHD) are observed in the matrix of the majority component (PS). The hexagonal formation of the PCHD cylinders is not continuous but the different dark and light domains which correspond to the PCHD and to the PS blocks respectively are distinct. The asymmetry of the two blocks is high enough to curve the interface towards the minority block (PCHD in this case), but the total free energy of the system is not minimized enough leading to cylinders, poorly formed in hexagonal packing.

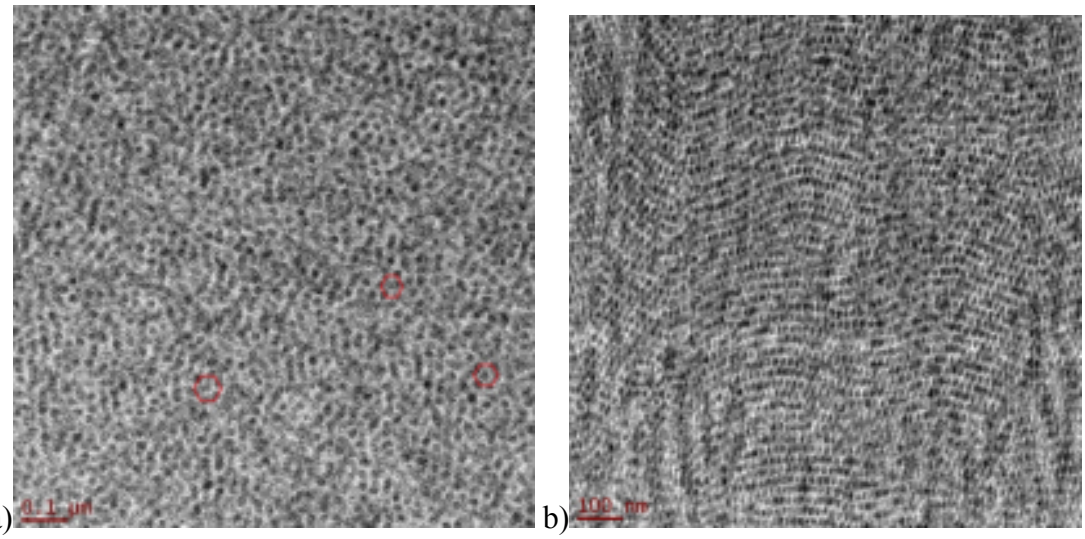

Figure 7.72: *a) TEM image of the annealed PS-b-PCHD-5 film b) TEM image of the unannealed PS-b-PCHD-5 film.*

Furthermore, the degree of polymerization is relatively high (N = 370) which implies that with further increase of the temperature, the χ interaction parameter will be decreased even more leading the system possibly to an order-order transition (spheres). This is also verified from the fact that the structure observed for the unannealed sections is more well-ordered than the one observed for the annealed one, which means that in lower temperature the system exhibits better microphase separation. The interface is minimized while there is a very good distinction between the two microphases comparing to the image from the annealed film. The observed morphology of the hexagonally packed cylinders of the PCHD block in a

PS matrix for the unannealed film is more periodic and continuous as it is evident from the TEM image.

Another significant observation is that the hexagonally packed cylinders appear for an increased volume fraction of the majority component (φ_{PS} = 79,4%). This verifies that conformational asymmetry shifts the order-order and order-disorder phase boundaries of the PS-b-PCHD system, which is something that has been proved experimentally and theoretically for other systems.[139,140,141] This asymmetry of the phase diagram has been attributed to differences in monomer volume and backbone flexibilities of the blocks leading to an overall conformational asymmetry which affects more the order-order rather than the order-disorder transitions. Furthermore, the conformational asymmetry affects the relative domain spacing between structures along their boundaries. This fact can explain the increase of the size of the PCHD cylinders in the annealed sample since Matsen and Bates,[141] by performing both SCFT and SST theoretical calculations, showed that at $\chi N = 60$ and when the volume fraction of the one component is above 50% and below 85%, the domain spacing is increased, while for volume fractions above 85% of the one component, the d spacing is decreased, an observation which is in accordance with the previously mentioned experimental results for the PS-b-PCHD-1 and PS-b-PCHD-2 annealed samples.

The following Figures (Figures 7.78a and 7.78b) present the annealed and unannealed PS-b-PCHD-8 films respectively.

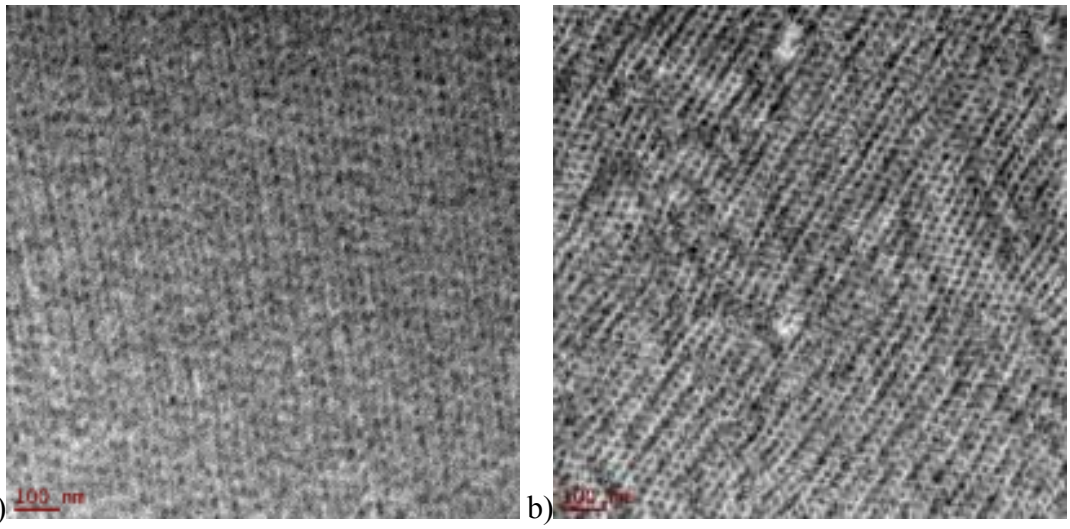

Figure 7.78: *a) TEM image of the annealed PS-b-PCHD-8 film b) TEM image of the unannealed PS-b-PCHD-8 film.*

This case resembles the aforementioned case of the PS-b-PCHD-5 annealed and unannealed films. The microphase separation for the annealed sample is low, but dark and light regions can be distinguished. The formation of spheres of the minority component (PCHD block), which are displayed darker, in a matrix of the majority component (PS block), which is displayed lighter can be observed. Additionally, the well-ordered structure of

hexagonally packed cylinders of the PCHD block in a matrix of the PS block seen for the unannealed sections rise questions whether an order-order transition occurs as the temperature is increased during the annealing process. The total molecular weight of this sample is very close to the molecular weight of PS-b-PCHD-5 sample (40.000 g/mol and 36.600 g/mol respectively) as well the degree of polymerization ($N_{PS\text{-}b\text{-}PCHD\text{-}8}$ = 391) but the TEM micrographs are identical only for the unannealed samples. The existence of the hexagonally packed cylinders of the minority component in the matrix of the majority at even higher volume fraction than that of PS-b-PCHD-5 sample indicates that the conformational asymmetry of this system is very high, which means that the ratio of the statistical segment lengths (α_A/α_B) of the two blocks is relatively large. Furthermore, as for the PS-b-PCHD-5 sample, the increase of the temperature (decrease of the χ parameter) affects the microphase separation creating less ordered structures. So far, poor-ordered structures have been observed for all the annealed films of the aforementioned systems except from the PS-b-PCHD-3 annealed case where the degree of polymerization is the lowest and by increasing the temperature, microphase separation is favored even more.

In Figures 7.79a and 7.79b the TEM images of the annealed and unannealed PCHD-b-PS-9 film sections respectively are presented.

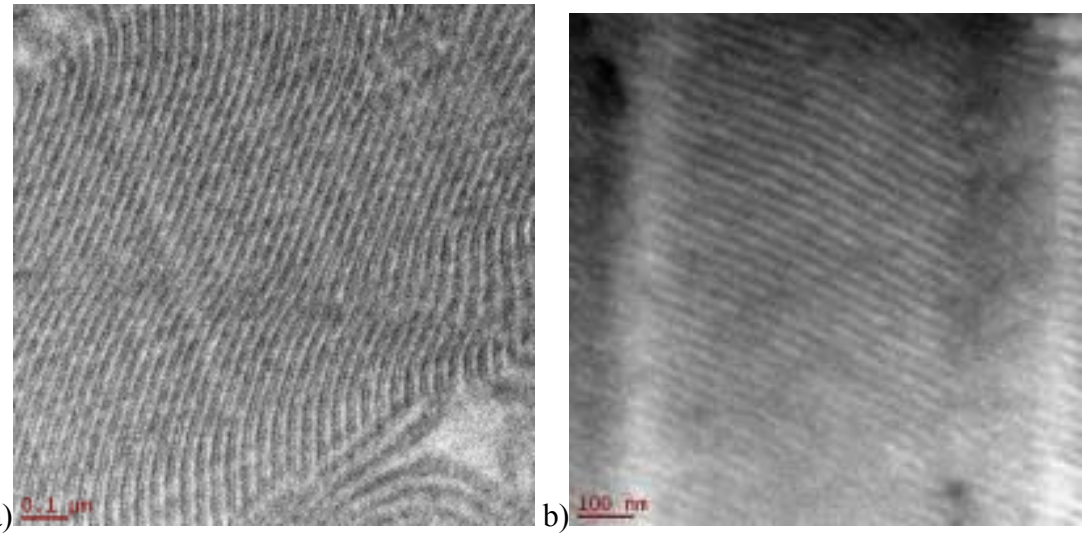

Figure 7.79: *a) TEM image of the annealed PCHD-b-PS-9 film b) TEM image of the unannealed PCHD-b-PS-9 film.*

It is easily observed that both images from the annealed and unannealed sections exhibit alternating lamellar morphology. The darker domains correspond to the PCHD block while the lighter to the PS block. The system is slightly asymmetric (φ_{PS} = 55,6%) and such morphology is consistent and with what has been observed for a PS-b-PCHD system (with 52% 1,2-microstructure though) from Natori et al.[3] The image from the unannealed sections seems to be less organized in comparison with the annealed one. Nevertheless, the lamellar morphology of the PS and PCHD blocks is distinct enough, while the domain size correlates

with the obtained volume fractions. In the case of the annealed PCHD-b-PS-9, it is clear that the increase of the temperature promoted the microphase separation even more and the lamellae of the PS and PCHD blocks are more distinct. Taking into account the previous mentioned results for other samples as well as the fact that the degree of polymerization is among the highest of all synthesized samples for this thesis (N = 556), it is believed that the system is well above the weak segregation regime, therefore, annealing is not affecting significantly the observed morphology.

Figures 7.80a and 7.80b represent the TEM images of the annealed and unannealed PS-b-PCHD-10 sections respectively.

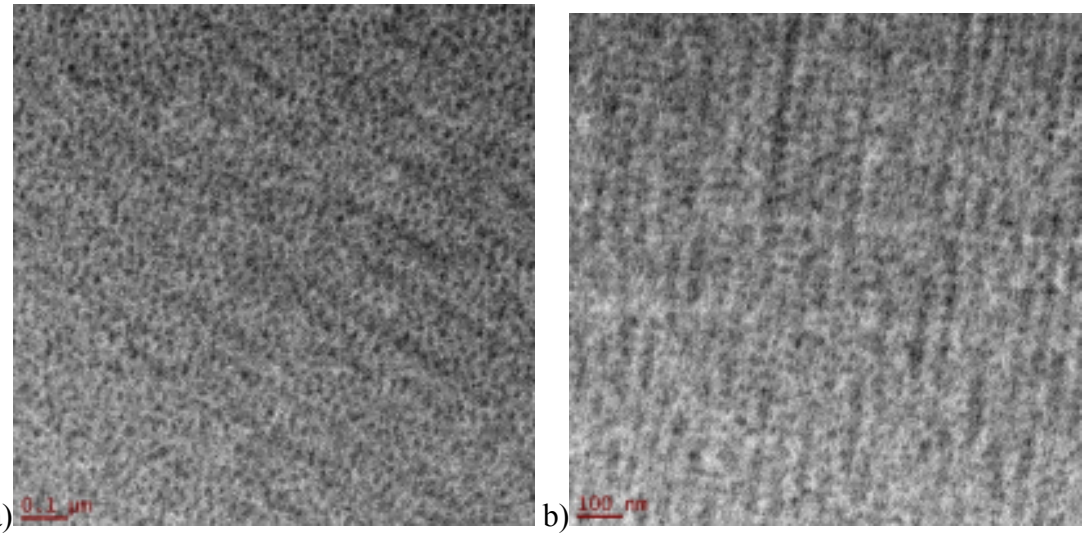

Figure 7.80: *a) TEM image of the annealed PS-b-PCHD-10 film b) TEM image of the unannealed PS-b-PCHD-10 film.*

Observing the TEM images of both annealed and unannealed samples it is understood that they exhibit poor-organized topography. Especially the TEM image of the unannealed film exhibits a very random structure with several darker regions which correspond to the stained PCHD block. It is clear that very distinct areas between the two blocks do not exist, which means that the interface of the PS and the PCHD blocks is flattened leading to partial mixing. Nevertheless, the existence of randomly oriented spheres of the minority component (darker domains) in a matrix of the majority component (lighter domains) can be stated. The fact that the PS-b-PCHD systems exhibit high conformational asymmetry correlates with the existence of this structure, even though it displays the highest volume fraction for the PS block (φ_{PS} = 91,2%) of all the synthesized linear diblock copolymers for this thesis. The annealed sample exhibits a slightly higher degree of microphase separation which can be described also as randomly oriented spheres of the minority PCHD blocks in the matrix of the majority PS blocks. The different regions are more distinct in this case implying that with the increase of the temperature, better microphase separation is adopted. However, these

assumptions are in great controversy with the conclusion made for the compositionally and molecularly almost similar PS-b-PCHD-2 annealed film, where no microphase separation was observed. The degree of polymerization for the PS-b-PCHD-10 annealed sample is slightly lower than that of the PS-b-PCHD-2 annealed sample (N = 444 and N = 457 respectively) which indicates that between these two values, significant changes may occur as far as the ODT is concerned. Concluding, the existence of even poor microphase separation at the annealed film is very important, taking into consideration the very high volume fraction of the PS block.

Figures 7.81(a,b) and 7.81c represent the TEM images from the PS-b-PCHD-11 annealed and unannealed films respectively. Figure 7.81d presents the FFT image for the structure observed in Figure 7.81b.

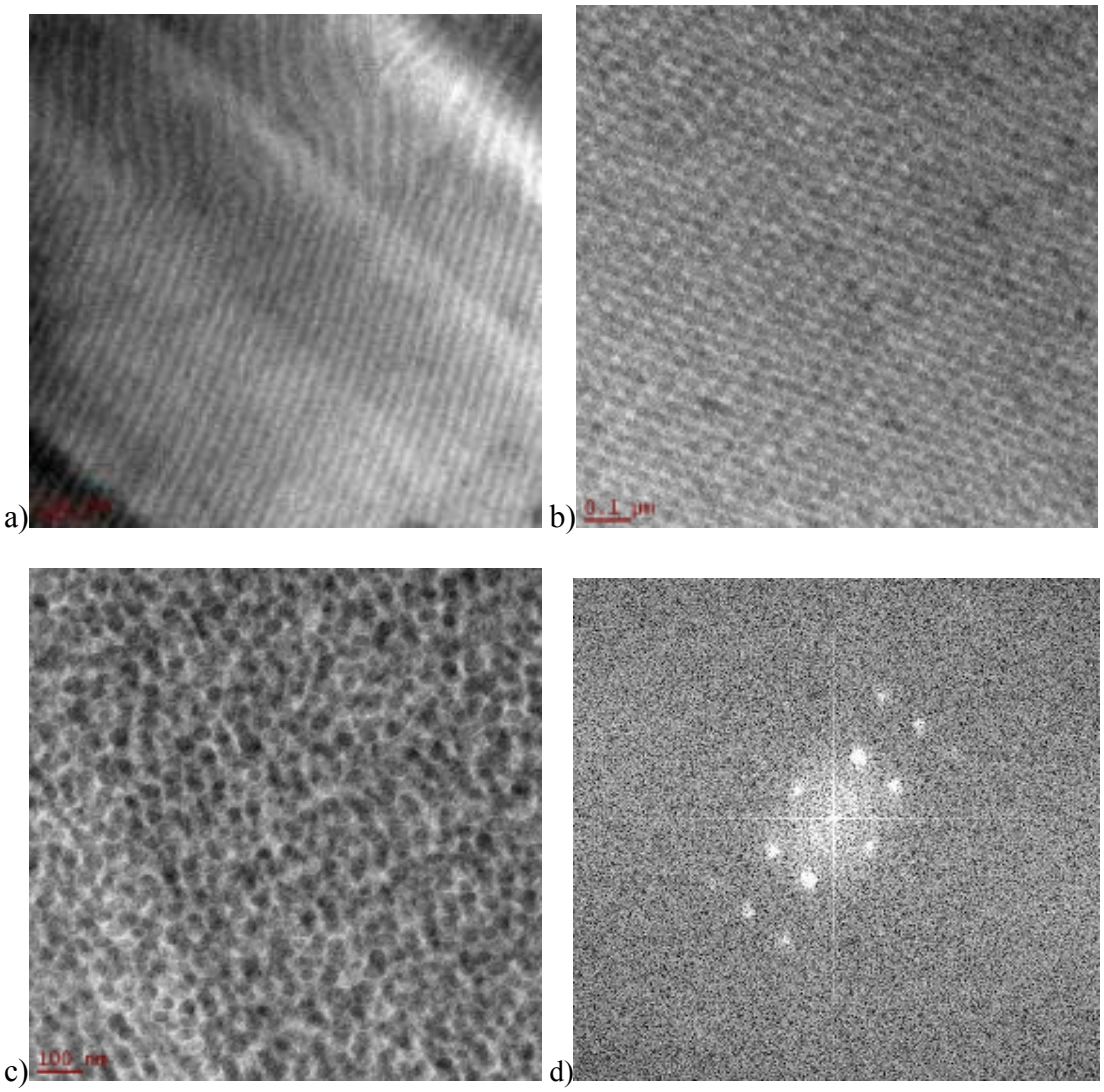

Figure 7.81: *a) TEM image of the annealed PS-b-PCHD-11 film for two days b) TEM image of the annealed PS-b-PCHD-11 film for 5 days c) unannealed PS-b-PCHD-11 film d) FFT image of the PS-b-PCHD-11 film for 5 days.*

In this case, three TEM micrographs are given corresponding to the annealed for two days (Figure 7.81a), to the annealed for 5 days (Figure 7.81b) and to the unannealed PS-b-PCHD-11 films (Figure 7.81c). The annealed for two days film exhibits alternating lamellae of the PCHD and PS segments, where the dark domains correspond to PCHD and the white to PS. The annealed for five days sample exhibits the double gyroid structure, which means that two independently interpenetrating and not interconnected bicontinuous three dimensional networks of the minority component (PCHD) are formed in a matrix of the majority component (PS). This is also indicated from the FFT image (Figure 7.81d) which exhibits approximately a two-fold projection (high symmetry axis of [110] type). Again in this case the dark domains correspond to PCHD stained with OsO_4 while the white domain corresponds to PS which does not react with the staining media. Both the observed morphologies are periodic and continuous. This very impressive difference indicates that the time of annealing also plays an important role in the microphase separation of a PS-b-PCHD sample. The double gyroid structure has been proven to be an equilibrium one and is normally observed for very narrow ranges of volume fractions. Actually, the DG has been identified at volume fractions for PS-b-PI diblock copolymers ranging from 27 to 33% for the PI. Recently, while studying the morphological behavior of PS-b-PDMS copolymers, it has been reported by Avgeropoulos and Thomas groups[142] that DG is observed for $\varphi_{minority}$ = 40 to 42% which includes the volume fraction of PCHD (φ_{PCHD} = 41,4% since φ_{PS} = 58,6%) in sample PS-b-PCHD-11. Therefore, additional studies via TEM are needed in order to completely verify the structure and add one more exception in the SSL phase diagram of Bates and Fredrickson for PS-b-PI copolymers. This very important observation indicates that the system undergoes an order-order transition by simply increasing the annealing time from two days to five, which means that the system probably lies upon the boundary between the lamellar and the double gyroid phase in the phase diagram of χN as a function of volume fraction. On the other hand, the unannealed sample exhibits poorly ordered cylinders of the PCHD block (dark domains) in a matrix of the PS block (lighter domains). The interface between the blocks is rather increased and by increasing the temperature, the system goes to more ordered topographies, but forming either the lamellar or the double gyroid phase.

In Figures 7.82a and 7.82b the TEM images of the annealed and unannealed PS-b-PCHD-12 films respectively are exhibited. Observing the TEM images for both the annealed and unannealed cases, it is clearly understood that they exhibit very well-ordered structures. The annealed sample exhibits hexagonally packed cylinders of the minority PCHD block in the matrix of the minority PS block. The PCHD cylinders appear darker due to staining with OsO_4 while the PS matrix appears white. The observed morphology is highly ordered and periodic in a wide range of the studied areas of the film.

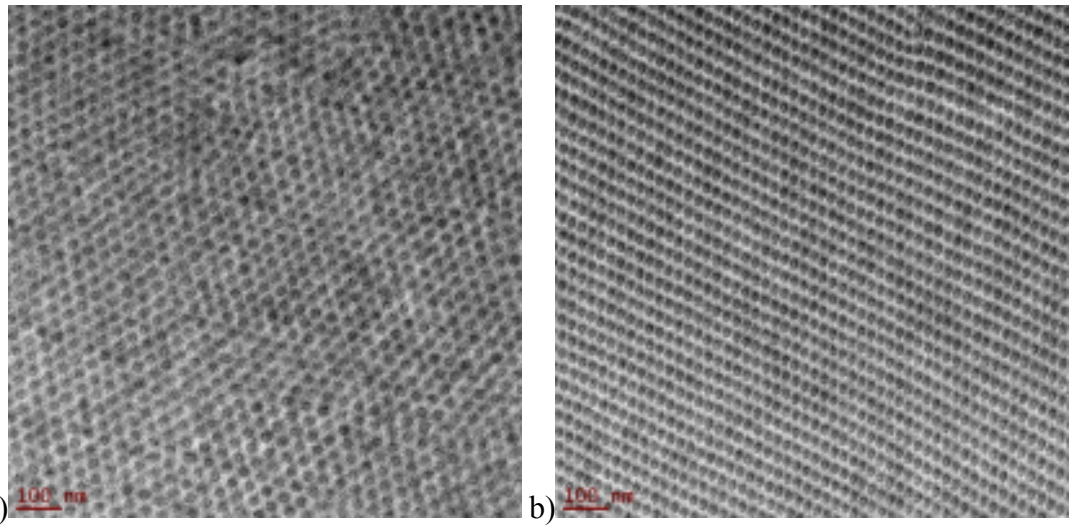

Figure 7.82: *a) TEM image of the annealed PS-b-PCHD-12 film b) TEM image of the unannealed PS-b-PCHD-12 film.*

According to the volume fractions of the two components, the expected morphology should be lamellar, but this is not the case. This indicates that, generally, the PS-b-PCHD linear diblock copolymers not only exhibit high conformational asymmetry but also the morphology of the hexagonally packed cylinders of the minority block in the matrix of the majority block covers a very wide range of volume fractions and χN values on the phase diagram and the lamellar phase is surprising narrow for $\varphi_{PS} > 50\%$, if a comparison is made with the well-established PS-b-PI phase diagram. Taking into account also what was previously reported about the highly self-organized structure of the PS-b-PCHD-3 annealed film, which exhibits similar volume fractions with the PS-b-PCHD-12 annealed film (φ_{PS} = 59,5% and φ_{PS} = 58,4 respectively) but very different molecular weights (17.800 g/mol and 40.000 g/mol respectively), it is indicated that the hexagonal packed cylinders are observed in lower as well in higher degrees of polymerization ($N_{PS\text{-}b\text{-}PCHD\text{-}3}$ = 190 and $N_{PS\text{-}PCHD\text{-}12}$ = 429). As far as the unannealed sample is concerned, it is also clear that it exhibits a very well self-organized structure of hexagonally packed cylinders of the minority PCHD blocks (dark areas) in a matrix of the majority PS blocks (white areas). The structure is highly periodic, while the size of the PCHD cylinders is slightly smaller compared to the cylinder size of the annealed sample, probably attributed to swelling of the domain size due to increase in temperature. As described for the PS-b-PCHD-3 sample, the opposite is happening when the degree of polymerization is low, where the segmental movements of the polymer chains are favored leading to better microphase separation.

However, the most important aspect is the large morphological discrepancies existing between the PS-b-PCHD-11 (annealed and unannealed) and the PS-b-PCHD-12 (annealed and unannealed) films studied, even though they exhibit identical volume fractions and degrees of polymerization ($N_{PS\text{-}b\text{-}PCHD\text{-}11}$ = 437 and $N_{PS\text{-}b\text{-}PCHD\text{-}12}$ = 429). As far as the annealed

PS-b-PCHD-12 sample is concerned, the existence of hexagonally packed cylinders for a volume fraction identical with that of the PS-b-PCHD-11 annealed case, which (depending) on annealing time) exhibits either the lamellar or the double gyroid morphology, provides new information about the phase boundaries of these three different morphologies for the given degrees of polymerization for the specific sequence of segments. Hence, it can be stated that these two almost identical samples lie upon the phase boundaries of two of the three observed phases and with minor changes in annealing time or the degree of polymerization, order-order transitions occur between the lamellar and the double gyroid phase and/or between the double gyroid and the hexagonally packed cylinders phase. These observations provide even more interesting information concerning the phase transformations of the PS-b-PCHD system regarding the phase diagram. As far as the unannealed film is concerned, which forms very well-ordered hexagonally packed cylinders as well, and in comparison with the unannealed PS-b-PCHD-11 film, quite disordered cylinders, it can be indicated that the system is very different from the relative annealed one, since order-order transitions are not observed. On the other hand, it is very clear that by increasing slightly only the volume fraction (from the PS-b-PCHD-11 sample to the PS-b-PCHD-12 sample), the system becomes very well-ordered, which is very puzzling.

In Figures 7.83a and 7.83b the TEM images of the PCHD-b-PS-13 annealed and unannealed films respectively are given.

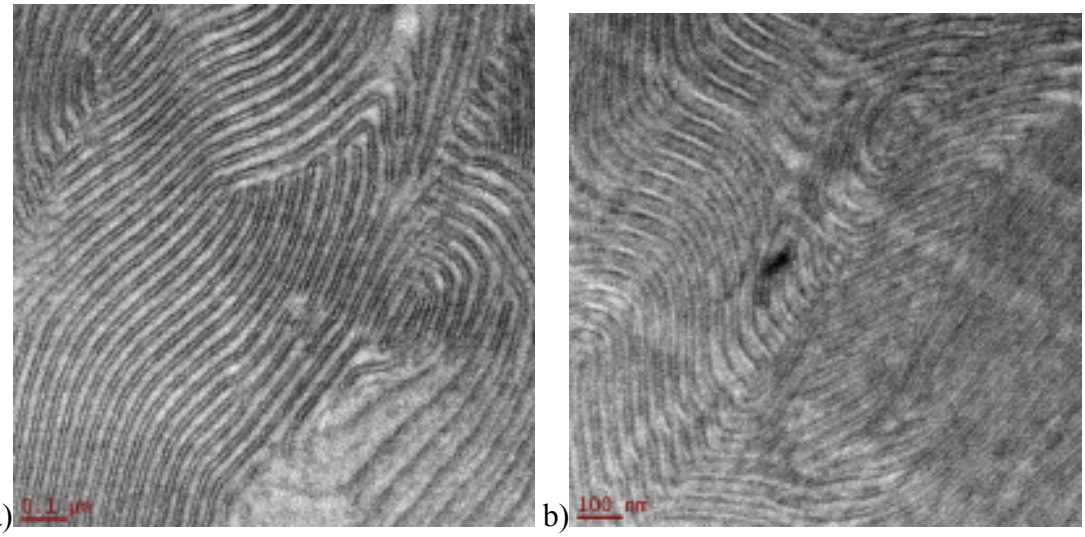

Figure 7.83: *a) TEM image of the annealed PCHD-b-PS-13 film b) TEM image of the unannealed PCHD-b-PS-13 film.*

It is observed that both films exhibit microphase separation with a very interesting and unique structure. This structure is the four-layer, three-phase lamellae morphology, which is normally observed in systems where three chemically different blocks exist. The unannealed PCHD-b-PS-13 sections exhibit a less ordered structure than the annealed one. As

for several previously mentioned samples, the annealing procedure promotes the microphase separation and the four-layer, three-phase lamellae morphology is even more distinct. Such morphology has never been reported before for a linear diblock copolymer, while there is one case where the interfacial staining of a linear diblock copolymer system is described forming this morphology, but this is not the case for the PCHD-b-PS-13 system.[143] Except from the fact that the observed morphology is unique, the volume fractions of the two blocks are very far from the usual values which may lead to lamellar morphology. This can be attributed to the high conformational asymmetry of the system, but more thorough investigation has to be performed.

A possible explanation for the observed morphology could be that the white domains are the unstained PS block, while the gray and black regions correspond to the 1,4- and the 1,2-microstructures of the PCHD block respectively. PCHD is the majority block which eventually increases the molar ratio of 1,2-PCHD in the whole system. If the randomness of the 1,2- vs. 1,4- microstructure is adopted then a possible schematic of how such a structure could be obtained is given in the following Figure 7.84.

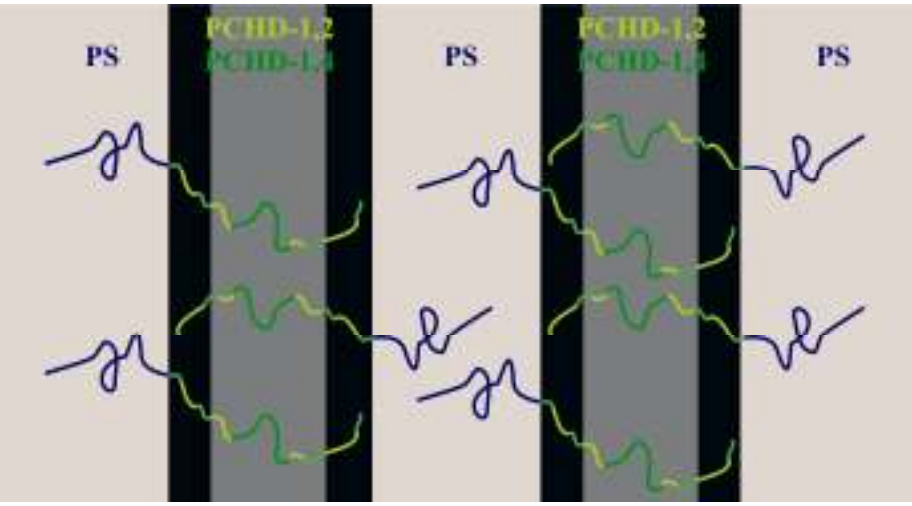

Figure 7.84: *Schematic presentation of the possible conformation of chains in order to explain a 3-phase topography from a 2-phase initial block copolymer(PCHD-b-PS-13).*

Furthermore, observing the unannealed case, the domain size of the two blocks coincides with the calculated volume fraction (φ_{PS} = 26,9%), while for the annealed sample it seems that the domain size of the PS lamellae has been increased. This can be attributed to minor swelling of the PS component due to the increase of the temperature.

The assumption that the obtained morphology corresponds to the projection normal to the cylindrical axis of a core-shell structure of polystyrene cylindrical cores surrounded by poly(cyclohexadiene) cylinders which are then hexagonally packed in a matrix of PS[137] does not correlates with the calculated volume fractions, which strengthens the existence of the lamellar morphology. Additionally, even though thorough study at the sections was applied,

no hexagonally close packed cylinders were observed, therefore, the adaptation of the assumption from the literature in not possible.

In Figures 7.85a and 7.85b, the TEM images of the annealed and unannealed PS-b-PCHD-14 films respectively are presented. Both the annealed and unannealed cases exhibit highly ordered microphase separation and long range order. The annealed sample exhibits probably the double gyroid structure, which elevates the previous mentioned results for the PS-b-PCHD-11 annealed film exhibiting the same structure and similar volume fractions.

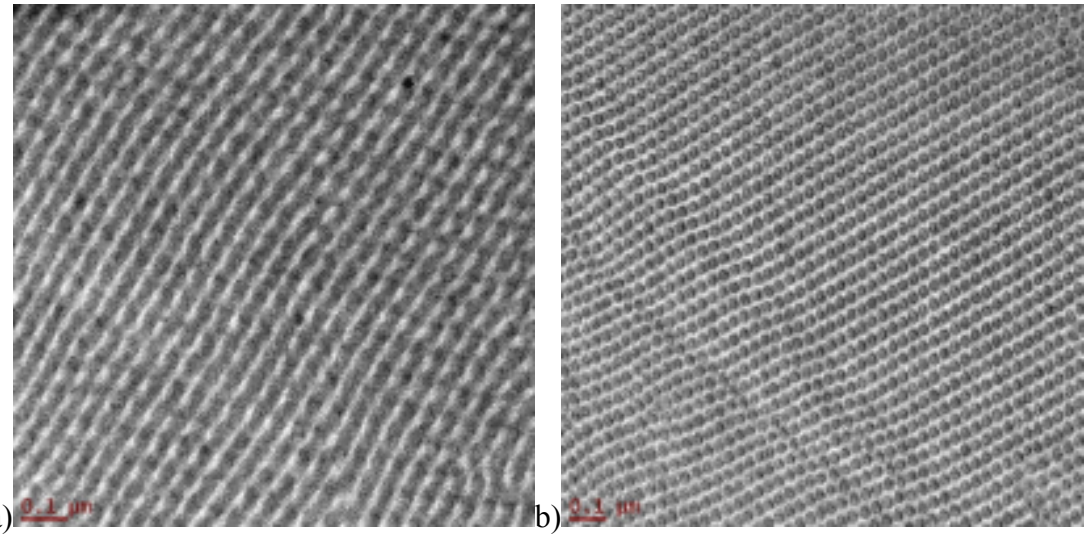

Figure 7.85: *a) TEM image of the annealed PS-b-PCHD-14 sample b) TEM image of the unannealed PS-b-PCHD-14 sample.*

This observation provides even more significant information concerning the existence of a double gyroid structure in the PS-b-PCHD systems and for the possible range of volume fractions that this structure is observed (which might be very narrow). The structure is highly periodic and consistent with the PCHD block appearing darker and the PS block appearing white. Furthemore, the observed double gyroid structure is very reasonable since the PS-b-PCHD-14 sample exhibits only slightly higher degree of polymerization than the PS-b-PCHD-11 sample ($N_{\text{PS-b-PCHD-14}}$ = 466 and $N_{\text{PS-b-PCHD-11}}$ = 437 respectively) for almost identical volume fractions. As far as the unannealed sample is concerned, it is believed that it exhibits a core shell structure of PS core surrounded by PCHD cylinders in the matrix of PS. This result has been reported previously by Mays et al. for similar volume fractions of the components[137] (φ_{PCHD} = 37 and 38%). They observed core-shell cylinders for both annealed and unannealed sections with the annealing procedure promoting the better microphase separation of core-shell cylinders. In the case of the PS-b-PCHD-14 sample this is not the case, but the reproduction of this structure in the unannealed sections provides significant information concerning the self-assembly of the PS-b-PCHD systems. The existence of the core-shell structure is strengthened by the fact that the domain size of the PCHD cylinders, in regard

with the matrix material, is larger than expected for the corresponding volume fraction of the PS-b-PCHD-14 sample.

In Figures 7.86a and 7.86b are represented the TEM images of the annealed and unannealed PCHD-PS-15 samples respectively. Analyzing the two TEM images it can be observed that both samples exhibit identical microphase separation. Hexagonally packed cylinders of the minority PCHD blocks (dark regions) in a matrix of the majority PS blocks (white regions) are formed in both the annealed and the annealed films, where in the case of the annealed sample, the cylinders appear slightly larger.

a) 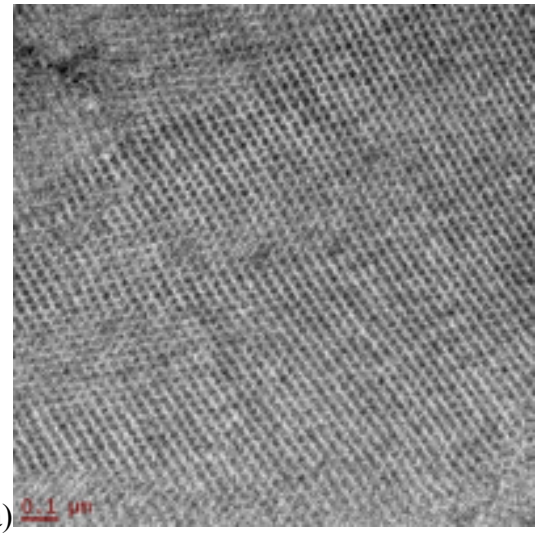 b) 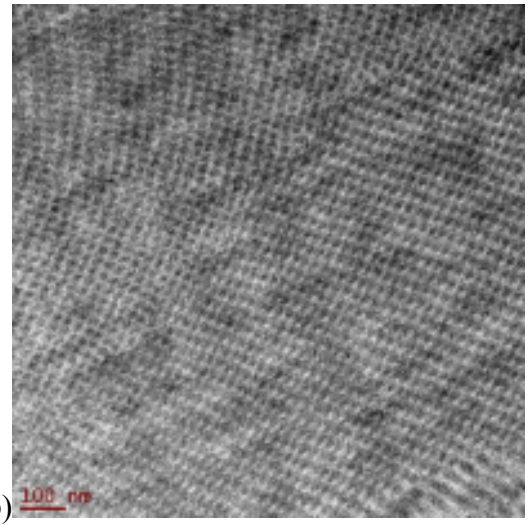

Figure 7.86: *a) TEM image of the annealed PCHD-PS-15 film b) TEM image of the unannealed PCHD-b-PS-15 film.*

Nevertheless, both structures are highly organized, exhibiting periodicity and consistency. This occurs due to the fact that the enthalpic factors of the free energy are favored resulting in the curving as well as the minimization of the interface. The morphology of hexagonally packed cylinders of the minority components in a matrix of the majority component for this volume fraction (φ_{PS} = 75,2%) correlates with the morphology observed for the PI-b-PS system,[140] even though the conformation asymmetry between these two systems is very different. Furthermore, the PCHD-PS-15 sample exhibits the highest degree of polymerization (N = 586%) among all the synthesized linear diblock copolymers for this thesis, but the increase in temperature does not alter the observed morphology nor the domain size as in some of the previously mentioned samples with relatively high degree of polymerization. This can be attributed to the volume fraction of the majority component which places this sample away from the OOT or ODT boundaries.

In Figures 7.87a and 7.87b the TEM images of the annealed and unannealed PS-b-PCHD-16 films are given. From the TEM images of the annealed and the unannealed sections respectively significant differences are evident. The unannealed film exhibits microphase

separation in contrast with the annealed sample which seems to be quite disordered. The morphology observed is the hexagonally closed packed cylinders of the minority PCHD blocks (darker regions) are formed in a matrix of the majority PS blocks (lighter regions). The hexagonal packing is rather poor and considering also the fact that the degree of polymerization is not that high (N = 356), it can be claimed that the system is probably in the intermediate segregation regime and near the ODT. This statement is further reinforced by the fact that the annealed sample is rather disordered which implies that by increasing the temperature (therefore, reducing the value of the χ interaction parameter), the entropic factors are favored instead of the enthalpic and the interface between the two blocks is increased leading possibly to partial mixing.

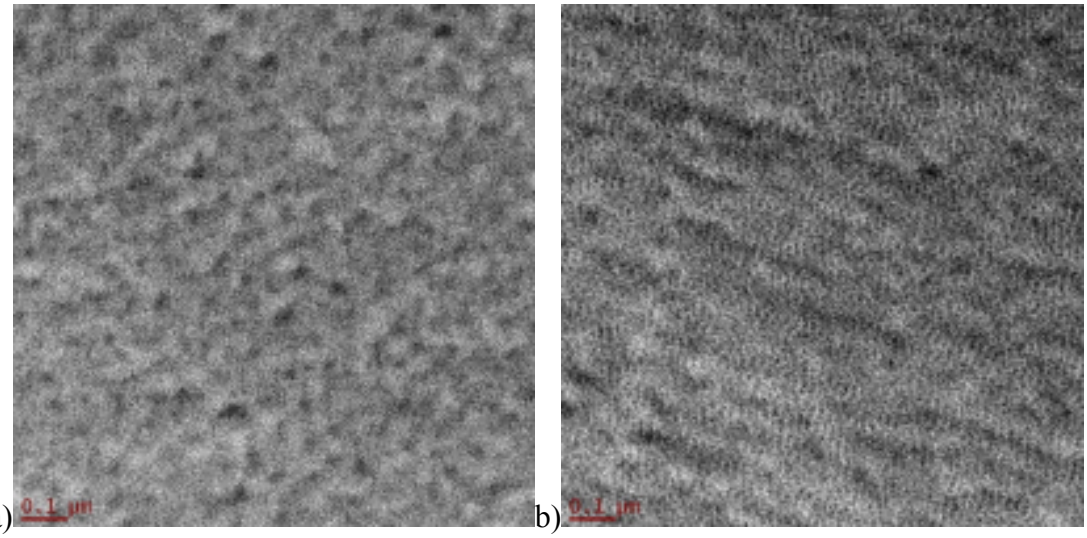

Figure 7.87: *a) TEM image of the annealed PS-b-PCHD-16 film b) TEM image of the unannealed PS-b-PCHD-16 film.*

This morphology for the corresponding volume fraction for the majority component (φ_{PS} = 57,8%) is unusual but is in good agreement with the previous mentioned observations for the PS-b-PCHD-12 sample concerning the range of existence of the hexagonally packed cylinder structure in the PS-b-PCHD linear diblock copolymer system. As it has been discussed before, this feature can be attributed to the high conformational asymmetry that is exhibited in the PS-b-PCHD system.

Figures 7.88a and 7.88b present the TEM images of the PS-b-PCHD-17 annealed and unannealed films respectively.

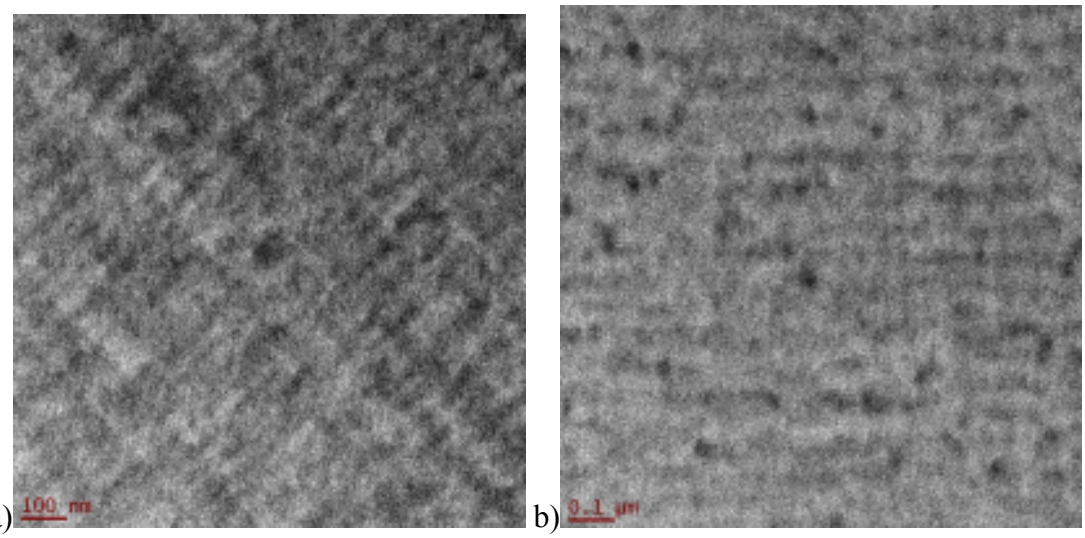

Figure 7.88: *a) TEM image of the annealed PS-b-PCHD-17 film b) TEM image of the unannealed PS-b-PCHD-17 film.*

Both TEM images exhibit disordered structures with several darker and lighter domains. The boundaries between these domains are not distinct and the existence of any well-ordered structure is not observed. The annealing process does not play any significant role in the promotion of microphase separation. PS-b-PCHD-17 linear diblock copolymer exhibits identical volume fraction with the PCHD-b-PS-15 sample (φ_{PS} = 72,4). However, the molecular weight of the PS-b-PCHD-17 sample is half of the relative one for the PCHD-b-PS-15 sample, thus its degree of polymerization is also significantly reduced (N = 300). This alternation explains why the PS-b-PCHD-17 sample is disordered while the PCHD-b-PS-15 sample exhibits microphase separation. Furthermore, this observation provides useful information concerning the order-disorder transition, suggesting that definitely between the range of N = 300 and N = 586, an order-disorder transition occurs from the disordered state to hexagonally packed cylinders, since both samples exhibit identical volume fractions.

In Figures 7.89a and 7.89b the TEM images of the annealed and unannealed PS-b-PCHD-18 sections are given. Analyzing the TEM images of the annealed case, it can be observed that it exhibits very poor order. There are darker and lighter regions but their boundaries are not distinct and the formation of any morphology is not observed. Therefore the interface is large, implying mixing of the two components. On the other hand, the unannealed sample is not disordered and exhibits relatively ordered microphase separation.

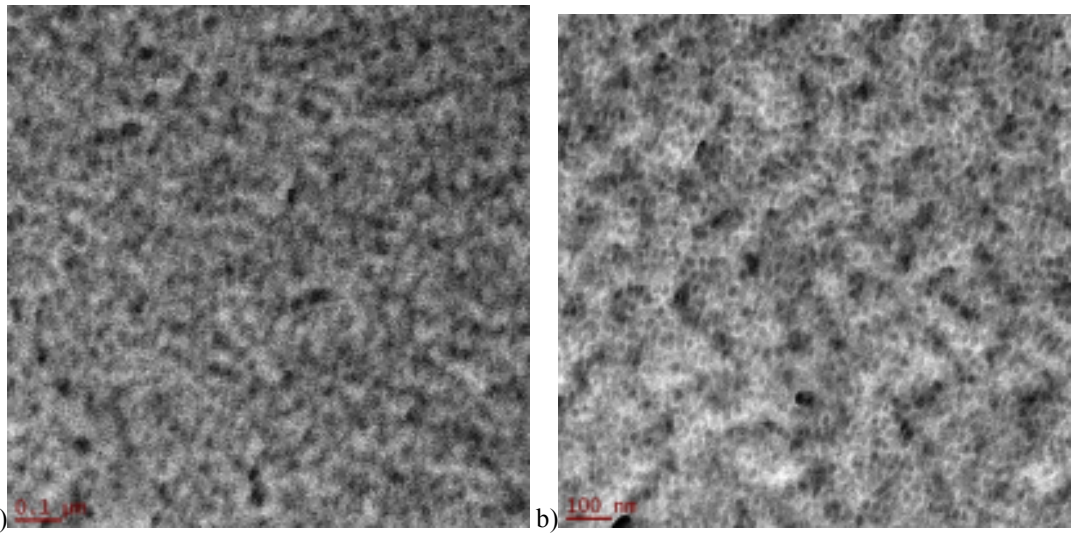

Figure 7.89: *a) TEM image of the annealed PS-b-PCHD-18 film b) TEM image of the unannealed PS-b-PCHD-18 film.*

Several domains exhibiting rather ordered hexagonally packed cylinders of the minority component (PCHD) in a matrix of the majority component (P) can be seen. The molecular characteristics of this sample are identical with those of the PS-b-PCHD-3 sample ($N_{PS\text{-}b\text{-}PCHD\text{-}18}$ = 189 and $N_{PS\text{-}b\text{-}PCHD\text{-}3}$ = 190 respectively) but their TEM images exhibit great discrepancies. The annealed film of the PS-b-PCHD-18 sample is less ordered than that of the PS-b-PCHD-3 sample, while the unannealed film of the PS-b-PCHD-18 sample is slightly more ordered than the relative one of the PS-b-PCHD-3 sample. This observation is provided from the great differences between the two annealed samples, where by increasing slightly the degree of polymerization (from 189 to 190), for almost identical volume fractions (φ_{PS} = 59,1% for the PS-b-PCHD-18 sample and φ_{PS} = 61,1 for the PS-b-PCHD-3 sample), a change occurs and the system prefers to make a transition from an almost disordered state to a highly ordered hexagonally packed cylinder state. This means that there is definitely an order-disorder transition occurring while the degree of polymerization is very slightly increased (from N = 189 to N =190 which is within the experimental error). This statement is strengthened by the fact that the system is probably in the weak segregation regime due to its low values of molecular weight and degree of polymerization.

Figures 7.90a and 7.90b represent the TEM images of the annealed and the unannealed PS-b-PCHD-19 sections respectively. In Figure 7.90c, a schematic of the morphology for the unannealed sample is presented also. Analyzing the TEM micrographs, it is observed that both samples exhibit microphase separation with the annealed one described as better well-ordered than the unannealed one. As it has been explained previously, this is reasonable, since the elevation of the temperature provides, in many cases, better microphase separation. The annealed sample exhibits a very interesting core-shell cylinder morphology that was observed also for the unannealed PS-b-PCHD-14 case. However, there are

significant differences between these two TEM images that lead to new assumptions. First of all, the lighter areas that correspond to the PS block cover a large area of the section, and the core PS seems to exhibit also large size.

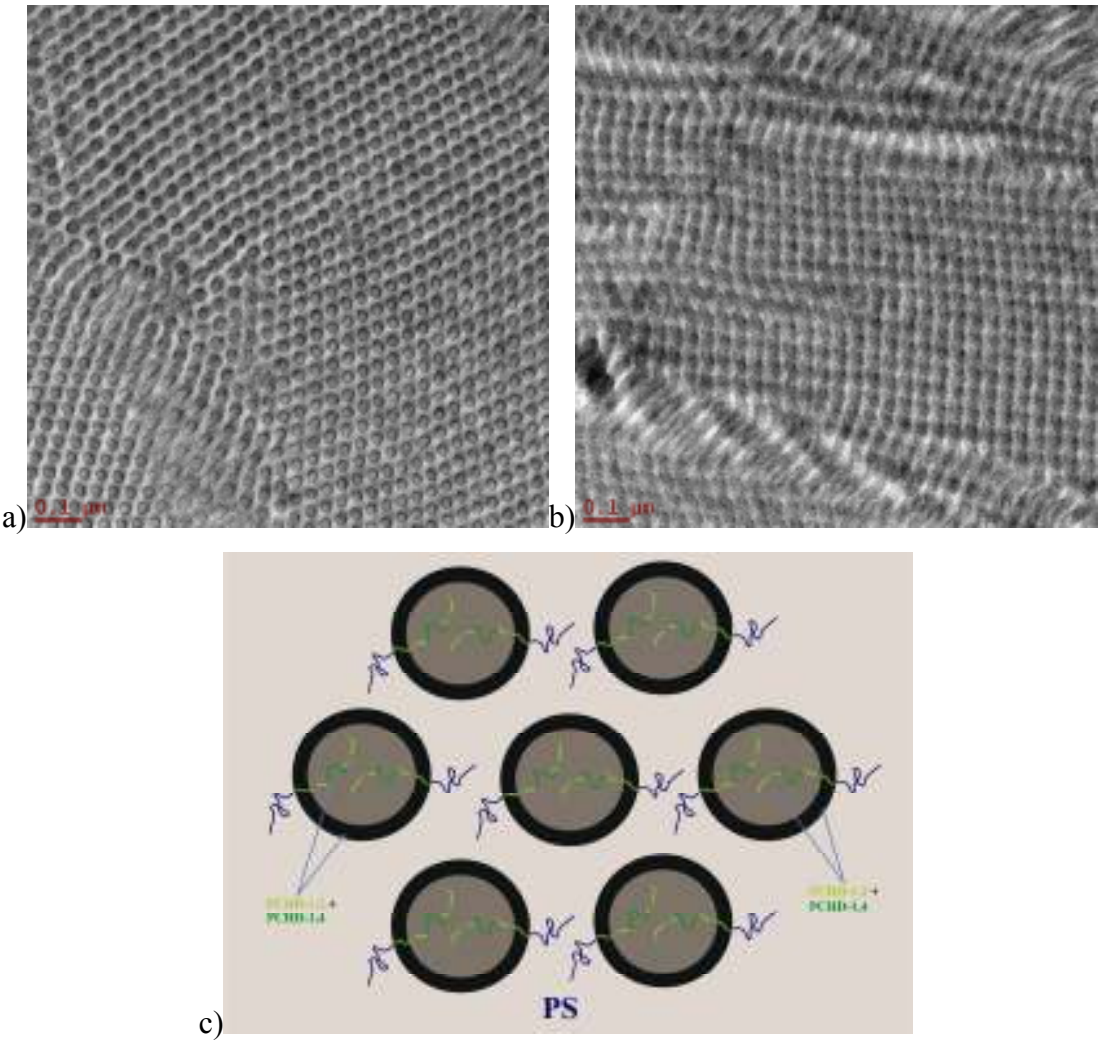

Figure 7.90: *a) TEM image of the annealed PS-b-PCHD-19 film b) TEM image of the unannealed PS-b-PCHD-19 film c) Schematic of the observed morphology for the annealed PS-b-PCHD-19 film.*

However, this observation comes in great disagreement with the fact that this sample exhibits PCHD majority (φ_{PCHD} = 54.4%), thus the core-shell cylinder case where the existence of PS core surrounded from PCHD cylinders, hexagonally packed in a PS matrix cannot be applied, taking also into account the domain sizes from the TEM image. This "dead-end" led to the assumption, which correlates with the PCHD-b-PS-13 case, that the system exhibits core-shell cylinders of the core 1,4-microstructure of the PCHD block (grey areas) surrounded by very narrow cylinders of the 1,2-microstructure of the PCHD block (black areas) in the matrix of the PS block (white areas). It is assumed that as the microphase separated system tends to form cylinders from the lamellar phase, and curving of the interface occurs towards the minority component, the 1,2-units of the PCHD block prefer to form a

layer between the polystyrene and the 1,4-units of the PCHD due to their stereochemistry and the fact that they exhibit lower flexibility.[136]

As far as the unannealed PS-b-PCHD-19 sample is concerned, a cubic structure is observed with dark and white regions corresponding to PCHD and PS respectively. The structure is well-organized and it seems like cylinders transforming into the double gyroid structure, since it does not exhibit any hexagonal packing. The volume fraction is almost the reversed from that of the PS-b-PCHD-11 (φ_{PCHD} = 54,4% for PS-b-PCHD-19, while φ_{PS} = 58,7% for PS-b-PCHD-11) which indicates the existence of another DG area on the phase diagram for $\varphi_{PS} < 50\%$. Annealing creates well-ordered structures with different morphology though, which is something that occurs often. More investigation has to be performed in order to verify the interesting assumption of the DG morphology in ranges lower than $\varphi_{PS} = 50\%$.

7.4.2 Small Angle X-Ray Scattering (SAXS)

SAXS studies of I(q) vs. q were performed for all samples but only the best results are presented here. The fact that the SAXS results were relatively poor even for very well-ordered cases as exhibited already from the TEM images can be explained by taking into account two factors:

a) As already mentioned at the experimental part the densities of PS and PCHD are very similar (1.05 g/ml and 1.10 g/ml respectively). Therefore, even when exposed for more time only a first peak and a very weak second are observed leading to very poor results.

b) The performance of these SAXS experiments through a more powerful X-ray source (e.g. Synchrotron facility) might lead to better results and assist in the confirmation of the topographies identified through the TEM images.

Furthermore, as already described at the morphological characterization through TEM, some discrepancies are observed at different molecular weights, volume fractions and block sequence. PS-b-PCHD and PCHD-b-PS are linear diblock copolymers with different sequence of the two blocks from which they are composed.

The most exciting result is that for sample PS-b-PCHD-13 annealed from chloroform at 120^0C. From the TEM it is evident that the morphology of 4-layer 3-phases is observed which is a structure only adopted, up to date at least, in linear ABC triblock terpolymers with almost equal volume fractions and approximately equal χ parameters between the adjacent segments ($\chi_{AB} \sim \chi_{AC} \sim \chi_{BC}$).

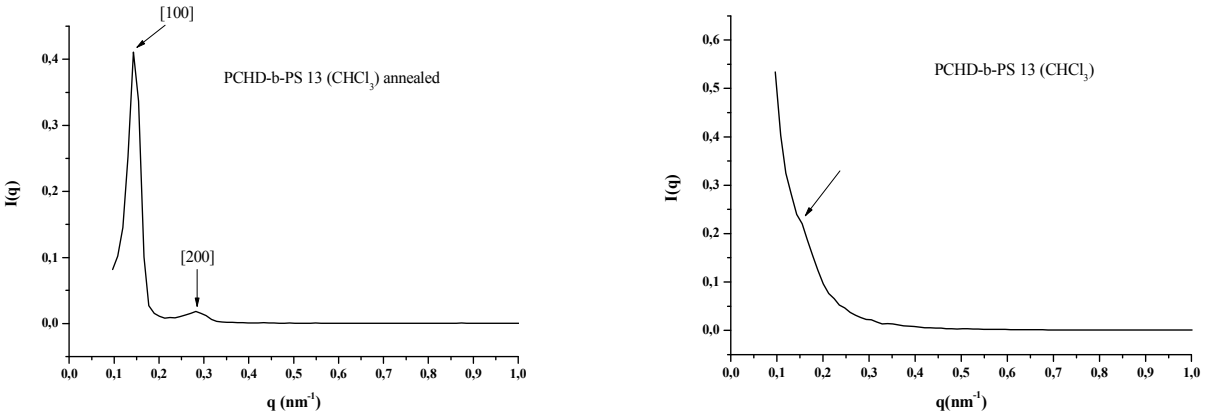

(a) **(b)**

Figure 7.91: *SAXS plots of I(q) vs. q for sample PS-b-PCHD-13 (a) for the annealed film cast from chloroform and (b) for the unannealed film cast from chloroform. The SAXS results are in partial agreement with the observations and conclusions from the TEM experiments.*

The SAXS plots of I(q) vs. q are given in Figure 7.91 where it is evident for the annealed cast from chloroform sample (Figure 7.91a) that two peaks are straightforward which correspond to reflection [100] and [200] respectively, leading to a ratio of 1:2 characteristic for alternating lamellae structures. Unfortunately, even though the TEM images for the unannealed cast from chloroform sample exhibit identical morphology with the annealed, but not as well-ordered, only one weak peak is evident (indicated with an arrow on the SAXS plot at Figure 7.91b).

In Figure 7.92 the SAXS plot of I(q) vs. q is given for sample PS-b-PCHD-12 cast from toluene and annealed at 120^0C. This is the only case where better order is being observed and at least 3 peaks are evident which lead to a ratio of 1:√3:√4 which corresponds ideally for hexagonally close packed cylinders, which is the case as observed from the TEM images.

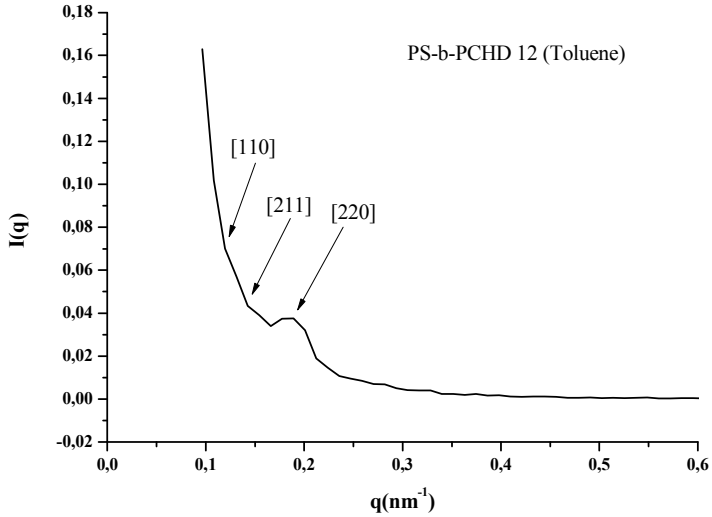

Figure 7.92: *SAXS plots of I(q) vs. q for sample PS-b-PCHD-12 for the unannealed film cast from toluene.*

The SAXS plot (Figure 7.93) for sample PS-b-PCHD-11 cast from toluene and annealed at 120^0C is consistent with what was observed from the TEM image. It was reported during the analysis of the TEM image that for the specific annealed sample a cubic structure is observed (since high symmetry projection of the [110] type is identified from the FFT image) and since only DG and OBDD have been identified for diblock copolymers it is assumed that the structure is one of these two cubic three dimensionally topographies. The SAXS plot seems to be more consistent with the OBDD structure but it is concluded that further and more analytical SAXS experiments should be made possibly at a Synchrotron source for complete verification.

From the TEM image that was given above (Figure 7.79a), the annealed sections of PS-PCHD-9 sample alternating lamellae were exhibited. From the SAXS pattern (Figure 7.94) the same sample exhibits peaks with ratio: 1:√3:√4:√7 which according to the international tables of crystallography these ratios are acquired for p6mm space group symmetry corresponding to hexagonally close packed cylinders (hcpc).

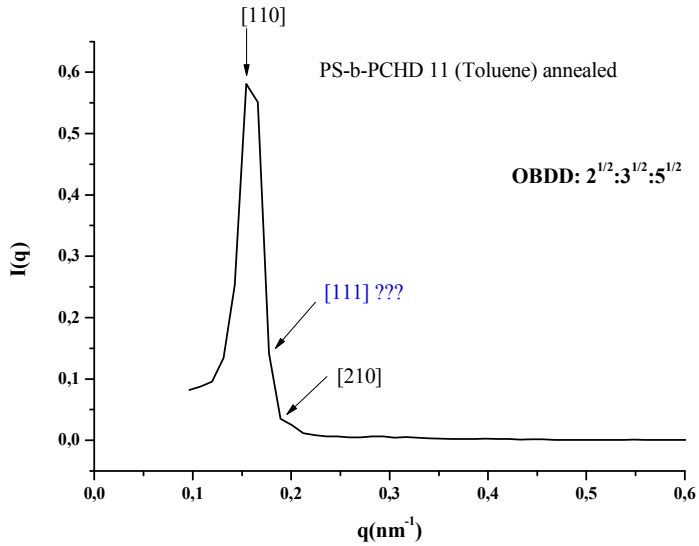

Figure 7.93: *SAXS plots of I(q) vs. q for sample PS-b-PCHD-11 for the annealed film cast from toluene.*

One possible explanation for the different results is that all the cylinders were horizontally oriented; therefore the sample was aligned and ordered in a specific direction; leading to observation of alternating layers. A schematic (Figure 7.95) is given below explaining this approach.

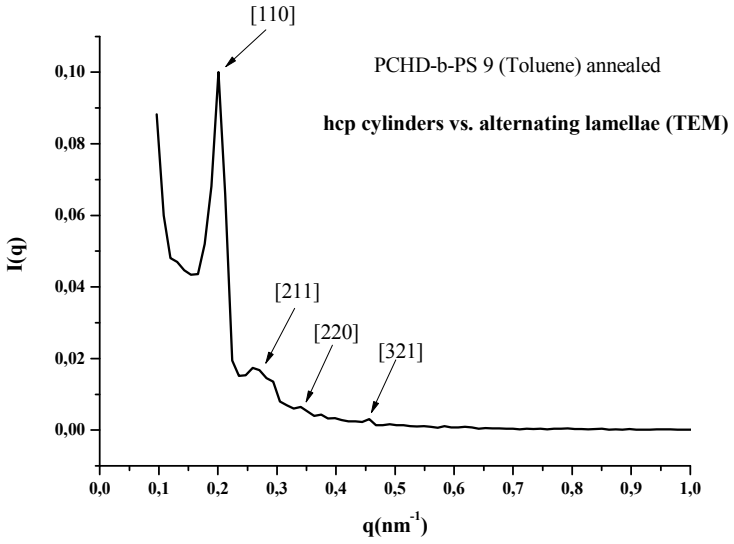

Figure 7.94: *SAXS plots of I(q) vs. q for sample PS-b-PCHD-9 for the annealed film cast from toluene.*

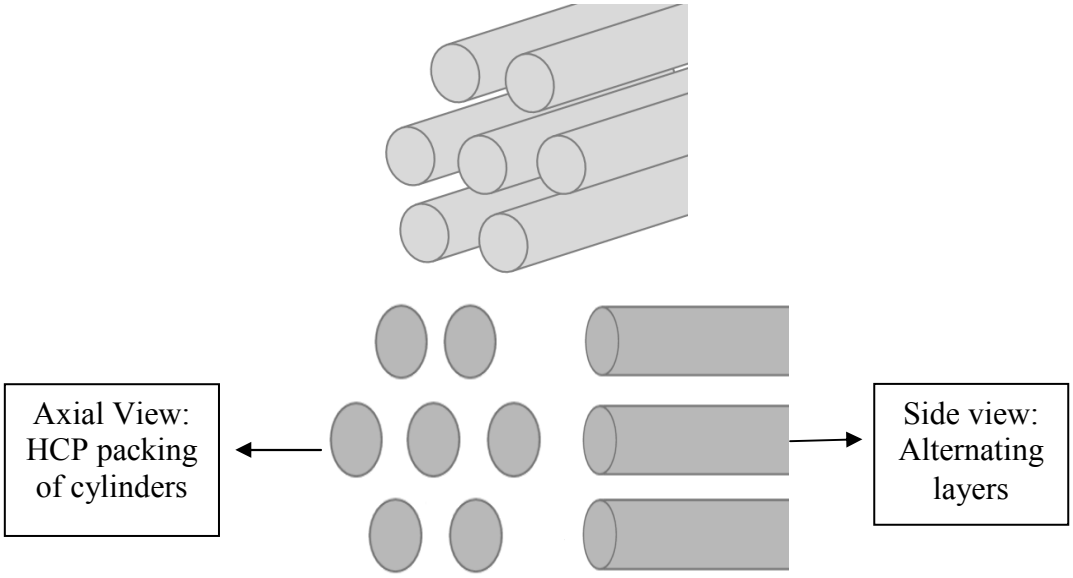

Figure 7.95: *Schematic representation of hexagonally close packed cylinders with intermediate (top) axial and side views respectively.*

In order to completely verify the differentiation between the TEM and SAXS results it is needed to examine the 2D pattern as taken from the SAXS instrumentation and conclude whether the sample is oriented. There are many cases observed in block copolymers in which orientation occurs from simple cast films of their dilute solutions from non-selective solvent for all segments involved due to the ability of such block copolymers to self-assemble. Additionally, if that is the case, it is needed to explore further the already prepared thin film (from casting) and take a cross section of the thin film in order to examine the side view.

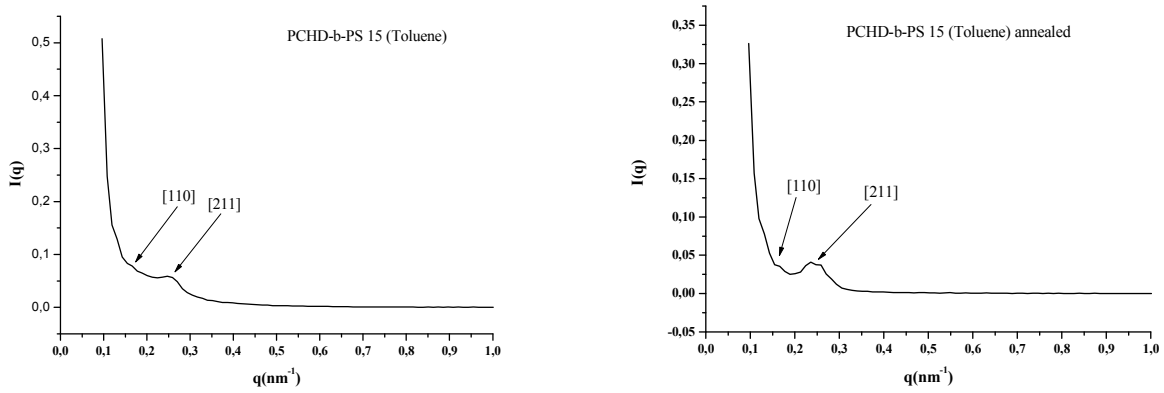

(a) **(b)**

Figure 7.96: *SAXS plots of I(q) vs. q for sample PS-b-PCHD 15 (a) for the annealed film cast from chloroform and (b) for the unannealed film cast from chloroform. The SAXS results are in partial agreement with the observations and conclusions from the TEM experiments.*

Finally, in Figure 7.96 the SAXS plots of I(q) vs. q are given for both annealed and unannealed films cast from toluene for sample PCHD-b-PS-15. It is evident that even though

the TEM images exhibited long range order that this is not the case for the SAXS patterns. Very rough estimation may occur and only two relevant peaks/shoulders can be verified leading to a ratio of 1:√3 which corresponds to hexagonally close packed cylinders of the one phase in the matrix of the other.

7.5 Conclusions - Future Work

The synthesis of the seventeen (17) linear diblock copolymers as well as the synthesis of the five (5) complex architecture copolymers is considered successful. The molecular characterization via size exclusion chromatography (SEC), membrane osmometry (MO) and proton nuclear magnetic resonance (^{1}H-NMR) spectroscopy indicated molecular and compositional homogeneity for all the samples. More specifically:

- ✓ The number average molecular weights obtained from size exclusion chromatography were verified through membrane osmometry for all synthesized samples.
- ✓ The molecular weight distributions of the first block of each diblock copolymer as well as of the final materials exhibited rather monomodal peaks with polydispersity indices varying from 1,04 to 1,23. For samples with I > 1,1, the PCHD block was either polymerized first and/or exhibited high molecular weight (> 15.000 g/mol). Minor or not at all side and/or termination reactions were observed during the analysis with molecular characterization techniques.
- ✓ The molecular weight distributions of the difunctional precursors as well as of the living arms for the complex architecture copolymers exhibited very narrow and monomodal peaks indicating the absence of any unwanted byproducts. The well-established chlorosilane chemistry led to well-defined final complex architecture copolymers.
- ✓ The fractionation procedure was established for all five (5) complex architecture copolymers in order to obtain the desirable final products. Several solvent/non-solvent systems were tried in order to find the optimum one.
- ✓ The weight fractions were also verified from the ^{1}H-NMR results, indicating molecular and compositional homogeneity for the synthesized samples. Furthermore, the 1,2- and 1,4-microstructures for the PCHD segments were calculated verifying the existence of high 1,4-microstructure for all samples (88-97%) due to the addition of the polar reagent DABCO.

The thermal analysis was performed via differential scanning calorimetry and the glass transition temperatures were measured for all synthesized linear diblock copolymers. The results indicated that significant dependence from the molecular weight and the volume fraction of PCHD segment is observed. More specifically:

- ✓ The glass transition temperatures varied from 102^0C to 107^0C for the PS majority materials, exhibiting minor dependence from the molecular weight alternation, while the PCHD majority materials exhibited increased glass transition temperatures (120^0C and 122^0C).
- ✓ Unique is the case of the fractionated PS-b-PCHD-4 (PCHD majority) sample which exhibited lower T_g than the aforementioned samples ($104,3^0$C). This was attributed to the absence of any unwanted byproducts resulting from side and/or termination reactions after the fractionation procedure.
- ✓ Additionally, exciting results were obtained for the cases of two samples (PCHD-PS-9 and PCHD-PS-15) that exhibited high glass transition temperatures ($115,4^0$C and $114,3^0$C respectively), even though they exhibit PS as the majority segment. This was attributed to the possible minor existence of byproducts from side and/or termination reactions during 1,3-CHD polymerization (since relatively high PCHD molecular weight for both samples was observed), which led to the increase of the T_g for the final materials.

The molecular characterization via transmission electron microscopy (TEM) and small angle X-ray scattering (SAXS) indicated that the two different blocks can self-assemble leading to known morphologies as well as several very interesting ones. More specifically:

- ✓ The preparation of thin films (50-75 nm) with the ultramicrotome is a tailored procedure which requests increased care in order to receive good and thin sections. The cryo mode was not used due to the increased glass transition temperatures of both segments and due to the embedding media which provided stiffness and stability.
- ✓ The polydiene block (PCHD) was stained with fresh aqueous solution (2% wt in water) of osmium tetroxide (OsO_4) for 45 minutes in order to increase the contrast in TEM. In this manner, the PCHD chains crosslink with the staining media increasing the electron density and therefore they appear darker in TEM micrographs.
- ✓ Structures that have been predicted theoretically and confirmed experimentally for other systems were observed, such as alternating lamellae, hexagonally closed packed (hcp) cylinders, spheres, double gyroid and maybe double diamond. Most of the corresponding morphologies were observed for different volume fractions than expected, since the PS-b-PCHD system exhibits high conformational asymmetry. It is evident that the variations in molecular weights as well as the annealing procedure play a significant role on the microphase separation of this system.
- ✓ Three unique morphologies were observed for three different diblock copolymers. More specifically, the core-shell cylinder morphology was observed for a PS majority diblock copolymer (PS-b-PCHD-14) consisting of PS shell, surrounded by PCHD

cylinders in a PS matrix. PCHD segments appear dark while PS segments appear white and this coincides with a case already reported in the literature by Mays et al.[137] These two systems exhibit similar molecular characteristics and volume fractions and the fact that the morphological behavior of a sample synthesized for this thesis, resembles the aforementioned behavior for the literature provide significant information elevating the confirmation of this unique morphology.

Furthermore, the four-layer three phase alternating lamellar morphology was observed via TEM for the first time for a linear diblock copolymer consisting of PCHD majority casted form chloroform (PCHD-b-PS-13). TEM images exhibited black, grey and white regions (Figures 7.83a and 7.83b) and the assumption that the black regions correspond to PCHD rich in 1,2-microstructure, the grey regions correspond to PCHD rich in 1,4-microstructure and the white regions correspond to PS, is made (Figure 7.84). SAXS plots of the annealed sample confirmed the existence of the lamellar morphology rising new information concerning the self-assembly of this system.

Additionally, the core-shell cylinder morphology was also observed for another sample (PS-b-PCHD-19) exhibiting PCHD majority segments. This clue led to the assumption that the system does not coincide with the previous mentioned and consists of a PCHD core, rich in 1,4-microstructure (grey regions), surrounded by a thin cylinder of PCHD rich in 1,2-microstructure (dark regions) in a matrix of PS segment (Figure 7.90c).

- ✓ SAXS plots for only five samples are presented due to relatively poor results even for very well-ordered cases as exhibited already from the TEM images. Such behavior could be attributed to the very similar density of both segments (1,05 g/ml for PS and 1,10 g/ml for PCHD), therefore, even when exposed for more time only a first peak and a very weak second are observed. Nevertheless, SAXS plots for these five samples confirm the results already exhibited from TEM micrographs. The most exciting case is the confirmation of the 3-phase, 4-layer alternating lamellar morphology for the PCHD-b-PS-13 sample, where the SAXS plot for the annealed sample confirm the observed topography from the TEM image, exhibiting the predictable first two reflections: [100] and [200].

The immediate future work and aims for the synthesized materials of this research work are listed below:

a) Morphological characterization via TEM and SAXS of the complex architecture copolymers.
b) SAXS measurements with a synchrotron source in order to obtain better results for the corresponding morphologies of the linear diblock copolymers, especially for those

that exhibit well-ordered structures in TEM images and verify whether or not similar electron density plays significant role.

c) Different annealing times and temperatures in order to understand the variations in morphological behavior related to these two factors. Especially for samples that exhibited poor order after annealing, lower temperatures have to be established (80^0C-110^0C) or even slightly above room temperature conditions (40^0C-50^0C), below the glass transition temperature of both segments.

d) Casting from different solvents, selective and non-selective, in order to verify whether the unique observed structures are equilibrium ones and to examine dependence on the selective solvent for the morphological behavior of the system.

e) Synthesis of more linear diblock copolymers of PCHD majority in order to cover a wider range of volume fractions and to investigate the microphase separation.

f) Additionally, thermal SAXS experiments and theoretical calculations, using the already reported results, must be performed in order to calculate the interaction parameter χ of these two polymers. This task is of a great importance and most of the steps towards this target have already been made through this research work.

g) Creation of the PS-b-PCHD $\chi N = f(\varphi)$ phase diagram. It is already proven that this system exhibits high conformational asymmetry and it would be very interesting to complete the morphological studies and receive an overall view of the different microphase separation for the specific system.

References

1. Natori I.; Imaizumi K.; Macromol. Symp. **2000,** 157**,** 143.
2. Imaizumi K.; Ono T.; Natori I.; Sakurai S.; Takeda K.; J. Polym. Sci., Polym. Phys. Ed. **2001**, 39, 13.
3. Natori I.; Imaizumi K.; Yamagishi H. ; Kazunori M.; J. Polym. Sci. Polym. Phys. Ed. **1998**, 36, 1657.
4. Bywater S.; Marcel V. B.; Smets G.; Szwarc M.; Worsfold D. J.; Adv. Polym. Sci., **1989,** 86, 147.
5. Young R. N.; Quirk R. P.; Fetters L. J.; J. Adv. Polym. Sci., **1984**, 56, 1.
6. Altares T. A.; Wyman D. P.; Allen V. R.; J. Polym. Sci., Part A, **1964**, 2, 4533.
7. Mays J. W.; Hadjichristidis. N.; Polym. Bull., **1989**, 22, 471.
8. Conlon D. A.; Crivello J. V.; Lee, J. L.; O' Brien M.; *Macromolecules*, **1989**, 22, 509.
9. Konigsberg I.; Jagur-Grodzinski J.; J. Polym. Sci., Polym.Chem., **1983**, 21, 2535.
10. Okay O.; Funke W.; Macromolecules, **1990**, 23, 2623.
11. Morton M.; Bostick E. E.; Clarke R. G.; J. Polym. Sci., Polym Chem, **1963**, 1, 475.
12. Hsieh H. L.; McKinney O. F.; J. Polym. Sci., Part B, **1966**, 4, 843.
13. Mavroudis A.; Avgeropoulos A.; Hadjichristidis N.; Thomas E.; Lohse D.; Chem Materials, **2003**, 15, 1976.
14. Xu Z.; Mays J. W..; Chen X.; Hadjichristidis N.; Schilling F. C.; Bair H. E.; Pearson, D. S.; Fetters, L.; Macromolecules, **1985**, 18, 2560.
15. Natori I.; Macromolecules, **1997**, 30, 3696
16. Mays J. W.; Hong K.; Macromolecules **2001**, 34, 782.
17. Allen R. D.; Long T. E.; McGrath J. E.; Polymer Bulletin, **1986**, 15, 127
18. Ekizoglou N.; Hadjichristidis N.; J. Polym. Sci., Polym. Chem., **2001**, 39, 1198.
19. Bellas V.; Iatrou H.; Hadjichristidis N.; Macromolecules, **2000**, 33, 6993
20. Colvin I. C.; Scinetific Glassblowing: An Introduction, **2008**.
21. A) Bahary W. S.; Lans J. H.; Rubber Chem. Technol., **1967**, 40, 1529. B) Burfield D. R.; Lim K-L.; Macromolecules, **1983**, 7, 1170.
22. Naumova S. F.; Dokl. Akad. Nauk B. SSR, **1975**, 19 (4), 346.
23. Naumova S. F.; Chem. Abtr., **1983**, 98 (22), 180717u.
24. Lenz R. W.; Mango L. A.; Chem. Abtr., **1972**, 77, 127102e
25. Craig D.; Shipman J. J.; Fowler R. B.; J. Am. Chem. Soc., **1961**, 83, 2885.
26. Stücklen H.; Thayer H.; Willis P.; J. Am. Chem. Soc. **1940**, 62, 1717.

27. Houtz R. C.; Adkins H.; J. Am. Chem. Soc., **1933**, 55, 1609.
28. Ballard D. G. H.; Courtis A.; Shirley I. M., Taylor S. C.; Macromolecules, **1988**, 21, 294.
29. McKean D. R.; Stille J. K.; Macromolecules, **1987**, 20, 1787.
30. Waratuke S. A.; Thorn M. G.; Fanwick P. E.; Rothwell, A. P.; Rothwell, I.; P. J. Am. Chem. Soc., **1999**, 121, 9111.
31. Sen A.; Thomas R. R.; Organometallics, **1982**, 1, 1251.
32. Sen A.; Lai, T. W.; Organometallics, **1982**, 1, 415.
33. Po R.; Santi R.; Cardasi M. A.; J. Polym. Sci., Polym. Chem., **2000**, 38, 3004.
34. Claverie J. P.; Gin D. L.; Conticello, V. P.; Hampton, P. D.; Grubbs, R. H.; Polym. Prepr. (Am. Chem. Soc., Div. Polym. Chem.) **1992**, 33, 1020.
35. Gin D. L.; Conticello V. P.; Grubbs R. H.; J. Am. Chem. Soc., **1994**, 116, 10507.
36. Marvel C. S.; Hartzell G. E.; J. Am. Chem. Soc. **1959**, 81, 448.
37. Frey, D. A.; Hasegawa, M.; Marvel, C. S.; J. Polym. Sci., Part A: Polym. Chem. Ed. **1963**, 1, 2057.
38. Mays J. W.; Hong K.; Macromolecules **2001,** 34, 782.
39. Cassidy P. E.; Marvel C. S.; Ray S.; J. Polym. Sci., Part A: Polym. Chem. Ed. **1965**, 3, 1553.
40. Sharaby Z.; Grodzinski J. J.; Martan M.; Vofsi D.; J. Polym. Sci., Polym. Chem., **1982**, 20, 901.
41. A) Francois B.; Zhong X. F. ; Makromol. Chem. **1990**, 191, 2735. B) Francois B.; Zhong X. F. ; Makromol. Chem. **1990**, 191, 2743.
42. Young R. N.; Fetters L. J.; Huang J. S.; Krishnamoorti R.; Polymer International, **1994**, 33, 217.
43. Zhong X. F.; Francois B.; Makromol. Chem., Rapid Commun., **1988**, 9, 411
44. Natori I.; Inoue S.; Macromolecules, **1998**, 31, 4687.
45. Williamson D. T.; Elman J. F.; Madison P. H.; Pasquale A. J.; Long T. E.; Macromolecules, **2001**, 34, 2108.
46. Wang X.; Xia J.; He J.; Yu F.; Li A.; Xu J.; Lu H.; Yang Y.; Macromolecules **2006,** 39, 6898.
47. Hong K.; Mays J. W.; Macromolecules, **2001**, 34, 3540.
48. Hong K.; Wan Y.; Mays J. W.; Macromolecules, **2001**, 34, 2482.
49. Tsoukatos T.; Hadjichristidis N.; J. Polym. Sci. Polym. Chem. , **2002,** 40, 2575.
50. Tsoukatos T.; Avgeropoulos A.; Hadjichristidis N.; Macromolecules **2002,** 35, 7928.
51. Uhrig D.; Hong K.; Mays J. W.; Kilbey S. M.; Britt P. F.; Macromolecules **2008**, 41, 9480.

52. Huang T.; Messman J. M.; Mays J. W.; Macromolecules **2008,** 41, 266.
53. Natori I.; Imaizumi K.; Macromol. Symp. **2000,** 157**,** 143.
54. Zhong X. F.; Francois B.; Makromol. Chem. **1991**, 192, 2277.
55. Kovacic P.; Jones M. B.; Chem. Rev. **1987**, 87, 357.
56. Yamamoto T.; *Prog. Polym. Sci.,* **1992**, 17, 1153.
57. Shacklette L. W.; Chance R. R.; Ivory D. M.; Miller G. G.; Baughman R. H.; Synth. Met., **1979**, 1, 307.
58. Shacklette L. W.; Elsembaumer R. L.; Chance R. R.; Sowa J.M; Ivory D. M.; Miller G. G.; Baughman R. H.; J. Chem. Soc., Chem. Commun., **1982**, 361.
59. Mignard E.; Hiorns R. C.; Francois B.; Macromolecules **2002,** 35, 6132.
60. Francois B.; Widawski G.; Rawiso M.; Cesar B.; Synthetic Metals, **1995,** 69, 463.
61. Francois B.; Widawski G.; Rawiso M.; Synthetic Metals, **1995**, 69, 491.
62. Mignard E.; Tachon C.; Francois B.; Synthetic Metals, **1999**, 102, 1246.
63. Natori I.; Natori S.; Sato H.; Macromolecules, **2006,** 39, 3168.
64. Natori I.; Sato H.; Jour. of Pol. Sci. Pol. Chem., **2006**, 44, 3526.
65. Williamson D. T.; Buchanan D.; Elkins C. L.; Long T. E.; Macromolecules, **2004,** 37, 4505.
66. Huang T.; Zhou H.; Hong K.; Simonson J. M.; Mays J. W.; Macromol. Chem. Phys. **2008**, 209, 308.
67. Hamley I. W.; Developments in Block Copolymer Science and Technology, **2004**.
68. Hadjichristidis N.; Pispas S.; Floudas G.; Block Copolymers: Synthetic Strategies, Physical Properties and Applications, **2003.**
69. Hadjichristidis N.; Pispas S.; Iatrou H.; Pitsikalis M.; J. of Polym. Sci. Pol. Chem., **2000**, 38, 3211.
70. Uhrig D.; Mays J. W.; J. Pol. Sci. Pol. Chem., **2005**, 43, 6179.
71. Rempp P.; Franta E.; Herz J. E.; Adv. Polym. Sci., **1989**, 86, 147.
72. Pitsikalis M.; Hadjichristidis N.; Pispas S.; Mays J. W.; Adv. Pol. Sc., **1998**, 135, 1.
73. Hadjichristidis N.; Pispas S.; Iatrou H.; Pitsikalis M.; Vlachos C.; Adv. in Pol. Sci., **1999,** 142.
74. Hadjichristidis N.; J. Pol. Sci. Pol. Chem., **1999**, 37, 857.
75. Hadjichristidis N.; Pispas S.; Iatrou H.; Pitsikalis M.; Chem. Rev. **2001,** 101, 3747.
76. Szwarc M.; Levy M.; Milkovich R.; J. Am. Chem. Soc. , **1956**, 78, 2656.
77. Morton M.; Anionic Polymerization: Principles and Practice, Academic Press, New York, **1983.**

78. Hsieh H. L.; Quirk R. P.; Anionic Polymerization: Principles and Practical Applications, Marcel Dekker Inc., New York, **1996.**
79. Hautekeer J. P.; Vashney S. K.; Fayt R.; Jacobs C.; Jerome R.; Teyssie P.; Macromolecules, **1990,** 23, 3893.
80. O'Driscoll K. F.; Tobolsky A. V.; J. Pol Sci Pol. Chem. **1959**, 132, 363.
81. Varshey K. S; Jacobs C.; Hautekeer J. ; Bayard P.; Jerome R.; Fayt R.; Teyssie P.; Macromolecules **1991**, 24, 4997.
82. Wang J. S.; Jerome R.; Bayard P.; Teyssie P.; Macromolecules **1994**, 27, 4908.
83. Paul D. R.; Barlow J. W.; J. Macromol. Sci., Rev. Macromol. Chem., **1980**, C18(1), 109.
84. Matsushita Y.; Shimizu N.; Nakao Y.; Choshi H.; Nagasawa M.; Polymer J., **1986**,18, 361.
85. Schindler A.; Williams J. L.; Polym. Prepr.; **1969**, 10(2), 832.
86. Grosius P.; Gallot Y.; Skoulios A.; Eur. Polym. J. **1970,** 6, 355.
87. Morton M.; Anionic Polymerization: Principles and Practice, Academic Press, New York, **1983.**
88. Burker M. C.; Vincent B.; Colloids & Surfaces **1984**, 8, 289.
89. Forster S.; Kramer E.;Macromolecules **1999**, 32, 2783.
90. Zilliox J. G.; Roovers J. E. L.; Bywater S.; Macromolecules **1975**, 8, 573.
91. Avgeropoulos A.; Dair B. J.; Hadjichristidis N.; Thomas E. L.; Macromolecules **1997**, 30, 5634.
92. Guyot P.; Favier J. C.; Fontanille M.; Sigwalt P.; Polymer **1982**, 23, 73.
93. Tung L. H.; Lo G. Y-S.; Macromolecules **1994**, 27, 1680.
94. Tung L. H.; Lo G. Y-S.; Macromolecules **1994**, 27, 2219.
95. Lo G. Y-S.; Otterbacher E. W.; Gatzke A. L.; Tung L. H.; Macromolecules **1994**, 27, 2233.
96. Bandermann F.; Speikamp H-D.; Weigel L.; Makromol. Chem. **1985**, 186, 2017.
97. Lo G. Y-S.; Otterbacher E. W.; Pews R. G.; L. H. Tung; Macromolecules **1994**, 27, 2241.
98. R. P. Quirk.; Ma J. J.; Polymer International **1991**, 24, 197.
99. Yu J. M.; Teyssie P.; Jerome R.; Macromolecules **1996**, *29,* 6090.
100. Yu J. M.; Dubois P.; Jerome R.; Macromolecules **1996**, 29, 7316.
101. Yu J. M.; Dubois P.; Jerome R.; J.Pol. Sci. Pol. Chem., **1997**, 35, 3507.
102. Yu J. M.; Yu Y.; Dubois P.; Teyssie P.; Jerome R.; Polymer, **1997**, 38, 12, 3091.
103. He J.; Knoll K.; Mckee G.; Macromolecules **2004,** 37, 4399.
104. Tong J. D.; Jerome R.; Polymer **2000**, 41, 2499.

105. Tong J. D.; Leclere P.; Doneux C.; Bredas J. L.; Lazzaroni R.; Jerome R.; Polymer **2000**, 41, 4617.
106. Li H. J.; Tsiang R. C-C.; Polymer **2000**, 41, 5601.
107. Sfika V.; Tsitsilianis C.; Macromolecules **2003,** 36, 4983.
108. Batra U.; Russel W. B.; Pitsikalis M.; Sioula S.; Mays J. W.; Huang J. S.; Macromolecules **1997**, 30, 6120.
109. Rahman M. S.; Samal S.; Lee J-S.; Macromolecules **2006**, 39, 5009.
110. Rahman M. S.; Changez M.; Samal S.; Lee J-S.; J. Nanosc. Nanotech. **2007**, 7, 1.
111. Roovers J.; Toporowski P. M.; Macromolecules **1981**, 14, 1174.
112. Gido S. P.; Lee C.; Pochan D. J.; Pispas S.; Mays J. W.; Hadjichristidis N.; Macromolecules **1996**, 29, 7022.
113. Iatrou H.; Avgeropoulos A.; Hadjichristidis N.; Macromolecules, **1994**, 27, 6232.
114. Meier D. J.; J. Polym. Sci. Pt. **1969**, C 26, 81.
115. Helfand E.; Macromolecules **1975**, 8, 522.
116. Helfand E.; Wasserman Z.R.; Macromolecules **1976**, 9, 879.
117. Helfand E.; Wasserman Z.R.; Macromolecules **1978**, 11, 961.
118. Semenov A.N.; Soviet Phys. JETP **1985**, 61, 733.
119. Papadakis C.M.; Almdal K.; Mortensen K.; Posselt D; J. Phys. II **1997**, 7, 1829.
120. Leibler L.; Macromolecules **1980**, 13, 1602.
121. Mayes A. M.; Olvera de la Cruz, M. Macromolecules, **1991**, 24, 3975.
122. Matsen M. W.; Phys Rev. Let. **1994**, 72, 2660.
123. Matsen M. W.; Bates S. F.; J. of Pol. Sci. Pol. Phys. **1997**, 6, 945.
124. Milner T. S.; Macromolecules, **1994**, 27, 2333.
125. Mayes A. M.; J. Chem. Phys. **1989**, 91, 7228.
126. Bates S. F.; Fredrickson G. H.; Macromolecules **1994**, 27, 1065.
127. A) Wu C-S.; Handbook of Size Exclusion Chromatography, **1995**, Marcel Dekker Inc., Vol 66. B) Benoit H.; Grubisic Z.; Rempp P.; Jour. Pol. Sc. Pol. Phys., **1996**, 10, 1707 (Polymer Letters, **1967**, 5, 753).
128. Brandolini A. J.; D. D. Hills; NMR of Polymers and Polymer Additives, **2000.**
129. Williams D. B.; Carter B. C.; Transmission Electron Microscopy A Textbook for Materials Science, **2009**.
130. Sawyer L. C.; Grubb D. T.; Mayers G. F; Polymer Microscopy, **2008**.
131. Schnablegger H.; Singh Y.; A Practical Guide to SAXS - Getting Acquainted with the Principles, **2006**.

132. Hubbell J. H.; Veigele W. J.; Briggs E. A.; Brown R. T.; Cromer D. T.; Howerton R. J.; J. Phys. Chem. Ref. Data **1975**, 4, 471.
133. Hubbell J. H.; Øverbø I.; J. Phys. Chem. Ref. Data **1979**, 8, 69.
134. Hild G.; Kohler A.; Rempp P.; Eur. Pol. Jour., **1980**, 6, 525.
135. Sawyer L. C.; Grubb D. T.; Meyers G. F.; Polymer Microscopy, **2008**.
136. Quirk R. P.; You F.; Zhu L. S.; Cheng Z. D.; Macromol. Chem. Phys. **2003**, 204, 755.
137. David J. L.; Gido S. P.; Hong K.; Zhou J.; Mays J. W.; Tan N. B.; Macromolecules **1999**, 32, 3216.
138. Tsoukatos, PhD Thesis, **2000**.
139. Floudas G.; Vazaiou B.; Schipper F.; Ulrich R.; Wiesner U.; Iatrou H.; Hadjichristidis N.; Macromolecules **2001,** *34,* 2947.
140. Khandpur A. K.; Hamley I. W.; Ryan J. A.; Bras W.; Almdal K.; Mortensen K.; Macromolecules **1995,** 28**,** 8796.
141. Politakos N.; Ntoukas E.; Avgeropoulos A.; Krikorian V.; Pate B. D.; Thomas E. L. ; Hill R. M.; J. of Polym. Sci. Polym. Phys., **2009**, 47, 2419.
142. Wang Y.; Coombs N.; Turak A.; Lu Z-H.; Manners I.; Winnik M. A.; Macromolecules 2007, 40, 1594.

Abstract

In this work, the synthesis via anionic polymerization of seventeen (17) linear diblock copolymers of the PS-b-PCHD or PS-b-PCHD type where PS: polystyrene and PCHD: poly(cyclohexadiene) as well as five (5) complex architecture copolymers exhibiting also PS and PCHD segments, is described. The complex architecture copolymers comprise from a linear triblock copolymer (PCHD-b-PS-b-PCHD), a linear pentablock copolymer [(PS-b-PCHD)-PS-(PCHD-b-PS)], an H-type copolymer [$(PCHD)_2$-PS-$(PCHD)_2$] and two super H-type copolymers [$(PCHD)_3$-PS-$(PCHD)_3$ and $(PS\text{-}b\text{-}PCHD)_3$-PS-$(PCHD\text{-}b\text{-}PS)_3$] respectively.

The complete synthesis of the final linear diblock copolymers was accomplished by the use of high vacuum techniques and monomer sequential addition. For the successful polymerization, sec-BuLi was used as the initiator and benzene as the solvent, while the polar additive DABCO was added in order for the PCHD segment to exhibit high 1,4-microstructure (87-98%). A wide range of volume fractions was chosen and accomplished ($0.25 < \varphi_{PS} < 0.94$) in order to study the morphological behavior of this system in great extent.

The synthesis of the complex architecture copolymers involved initially the use of the difunctional initiator sodium/naphthalenide in order to synthesize the difunctional PS backbone in a benzene/THF solvent mixture (benzene:THF/1.2:1). The linking reaction with the living arms, which were either PCHD homopolymer or PS-b-PCHD diblock copolymer, was accomplished by using well-established chlorosilane chemistry. More specifically, the $(CH_3)_2SiCl_2$, $(CH_3)SiCl_3$ and $SiCl_4$ chlorosilane agents were initially linked with the backbone ($Na^{(+)(-)}PS^{(-)(+)}Na$) and then with the corresponding living polymer under absolutely controlled conditions.

The molecular characterization was performed via size exclusion chromatography (SEC) and membrane osmometry (MO) to confirm the $\overline{M}_n$ values and the molecular weight distribution. Also, proton nuclear magnetic resonance (^{1}H-NMR) spectroscopy was adopted to verify the type of the predictable microstructure for the PCHD segment as well as to identify the composition of each block. Furthermore, differential scanning calorimetry (DSC) measurements were performed in order to confirm the glass transition temperatures of the samples and their dependence from the molecular weight and the volume fraction. The results indicated

that all samples exhibited low molecular weight distribution and molecular as well as compositional homogeneity.

The morphological characterization of the linear diblock copolymers was performed via transmission electron microscopy (TEM) and small angle X-ray scattering (SAXS). All morphologies reported in the literature were observed, most of them for different volume fractions than expected, while unique morphologies are exhibited providing new information concerning the microphase separation of the PS-b-PCHD system. Further studies should also be made in order for the SAXS to completely verify the TEM results since a few discrepancies were encountered.

Περίληψη

Στην συγκεκριμένη ερευνητική εργασία περιγράφεται η σύνθεση μέσω ανιοντικού πολυμερισμού δεκαεφτά (17) γραμμικών δισυσταδικών συμπολυμερών του τύπου PS-b-PCHD ή PS-b-PCHD όπου PS: πολυστυρένιο και PCHD: πολυ(κυκλοεξαδιένιο) καθώς και πέντε (5) συμπολυμερών πολύπλοκης αρχιτεκτονικής αποτελούμενα επίσης από συστάδες PS και PCHD. Τα πολύπλοκης αρχιτεκτονικής δείγματα αποτελούν ένα (1) γραμμικό τρισυσταδικό συμπολυμερές του τύπου (PCHD-b-PS-b-PCHD), ένα (1) γραμμικό πεντασυσταδικό συμπολυμερές του τύπου [(PS-b-PCHD)-PS-(PCHD-b-PS)], ένα (1) H-type συμπολυμερές [$(PCHD)_2$-PS-$(PCHD)_2$] και δύο (2) super H-type συμπολυμερή [$(PCHD)_3$-PS-$(PCHD)_3$ και $(PS\text{-}b\text{-}PCHD)_3$-PS-$(PCHD\text{-}b\text{-}PS)_3$] αντίστοιχα.

Η σύνθεση των τελικών δειγμάτων ολοκληρώθηκε με την χρήση της γραμμής υψηλού κενού και την μέθοδο της διαδοχικής προσθήκης μονομερών. Για τον επιτυχημένο πολυμερισμό χρησιμοποιήθηκε ο απαρχητής sec-BuLi σε διαλύτη βενζόλιο, ενώ πραγματοποιήθηκε η χρήση του πολικού συστατικού DABCO ώστε η συστάδα του PCHD να εμφανίζει υψηλή 1,4-μικροδομή(87-98%). Συντέθηκε ένα μεγάλο εύρος κλασμάτων όγκου ($0.25 < \varphi_{PS} < 0.94$) έτσι ώστε να εξεταστεί αναλυτικά η μορφολογική συμπεριφορά του συστήματος.

Η σύνθεση των πολύπλοκης αρχιτεκτονικής συμπολυμερών περιελάμβανε αρχικά την χρήση του διδραστικού απαρχητή νάτριο/ναφθαλίνιο ώστε να συντεθεί το διδραστικό πολυστυρένιο που αποτελεί την μεσαία συστάδα. Ο πολυμερισμός πραγματοποιήθηκε σε διάλυμα βενζολίου/THF σε αναλογία 1,2:1 έτσι ώστε να αυξηθεί η διαλυτότητα του διδραστικού απαρχητή. Η αντίδραση σύζευξης με τα ενεργά άκρα, που αποτελούνταν είτε από PCHD ή από (PS-b-PCHD), πραγματοποιήθηκε χρησιμοποιώντας γνωστή χημεία χλωροσιλανίων. Πιο συγκεκριμένα τρία διαφορετικά χλωροσιλάνια χρησιμοποιήθηκαν, το διχλωροδιμεθυλοσιλάνιο [$(CH_3)_2SiCl_2$], το χλωροτριμεθυλοσιλάνιο [$(CH_3)SiCl_3$] και το τετραχλωροσιλάνιο ($SiCl_4$) ώστε να συζευχθούν με την διδραστική συστάδα ($Na^{(+)(-)}PS^{(-)(+)}Na$) και στην συνέχεια με τα ζωντανά άκρα αποτελούμενα από PCHD ή από (PS-b-PCHD).

Ο μοριακός χαρακτηρισμός των δειγμάτων πραγματοποιήθηκε μέσω της χρωματογραφίας αποκλεισμού μεγεθών (size exclusion chromatography - SEC) και

οσμομετρίας μεμβράνης (membrane osmometry - MO) ώστε να πιστοποιηθούν τα μέσα μοριακά βάρη κατά αριθμό $\overline{M}_n$ και οι κατανομές μοριακών βαρών. Επίσης χρησιμοποιήθηκε η φασματοσκοπία πυρηνικού μαγνητικού συντονισμού πρωτονίου [proton nuclear magnetic resonance (^{1}H-NMR) spectroscopy] ώστε να επιβεβαιωθούν τα κλάσματα μάζας και η ομοιογένεια ως προς την σύσταση και το μοριακό βάρος, καθώς επίσης και να υπολογιστούν τα ποσοστά των μικροδομών 1,2- και 1,4- για την συστάδα του πολυ(κυκλοεξαδιενίου). Επίσης, υιοθετήθηκε η διαφορική θερμιδομετρία σάρωσης (differential scanning calorimetry - DSC) ώστε να προσδιοριστούν οι θερμοκρασίες υαλώδους μετάπτωσης (T_g) των τελικών δειγμάτων και να μελετηθεί η εξάρτηση από το μοριακό βάρος και την αλληλουχία των συστάδων.

Τέλος, ο μορφολογικός χαρακτηρισμός των γραμμικών δισυσταδικών συμπολυμερών πραγματοποιήθηκε με την χρήση της ηλεκτρονικής μικροσκοπίας διέλευσης (transmission electron microscopy -TEM) και της σκέδασης ακτινών-Χ υπό μικρές γωνίες (small angle X-ray scattering - SAXS). Παρατηρήθηκαν όλες οι γνωστές μορφολογίες από την βιβλιογραφία αλλά για αρκετά διαφορετικά κλάσματα όγκου από τα αναμενόμενα, ενώ μοναδικές μορφολογίες παρατηρήθηκαν προσφέροντας νέες πληροφορίες για τον μικροφασικό διαχωρισμό του συστήματος PS-b-PCHD. Επίσης, πιο αναλυτικές μετρήσεις μέσω SAXS (Σύγχροντρο ή/και μεγαλύτερο χρονικό διάστημα έκθεσης στην δέσμη των ακτινών-Χ) πρέπει να πραγματοποιηθούν ώστε να επιβεβαιωθούν οι μορφολογίες που παρατηρούνται μέσω TEM.